Czech Technical University in Prague
Faculty of Mechanical Engineering
Department of Energy Engineering

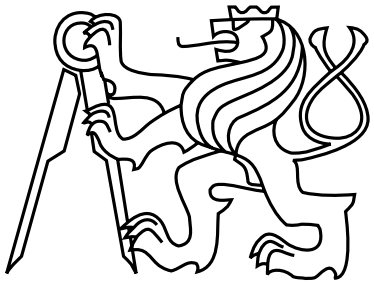

PhD Thesis

Formation of NO_X in oxy-fuel combustion in a bubbling fluidized bed

Ing. Matěj Vodička

Supervisor: prof. Ing. Jan Hrdlička, Ph.D.

Study Programme: Energy and Process Engineering

March 13, 2023

Aknowledgements

I would like to thank my supervisor Prof. Jan Hrdlička, Ph.D., for his support throughout my studies, for creating pleasant conditions for the successful completion of my thesis and for the valuable advice and comments he had on my work.

I also thank all the staff of the Department of Energy Engineering for creating a favorable environment, especially Ing. Pavel Skopec, Ph.D., for the enormous amount of selfless help and work done together, and Petr Stříž for his always efficient and prompt solutions to technical problems.

My greatest thanks go to my family, who created favourable conditions for me to complete my Ph.D. studies, in particular to my beloved wife Patricie, who has always been a great support, and to my daughter Magdaléna, who has been a great source of motivation.

This work was supported by the Grant Agency of the Czech Technical University in Prague, Student Grant Competition, grant No. SGS16/211/OHK2/3T/12, by Norway Grants 2009-2014, under CZ08 Programme, Fund for Bilateral Relations at Programme Level, Initiative No. NF-CZ08-BFB-1-026-2017, and by the Ministry of Education, Youth and Sports under OP RDE grant number CZ.02.1.01/0.0/0.0/16_019/0000753 "Research centre for low-carbon energy technologies". All grants are gratefully acknowledged.

Declaration

I hereby declare that I have completed this thesis independently and that I have listed all the literature and publications used.
I have no objection to usage of this work in compliance with the Act §60 No. 121/2000 Coll., the Copyright Law, and with the rights connected with the copyright act including the changes in the act.

In Prague on January 3, 2023 .....

Abstract

Oxy-fuel combustion is a technology for CO_2 capture and storage (CCS). Its main advantages compared to other CCS technologies are low demand for the newly built area and the possibility of retrofitting this technology to existing units. Therefore, it is very promising, in particular for the decentralized energy systems. One of the most common types of facilities for combustion of solid fuels used for combined heat and power production are bubbling fluidized bed (BFB) boilers. This thesis is focused on the formation of nitrogen oxides (NO_X) in the oxy-fuel combustion in BFBs. The combustion process is inevitably accompanied by the formation of gaseous pollutants such as NO_X. These do not pose any risk to the environment in the case of oxy-fuel combustion, since the flue gas is not directly released to the atmosphere. However, they can be dangerous for systems of CO_2 processing, transport, storage, or utilization. It is essential to understand the formation of NO_X in the oxy-fuel combustion process to minimize it. A comprehensive review of the current state of the art revealed that there is a lack of studies on the formation of NO_X in the oxy-fuel combustion in BFBs.

A one-dimensional numerical model of the oxy-fuel combustion in a BFB is presented in this thesis. The model is based on the principle of a plug flow reactor (PFR) with calculation of flue gas composition using chemical kinetics. Four mechanisms describing the kinetics of the formation of nitrogen oxides were adapted and tested within the model. The most convenient mechanism was then applied for detailed analysis. The numerical results were experimentally verified using a $30\,kW_{th}$ BFB combustor operating in full oxy-fuel combustion with real flue gas recirculation (FGR). Since BFBs are facilities typical for their ability to combust different types of fuel, two fuels were used in the numerical and experimental tests, Czech lignite and spruce wood pellets. The sensitivity of the formation of NO_X to the most important parameters of the combustion process was studied. These were the oxygen stoichiometry, the temperature of the fluidized bed, and the staged supply of oxygen. The formation of NO_X in the oxy-fuel and air-combustion was also compared within the experiments.

The numerical and experimental results showed in agreement that the formation of NO_X is strongly dependent on the oxygen stoichiometry for both fuels. The availability of oxygen is essential for the oxidation of nitrogen compounds, which are precursors to the formation of NO_X. On the contrary, the effect of fluidized bed temperature on the formation of NO_X was not so clear. The model predicted a very weakly decreasing trend of the NO_X concentration in the flue gas as the temperature increased in the studied range of values (from 800 to 1 000 °C) for both fuels. The experimental results showed a possitive sensitivity of concentrations of NO_X to increasing of the temperature (in the same range) for lignite combustion and no effect of temperature for the combustion of wooden pellets. There was a good agreement in

the numerical and experimental results in the study of the effect of staged supply of oxygen. The formation of NO_X was continuously depressed with increasing ratio of volumetric flows of secondary and primary oxygen in the range from 0 to 1.2. The experimental comparison of the formation of NO_X in the oxy-fuel and air-combustion regime showed that despite the relative concentrations of NO_X being higher in the oxy-fuel combustion (because of the lower volume of the formed flue gas), the absolute amount of formed NO_X is significantly lower.

To verify the results and to validate the numerical model, additional experiments of the oxy-fuel fuel combustion were carried out in a pilot-scale $500\,kW_{th}$ combustor. These tests showed the speciation of NO, NO_2, and even of N_2O, since their concentrations in the flue gas were measured separately. The results showed that the average shares of NO, NO_2, and N_2O in the formed nitrogen oxides were 88.4 %, 2.8 %, and 8.8 %, respectively. That was in good agreement with the numerical results obtained with the selected kinetic mechanism.

Abstrakt

Oxy-fuel spalování je jednou z technologií pro záchyt CO_2 ze spalin (CCS). Jejími hlavními výhodami ve srovnání s jinými technologiemi CCS jsou nízké nároky na nově zastavěné plochy a možnost dodatečné instalace této technologie do stávajících bloků. Proto je velmi perspektivní, zejména pro zdroje pro kombinovanou výrobu elektřiny a tepla. Jedním z nejběžnějších typů zařízení na spalování tuhých paliv používaných v teplárenství jsou kotle s bublinkovou fluidní vrstvou (BFB). Tato práce je zaměřena na tvorbu oxidů dusíku (NO_X) při oxy-fuel spalování v kotlích s bublinkovou fluidní vrstvou. Proces spalování je nevyhnutelně doprovázen tvorbou plynných znečišťujících látek, jako jsou NO_X. Ty v případě oxy-fuel spalování nepředstavují riziko pro životní prostředí, protože spaliny nejsou přímo vypouštěny do ovzduší. Mohou však mít škodlivé vlivy v systémech zpracování, přepravy, skladování nebo využití CO_2. Aby bylo možné tvorbu NO_X při oxy-fuel spalování minimalizovat, je potřeba jí nejprve dobře porozumět. Přehled současného stavu poznání ukázal, že existuje nedostatek studií popisujících tvorbu NO_X při oxy-fuel spalování v kotlích s bublinkovou fluidní vrstvou.

V této práci je představen jednorozměrný numerický model oxy-fuel spalování v ohništi s bublinkovou fluidní vrstvou. Tento model je založen na principu plug-flow reaktoru (PFR) s výpočtem složení spalin pomocí reakční kinetiky. V rámci modelu byly testovány čtyři mechanismy popisující reakční kinetiku tvorby oxidů dusíku. Nejvhodnější mechanismus byl poté použit pro podrobnou analýzu. Numerické výsledky byly experimentálně ověřeny pomocí laboratorního spalovacího zařízení s bublinkovou fluidní vrstvou o výkonu $30\,kW_{th}$ pracujícího v úplném oxy-fuel režimu spalování se skutečnou recirkulací spalin. Vzhledem k tomu, že kotle s bublinkovou fluidní vrstvou jsou zařízení typická svou schopností spalovat různé druhy paliv, byla při numerických i experimentálních testech použita dvě paliva, české hnědé uhlí a pelety ze smrkového dřeva. Byla studována citlivost tvorby NO_X na nejdůležitější parametry spalovacího procesu. Těmi byly stechiometrie kyslíku, teplota fluidní vrstvy a stupňovitý přívod kyslíku. V rámci experimentů byla rovněž porovnána tvorba NO_X při oxy-fuel spalování a při běžném spalování se vzduchem.

Numerické a experimentální výsledky shodně ukázaly, že tvorba NO_X je u obou paliv silně závislá na stechiometrii kyslíku. Dostupnost kyslíku je klíčová pro oxidaci dusíkatých sloučenin, které jsou prekurzory tvorby NO_X . Naopak vliv teploty fluidní vrstvy na tvorbu NO_X nebyl tak jednoznačný. Model předpověděl velmi slabě klesající závislost koncentrace NO_X ve spalinách na teplotě ve zkoumaném rozsahu hodnot (od 800 do 1 000 °C) pro obě paliva. Experimentální výsledky ukázaly pozitivní závislost koncentrací NO_X na zvyšování teploty (ve stejném rozsahu) při spalování hnědého uhlí a žádný vliv teploty při spalování dřevěných pelet. Při studiu vlivu stupňovitého přívodu kyslíku byla zjištěna dobrá shoda numerických a experimentálních výsledků. Tvorba NO_X se plynule snižovala s rostoucím

poměrem objemových průtoků sekundárního a primárního kyslíku v rozmezí od 0 do 1,2. Experimentální porovnání tvorby NO_X v oxy-fuel a vzduchovém spalovacím režimu ukázalo, že přestože relativní koncentrace NO_X jsou vyšší při oxy-fuel spalování (z důvodu menšího objemu vznikajících spalin), absolutní množství vzniklých NO_X je výrazně nižší.

Pro ověření výsledků a validaci numerického modelu byly provedeny další experimenty oxy-fuel spalování v pilotním spalovacím zařízení s bublinkovou fluidní vrstvou o výkonu $500\,kW_{th}$. Tyto testy ukázaly speciaci NO, NO_2 a dokonce i N_2O, protože jejich koncentrace ve spalinách byly měřeny odděleně. Výsledky ukázaly, že průměrné podíly NO, NO_2 a N_2O ve vznikajících oxidech dusíku byly 88,4 %, 2,8 % a 8,8 %. To bylo v dobrém souladu s numerickými výsledky získanými pomocí zvoleného mechanismu reakční kinetiky.

Contents

List of Figures

List of Tables

Nomenclature

Abbreviations

ASU Air separation unit

BFB Bubbling fluidized bed

CCS Carbon capture and storage (sequestration)

CCU Carbon capture and utilization

CFB Circulating fluidized bed

CFD Computational fluid dynamics

CLC Chemical looping combustion

CPU CO_2 purification unit

DFG Dry flue gas

EFR Entrained flow reactor

EOR Enhanced oil recovery

ETS Emissions trading system

FGR Flue gas recirculation

IGCC Integrated gasification combined cycle

JSR Jet stirred reactor

LHV Lower heating value [$MJ \cdot kg^{-1}$]

LWA Lightweight ceramic aggregate

PAN Peroxy-acetyl nitrate

PFR Plug flow reactor

PSD Particle sized distribution

RRSB Rosin-Rammler-Sperling-Bennet

SNCR Selective non-catalytic reduction

TOC Total organic carbon

WFG Wet flue gas

Greek symbols

η Dynamic viscosity [Pa·s]

λ Ratio of the oxygen excess [−]

ω Fuel devolatilization function [−]

ϕ Volumetric fraction of a component [% vol., ppmv]

ϕ_s Sphericity of solids [−]

ψ Ratio of secondary to primary oxygen volumetric flows [−]

ρ_b Bulk density of solid material [$\mathrm{kg \cdot m^{-3}}$]

ρ_g Density of fluidizing gas [$\mathrm{kg \cdot m^{-3}}$]

ρ_s Density of solid material [$\mathrm{kg \cdot m^{-3}}$]

ε_{mf} Voidage of the bed at minimum fluidization velocity [−]

Lower indexes

bed, *B* In the dense bed section

eq At the state of equilibrium

prim In the primary gas

Roman symbols

$\dot{V}_{\mathrm{O_2},prim}$ Volumetric flow of primary oxygen [$\mathrm{m^3_N \cdot h^{-1}}$]

$\dot{V}_{\mathrm{O_2},sec}$ Volumetric flow of secondary oxygen [$\mathrm{m^3_N \cdot h^{-1}}$]

Ar Archimedes number [−]

$\mathrm{Re}_{p,mf}$ Reynold's number for particles at minimum fluidization velocity [−]

A Pre-exponential factor of the rate constant [$\mathrm{cm^3 \cdot mole^{-1} \cdot s^{-1}}$, $\mathrm{cm^6 \cdot mole^{-2} \cdot s^{-1}}$]

A_{bed} Cross-section of the dense bed section [$\mathrm{m^2}$]

A_{freeb} Cross-section of the freeboard bed section [$\mathrm{m^2}$]

b Coefficient representing the particle size range

b Temperature exponent [−]

d_p Particle size [mm]

d_p^* Dimensionless particle size [−]

d_{10} 1^{st} decile particle size [mm]

d_{50} Median diameter [mm]

d_{90} 9^{th} decile particle size [mm]

d_{mean} Mean particle size [mm]

d_{mode} Mode particle size [mm]

dt Time step [s]

dt_{bed} Time step within the dense bed section [s]

E_a Activation energy [$\text{cal} \cdot \text{mole}^{-1}$]

EF Emission factor of gaseous pollutant [$\text{mg} \cdot \text{MJ}^{-1}$]

g Gravity acceleration [$\text{m} \cdot \text{s}^2$]

h Height [m]

$h_{\text{O}_2,sec}$ Height where the secondary oxygen is supplied [m]

h_{BFB} Height at which the boundary between dense bed and freeboard section is [m]

h_{freeb} Height at which the cross-section of the PFR reactor changes [m]

h_{max} Height in which the last thermocouple is placed in the freeboard section of the BFB combustor [m]

h_{total} Totel height of the PFR reactor [m]

k_f Forward rate constant [$\text{cm}^3 \cdot \text{mole}^{-1} \cdot \text{s}^{-1}$, $\text{cm}^6 \cdot \text{mole}^{-2} \cdot \text{s}^{-1}$]

m_{fuel} Mass flow of fuel [$\text{kg}\cdot\text{h}^{-1}$]

n Coefficient representing the polydispersity of the studied sample

n_{steps} Number of steps of the time integration [−]

R Universal gas constant [$\text{cal} \cdot \text{K}^{-1} \cdot \text{mole}^{-1}$]

$R(x)$ Cummulative weight of particles larger than x [−]

T Thermodynamic temperature [K]

t Temperature [°C]

t_0 Time matrix for the time integration [s]

u^* Dimensionless gas velocity [−]

u_0 Superficial gas velocity [m·s^{-1}]

u_{mf-90} Minimum fluidization velocity for d_{90} [m · s^{-1}]

u_{mf} Minimum fluidization velocity [m · s^{-1}]

u_{t-90} Terminal particle velocity for d_{90} [m · s^{-1}]

u_t Terminal particle velocity [m · s^{-1}]

$V_{O_2,min}$ Minimum specific volume of oxygen needed for complete combustion [m^3_N · kg^{-1}]

V_{O_2} Specific volume of oxygen available for combustion [m^3_N · kg^{-1}]

V_{air} Specific volume of air in the primary gas [m^3_N · kg^{-1}]

$V_{FG,dry}$ Specific volume of dry flue gas [m^3_N · kg^{-1}]

$V_{FG,wet}$ Specific volume of wet flue gas [m^3_N · kg^{-1}]

V_{FGR} Specific volume of recirculated flue gas [m^3_N · kg^{-1}]

w Mass fraction [−]

X Mole fraction [−]

x Particle size [mm]

$y(x)$ Function of the particle size distribution [1 · mm^{-1}]

z Current height in the plug flow reactor [m]

N−NO Conversion ratio of fuel nitrogen to NO [% mole]

Chapter 1

Introduction

Global warming is one of the most talked about environmental issues in recent years and is believed to be partly triggered by the increase in greenhouse gas emissions originating in excessive anthropogenic activities [1]. Therefore, most countries in the world have a duty to reduce greenhouse gas emissions thanks to countersigning the United Nations Framework Convention on Climate Change [2]. Carbon dioxide (CO_2), which belongs to this group of gases, is emitted from a large number of different applications, but one of the main contributors to its formation is the fossil fuel-based power production industry [1]. Several technologies (commonly called 'carbon capture and storage' or 'carbon capture and sequestration' (CCS) and 'carbon capture and utilization' (CCU)) were developed to reduce CO_2 emissions from energy production. Using these technologies, CO_2 is captured from the flue gas stream. The cleaned flue gas is released into the atmosphere, while CO_2 is purified, compressed, and transported to the place of utilization or storage. Unfortunately, these technologies require sizable investment costs and bring a significant reduction of the efficiency of energy conversion (in the case of coal fired power plants in the range from 15 to 28 % [3]). The need to capture CO_2 from the flue gas streams, in spite of the drawbacks of CCS/U technologies, comes from the steeply increasing prices of the so-called CO_2 credits that are traded within emissions trading systems (ETS), particularly in European Union by the EU ETS [4]. In fact, the EU ETS system was initially launched as a financial source of

decarbonization and, in parallel, as a tool to force energy producers to reduce CO_2 emissions from energy production.

1.1 Technologies for CO_2 capture

Technologies for CO_2 capture can be classified into three categories based on the principle of CO_2 capture:

- post-combustion capture,
- pre-combustion capture, and
- technologies with modified combustion.

The basic process scheme of these categories is given in Figure 1.1.

The post-combustion capture is the most straightforward and it can be easily retrofitted into already operating power plants, since CO_2 is captured from the flue gas downstream of all conventional flue gas cleaning technologies (e.g., particle filter, desulfurization unit or denitrification unit) [5]. CO_2 can be captured from the flue gas using various technologies, for example, absorption, adsorption, membrane, or cryogenic separation.

In the pre-combustion capture, the fuel is gasified using steam-oxygen gasification agent and CO_2 is captured from the gas produced before the combustion process. This technology is realized through the integrated gasification combined cycle (IGCC), which combines gasification and electricity generation using combustion and steam turbines. The gasifier converts the primary fuel into a syngas, which consists mainly of H_2, CO, and CO_2. Syngas is reformed using the water-gas-shift reaction where CO reacts with H_2O forming H_2 and CO_2. Then, CO_2 is separated from the reformed gas, typically by the absorption or adsorption process. The final product is H_2, which is burned in the IGCC combustion turbine. Although IGCC combined with the capture of CO_2 should have promising efficiency and operational costs, plant construction is associated with high capital costs [5, 6, 7]. It is also not feasible to retrofit conventional combustion plants with this technology [5, 6, 7].

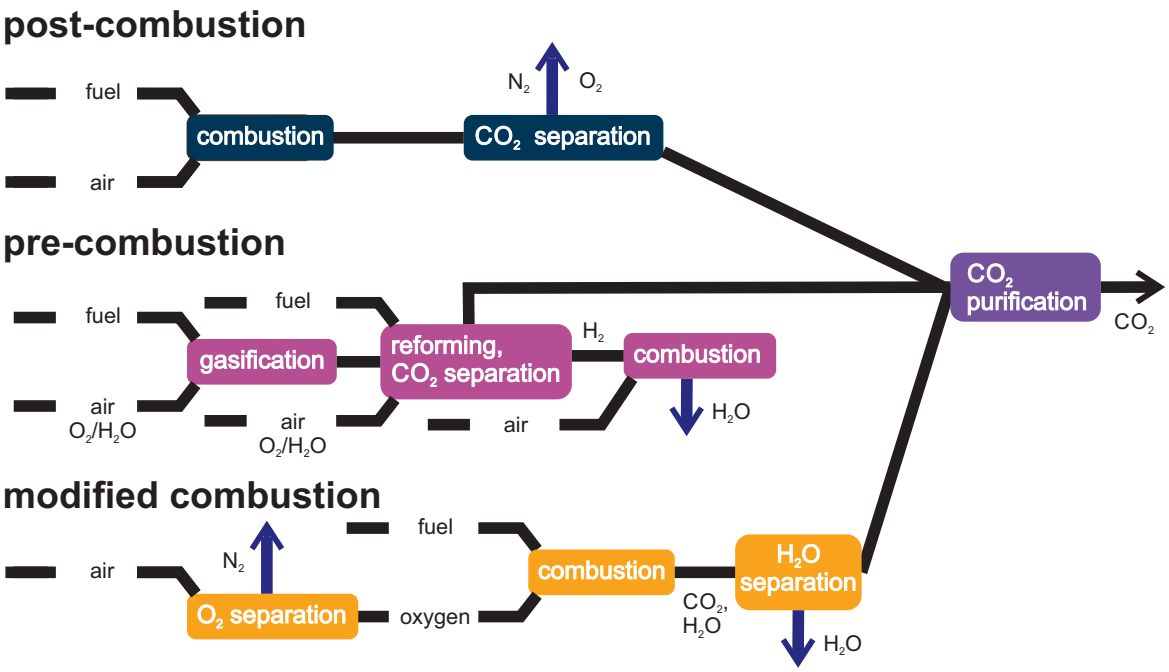

Figure 1.1: Process scheme of CCS technologies - post-combustion, pre-combustion and oxy-fuel-combustion.

The technologies with modified combustion are two: chemical looping combustion (CLC) and the oxy-fuel combustion. In both of them, oxygen is used to oxidize the fuel instead of air, which means that almost no molecular nitrogen is present in the combustion zone. In CLC, oxygen is provided to the process by a metal-based oxygen carrier, whereas in oxy-fuel combustion, oxygen is provided in molecular form from an air separation unit (ASU). As a result, the flue gas consists primarily of CO_2 and water vapor, which can be easily separated by condensation. This means that the CO_2 capture process itself is much more straightforward than for the so-called post-combustion capture, where nitrogen is still present in the hot flue gas. The CLC technology consists of two interconnected reactors with circulating fluidized beds (CFBs) between which a metal oxygen carrier is circulating. In the first reactor, the metal carrier is oxidized using air or water vapor. In the second reactor, where the fuel is introduced, the metal carrier is reduced, releasing oxygen available for the fuel oxidation. The process of oxy-fuel combustion is generally less technologically complicated. Here, the oxygen that is brought to the combustion chamber to oxidize the fuel comes directly

from a cryogenic ASU, and the process is carried out in a way similar to that of conventional combustion. However, this relative simplicity of capture comes with the penalty of expensive and inflexible oxygen production [5]. Nevertheless, it is the simplest CCS technology, which can certainly find wide application in practice.

The advantage of oxy-fuel combustion in comparison to other CO_2 capture technologies is that it can be easily retrofitted to boilers that have been operated without excessive demands on a newly built area [5, 8]. Several techno-economical studies indicated that the oxy-fuel combustion should be the most energy and cost efficient of the CO_2 capture technologies [5, 9, 10, 11]. Retrofitting can save significant investment costs, which is essential, especially for smaller heat power plants. Oxy-fuel combustion is a new technology that has not been applied in industry yet, but which has a very promising potential.

The application of oxy-fuel combustion on bubbling fluidized bed boilers is a specific case that is studied within this thesis. Bubbling fluidized bed (BFB) boilers are facilities with a power load that typically varies between $10-50$ MW. They are capable of combusting various types of solid fuels and even a variety of low-grade fuels with high moisture content [12]. The fluidized bed temperature typically varies in the range from 800 to 1 000 °C. Such a low combustion temperature contributes to the decrease in the formation of gaseous pollutants (particularly NO_X) and allows in situ desulfurization in the fluidized bed [13, 14]. These facts make BFB boilers very popular in the heat power production industry.

1.2 Motivation and scope of the thesis

Before compression and further processing of CO_2, the stream of the flue gas has to be cleaned and some of the components have to be removed, typically acidic gases (SO_X and NO_X). Generally, they can be considered as trace components in terms of their typical concentrations. The maximum levels allowed for these trace components according to Abbas et al. [15] are given in Table 1.1. The cleaning process is carried out in a so-called CO_2 purification unit (CPU), which consists of three parts: I) a sour compression unit where

Table 1.1: Maximum allowed levels of impurities in the CO_2 stream for the overall range of applications [15].

Component	Level of impurity [vol. % or ppmv]
H_2O	< 50 ppmv
O_2	< 10 ppmv
non-condensable gases (N_2, Ar, H_2)	< 4 %
CO	$< 2\,000$ ppmv
NO_X	< 100 ppmv
SO_X	< 50 ppmv
TOC	< 2 %
H_2S	$< (10 - 50)$ ppmv
CO_2	> 95 %

acidic gases are separated; II) a dehydration unit where water is separated; and III) a cryogenic unit where oxygen and non-condensable gases (N_2, Ar, H_2) are separated [16]. Since the cleaning process demands very expensive equipment and a significant amount of energy, it is essential to reduce the content of the unwanted components in the flue gas stream as much as possible prior to the CPU using conventional techniques, which are more cost and energy efficient.

Particularly, this thesis is focused on characterization of the formation of nitrogen oxides in oxy-fuel combustion in a BFB. The term 'nitrogen oxides' comprise generally all oxides of nitrogen, but in terms of gaseous products of combustion of solid fuels, we speak mainly about nitric oxide (NO), nitrogen dioxide (NO_2), and nitrous oxide (N_2O). The former two are dangerous gaseous pollutants and their emissions are regulated and restricted in the case of conventional air-combustion of solid fuels. N_2O is not a harmful gas (it is used in pharmacy as it produces insensibility to pain when inhaled), however it has a strong greenhouse effect. Because it is present in flue gases only in small concentrations (in units or tens of ppmv), it is not an object of emission limits. In the case of oxy-fuel combustion (and other combustion systems combined with CCS technologies), the maximum concentrations of impurities (Table 1.1) are not specified due to emission limits in general, because it is assumed that no gas is emitted to the atmosphere. They are based on technical demands

for transport and storage and on environmental demands in the place of deployment. The limit of 100 ppmv for NO_X (comprising NO and NO_2) is set mainly due to health and safety reasons (in the case of gas leakage) [17] and because of risks of corrosion. NO can catalyze the conversion of SO_2 to H_2SO_4, which has a strong corrosive potential [18]. NO oxidizes to NO_2 at lower temperatures and higher pressures (e.g. in the CPU) and NO_2 can react with H_2O forming HNO_3, which is also a strong corrosive acid. In the case of CO_2 storage, NO and NO_2 can react with formation and cap rocks and affect the injectivity and storage integrity [18]. Therefore it is necessary to characterize the impacts of the operation parameters of the oxy-fuel combustion process in a BFB on the formation and reduction of NO_X, since it is crucial to minimize their presence in the outlet CO_2 stream.

N_2O (unlike NO and NO_2) is not an acid gas and has no dangerous impact on CO_2 transport and storage systems. It can also be formed in the CO_2 purification process in the sour compression unit as a by-product of the NO and NO_2 reduction [16, 19]. Therefore, it is not an object of the maximum allowed levels of impurities in the stream of CO_2. However, because of its greenhouse potential, its formation in the oxy-fuel combustion in a BFB is involved in this study.

Chapter 2

Oxy-fuel combustion

First, the idea of replacing combustion air with pure oxygen was postulated by Horn and Steinberg [20] and Abraham et al. [21] simultaneously in 1982. They proposed an oxygen-coal-fired system producing a stream of liquefied CO_2 that could be used for enhanced oil recovery (EOR) from oil wells. Since then, oxy-fuel technology has been in the scope of many research groups all over the world. Around 2010, several large pilot units and plants were built or retrofitted, for example, Vattenfall's 30 MW_{th} plant in Schwarze Pumpe, Germany (2008) [22]; Total's 30 MW_{th} retrofitted boiler in the Lacq complex, France (2009) [23]; CIUDEN's 30 MW_{th} circulating fluidized bed (CFB) unit in Leon, Spain (2010) [24]; or Callide A 30 MW_{el} retrofitted oxy-fuel plant in Queensland, Australia (2011) [25]. These projects ended within a few years of research, some of them with the conclusion that the oxy-fuel technology as well as other CCS technologies were not viable at that time [26]. However, since then, oxy-combustion has been in the scope of many researchers who have continued to study this technology, particularly under laboratory-scale conditions, describing its fundamental aspects and the specifics of its application in various types of boilers, and currently even large industry corporations are interested in CCS and CCU technologies again [27]. Several comprehensive reviews of oxy-fuel combustion have been published, for example, by Wall et al. [28], Toftegaard et al. [5] and Scheffknecht et al. [29].

As mentioned in Chapter 1, the major part of the oxy-fuel flue gas consists of CO_2 and water vapor. The concentration of water vapor is particularly dependent on the properties of the fuel, since it comes from the moisture of the fuel and from the hydrogen bound in the combustibles. The sum of the volumetric fractions of CO_2 and H_2O in the flue gas can reach about 90 % and depends mainly on the oxygen stoichiometry, the degree of false air ingress, and the purity of oxygen. The residual share consists mainly of O_2, which is fed into the primary gas in excess to ensure the stability of the combustion process. Other components are Ar (being an impurity in the oxygen stream coming from the air separation unit), N_2 (introduced into the boiler with air ingress) and trace gaseous pollutants, for example CO, SO_2 and NO_X. For illustration, a comparison of typical specific volumes of flue gas and of its composition in the case of air- and oxy-combustion of lignite is given in Table 2.1. Volumes and volumetric fractions were calculated for ideal combustion at ratio of the oxygen excess $\lambda = 1.2$. This ratio is defined in Equation (2.1).

$$\lambda = \frac{V_{O_2}}{V_{O_2,min}} \tag{2.1}$$

Here, V_{O_2} is the specific volume of oxygen available for combustion and $V_{O_2,min}$ is the minimum specific volume of oxygen needed for complete combustion. The fuel considered for this calculation was used in this study and is described in Section 5.2.2. Air of 1.6 % content of water vapor and oxygen of 100 % purity were also considered within the calculation. It can be seen that the specific volume of wet flue gas formed per 1 kg of combusted fuel is about 3.4 times smaller in the case of oxy-fuel combustion. Due to the lower specific volume of flue gas, the relative concentration of O_2 in wet flue gas is then about 3.4 times higher in the case of oxy-fuel combustion compared to the air-combustion, although the oxygen excess ratio is the same for both combustion regimes.

Table 2.1: Comparison of specific volumes (per kg of fuel) and composition of flue gas formed in air- and oxy-combustion of lignite at ratio of the oxygen excess $\lambda = 1.2$.

			Air-combustion	Oxy-combustion
Specific volumes of flue gas:				
Volume of dry flue gas (DFG)	$V_{FG,dry}$	$\mathrm{m_N^3 \cdot kg^{-1}}$	5.08	0.99
Volume of wet flue gas (WFG)	$V_{FG,wet}$	$\mathrm{m_N^3 \cdot kg^{-1}}$	5.91	1.73
Volumetric fractions in wet flue gas:				
Vol. fraction of O_2	ϕ_{O_2}	% vol.	3.07	10.45
Vol. fraction of CO_2	ϕ_{CO_2}	% vol.	13.6	46.25
Vol. fraction of N_2	ϕ_{N_2}	% vol.	68.49	0.25
Vol. fraction of H_2O	ϕ_{H_2O}	% vol.	13.94	42.72
Vol. fraction of SO_2	ϕ_{SO_2}	% vol.	0.09	0.33
Vol. fraction of Ar	ϕ_{Ar}	% vol.	0.81	0

2.1 Oxy-fuel combustion in bubbling fluidized bed

The BFB boiler furnace is filled with bulk inert material that is fluidized by a fluidization gas. The fuel fed into the fluidized bed is mixed with this inert material by the movement of solids (caused by the fluidization gas) and amounts only about 1–2 % of the total mass of solids [30]. The type of used inert material depends on the combusted fuel. In the case of fuels with a higher ash content, such as coal or sewage sludge, the inherent ash is usually used as the bed material. In the case of fuels of lower ash content or fuels with ash of unsuitable fluidization properties, such as plant derived biomass, an external bed material has to be used. The most commonly used external bed material for biomass combustion is silica sand. Utilization of alternative materials such as allumina sand, calcite, magnesite, and olivine has been the subject of several studies [31, 32, 33, 34, 35, 36, 37, 38].

2.1.1 The primary gas in oxy-fuel combustion in a BFB

Fluidization is driven by the primary gas (also called fluidization gas), which has three particular functions:

1. It drags solid particles (which means that it maintains the fluidization);

2. It oxidizes fuel in the primary combustion zone;

3. It contributes to the heat balance of the fluidized bed in order to reach a desired temperature.

In conventional air combustion, the fluidization gas consists of primary air and, in some cases, recirculated flue gas (FGR). The FGR brings a degree of freedom into the combustion control process, since it only participates in the drag of solids and in the fluidized bed heat balance, but it does not fully contribute to the fuel oxidation.

In oxy-combustion, the fluidization gas is a mixture of almost pure oxygen and FGR. Compared to conventional air-combustion, the FGR is essential, particularly for provision of sufficient flow of the fluidization gas and for serving as a heat carrier. Without the FGR, the flow of oxygen supplied for the oxidation of the fuel would not be able to properly fluidize the bed alone. Additionally, the fluidized bed temperature would be several times higher than it should be with respect to the thermal stability of the fluidized bed. The adiabatic flame temperature can exceed 3 000 °C in the oxy-fuel combustion without the FGR [39]. The FGR initially has the same composition as the flue gas leaving the combustion chamber, but it can lose a part of the water vapor depending on the temperature of the FGR stream. If the FGR temperature is lower than the temperature of the dew point corresponding to the partial pressure of H_2O in the FGR, the water vapor condenses. Depending on whether condensation appears or not, the flue gas recirculation is called dry or wet, respectively.

For illustration, a comparison of the primary gas composition and of its specific volumes in air- and in oxy-combustion of lignite is shown in Table 2.2. The values shown in this table contribute to the balance of complete combustion for air- and oxy-fuel combustion modes that was shown in Table 2.1. The composition of FGR was considered the same as the composition of the flue gas reported in Table 2.1. Specific volumes of air and oxygen correspond to the ratio of oxygen excess $\lambda = 1.2$. The specific volume of FGR (V_{FGR}) equal to $0.3 \cdot V_{air}$ was used in the balance in the case of air-combustion. Here V_{air} is the specific volume of air in the primary gas. This ratio of V_{FGR} and V_{air} can reach values in a wide

Table 2.2: Comparison of specific volumes (per kg of fuel) and compositions of the primary gas in air- and oxy-combustion of lignite at ratio of the oxygen excess $\lambda = 1.2$, volumetric flow of FGR $V_{FGR} = 0.3 \cdot V_{air}$ for air-combustion, and the same specific volume of primary gas for both combustion regimes.

			Air-combustion	Oxy-combustion
Specific volumes of primary gas components:				
Volume of air/O_2	V_{air}/V_{O_2}	$m^3_N \cdot kg^{-1}$	5.2	1.09
Volume of FGR	V_{FGR}	$m^3_N \cdot kg^{-1}$	1.56	5.67
$\sum$ Volume of primary gas	$V_{prim-gas}$	$m^3_N \cdot kg^{-1}$	6.76	6.76
Volumetric fractions of primary gas components:				
Vol. fraction of O_2	ϕ_{O_2}	% vol.	16.61	24.92
Vol. fraction of CO_2	ϕ_{CO_2}	% vol.	3.16	38.78
Vol. fraction of N_2	ϕ_{N_2}	% vol.	74.9	0.21
Vol. fraction of H_2O	ϕ_{H_2O}	% vol.	4.42	35.82
Vol. fraction of SO_2	ϕ_{SO_2}	% vol.	0.02	0.28
Vol. fraction of Ar	ϕ_{Ar}	% vol.	0.88	0

range from 0 to more than 1 depending on the type of combustor and operating parameters, but the value of 0.3 is widely used in experimental studies [40, 41]. The specific volume of wet FGR in the case of oxy-fuel combustion was balanced in order to reach the same total specific volume of primary gas $V_{prim-gas}$ as in the case of air-combustion.

The composition of the primary gas plays a crucial role in the combustion process in BFBs. It affects the physical properties of the primary gas and thus its fluidization and heat-carrying capabilities.

It also has consequences for the chemical kinetics of the combustion process. The fact that combustion air is substituted with oxygen and recirculated flue gas generally results in an increase in the concentration of CO_2 in the flue gas, as well as an increase in the relative concentrations of all other flue gas species, including pollutants such as NO_X, SO_2, or CO. Regardless of the order and how close to equilibrium a chemical reaction is, a higher concentration of the product always slows the chemical reaction rates. There is also an impact of the FGR condition. If the FGR is dry, the concentrations of all combustion products (except H_2O) are even higher than in the case of wet FGR.

When the formation of gaseous pollutants in the oxy-fuel combustion is studied, the primary gas is clearly important, and therefore the composition and state of the FGR are clearly important. In large-scale applications, it is more likely that a high-temperature wet FGR will be used. Using a dry FGR would essentially mean integration of a condenser into the FGR stream. When the temperature of the flue gas decreases along the FGR path from the combustor outlet to the primary fluidization fan, acid gases such as NO_X, SO_2, or SO_3 can form mineral acids that condense before condensation of water vapor. The liquid acids (even if diluted) can have a strong corrosive effect on the flue gas ducts and other combustor equipment. The use of non-corrosive materials for the FGR path would be costly, and prevention of condensation in terms of keeping the FGR temperature above the dew point seems to be a better way.

It should be noted that the oxy-fuel fludized bed combustion has not yet been deployed in the industry on a commercial scale. Table 2.3 gives a summary of laboratory and pilot-scale experimental facilities and a review of experimental studies on oxy-fuel combustion carried out in the world between 2011 and 2020. It can be seen that most of the studies were performed using facilities with fluidized beds, particularly with CFBs. Several studies on nitrogen formation in oxy-fuel combustion in a BFB have also been published. However, in almost all of them, the real FGR was substituted by a dry mixture of clean gases from pressurized cylinders. Only de las Obras-Loscertales et al. [42] and de Diego et al. [43] included in their FGR water vapor and in only about 15 % vol., which is significantly lower than could be reached in the case of lignite or biomass combustion. It was already mentioned that several large-scale projects focused on the oxy-fuel combustion were carried out around 2010. These were the Vattenfall's 30 MW_{th} plant for pulverized coal in Schwarze Pumpe, Germany [22]; Total's 30 MW_{th} boiler for pulverized coal in the Lacq complex, France [23]; CIUDEN's 30 MW_{th} CFB unit in Leon, Spain [24, 81]; or Callide A 30 MW_{el} retrofitted oxy-fuel plant in Queensland, Australia (2011) [25, 82, 83, 84, 85]. Facilities used within these projects are not included in Table 2.3, since only very limited results from these projects

Table 2.3: Review of published experimental tests and of existing facilities for the oxy-fuel combustion of solid fuels.

Institution	Facility	FGR type	Fuel	Scope of the study	References
Instituto de Carboquímica, Zaragoza, Spain	3 kW_{th} BFB	simulated	coal (anthracite, bituminous, lignite)	fate of NO, N_2O, CO, SO_2, and Hg	[42, 43, 44], [45, 46]
School of Energy and Environment, Southeast University, Nanjing, China	50 kW_{th} CFB	real	coal (anthracite, bituminous)	NO formation	[47]
	10 kW_{th} CFB	not mentioned	co-firing coal and biomass	NO formation	[48]
Center of Research of Energy Resources and Consumptions, Zaragoza, Spain	90 kW_{th} BFB	simulated	coal (anthracite, bituminous, lignite) co-firing coal and biomass	fate of NO, CO, and SO_2, solids composition, deposits, corrosion	[49, 50, 51], [52, 53], [54, 55]
Institute of Advanced Energy Technologies, Czestochowa University of Technology, Poland	100 kW_{th} CFB	simulated	coal (bituminous)	fate of NO_X precursors, NO_X formation	[56]
VTT Technical Research Centre of Finland	100 kW_{th} CFB	real	coal (anthracite, bituminous)	formation of NO and N_2O	[57]
Faculty of Engineering, University of Nottingham, UK	20 kW_{th} BFB	simulated	biomass (miscanthus, wheat straw, wood)	formation of NO_X and CO	[58]
Department of Mechanical Engineering, Birla Institute of Tech. and Science, Pilani, India	20 kW_{th} BFB	real	oxygen enriched co-firing of coal, biomass, and sewage sludge	formation of NO_X and CO, temperature profiles	[59, 60]
Future Energy Plant Convergence Res. Center, Korea Institute of Energy Research, South Korea	100 kW_{th} CFB	real	coal (bituminous, sub-bituminous, lignite) co-firing of coal and biomass	oxy-fuel characteristics, CO_2 purity	[61, 62, 63]
Natural Resources Canada, CanmetENERGY, Ottawa, Canada	100 kW_{th} CFB	real	coal (bituminous), coke, co-firing of coal and biomass	oxy-fuel char., pollutants formation, ash characterization	[64, 65, 66]
	800 kW_{th} CFB	real	coal (bituminous, anthracite)		[67, 68]
Inst. of Eng. Thermophysics, Chinese Academy of Sciences, Beijing, China	lab-scale el. heated BFB	simulated	coal (bituminous) co-firing of coal and biomass	NO_X reduction over char	[69, 70]
Institute of Combustion and Power Plant Technology, Universität Stuttgart, Germany	20 kW_{th} pulverized fuel	simulated	coal (bituminous, lignite), oil shale	fate of NO_X, CO, SO_2, SO_3, and Hg, oxy-fuel characteristics	[71, 72] [73, 74]
	150 kW_{th} CFB	real	coal (bituminous)		[75]
	500 kW_{th} pulverized fuel	real	coal		[76]
Department of Chemical Engineering, Monash University, Victoria, Australia	lab-scale BFB	simulated	coal (brown)	oxy-fuel and ash characteristics	[77, 78]
	10 kW_{th} BFB	simulated	coal (brown)	fate of Hg, Se, Cr, and As	[79, 80]

have been published (except for the Callide project, which was, however, focused only on the combustion of pulverized coal).

As it infers from the paragraphs above and from the review in Table 2.3, it is essential to study the oxy-fuel combustion in a BFB with real wet FGR, as there is a significant lack of knowledge. In particular for the study of formation gaseous pollutants, it is necessary to bring the conditions of the experiments as close as possible to the future large-scale applications. It can be expected that operation of BFB combustors under oxy-fuel conditions with real wet FGR will bring lesser freedom of choice of operating parameters and only narrower ranges of these parameters will be possible compared to laboratory-scale experiments with artificial atmospheres or electrically heated devices. However, such results will surely have a greater benefit for a real practice despite these drawbacks.

2.1.2 Fluidization process in oxy-fuel combustion in a BFB

It was mentioned in Section 2.1.1, that the composition of the primary gas affects its fluidization properties. Within this Section, calculation of characteristic fluidization velocities is explained, which can help to quantify how the fluidization process can be affected. The numerical approach was taken from [86].

First, it is necessary to describe the process of fluidization, when a bed of solid particles is transformed into a fluid-like state. If a fluid passes upward through a bed of fine particles at a still higher velocity, at certain point all the particles are just suspended by the gas or liquid. At this moment, the drag force between the solid particles and the fluid counterbalances the weight of the particles and the bed is in a state of minimum fluidization, which can be characterized by a minimum fluidization velocity [86].

In the case where gas passes through the bed, the minimum fluidization velocity is obtained just from the force balance of particles dragged by the moving gas stream in the gravity field. After rearrangement, the balance can be expressed using the Ergun equation

in the following form:

$$\frac{1.75}{\varepsilon_{mf}^3 \phi_s} \mathrm{Re}_{p,mf}^2 + \frac{150(1-\varepsilon_{mf})}{\varepsilon_{mf}^3 \phi_s^2} \mathrm{Re}_{p,mf} = \mathrm{Ar} \tag{2.2}$$

where ε_{mf} is the voidage of the bed at the minimum fluidization velocity, ϕ_s is the sphericity of the solids, $\mathrm{Re}_{p,mf}$ is the Reynolds number of particles at the minimum fluidization velocity defined in Equation (2.3) and Ar is the Archimedes number defined in Equation (2.4).

$$\mathrm{Re}_{p,mf} = \frac{d_p \cdot u_{mf} \cdot \rho_g}{\eta} \tag{2.3}$$

In Equation (2.3), d_p is the characteristic size of solid particles. For minimum fluidization conditions, the mean or mode from a particle size distribution (PSD) analysis is typically used. u_{mf} is the minimum fluidization velocity, ρ_g is the density of the fluidizing gas, and η is its dynamic viscosity.

$$\mathrm{Ar} = \frac{d_p^3 \cdot \rho_g (\rho_s - \rho_g) g}{\eta^2} \tag{2.4}$$

where ρ_s is the density of the solids and g is the acceleration of gravity. This set of equations can be used to calculate the minimum fluidization velocity for any particle size. For example, inserting the particle size d_{90} gives the so-called minimum velocity of complete fluidization, indicating that 90 % of the particles are at or above their corresponding minimum fluidization velocity, and the bed can be considered fully fluidized.

If the gas passes through the fluidized bed at still increasing velocity, at one moment, the upper surface of the bed disappears and solids are carried out of the bed with the gas. The corresponding gas velocity is called the terminal velocity and can be obtained using the dimensionless particle size d_p^* and the dimensionless gas velocity u^* from the following expression [86]:

$$u_t^* = \left[\frac{18}{\left(d_p^*\right)^2} + \frac{2.335 - 1.744\phi_s}{\left(d_p^*\right)^{0.5}} \right]^{-1} \tag{2.5}$$

where

$$d_p^* = d_p \left[\frac{\rho_g (\rho_s - \rho_g) g}{\eta^2} \right]^{1/3} = \mathrm{Ar}^{1/3} \tag{2.6}$$

and

$$u^* = u \left[\frac{\rho_g^2}{\eta(\rho_s - \rho_g)g} \right]^{1/3} = \frac{\mathrm{Re}_p}{\mathrm{Ar}^{1/3}} \tag{2.7}$$

During combustion in a BFB, the superficial velocity must always be higher than the minimum fluidization velocity. The optimal range of the superficial velocity is theoretically between the velocity of complete fluidization u_{mf-90} and the terminal velocity u_t.

In Equations (2.2–2.7), the composition of the primary gas affects the density of the gas ρ_g and the viscosity η. Comparison of these parameters of primary gas in the air- and oxy-combustion at various temperatures in the range typical for BFB combustors is given in Table 2.4. The compositions of the primary gas given in Tabble 2.2 were used for the calculation. It can be seen that both the viscosity and the density of the primary gas are higher in the case of oxy-fuel combustion. At 800 °C, the viscosity is about 10 % higher and at 1 000 °C, it is about 13.2 % higher. The density is about 10.4 % higher regardless the gas temperature. Both variables appear in the definition of Reynolds number (Equation (2.3)) and Archimedes number (Equation (2.4)). Although the higher values in the case of oxy-fuel combustion have a negligible effect on the Reynolds number (since density is in the numerator and viscosity in the denominator), they noticeably affect the Archimedes number (where the viscosity in the denominator is squared). As a consequence, the minimum fluidization velocity can be about 25 % lower in the case of oxy-fuel combustion compared to air-combustion, while the terminal velocity can be about 15 % lower. The lower minimum fluidization velocity does not represent any risk for oxy-fuel combustion in a BFB, but the lower terminal velocity can cause unwanted pneumatic transport of the fluidized bed materials at some operating regimes. Therefore, the superficial gas velocity has to be checked carefully during oxy-fuel combustion.

2.1.3 Fluidized bed materials for oxy-fuel combustion in a BFB

The composition of primary gas (and of the combustion atmosphere) can also affect the process of fluidization in another way, by affecting the fluidized bed material. Fuel itself

Table 2.4: Comparison of viscosity and density of the primary gas in the air- and oxy-fuel combustion.

Temperature	°C	800	900	1 000
Viscosity η				
Air-combustion	$\mathrm{Pa \cdot s}$	$4.39 \cdot 10^{-5}$	$4.63 \cdot 10^{-5}$	$4.87 \cdot 10^{-5}$
Oxy-combustion	$\mathrm{Pa \cdot s}$	$4.83 \cdot 10^{-5}$	$5.17 \cdot 10^{-5}$	$5.51 \cdot 10^{-5}$
Density ρ_g				
Air-combustion	$\mathrm{kg \cdot m^{-3}}$	0.33	0.30	0.28
Oxy-combustion	$\mathrm{kg \cdot m^{-3}}$	0.36	0.33	0.30

amounts only to 1–2 % of the total mass of the material in the fluidized bed [30]. The residue has to be a material inert to combustion reactions, which carries the fuel particles and evenly distributes them in the volume of the fluidized bed. This inert material can be the inherent ash of the fuel if the fuel has a sufficient amount of ash of suitable fluidization properties (e.g., coal or sewage sludge in convenient particle size). However, for primary biomass of both wooden and non-wooden origin, it is specific that it contains a very small amount of inherent ash. To use biomass as a fuel for combustion in a fluidized bed, the bed material must therefore necessarily be of an external origin. The term "external" refers to an inert material that is not an integral part of the combusted fuel and must be supplied externally to the combustor.

For a stable combustion process, the external bed material must have suitable properties. Mainly, it has to be easily and evenly fluidizable, it cannot have a negative impact on the formation of gaseous pollutants, and it must not tend to form eutectics and agglomerates. Agglomeration of the fluidized bed causes an increase in the mean particle size of the bed and consequently in the minimum fluidization velocity, which can lead to defluidization of the bed and shutdown of the facility [87]. Comprehensive reviews of particle agglomeration mechanisms during fluidized bed thermal processes were published by Olofsson et al. [88], Bartels et al. [89], Morris et al. [90], Scala [91], or Kuba et al. [92]. Generally, there are two main mechanisms of agglomeration: coating-induced agglomeration and melt-induced agglomeration. Several mechanisms based on physical principles were also reported, but they

can be largely explained by the former two. In the coating-induced agglomeration, the bed particles are coated with a K-silicate or Ca-silicate melt layer covered by an outer ash layer. When coated particles collide, a K-silicate or Ca-silicate neck is formed. The continuously growing agglomerate has a high potential for sintering at a sufficient temperature [90]. In melt-induced agglomeration, the alkali-silicate melt from the fuel ash adheres to the bed particles and agglomerates them together [90].

The most frequently used external bed material for conventional air-combustion is silica sand, although due to the high Si content it is prone to agglomeration problems. According to Morris et al. [90], replacing silica sand based on SiO_2 with materials with a predominant content of Mg, Ca, or Al reduces the available silica and therefore reduces the agglomeration, which was also confirmed by [31, 33, 35, 36, 38, 93]. Other bed materials, such as alumina, olivine, or sepiolite, can be used with advantage. The defluidization time, that is, the time before the defluidization associated with agglomeration occurs, was found to be increased by using olivine instead of silica sands, particularly for fuels predisposed to melt-induced agglomeration, such as wheat straw [94].

The impact of long-term exposure of the external fluidized bed materials to the oxy-fuel combustion atmosphere at high temperatures on material performance and proneness to agglomeration is unknown. Research on this topic is very desirable, since oxy-fuel combustion of biomass is a promising combination that leads to negative overall CO_2 production. Although the study of fluidized bed materials for oxy-fuel combustion is not directly within the scope of this thesis, this study can contribute in part to the current state of the art within this topic.

Chapter 3

Nitrogen oxides formation in a combustion process

As mentioned in Section 1.2, the most important oxides of nitrogen formed in the combustion process are nitric oxide (NO), nitrogen dioxide (NO_2), and nitrous oxide (N_2O). The former two are toxic gases collectively called NO_X. Nitrous oxide is not a harmful gas, but has a strong greenhouse effect. Properties of these oxides will be described in Section 3.1. In the combustion process, they are formed through different mechanisms, either from a molecular nitrogen (normally fed to the furnace in the combustion air) or from a nitrogen bound in the fuel. The mechanisms of formation of NO, NO_2, and N_2O will be described in Sections 3.2, 3.3, and 3.4, respectively. The specific aspects of oxy-fuel combustion in a BFB that affect the formation of nitrogen oxides will be described in Section 3.5.

3.1 Nitrogen oxides

3.1.1 NO

Nitric oxide is a colorless toxic gas. Its boiling temperature is -151.8 °C at atmospheric pressure. Nitric oxide is a free radical, which means it has an unpaired electron. It is the most

dominant part of NO_X formed in the combustion of fossil fuels in stationary sources, however, it can easily oxidize and form NO_2. NO contributes to the depletion of the stratospheric ozone layer through the following reaction [95]

$$NO + O_3 \overset{hv}{\rightleftharpoons} NO_2 + O_2 \tag{3.1}$$

and can contribute to the deposition of acid rain through the reaction sequence (3.2) - (3.3), when it reacts with the hydroperoxy radical and forms nitric acid [96].

$$NO + HO_2 \longrightarrow NO_2 + OH \tag{3.2}$$

$$NO_2 + OH \longrightarrow HNO_3 \tag{3.3}$$

The reaction (3.1) is used as well in order to measure the concentration of NO in the flue gas, since the reaction of nitric oxide with ozone is accompanied by a light emission proportional to the amount of nitric oxide in the sample. The intensity of the electromagnetic waves is measured using a photodetector.

3.1.2 NO_2

Nitrogen dioxide is a brown aggressive and toxic gas with a boiling temperature of 21.2,°C. Its direct formation is mainly negligible in the combustion of solid fuels and occurs only if the flue gas is rapidly cooled [97]. NO_2 is mostly formed through the oxidation of NO according the equation (3.4), usually at lower temperatures [98] and higher pressure.

$$2\,NO \rightleftharpoons N_2O_2 \xrightarrow{O2} 2\,NO_2 \tag{3.4}$$

The temperature coefficient of this reaction is negative, so the reaction speed is highest at low temperatures [97]. However, significant NO_2 concentrations can be found in the flue gas from gas turbines [99].

The nitrogen dioxide altogether with non-methane hydrocarbons participates in the chemical reaction sequence (3.5) - (3.8) that produces tropospheric ozone contributing to photochemical smog [100, 101]. First, NO_2 is decomposed by photolysis

$$NO_2 + h\nu\,(\lambda < 420\,\text{nm}) \longrightarrow NO + O \tag{3.5}$$

and then, the $O^\bullet$ radical reacts with the atmospheric O_2 in a three-body reaction immediately.

$$O_2 + O + M \longrightarrow O_3 + M, \tag{3.6}$$

where the collision partner can be a gas-phase molecule, usually of N_2, O_2, Ar, or He [102]. So far, only the amount of O_3 proportional to the original NO_2 concentration could be formed. However, peroxy radicals originating from hydrocarbons can react with NO forming another NO_2, which can be a source of more ozone.

$$RCH_2 + O_2 \longrightarrow RCH_2OO \tag{3.7}$$

$$RCH_2OO + NO \longrightarrow NO_2 + RCH_2O \tag{3.8}$$

Furthermore, organic radicals accumulate the NO_2 content in the atmosphere through the formation of various compounds, particularly peroxy-acetyl nitrate (PAN).

3.1.3 N_2O

Nitrous oxide is a colorless gas. Due to the tight N−N bond it is very stable in the atmosphere with a half-life period exceeding 100 years [97]. Its boiling temperature is −88.5 °C. At elevated temperatures, it is a strong oxidizer. Although it is not involved in the NO_X group and its formation in the combustion of fossil fuels from stationary sources is not restricted by legislation, nitrous oxide is a greenhouse gas and contributes significantly to the depletion of stratospheric ozone. However, the power producing industry is only a minor producer of N_2O compared to agricultural soil management [103]. The concentrations of N_2O in the stream

of CO_2 to be captured or utilized are not mentioned in most studies on the CO_2 purity requirements and neither in studies on the performance of CO_2 purification units although the yields of N_2O can sometimes be comparable to those of NO_2.

3.2 Mechanisms of the NO formation in a combustion process

Nitric oxide originating from the combustion of solid fuels is formed from molecular nitrogen obtained in the combustion air or from nitrogen-containing organic compounds in the fuel (referred to as fuel-bound nitrogen). There are three generally well-described mechanisms of NO formation. Two of them are based on the oxidation of gas-phase molecules of N_2, the third is based on the oxidation of fuel-bound nitrogen, which is particularly found in NO^- or NH_2^- functional groups and heterocyclic hydrocarbons containing nitrogen, for example, pyridine [99]. The formation of NO from N_2 at high temperatures in the post-flame zone was first described by Zeldovich et al. [104] and is generally called the thermal formation mechanism, often referred to as the Zeldovich mechanism. The second mechanism, based on molecular nitrogen oxidation, is called the prompt mechanism. It was first postulated by Fenimore [105] who observed that in the case of a fuel-rich hydrocarbon flame, NO can be formed already in the flame zone. Hence, the prompt mechanism is sometimes called the Fenimore mechanism. In the case of combustion of fuels containing bound nitrogen, the majority of NO is formed through the fuel mechanism. Hydrocarbons containing nitrogen are thermally decomposed prior to entering the combustion zone, forming low molecular weight nitrogen-containing compounds (mainly HCN and to a lesser extent also ammonia) that can rapidly oxidize to NO. Reviews on the mechanisms of formation of NO were published by Miller and Bowman [106] and Bowman [107, 108].

3.2.1 Thermal NO

The thermal mechanism of formation of NO comprises the chain of reactions (3.9) and (3.10) initiated by oxygen atoms (from the H_2-O_2 radical pool or from the dissociation of O_2) attacking the nitrogen molecule [99].

$$O + N_2 \rightleftharpoons NO + N \tag{3.9}$$

$$N + O_2 \rightleftharpoons NO + O \tag{3.10}$$

It is common to include also the reaction (3.11) in the thermal mechanism, although the concentration terms in the rate expression of this reaction would be very small, since both reacting species are radicals.

$$N + OH \rightleftharpoons NO + H \tag{3.11}$$

The set of reactions (3.9 - 3.11) is usually referred to as the extended Zeldovich mechanism. Due to the need to break the tight N_2 bond, the reaction that controls the rate of this mechanism is the reaction (3.9). Invoking a steady-state approximation for the concentration of N atoms and making a partial equilibrium assumption for the O atom, the maximum formation rate of NO can be expressed using Equation (3.12) [107].

$$\frac{d[NO]}{dt} = 1.45 \cdot 10^{17} \cdot T^{-1/2} \cdot \exp(-69\,460/T) \cdot [O_2]_{eq}^{1/2} \cdot [N_2]_{eq} \quad [\mathrm{mol \cdot cm^{-3} \cdot s^{-1}}] \tag{3.12}$$

From this equation, it is apparent that the formation of NO through the thermal mechanism depends mainly on the temperature of the flue gas and slightly also on the O_2 concentration in the flue gas. And obviously, the formation of NO would depend on the concentration of N_2, which can play a significant role in oxy-fuel combustion, but in air-combustion, it can

hardly be taken as a variable. Under 1 800 K, the thermal mechanism is generally considered irrelevant.

3.2.2 Prompt NO

Although the thermal mechanism explains the formation of NO in the burned gas zone, it cannot clarify the formation of NO in front of fuel-rich hydrocarbon flames, which was first observed by Fenimore [105]. He claimed that there has to be another NO formation mechanism different from the thermal mechanism, which plays a role in the flame region. He called the NO "prompt" NO. Since he did not find any prompt NO in the CO-air and H_2-air flames, he claimed that the NO formation mechanism could include reactions (3.13) and (3.14). Then, N atoms could form nitric oxide through Equations (3.10) and (3.11) and CN could produce NO through the reaction with oxygen molecule or oxygen atom as well.

$$CH + N_2 \rightleftharpoons HCN + N \tag{3.13}$$

$$C_2 + N_2 \rightleftharpoons 2\,CN \tag{3.14}$$

Lately, Hayhurst and Vince [109] have proved that prompt NO formation in moderately fuel-rich systems is proportional to the number of carbon atoms present per unit volume and that it is independent of the type of original hydrocarbon. This meant that reactions (3.13) and (3.14) cannot be the main contributors, as it is unlikely that C_2 and C_2H could be formed from CH_4 with an efficiency half that of C_2H_2 of one-third that of C_3H_6 or C_3H_8 [99]. The main kinetic route to prompt NO appears to follow reactions (3.15) - (3.19).

$$HCN + O \rightleftharpoons NCO + H \tag{3.15}$$

$$NCO + H \rightleftharpoons NH + CO \tag{3.16}$$

$$NH + (H, OH) \rightleftharpoons N + (H_2, H_2O) \tag{3.17}$$

$$N + OH \rightleftharpoons NO + H \tag{3.18}$$

$$N + O_2 \rightleftharpoons NO + O \tag{3.19}$$

According to Bowman [107], the prompt NO (defined as NO formed at a rate faster than that calculated from the equilibrium of the thermal mechanism of formation of NO) could be formed from three different sources:

1. non-equilibrium O and OH concentrations in the reaction zone and burned gas, which could accelerate the rate of thermal mechanism,

2. a reaction sequence, described in Figure 3.1 and by equations (3.15) - (3.19), which is initiated by reactions of hydrocarbon radicals, present in and near the reaction zone, with molecular nitrogen (the mechanism proposed by Fenimore [105]),

3. reaction of O-atoms with molecular nitrogen to form N_2O through a three-body recombination reaction

$$O + N_2 + M \longrightarrow N_2O + M \tag{3.20}$$

and subsequent reaction of N_2O to form NO via

$$N_2O + O \longrightarrow NO + NO \tag{3.21}$$

The relative importance of these sources of the prompt NO depends on the conditions in the combustor. The non-equilibrium O an OH radicals concentration tends to enhance the NO formation most significantly in non-premixed flames, in stirred reactors for lean conditions, and in low pressure premixed flames, accounting for up to 80,% of the prompt NO formation [107]. The Fenimore mechanism is dominant in the fuel-rich combustion of premixed hydrocarbons and in the diffusion flames of hydrocarbons, accounting for more than 50 % of the total formation of NO [107]. The formation of NO through the mechanism of N_2O is most significant for low fuel-air ratios, low flue gas temperatures, and high pressures. It is most important in conditions where the total NO formation rate is very low.

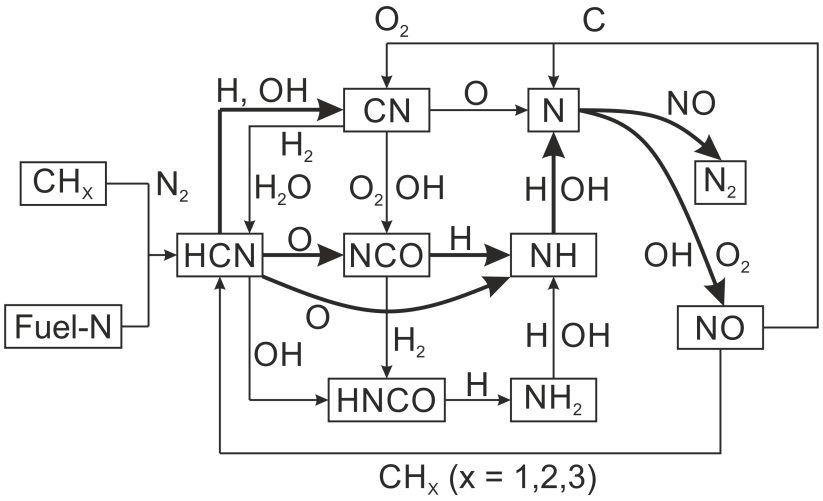

Figure 3.1: Reaction path diagram illustrating the major steps in prompt NO formation, conversion of fuel-N through the oxidation of HCN, and reburning [106].

3.2.3 NO from the fuel-bound N

Fuel-bound nitrogen is an important source of NO in the combustion of fossil fuels and biomass. It is particularly important for the combustion of coal, which typically contains $0.5-2.0\,\%$ wt. of nitrogen, and for the combustion of non-wooden biomass, where its content can reach up to $5\,\%$ wt. The degree of conversion of fuel-N to NO is nearly independent of the type of nitrogen compound, but is significantly dependent on the local combustion environment [106]. In the furnace, fuel is thermally decomposed, producing volatile and char compounds. Fuel-bound nitrogen is distributed between the char and volatiles depending on the fuel structure and devolatilization conditions, such as temperature, heating rate, oxygen concentration, or residence time. In case of lower temperatures or shorter residence times, nitrogen preferably remains in the char, while at higher temperatures, it is rather a part of the volatiles [110]. The fuel structure affects the fuel-N mechanism so that the rate of devolatilization increases with increasing oxygen content in the fuel, which means that it increases with decreasing fuel rank [110].

The gas phase volatile nitrogen reaction sequence is initiated by a rapid and almost quantitative conversion of the parent nitrogen compounds to hydrogen cyanide and ammonia [106]. HCN appears to be the principal product when fuel nitrogen is bound to an

aromatic ring, and NH_3 when fuel nitrogen is in the form of amines. The formed HCN and NH_3 are oxidized simultaneously, and HCN and NH_3 are considered the main sources of NO and N_2O. Since the production of NO from fuel-bound nitrogen involves reactions important in the oxidation of HCN and NH_3, the fuel-N mechanism is similar to the prompt NO mechanism and can be described using the reaction sequence shown in Figure 3.1.

The reaction mechanism given in the Figure 3.1 shows as well a pathway to recycle NO formed in the combustion process back to cyano compounds by reaction of NO with small hydrocarbon radicals. Under fuel-rich conditions, these compounds can preferably react to form N_2. This process is often referred to as reburning [107]. The scheme of oxidation of NH_3 to NO is given in Figure 3.2. In addition to the reaction steps shown in the diagram, there are also reactions that form N_2 that do not involve NO [106].

Char-N oxidation is a complex and difficult-to-describe process consisting of various heterogeneous reactions and subsequent homogeneous reactions. Moreover, the experimental characterization of this process is complicated by the simultaneous release of volatile N or by subsequent reactions of the primary products. The output of char-N oxidation comprises a number of species (NO, N_2O, HCN, NH_3, HCNO, N_2) [110]. Char-N conversion to NO varies from 30 % to almost 100 % and it is assumed that NO is the main product of char-N oxidation [110]. The active surface of char can also catalyze a number of reactions either NO forming or reducing, for example, the reduction by CO or H_2 and oxidation of NH_3 to NO. Experiments of highly devolatilized small single particle combustion have shown that char-N is oxidized to NO with a yield of 75–100 % and that NO yields far below 100 % are caused by subsequent reduction of NO in the porous structure of the parent char particle or of other char particles [110, 111].

Although details have yet to be clarified, the general reaction mechanism of char-N oxidation and further NO reduction on the char surface appears to have been sufficiently described in recent time. The following discussion follows the review presented by Glarborg et al. [110].

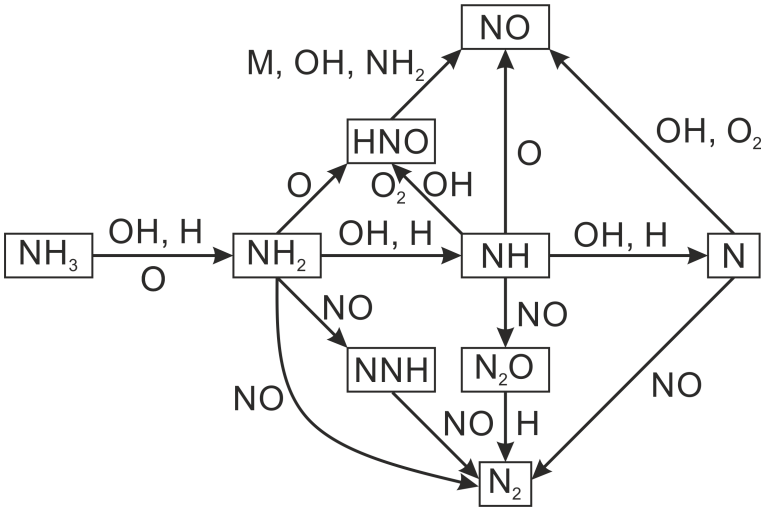

Figure 3.2: Reaction path diagram for the oxidation of ammonia in flames [106].

The first step is the formation of NO through a reaction

$$\mathrm{C(N) + O_2 \longrightarrow NO + C(O)} \tag{3.22}$$

where C(N) and C(O) refer to nitrogen and oxygen species on the surface of the char. The formed NO may be subsequently reabsorbed on the char surface by dissociative chemisorption

$$\mathrm{2\,C_f + NO \longrightarrow C'(N) + C(O)} \tag{3.23}$$

Here, $\mathrm{C_f}$ denotes a free carbon site, while C'(N) are nitrogen species on the char surface, which may be different from the char-N C(N). The reaction (3.23) can lead to an accumulation of N on the char surface, at least at lower temperatures. The reaction of gaseous NO with nitrogen species on the surface of char C'(N) can lead to a reduction of NO and the formation of molecular nitrogen according the equation (3.24).

$$\mathrm{C'(N) + NO \longrightarrow N_2 + C(O)} \tag{3.24}$$

Another option for the formation of free nitrogen could be the state recombination of two C'(N) species according the equation (3.25). However, the route (3.25) should be dominant

in the temperature range 900 – 1200 K [112, 113].

$$C'(N) + C'(N) \longrightarrow N_2 + 2\,C_f \tag{3.25}$$

Char-N oxidation can be affected by various parameters of the combustion process. The NO yields decrease with an increase of the volumetric fraction of NO, of the particle size, of the pressure, and of the char reactivity. Both increased particle size and pressure yield a longer residence time for NO in the porous structure and, consequently, a larger reduction.

3.3 Mechanisms of the NO_2 formation in a combustion process

Although the direct formation of nitrogen dioxide is almost negligible, the possible reaction sequence of formation and destruction of NO_2 is fairly well known [106, 107]. NO_2 is formed by the reaction of nitric oxide with the hydroperoxy radical described by the equation (3.2). The HO_2 is relatively stable in low-temperature regions where it can react with NO transported by diffusion from high-temperature regions. The rate of the reaction (3.2) is strongly dependent on the concentration of HO_2, which is formed mainly through the reaction (3.26) from the oxidation of H atoms transported from high temperature regions.

$$H + O_2 + M \rightleftharpoons HO_2 + M \tag{3.26}$$

The destruction of NO_2 can follow the reactions (3.27) and (3.28), where the former is the principal.

$$NO_2 + H \rightleftharpoons NO + OH \tag{3.27}$$

$$NO_2 + O \rightleftharpoons NO + O_2 \tag{3.28}$$

It can be seen that the reaction (3.26) and (3.27) are competitive, as both need free H atoms.

The NO_2 is consumed rapidly at elevated temperatures. Its lifetime is usually less than 10 ms at 1 500 K which indicates that the NO_2 formation can be of importance only in facilities with lower combustion temperatures [107].

3.4 Mechanisms of the N_2O formation in a combustion process

Nitrous oxide is formed in the early phases of combustion at low temperatures. At higher temperatures, it decomposes into NO. The lifetime of N_2O in zones with a temperature greater than 1 500 °C is typically less than 10 ms [107]. However, in low-temperature combustion, such as in fluidized bed combustors, and in the cases of some post-combustion NO_X reduction systems, N_2O emissions may be significant. The main gas phase reactions that lead to formation of N_2O in the combustion of fossil fuels are

$$NCO + NO \longrightarrow N_2O + CO \tag{3.29}$$

$$NH + NO \longrightarrow N_2O + H \tag{3.30}$$

In the case of combustion of natural gas at lower temperatures and elevated pressures, N_2O can also be formed according the three-body reaction (3.31).

$$O + N_2 + M \longrightarrow N_2O + M \tag{3.31}$$

The primary steps of N_2O removal are described using the equation (3.32) and (3.21).

$$H + N_2O \longrightarrow N_2 + OH \tag{3.32}$$

3.5 NO_X formation in the oxy-fuel combustion in a bubbling fluidized bed

The changes in the combustion environment when changing from air- to oxy-fuel combustion significantly influences the nitrogen chemistry and the formation of nitrogen oxides. The near absence of molecular nitrogen N_2 is obviously of importance for thermal and prompt formation of NO_X, however, the dominance of CO_2 and H_2O and the high relative concentration of combustion products also affect the oxidation of fuel-bound nitrogen. The following text presents a review of experimental studies on impacts of oxy-fuel combustion environment on the formation of nitrogen oxides. Not all studies are related to BFBs, but here only the observations relevant for BFBs are reported.

Zhu et al. [114] examined the effect of the introduction of water vapor into the fluidized bed on the formation of NO_X. They concluded that the addition of H_2O to the combustion chamber enhances the reduction of NO_X at low to moderate (up to 30 % vol.) oxygen concentrations at the inlet gas due to the inhibited release of volatile N species. At higher oxygen concentrations, H_2O would tend to react with O_2 and form more OH radicals, resulting in an increased formation of NO_X compared to the situation without the addition of H_2O. Duan et al. [47] studied the impact of a CO_2 atmosphere on NO_X precursor formation using a tube furnace and FTIR gas analyzer. They observed that CO_2 influences both NH_3 and HCN formation. The HCN yields were significantly enhanced compared to those obtained in an atmosphere of Ar, while the NH_3 yields were suppressed. Giménéz-López et al. [115] studied HCN oxidation in an O_2 /CO_2 atmosphere, corresponding to oxy-fuel combustion, and observed considerable inhibition compared to air-combustion. This inhibition of HCN formation is due to the competitive reaction of CO_2 and hydrogen radicals. As a result, a depressed fuel-N/NO_X conversion ratio can be expected in the oxy-fuel regime, which was confirmed by Lupiáñez et al. [49] in a 90 kWth BFB combustor.

According to Normann et al. [116], the elevated CO_2 concentration can also lead to changes in the radical pool of the combustion process, mainly through the reaction

$$CO_2 + H \rightleftharpoons CO + OH \tag{3.33}$$

Here, the higher concentration of hydroxyl radicals (OH) can promote the formation of NO from volatile-N, but also, as mentioned above, CO can reduce NO in proximity to the particles through the reaction [49]

$$NO + CO \rightleftharpoons \frac{1}{2}N_2 + CO_2 \tag{3.34}$$

This reaction can be particularly significant, since the formation of CO in oxy-fuel combustion is enhanced by the heterogeneous Boudouard reaction that uses the unburned fuel char

$$CO_2 + C^{(S)} \longrightarrow 2\,CO \tag{3.35}$$

which can also lead to another reduction of NO_X emission [116].

Zhou et al. [117] studied the conversion of fuel-N to NO during devolatilization and char combustion in an oxy-fuel combustion atmosphere using a laboratory-scale flow tube reactor and observed that the formation of NO is promoted by an increase in temperature in the range $700-900\,^{\circ}C$, both from the oxidation of volatile and char-N. However, while the impact on the volatile-N to NO conversion ratio was very small, the formation of NO from char-N appeared to be very temperature sensitive. The temperature of the burning char particle is mainly dependent on the concentration of O_2 and the size of the char particle [118]. Within an oxy-fuel combustion atmosphere, the diffusivity of O_2 toward the char particle is reduced, which, together with the enhanced gasification, can decrease the temperature of the burning char particle compared to the air-combustion atmosphere [119, 120]. This decrease is most dominant at higher temperatures, but is significant even for the typical bubbling fluidized

bed temperature range. The formation of NO_X from combustion of chars is expected to be lower for oxy-fuel combustion than for air-combustion in terms of absolute values.

The effect of oxy-fuel combustion on the formation of N_2O has not yet been an object of many studies. It can be assumed that the lack of molecular nitrogen in the combustion atmosphere would lead to a depression of reaction (3.31) compared to air-combustion. Since the other main routes of N_2O formation (Equations (3.29) and (3.30)) contain NO as a reagent, the yields of N_2O would depend on the impact of oxy-fuel atmosphere on the formation of NO. Kosowska-Golachowska et al. [121] studied the combustion of various biomass fuels and bituminous coal under oxy-fuel conditions in a bench-scale CFB and observed a decrease in the formation of N_2O for all fuels in the oxy-fuel combustion compared to the air-combustion. They examined the impact of the composition of the fluidization gas on the formation of N_2O and observed that with each increase in the concentration of O_2 in fluidization gas in the range from 21 to 40 % vol., the concentration of N_2O decreased slightly. De las Obras-Loscertales et al. [45] studied the formation of NO and N_2O in the oxy-fuel combustion of anthracite, bituminous coal, and lignite in a laboratory-scale BFB and examined the impacts of fluidized bed temperature and also of the concentration of O_2 in the fluidization gas. They observed that the formation of N_2O was significantly depressed with each increase in fluidized bed temperature in the range from 820 to 960 °C for all fuels, but did not observe any effect of the concentration of O_2 in the fluidization gas on the yields of N_2O.

3.5.1 NO_X reducing measures

Generally, a reduction of oxygen availability for the oxidation of both char and volatile nitrogen in the fluidized bed altogether with low bed temperature seems to be the right approach to achieve a lower NO_X formation from oxy-fuel combustion in a BFB. However, the possibilities of decreasing the temperature and the oxygen excess are limited with respect to the formation of other gaseous pollutants than NO_X. Incomplete carbon combustion accompanied by an increase in CO and TOC formation begins to be significant at low excess

of oxygen or at fluidized bed temperatures below 800 °C. Furthermore, in situ desulfurization in the BFB with added limestone reaches its maximum efficiency at approx. 880 °C and becomes ineffective at lower temperatures in the oxy-fuel combustion [122]. To operate the BFB at low oxygen excess and simultaneously prevent intensive CO formation, the oxidizer can be separated into two or even more streams. The first stream is mixed with the FGR and introduced into the BFB as the primary gas. The second stream (and possibly the consequent streams) is introduced into the freeboard section above the fluidized bed. In the primary combustion zone, there are fuel-rich conditions (stoichiometric or even sub-stoichiometric oxygen/fuel ratio) that cause a smaller conversion of the NO_X precursor to NO_X and favor the formation of N_2. Furthermore, already formed NO can be further reduced through a) reburning reactions (described in Section 3.2.3) with released fuel-N (mainly HCN and NH_3), or b) through reactions with carbon compounds that were not yet completely oxidized, or c) on the surface of the char through catalytic reactions [123, 124]. The gaseous products of incomplete combustion, CO and TOC (that are inevitably formed under such conditions), are subsequently oxidized in the freeboard section, where the secondary oxidizer is introduced. The efficiency of NO_X reduction through staged injection of oxygen is significantly dependent on residence time in the primary zone with reduction conditions [124, 125]. The optimum residence time in the reduction zone may vary according to the fuel structure. For a brown coal, it is about 1.5 s [125]. If the residence time in the reduction zone is too short, NO can be further formed in a significant amount in the secondary oxidation zone [124].

In the case of pulverized coal or natural gas combustion, staged fuel feeding or FGR can be an alternative NO_X measure to staged injection of oxidizer. Staged fuel feeding operates on a similar principle of NO_X reduction as staged injection of the oxidizer, reduction of already formed NO in a zone with sub-stoichiometric conditions. In this case, the combustion chamber is separated into three subsequent zones placed downstream the flue gas: a) primary zone with over-stoichiometric conditions terminated by the secondary fuel inlets (burners), b) NO reburning zone bounded by the secondary burners upstream and by the inlets of the secondary oxidizer downstream, and c) burnout zone downstream the secondary oxidizer

inlets with over-stoichiometric conditions [125]. However, staged fuel feeding cannot be applied in the case of oxy-fuel combustion in the BFB with the fuel of particle size typically used in BFBs. The fuel would fall back to the bed immediately, and the sub-stoichiometric reduction zone would not be created. Theoretically, an alternative fuel (natural gas, oil, or pulverized solid fuel) can be used in the secondary zone to reduce NO. Nevertheless, utilization of these more expensive fuels (or fuel preparation methods) in BFBs decreases one of the main advantages of this type of combustors, which is the ability to monocombust lower quality fuels.

Another measure used in conventional combustion systems to reduce NO_X is the FGR, which contributes to the NO_X reduction in two ways. Firstly, it reduces the temperature of the flame, causing a lower NO formation, and secondly, it recycles the already formed NO_X which can be reduced through the reburning mechanism under fuel-rich conditions [126]. However, in the case of oxy-fuel combustion in a BFB, the FGR must perform the necessary functions for stable combustion (described in Section 2.1.1). Its contribution to the NO_X reduction is appreciated, however, it cannot be further optimized by changing the FGR parameters.

3.5.2 Modeling of NO_X formation under oxy-fuel conditions

Modeling of NO_X chemistry in a combustion process has been of scientific interest for almost as long as it has been studied. Many authors published models that employed various numerical approaches and different mechanisms of chemical kinetics. Glarborg et al. [139] published a comprehensive state of the art on NO_X formation and destruction in combustion based on the work reported over the last four decades. The NO_X modeling in oxy-fuel combustion process has been also a subject of a few studies, but none of these are focused on combustion in a BFB or on combustion at conditions similar to those usually reached in BFBs. A review of these studies is given in Table 3.1. Within most of them, combustion of natural gas or pulverized coal at temperatures in a range from 1 000 to 1 500 °C was modeled. Sometimes even at elevated pressures. Only Krzywański et al. [128] modeled

Table 3.1: Review of published numerical studies on the formation of NO_X in oxy-fuel combustion.

Author, year, reference	Scope of the study	Model type	Kinetic mechanism	Facility
Hashemi et al. (2011) [127]	NO_X formation in oxy-fuel combustion of coal in an entrained flow reactor (EFR)	chemical kinetics in an EFR	Hashemi et al. (2011) [127]	EFR
Krzywański et al. 2011, [128]	CO_2, CO, SO_2, NO_X and O_2 emissions from the combustion of solid fuels in a circulating fluidized bed boiler	Peters's model of CFB hydrodynamics	Krzywański et al. (2010) [129], Krzywański et al. (2011) [128]	CFB
Schluckner et al. 2020, [130]	(1) predict the flame shape and temperature, (2) calculate the OH and CH emissions driving the NO_X formation, (3) fast and accurately predict the NO_X emissions during oxy-fuel combustion and during the presence of low nitrogen amounts in the oxidizer	CFD	(Skeletal25) Peeters 1995 [131]	natural gas jet burner
Schluckner et al. 2020, [132]	Numerical and experimental comparison of NO_X formation in two different natural gas jet burners	CFD	(Skeletal25) Peeters 1995 [131]	natural gas jet burner
Yadav and Mondal 2020, [133]	NO_X formation in oxy-coal swirl burner	CFD	Yadav and Mondal (2020) [133]	swirl burner
Liang et al. 2021, [134]	NO formation from homogeneous and heterogeneous reactions in oxy-ful combustion of coal at elevated pressures	chemical kinetics in a PFR	Aho et al. (1995) [135], Mendiara and Glarborg (2009) [136], GRI-mech 3.0 [137], Hashemi et al. (2011) [127]	pressurized flow reactor
Rahman et al. 2021, [138]	NO_X formation in jet stirred reactor (JSR) under oxy-fuel conditions with elevated pressure	chemical kinetics in a JSR	Glarborg et al. (2018) [139]	JSR
Rahman et al. 2022, [140]	NH_3 oxidation and NO formation in a plug flow reactor (PFR) under oxy-fuel conditions with elevated pressure	chemical kinetics in a PFR	Glarborg et al. (2018) [139]	PFR

Table 3.2: Review of published kinetic mechanisms of nitrogen chemistry in a combustion process.

Mechanism, reference	Year	Reactions	Species	Note
Miller and Bowman, [106]	1989	234	53	general combustion process
Aho et al., [135]	1995	339	55	pulverized coal combustion
GRI-Mech 2.11, [141]	1997	277	49	natural gas combustion and reburning
GRI-Mech 3.0, [137]	1999	325	53	natural gas combustion and reburning
Mendiara and Glarborg, [136]	2009	757	95	NH_3 chemistry in oxy-fuel combustion of CH_4
Krzywański et al., [129]	2010	34	23	oxy-fuel combustion of solid fuels in a CFB
Krzywański et al., [128]	2011	43	24	oxy-fuel combustion of solid fuels in a CFB
Hashemi et al., [127]	2011	768	107	oxy-fuel combustion of pulverized coal
Glarborg et al., [139]	2018	1395	151	general combustion process

oxy-fuel combustion of coal in a circulating fluidized bed, however, with a small set of chemical reactions. The residence times of fuel particles in an oxidation zone are significantly different in CFBs compared to those in BFBs. Therefore, the results of this study are hardly comparable with the results reached in BFBs. Based on the review, it can be concluded that numerical studies of the formation of nitrogen oxides in BFBs are missing in the current state of the art.

The conversion of nitrogen through homogeneous reactions can be modeled using a number of detailed kinetic mechanisms consisting of hundreds of elementary reactions. A review of published mechanisms is given in Table 3.2. Usually, these mechanisms are based on kinetic parameters experimentally determined at particular conditions, and hence they should be used for modeling of process at similar conditions. However, modeling of heterogeneous reactions brings significant uncertainties in the size of the available reaction surface and its activity. Therefore, published numerical studies of solid fuel combustion are simplified and often rely on the chemistry of homogeneous reactions. Within the numerical studies of oxy-fuel combustion of solid fuels published by Hashemi et al. [127], Yadav and Mondal [133] or Liang et al. [134], it was considered that char-N converts to NO fully or at a rate proportional to the conversion of char-C to CO with the rest released as N_2. Krzywański et al. [128] considered that char-N reacts only with NO forming N_2O. No other heterogeneous reactions were involved in these studies.

Chapter 4

Goals and novelty of the thesis

This thesis is focused on the formation of nitrogen oxides in oxy-fuel combustion in a BFB. A review of the current state of the art revealed that there is a lack of both numerical and experimental studies that would comprehensively cover this topic. Within the published numerical studies, no special interest has been given to the environment of BFBs or at least to conditions that would be similar to those of atmospheric oxy-fuel BFBs. Within the published experimental studies, almost all works were performed with simulated FGR consisting of an artificial mixture of pure gases and not with real wet FGR. This thesis contributes to the state-of-the-art and brings the missing information. Goals of this thesis are: development of a numerical model, simulation of the formation of nitrogen oxides in the oxy-fuel combustion, design and construction of the experimental facility, and the experimental verification of the numerical results. Particularly, they can be described by the following points:

1. design of a numerical model of the formation of nitrogen oxides in a BFB combustor operating under oxy-fuel conditions using chemical kinetics,

2. numerical simulation of the formation of nitrogen oxides in a BFB combustor operating under oxy-fuel conditions,

3. design and construction of an experimental 30 kW_{th} laboratory-scale BFB combustor, which could be operated under full oxy-fuel conditions with real wet FGR and with various fuels,

4. experimental verification of the nitrogen oxides formation in the 30 kW_{th} BFB facility operating under full oxy-fuel conditions with real flue gas recirculation, and experimental validation of the numerical model.

The purpose of the numerical model is to clarify the effects of the operational parameters of the combustion process and their importance in the formation of nitrogen oxides (rather than to precisely predict their concentrations in the flue gas from different types of combustors). In addition, the model can be used to explain the observed experimental results in detail. Therefore, a one-dimensional plug flow reactor (PFR) model is proposed. The PFR is a model concept that is used to describe a chemical or physical process with a large number of subsequent steps. It cannot include the hydrodynamics of the fluidized bed, but when proper boundary conditions are established, it can give valuable and plausible results without enormous computational demands. The core of the model is based on a mechanism of reaction kinetics, which includes definitions of chemical compounds, chemical reactions, kinetic data of these reactions, and thermal and transport properties. The goal of the numerical work is not to create such a mechanism, but to employ an existing one and apply it in a model under the specific conditions of oxy-fuel combustion in a BFB. Four different mechanisms of reaction kinetics are applied within the model. These mechanisms were particularly assembled to study nitrogen chemistry during combustion processes under various conditions using different fuels. The PFR model is based on physical parameters of the 30 kW_{th} laboratory-scale BFB combustor to ensure the highest possible comparability of obtained results.

Both the numerical and experimental studies presented in this thesis are performed for two different types of fuel, Czech lignite and wooden biomass. These types of fuel are typical for their application in BFBs and differ significantly in their nitrogen content, share of volatiles, and structure of nitrogen compounds. The fact that the full oxy-fuel combustion

process is realized in a facility equipped with a real FGR makes the experimental results of great importance. It also verifies the limits of the attainable operating parameters and shows the possible drawbacks of the technology.

Chapter 5

Material and methods

5.1 Numerical modeling

5.1.1 Model description

An one-dimensional mathematical model of the BFB combustor was proposed using a plug flow reactor (PFR) concept to gain a deeper understanding of the formation of nitrogen oxides in the oxy-fuel combustion in the BFB. The model was assembled using the Cantera [142] toolkit to calculate chemical kinetics, thermodynamics, and transport processes in Python code.

The PFR model is a common model that is used to describe chemical mechanisms based on reaction kinetics in continuous-flow systems. The composition of the mixture studied using the PFR is calculated in a large number of small time steps, where the volume of each time step represents a single batch reactor. The resulting composition of the mixture in one step is used as the initial composition in the subsequent step. Only forward flow is considered within the reactor, there is no backflow or mixing. In each step (plug), ideal mixing and uniform conditions are considered. However, external parameters, such as temperature, pressure, or velocity, can change along the flow.

In a BFB, the solids circulate, move dynamically along the bed, spout, and then fall back. Such phenomena cannot be described using 1-D PFR at all. Within the proposed model, the hydrodynamics of the fluidized bed was omitted as well as heterogeneous reactions, which were replaced with homogeneous reactions of typical char-reaction products. This simplification could without question affect the numerical results and make them less accurate. However, several assumptions were made that can justify such an approach:

- The solid fuel was substituted with volatiles and gaseous products of char combustion.
- Fuels with high volatile content were applied in the study, which makes the char combustion of less importance.
- The gas residence time inside the bed was very small because of the small free cross section and high velocity inside the bed, which made the catalytic effect of the surface of the solid particles less important.

To provide model outputs comparable with experimental results, the physical and operating parameters of the PFR were set according to the corresponding parameters of the facility used in the experimental part of this thesis. The PFR scheme is given in Figure 5.1. The superficial gas velocity, the fuel load, and the temperature profile along the height of the combustor were set as the source terms according to the measured data. The experiments, which had been carried out before the model was created, had shown that the temperature in the dense bed section of the fluidized bed does not change much with height (up to 10 °C), so the temperature in the bed in the model was also considered independent of height. Above the bed, the temperature decreased because the heat loss to the reactor walls was greater than the heat released from the oxidation of the remaining combustibles. The absolute value of the decrease in temperature between the fluidized bed and the outlet of the combustor varied in operating time (from 250 to 320 °C) and depended mostly on the operating time of the facility and the volatile content of the fuel. In particular, the temperature difference was larger after the combustion process was started and decreased with the operating time due to the accumulation abilities of the insulation and of the stainless steel construction.

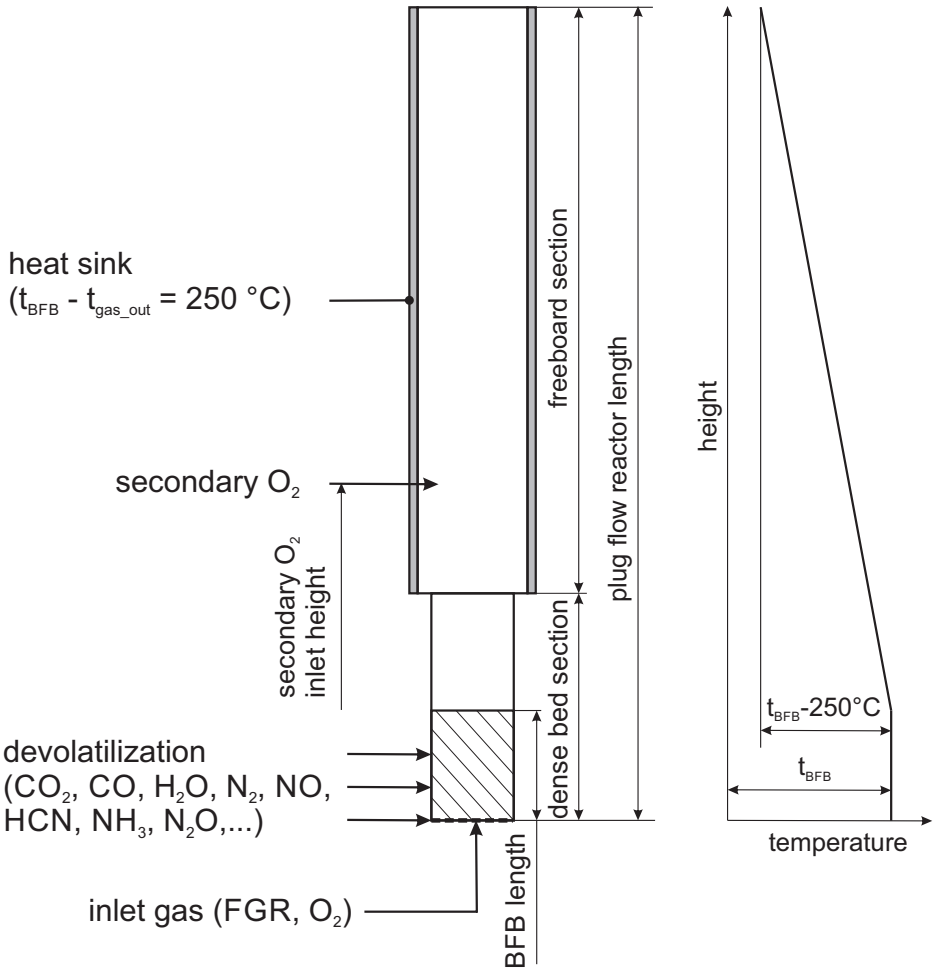

Figure 5.1: Scheme of the plug flow reactor model with an indicated temperature height profile.

The value of 250 °C was used in the model as the typical temperature drop between the bed and the combustor outlet. The temperature decreases linearly within the model between the top of the dense bed and the reactor outlet. The considered temperature profile is given in Figure 5.1. The dimensions and other physical parameters of the PFR model are given in Table 5.1. The grid of the numerical PFR reactor model was based on time steps. The duration of each time step was chosen according to the residence time of the gas - differently in the fluidized bed zone (0.000 4 s) and in the freeboard zone (0.004 73 s) providing 400 steps in the fluidized bed and 600 steps in the freeboard section. The devolatilization occurred at each step of the BFB zone in an amount equivalent to the fuel load at the time step. The

Table 5.1: Physical properties of the PFR model.

Parameter	Unit	Value
Dense bed cross-section	m^2	0.03375
Freeboard cross-section	m^2	0.06
BFB length	m	0.3
Dense bed section length	m	0.62
PFR length	m	2.2
Secondary oxygen inlet height	m	0.74
Superficial gas velocity at the inlet (u_0)	$m_N \cdot s^{-1}$	0.412
Voidage in the fluidized bed (ε_m)	-	0.6

total calculation time was set to the value of 3 s. The gas reached the outlet of the facility in this time under all modeled conditions. If the gas reached the top of the PFR sooner than in 3 s, its temperature was set to 200 °C, which corresponds to the FGR temperature after some time. No change in the gas composition was observed in the results at this additional time. The reason why this approach was chosen is that it would be difficult to terminate the calculation process exactly at the time when the gas reached the outlet. At different modeled conditions, the gas reached the outlet of the PFR at various times as a result of a variable gas density dependent on the gas composition and temperature.

The numerical model was based on the calculation of homogeneous combustion reaction kinetics. First, the GRI-mech 3.0 mechanism [137] had been used within the proposed model. The results achieved were published in a peer-reviewed journal [158] and in a conference proceedings [159]. This mechanism was originally designed to model natural gas combustion, including NO formation and reburning, and contains 325 reactions and 53 species. However, the model predicted unrealistically high concentrations of NO_2 in the flue gas using the GRI-mech 3.0 mechanism. Discrepancies in NO/NO_2 shares were observed also by Rahman et al. [138, 140] and Mulvihill et al. [143]. Therefore, a comparison of the performance of the model with the four most cited mechanisms of nitrogen chemistry in combustion process was realized. The results are given in Appendix A. The mechanisms published by Glarborg et al. [139], Hashemi et al. [127], and Miller and Bowman [106] were compared with the GRI-mech 3.0 mechanism. The kinetic parameters of the reactions, which are most important for

Table 5.2: Kinetic parameters of the most important reactions for the formation of nitrogen oxides within the applied mechanisms.

	Glarborg et al., [139]			GRI-Mech 3.0, [137]		
Reaction	A	b	E_a	A	b	E_a
$NO + HO_2 \leftrightarrow NO_2 + OH$	$2.1 \cdot 10^{12}$	0	−497	$2.11 \cdot 10^{12}$	0	−480
$N + O_2 \leftrightarrow NO + O$	$5.9 \cdot 10^{09}$	1	6280	$9.00 \cdot 10^{09}$	1	6500
$N + OH \leftrightarrow NO + H$	$3.8 \cdot 10^{13}$	0	0	$3.36 \cdot 10^{13}$	0	385
$NO_2 + H \leftrightarrow NO + OH$	$1.3 \cdot 10^{14}$	0	362	$1.32 \cdot 10^{14}$	0	360
$NO_2 + O \leftrightarrow NO + O_2$	$1.1 \cdot 10^{14}$	−0.52	0	$3.90 \cdot 10^{12}$	0	−240
$HONO + OH \leftrightarrow H_2O + NO_2$	$1.7 \cdot 10^{12}$	0	−520	NI*	NI*	NI*
$HNO_2 + OH \leftrightarrow H_2O + NO_2$	$4.0 \cdot 10^{13}$	0	0	NI*	NI*	NI*
$H + N_2O \leftrightarrow N_2 + OH$	$6.4 \cdot 10^{07}$	1.835	13 492	$3.84 \cdot 10^{14}$	0	18 880
$NO + O + M \leftrightarrow NO_2 + M$	$4.72 \cdot 10^{24}$	−2.87	1550	$1.06 \cdot 10^{20}$	−1.41	0
$N_2O + M \leftrightarrow N_2 + O + M$	$6.0 \cdot 10^{14}$	0	57 444	$6.37 \cdot 10^{14}$	0	56 640
$H + O_2 + M \leftrightarrow HO_2 + M$	$6.37 \cdot 10^{20}$	−1.72	524.8	$2.8 \cdot 10^{18}$	−0.86	0
$H + O_2 + N_2 \leftrightarrow HO_2 + N_2$	NI*	NI*	NI*	$2.6 \cdot 10^{19}$	−1.24	0
	Hashemi et al., [127]			Miller and Bowman, [106]		
Reaction	A	b	E_a	A	b	E_a
$NO + HO_2 \leftrightarrow NO_2 + OH$	$2.1 \cdot 10^{12}$	0	−497	$2.1 \cdot 10^{12}$	0	−479
$N + O_2 \leftrightarrow NO + O$	$6.4 \cdot 10^{09}$	1	6280	$6.4 \cdot 10^{09}$	1	6280
$N + OH \leftrightarrow NO + H$	$3.8 \cdot 10^{13}$	0	0	$3.8 \cdot 10^{13}$	0	0
$NO_2 + H \leftrightarrow NO + OH$	$1.3 \cdot 10^{14}$	0	362	$3.5 \cdot 10^{14}$	0	1500
$NO_2 + O \leftrightarrow NO + O_2$	$1.1 \cdot 10^{14}$	−0.52	0	$1.0 \cdot 10^{13}$	0	600
$HONO + OH \leftrightarrow H_2O + NO_2$	$1.7 \cdot 10^{12}$	0	−520	NI*	NI*	NI*
$HNO_2 + OH \leftrightarrow H_2O + NO_2$	$4.0 \cdot 10^{13}$	0	0	NI*	NI*	NI*
$H + N_2O \leftrightarrow N_2 + OH$	$3.3 \cdot 10^{10}$	0	4729	$7.6 \cdot 10^{13}$	0	15 200
$NO + O + M \leftrightarrow NO_2 + M$	$4.72 \cdot 10^{24}$	−2.87	1550	$1.1 \cdot 10^{16}$	0	66 000
$N_2O + M \leftrightarrow N_2 + O + M$	$4.0 \cdot 10^{14}$	0	56 600	$1.6 \cdot 10^{14}$	0	51 600
$H + O_2 + M \leftrightarrow HO_2 + M$	$3.5 \cdot 10^{16}$	−0.41	−1116	$3.61 \cdot 10^{17}$	−0.72	0
$H + O_2 + N_2 \leftrightarrow HO_2 + N_2$	$6.37 \cdot 10^{20}$	−1.72	520	NI*	NI*	NI*

* The reaction is not included in the mechanism.

the formation of nitrogen oxides, included in these mechanisms are given in Table 5.2. There, A, b, and E_a are the parameters of the Arrhenius function (Equation (5.1)), particularly A is the preexponential factor, b is the temperature exponent, and E_a is the activation energy [144].

$$k_f = A \cdot T^b \cdot e^{-\frac{E_a}{R \cdot T}} \tag{5.1}$$

Using the Arrhenius function, a dependence of a forward rate constant k_f of an elementary reaction on the thermodynamic temperature T can be described. The unit of order constant depends on the rate of the reaction. For reactions of second order, the unit is $cm^3 \cdot mol^{-1} \cdot s^{-1}$, while for reactions of third order, it is $cm^6 \cdot mol^{-2} \cdot s^{-1}$. The unit of the preexponential factor A is the same as that of the rate constant. R in Equation (5.1) is the universal gas constant.

The impacts of the O_2 concentration in the flue gas, the fluidized bed temperature, and the oxygen staging on the formation of NO, NO_2, and N_2O in the case of lignite and wood combustion obtained using these mechanisms are given in Figures 6.1 - 6.4 and A.1 - A.8. On the basis of these results, the mechanism presented by Hashemi et al. was found to be the most suitable for the application on oxy-fuel combustion in a BFB and was further used within the model.

As mentioned above, the simplification introduced by neglecting the heterogeneous char reactions was compensated by including typical products of char combustion in the volatiles. The composition of volatiles after devolatilization and char combustion was determined using data published by Winter et al. [145] and Konttinen et al. [146] (for combustion of lignite), by Konttinen et al., Anca-Couce et al. [147], and Brunner et al. [148] (for combustion of wooden biomass), based on fuel properties and the stoichiometry of the oxy-fuel combustion. The corresponding shares of volatile components and char combustion products used in the numerical simulations were calculated based on the devolatilization ratios of H, N, and O (given in Table 5.3) and the conversion ratios of fuel bound nitrogen and carbon (given in Table 5.4). These shares are given in Table 5.5. The shares of N_2, H_2, and O_2 are the results of the balance of N, H, and O in the volatiles and char combustion products. The negative value of O_2 indicates that oxygen bound in the fuel structure (char or volatile) is not sufficient for the formation of other components and therefore it must be supplied as an oxidizer. Neither of the studied kinetic mechanisms includes sulfur and its reactions, therefore it was not included in the calculated gas composition. However, this disadvantage can be accepted, as the sulfur does not affect the nitrogen chemistry significantly.

Table 5.3: Devolatilization ratios of H, O, and N bound in the fuel [146].

Devolatilization ratios	Lignite [%]	Wooden biomass [%]
H	0.94	0.977
N	0.4	0.561
O	0.85	0.987

Table 5.4: Conversion ratios of nitrogen and carbon bound in the fuel [145, 147, 148].

Conversion ratios	Lignite		Wooden biomass	
	Volatiles [%]	Char [%]	Volatiles [%]	Char [%]
N−NH_3	0.3	0.03	0.3	0.3
N−HCN	0.1	0.035	0.5	0.5
N−NO	0.4	0.18	0.15	0.15
N−N_2O	0.03	0.005	0.005	0.005
C−CH_4	0.35	0	0.35	0
C−C_2H_6	0.25	0	0.1	0
C−CO	0.35	0.1	0.5	0.1

Table 5.5: Shares of volatile components and gaseous products of char combustion used within the numerical model.

Component	Lignite		Wooden biomass	
	Volatiles [g/kg_{fuel}]	Char [g/kg_{fuel}]	Volatiles [g/kg_{fuel}]	Char [g/kg_{fuel}]
NH_3	1.137	0.171	0.557	0.436
HCN	0.601	0.316	1.473	1.152
NO	2.671	1.803	0.491	0.384
N_2O	0.147	0.037	0.012	0.009
N_2	0.530	3.506	0.069	0.054
CH_4	91.839	0	171.455	0
C_2H_6	61.478	0	45.909	0
CO	160.350	70.388	427.655	22.343
CO_2	35.992	995.343	67.193	315.949
H_2	5.426	2.581	8.667	1.319
O_2	−8.224	−745.287	80.775	−237.763
H_2O	211.2		78	

Algorithm 1 Numerical PFR model of oxy-fuel combustion in a BFB.

Set physical properties: h_{total}, h_{BFB}, h_{freeb}, $h_{O_2,sec}$, A_{bed}, A_{freeb}
Set operational parameters: u_0, t_0, n_{steps}, dt, dt_{bed}, m_{fuel}, ϕ_{O_2}, ψ
Define the fuel devolatilization function: ω $(f(m_{fuel}, V_i))$
for j $\in \langle 1, 10 \rangle$ **do**
    Calculate primary gas composition $(f(\phi_{O_2}, \phi_{n,FGR}))$
    Calculate volume of FGR $(f(\phi_{O_2}))$
    procedure PERFORM TIME INTEGRATION(dt, dt_{bed})
        Calculate: gas composition, ρ_i, t_i, m_i, $\sum m$, u_i, h_i
        if $h_i < h_{BFB}$ **then**
            Use: dt_{bed}, A_{bed}; Import ω $(f(m_{fuel}, V_i))$
        else if $h_{BFB} < h_i < h_{freeb}$ **then**
            Use: dt, A_{bed}
        else if $h_i > h_{freeb}$ **then**
            Use: dt, A_{freeb}
        else if $h_i = h_{O_2,sec}$ **then**
            Introduce: $V_{O_2,sec}$
        end if
    end procedure
    Calculate FGR composition $(f(\text{gas composition}, t_{FGR}))$
end for

In each step of the PFR, the numerical model calculated the gas composition, flow rate, and velocity. Initially, the gas consisted of a mixture of O_2, CO_2, and H_2O. In the steps in the BFB section, the mixture of volatiles and char combustion products according to Table 5.5 was introduced proportionally to the fuel load and the time duration of each step. The gas velocity in the PFR reflected the voidage in the fluidized bed and the gas density. In the case of combustion modeling with staged injection of O_2, only part of the total amount of the introduced O_2 was included in the primary stream. The remaining part was added when the calculation reached the height of the secondary O_2 injection port. The FGR was respected in the calculation through 10 iterations of the whole computation loop, where the output composition of the flue gas was used as the source term for the calculation of the FGR composition. The content of water vapor in the FGR depended on the FGR temperature measured within the experiments. A simplified algorithm of the numerical PFR model is given in Algorithm 1. A calculation performed within each step of the PFR inside the dense bed is illustrated in Figure 5.2.

$i+1$

i :

load mass fractions w_n^{i-1} from Cantera,

$$w_n^i = \frac{w_n^{i-1} \cdot \sum m^{i-1} + w_n^0 \cdot A_{bed} \cdot \varepsilon_{mf} \cdot \rho^{i-1} \cdot dt_{bed} \cdot u^{i-1} + \omega_n}{\sum m^{i-1} + A_{bed} \cdot \varepsilon_{mf} \cdot \rho^{i-1} \cdot dt_{bed} \cdot u^{i-1} + \sum \omega},$$

store mass fractions w_n^i to Cantera,

load gas density ρ^i from Cantera,

$$m^i = A_{bed} \cdot \varepsilon_{mf} \cdot \rho^{i-1} \cdot dt_{bed} \cdot u^{i-1},$$

$$u^i = \frac{m^i}{A_{bed} \cdot \varepsilon_{mf} \cdot \rho^i \cdot dt_{bed}},$$

$$h^i = h^{i-1} + u^i \cdot dt_{bed}.$$

$i-1$

Figure 5.2: Calculation performed in each step of the PFR within the dense bed section.

5.1.2 Numerical tests

The impacts of O_2 concentration in dry flue gas (representing the impact of oxygen stoichiometry), fluidized bed temperature, and staged supply of oxygen on the formation of nitrogen oxides were studied similarly to within experimental tests. In the cases of tests with variable O_2 concentration in flue gas and variable fluidized bed temperature, only primary oxygen was introduced to the PFR. In the case of staged oxygen supply, the ratio of secondary to primary oxygen ψ was variable. Other parameters were always kept constant. The fuel load and gas velocity were set according to the average experimental values achieved for both fuels. The matrix of parameters used within the model is given in Table 5.6.

Table 5.6: Matrix of parameters used within the numerical model.

Parameter	Unit	Impact of:		
		Oxygen stoichiometry	BFB temperature	Oxygen staging
$\phi_{O_2}^{DFG}$	[% vol.]	3, 6, 9	6	6
t_{BFB}	[°C]	880	840, 880, 920, 960	880
ψ	[−]	0	0	0, 0.5, 1, 1.25, 1.5
m_{fuel} lignite	[kg·h^{-1}]		3.8	
m_{fuel} wood	[kg·h^{-1}]		10.8	

5.2 Experimental set-up

5.2.1 Experimental equipment

30 kW$_{th}$ BFB facility

The main experimental part of this thesis was carried out using a 30 kW$_{th}$ BFB combustor, located in the laboratory of the Department of Energy Engineering of the Faculty of Mechanical Engineering of the Czech Technical University in Prague. This facility was built in 2013/2014 and has since been used for a number of studies on air- and oxy-fuel combustion, for example [160, 161, 162, 163, 164, 165]. The author of this thesis contributed to the original design and construction of this facility. To meet the objectives of this thesis, the facility was also improved by several modifications. Its overall scheme is given in Figure 5.3. The reactor itself has a modular construction made of stainless steel. Its walls are insulated from the outside using Fiberfrax® Duraboard®. The height of the combustor is 2.7 m (2.05 m from the fluidizing gas distributor (1) to the top of the reactor). Its cross section is 0.15 × 0.225 m in the dense bed section (2) and 0.2 × 0.3 m in the freeboard section (3) to slow down the flue gas and increase its residence time. Fuel is supplied by a screw conveyor (4), the height of the fluidized bed is limited by the spillway (5) mounted in the wall (265 mm above the distributor of the fluidizing gas). Fly ash is separated from the flue gas stream by the cyclone particle separator (6). In the oxy-fuel combustion regime, oxygen of 99.5% purity from pressurized or cryogenic vessels is used as an oxidizer. The bed material

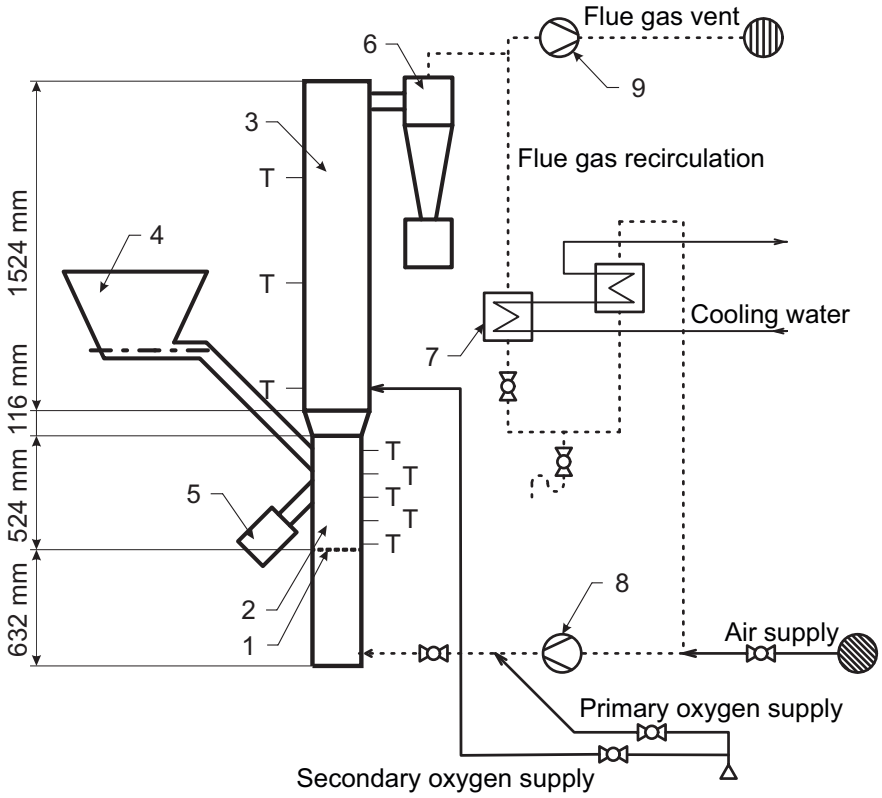

Figure 5.3: Scheme of the 30 kW_{th} experimental BFB facility. 1) distributor of the fluidizing gas, 2) dense bed section, 3) freeboard section, 4) screw conveyor, 5) fluidized bed spillway, 6) cyclone particle separator, 7) FGR coolers, 8) primary fan, 9) flue gas fan. The 'T' signs indicate temperature measurement points.

is fluidized by a mixture of recirculated flue gas and oxygen. The FGR is taken downstream of the cyclone particle separator, through two water coolers (7) to the suction pipe of the primary fan (8). At the pressure pipe of the primary fan, the primary oxygen is mixed with the recirculated flue gas. To protect the primary fan from high temperatures and from the risks that could be caused by the condensation of water vapor simultaneously, the FGR is cooled to approximately 150 °C in the water coolers. This temperature is higher than the dew point of the flue gas, therefore, the FGR is wet and the water vapor does not condense before the primary fan. The facility is also equipped with a secondary supply of oxygen to study the impact of staged combustion on the formation of gaseous pollutants. Secondary oxygen is supplied through two inlets into the freeboard section. Their cross section is designed to provide sufficient outflow velocity (more than 3 $m \cdot s^{-1}$ at minimal volumetric flow,

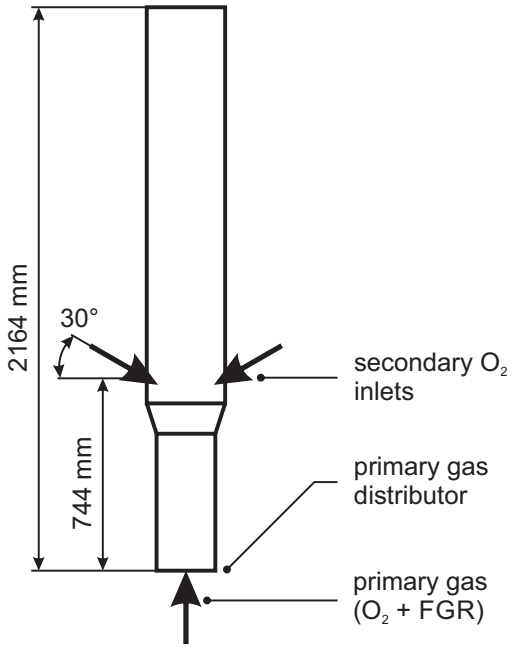

Figure 5.4: Scheme of the experimental facility axial cross-section with the position of the secondary oxygen inlets.

referenced to normal conditions). The inlets are oriented tangentially to the flue gas stream in the radial cross-section, each from the opposite wall of the combustor. Their location and orientation in the axial cross section are shown in Figure 5.4. Pure oxygen (also of 99.5% purity) was used as the secondary oxidizer. The facility was operated at over pressure conditions with the flue gas fan (9) turned off in the case of the oxy-fuel combustion to prevent an air ingress and flue gas dilution. The start-up of the facility was always realized in the air-combustion regime, when the primary air was heated by an electric heater. During the switch from air-combustion to oxy-combustion, the air intake pipe was closed by a valve.

The vertical profile of the temperature along the combustor is measured using five thermocouples in the dense bed section and three thermocouples in the freeboard section indicated in Figure 5.3 by the 'T' signs. The lowest thermocouple is placed very close to the distributor of the fluidization gas, so the temperature that it measures can be affected by the streams of the still cool fluidization gas. The only thermocouples completely immersed in the bed are the two lowest. The third lowest is placed on the surface of the bed (when the bed does not fluidize). The temperature referred to in this thesis as the bubbling fluidized

bed temperature t_{BFB} represents the value measured by the second lowest thermocouple. Volumetric flows of air and FGR were calculated from pressured drops of orifices placed in the air and FGR ducts. Pressure drops were measured with Omega PX277 differential pressure transducers. The regulation of these flows was carried out through the frequency of the primary fan electric motor and by the settings of the valves in the air and FGR ducts. The volumetric flows of primary and secondary oxygen were measured and regulated by Bürkert MFC8626 mass flow controllers. Fuel mass flow was regulated by the timing and frequency change of the electric motor of the screw conveyor and was determined by calibration.

The composition of the flue gas was continuously analyzed. The volumetric fractions of CO_2, O_2, CO, SO_2, and NO_X (the sum of NO + NO_2) were measured. The flue gas was sampled downstream the cyclone separator and upstream the flue gas fan. The flue gas analysis consisted of a sampling probe with heated ceramic filter, heated sampling line, secondary sample filtration, cooling to 5 °C, pump, and a set of online gas analyzers. The volumetric fractions of CO, NO_X, and SO_2 were measured by Hartmann&Braun Uras 10E instruments, which work on the NDIR principle. The volumetric fraction of CO_2 was measured with a Fuji ZRJ instrument, which also uses the NDIR method. The volumetric fraction of O_2 was measured by a paramagnetic method, using a M&C PMA 12 instrument.

500 kW_{th} pilot-scale BFB facility

Because the 30 kW_{th} BFB facility was equipped only with an NDIR sensor measuring the sum of volumetric fractions of NO and NO_2, additional experiments were performed using a pilot-scale 500 kW_{th} BFB combustor to verify the shares of NO, NO_2, and N_2O in nitrogen oxides formed in oxy-fuel combustion in a BFB. This facility was equipped with multiple analyzers for on-line measurement of the flue gas composition: extractive UV analyzer for the measurement of NO and NO_2 concentrations, paramagnetic sensor for O_2 concentration, NDIR (nondispersive infrared) analyzers for SO_2, CO, CO_2, N_2O, and NO_X (sum of NO and NO_2 after conversion of NO_2 to NO) concentrations, flame ionization detector for the measurement of TOC (total organic carbon), and laser diode analyzer for NH_3 concentrations.

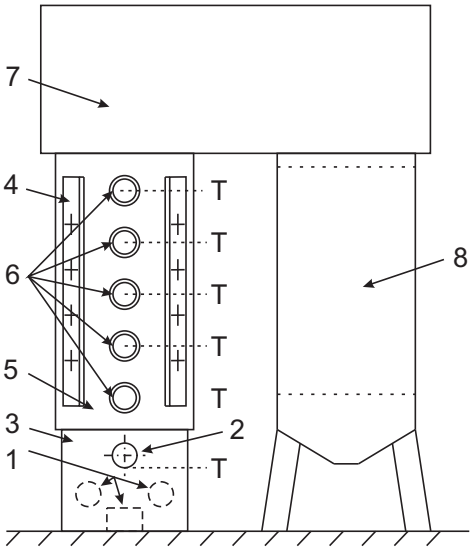

Figure 5.5: Scheme of the 500 kW_{th} pilot-scale BFB facility. 1) primary gas inlets, 2) fuel feeder, 3) fluidized bed region, 4) secondary air distributors, 5) freeboard section, 6) inspection windows, 7) crossover pass, and 8) heat exchanger. The 'T' signs indicate the temperature measurement points.

The scheme of the pilot-scale BFB combustor is given in Figure 5.5. The facility consists of three main sections: the BFB combustion chamber (dense bed and freeboard section), the crossover pass, and the heat exchanger. The fluidization gas, formed by primary air (or oxygen) and recirculated flue gas (FGR), enters the bed trough distributor consisting of 36 nozzles placed in 6 rows. The distributor was described in detail by Skopec et al. [149]. The combustion chamber has a cylindrical cross section and is insulated with a fireclay lining with a water-cooled surface. The temperature in the dense bed is measured using four thermocouples. In the freeboard section, the facility is equipped with 6 pairs of thermocouples along the height (the first thermocouple of the pair is placed near the wall, the second in the core of the freeboard section). Secondary air (or pure oxygen) is supplied to the freeboard section by 4 distributors placed evenly on the perimeter. Each distributor can provide the secondary air inlet at 4 different heights. For the experiments, secondary oxygen inlets were used at a height of 550 mm above the fluidized bed. From the freeboard section, the flue gas continues to an empty crossover pass with water-cooled surface and then enters a heat exchanger. Downstream of the heat exchanger, the fly ash is separated from the flue gas in

a cyclone particle separator and in a subsequent fabric particle filter. The cleaned flue gas is driven by a flue gas fan into a stack or is recirculated into the primary gas by a primary fan. This facility has been used for a number of studies on air-combustion, for example [166, 167, 168, 169].

5.2.2 Materials

Fuel

The experiments were carried out with two fuels, a Czech lignite Bílina HP1 135 and pellets of A1 quality from spruce wood. The proximate and ultimate analysis of these fuels is given in Table 5.7. The share of combustibles in the fuel is the balance to the proximate analysis, and the share of oxygen in the combustibles is the balance to the ultimate analysis. Lignite was sieved to extract the fraction of particles larger than 8 mm, which could get stuck in the screw conveyor and destabilize the fluidization process.

Fluidized bed materials

The lignite contains a significant content of ash, which was used as the fluidized bed material for experimental tests with this type of fuel. On the other hand, spruce wood contains only a small amount of inherent ash, which also has inconvenient fluidization properties (e.g., to fine particles and low density of particles). Therefore, a fluidized bed material of an external origin had too be used for the combustion of wooden pellets. A lightweight ceramic aggregate (LWA) (produced from a thermally expanded clay-based mineral) was selected in two particle size distributions (PSDs) for this purpose. It has a porous structure and a high content of aluminum oxide and ferric oxide (approx. 25 % and 15 %, respectively) and its advantage compared to other materials is the very low density and the bulk density (approximately $1\,000\,\mathrm{kg}\cdot\mathrm{m}^{-3}$ and $500\,\mathrm{kg}\cdot\mathrm{m}^{-3}$, respectively). A lower density of the material in the bed causes a lower pressure drop in the fluidized bed. By using a lighter material, it is possible to reduce the power load of the fluidization fan, which contributes significantly to the operating

Table 5.7: Proximate and ultimate analysis of the Czech lignite (Bílina HP1 135) and pellets from spruce wood of A1 quality used during the experiments. Standards used for the fuel analysis: LHV - ISO 1928 [150], water content - ČSN 44 1377 [151], ash content - ISO 1171 [152], ultimate analysis determined by Thermo Scientific FlashEA 112.

	as received			dry ash free				
	LHV [MJ · kg^{-1}]	water [wt. %]	ash [wt. %]	C [wt. %]	H [wt. %]	N [wt. %]	S [wt. %]	volatiles [wt. %]
lignite	17.6	21.1	9.9	72.3	6.3	1.1	1.3	47.0
wooden pellets	16.4	7.8	1.5	51.0	6.9	0.3	0.003	84.6

costs of the facility. Furthermore, LWA production is flexible to different particle sizes of the material; thus, it could be adapted to the respective fuel, which is very beneficial for biomass combustion.

The bed materials were analyzed for particle size on the basis of the mass distribution. The analysis provided a mass fraction of the particles of respective size, which was then fitted with the Rosin-Rammler-Sperling-Bennet (RRSB) distribution equation, using the least squares method. The RRSB approximation can be described with the following equation:

$$R(x) = \exp(-b \cdot x^n) \tag{5.2}$$

where $R(x)$ is the cumulative weight of particles greater than x, b is the coefficient representing the particle size range, and n is the coefficient representing the polydispersity of the studied sample [153]. The PSD curve can be obtained as the first derivative of Equation (5.2) and can serve as a mathematical tool to obtain the desired particle size characteristics. The distribution curves of the studied samples of materials are shown in Figure 5.6.

The distribution equation provides essential information to evaluate the fluidization properties. The arithmetic mean, mode, median, 1$^{\text{st}}$ decile (d_{10}), and 9$^{\text{th}}$ decile (d_{90}) particle size were evaluated. The density and bulk density were analyzed along with the particle size. Lignite ash can be classified as Geldart B particles which are well fluidizable and form vigorous bubbles. The LWA population referred to as 'P3' belongs to the D particle class in the Geldart classification, which is difficult to fluidize in deep beds, it spouts, and forms explod-

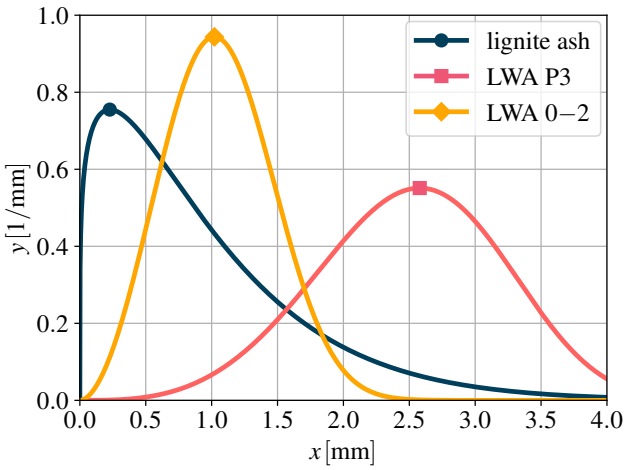

Figure 5.6: Particle size distribution curves of the fluidized bed materials.

Table 5.8: Results of the particle size distribution analysis of the fluidized bed materials.

		Liginite ash	LWA P3	LWA 0−2
ρ_s	$\mathrm{kg \cdot m^{-3}}$	2 195	815	1088
ρ_b	$\mathrm{kg \cdot m^{-3}}$	795	480	570
d_{mean}	mm	0.37	2.73	1.07
d_{mode}	mm	0.23	2.58	1.02
d_{10}	mm	0.15	1.58	0.54
d_{50}	mm	0.74	2.53	1.05
d_{90}	mm	1.77	3.41	1.59

ing bubbles or channels [154]. The LWA population referred to as '0−2' is on the boundary between B and D particle types in the Geldart classification. The physical properties of the bed materials are given in Table 5.8.

Fluidization velocity analysis

The minimum fluidization velocities, the minimum complete fluidization velocities, and the terminal velocities were calculated for three different conditions of the fluidization gas. First, the properties of the gas corresponded to air at 20 °C ($\rho_g = 1.20\,\mathrm{kg \cdot m^{-3}}$, $\eta = 1.8 \times 10^{-5}$ Pa·s), secondly to air at 850 °C ($\rho_g = 0.29\,\mathrm{kg \cdot m^{-3}}$, $\eta = 3.8 \times 10^{-5}$ Pa·s) and thirdly, they corresponded to oxy-fuel flue gas at 850 °C ($\rho_g = 0.34\,\mathrm{kg \cdot m^{-3}}$, $\eta = 4.94 \times 10^{-5}$ Pa·s). The fluidizing gas temperature of 850 °C was chosen in two cases, because when the fluidizing

Table 5.9: Minimum fluidization velocities u_{mf}, terminal velocities u_t (calculated for d_{mean}), minimum velocities of complete fluidization u_{mf-90}, and complete terminal velocities u_{t-90} (calculated for d_{90}) of the selected fluidized bed materials. The experimental values are in brackets.

Conditions			Lignite ash	LWA P3	LWA 0−2
calculation (experimental) results					
air at 20 °C	u_{mf}	$\mathrm{m \cdot s^{-1}}$	0.37 (0.42)	0.61 (0.62)	0.40 (0.38)
	u_{mf-90}	$\mathrm{m \cdot s^{-1}}$	1.72	0.76	0.65
	u_t	$\mathrm{m \cdot s^{-1}}$	2.02	4.54	3.09
	u_{t-90}	$\mathrm{m \cdot s^{-1}}$	5.47	5.31	4.06
air at 850 °C	u_{mf}	$\mathrm{m \cdot s^{-1}}$	0.21	0.65	0.27
	u_{mf-90}	$\mathrm{m \cdot s^{-1}}$	2.59	0.99	0.62
	u_t	$\mathrm{m \cdot s^{-1}}$	2.36	8.54	4.95
	u_{t-90}	$\mathrm{m \cdot s^{-1}}$	10.23	10.26	7.24
oxy-fuel at 850 °C	u_{mf}	$\mathrm{m \cdot s^{-1}}$	0.16	0.52	0.21
	u_{mf-90}	$\mathrm{m \cdot s^{-1}}$	2.21	0.82	0.50
	u_t	$\mathrm{m \cdot s^{-1}}$	1.95	7.70	4.31
	u_{t-90}	$\mathrm{m \cdot s^{-1}}$	9.20	9.31	6.45

gas passes through the bed of hot material, it is heated to the bed temperature within a few millimeters above the distributor of the fluidizing gas [155]. The properties of the oxy-fuel flue gas were included because in oxy-fuel combustion in BFB, the mixture of flue gas recirculation and pure oxygen is used as the fluidization gas. The minimum fluidization velocities of all bed materials were also experimentally verified by measuring the correlation of bed pressure drop and superficial fluidizing gas velocity u_0. This method can be found in [86]. This test was carried out using air at 20 °C as fluidization gas. The calculated minimum fluidization velocities u_{mf} (for d_{mean}), the complete fluidization velocities u_{mf-90} (for d_{90}), and the terminal velocities u_t (for d_{mean}), as well as the experimentally determined minimum fluidization velocities, are given in Table 5.9. All materials were able to form the BFB relatively well.

The terminal velocity for the mean diameter of the lignite ash is lower than its velocity of complete fluidization at 850 °C, since this material is very polydisperse and contains a significant amount of both fine and coarse particles. One of the experimental goals was to

determine the impact of the superficial gas velocity (and therefore the impact of the gas residence time) on the formation of NO_X. The levels of superficial velocity were approximately at 1, 1.5, and $2\,m \cdot s^{-1}$. Therefore, the superficial velocity could be higher than the terminal velocity for the mean diameter of the lignite ash in some experiments. These experiments had to be accompanied by the loss of fine particles, and the PSD of the lignite ash had to be shifted toward coarser particles. However, no immediate consequences were observed in the fluidization process and combustion performance. In the case of combustion of spruce wood, the finer PSD '0–2' of LWA was used for tests with a superficial velocity of 1 and $1.5\,m \cdot s^{-1}$ and coarser PSD 'P3' was used for tests with a superficial velocity of $2\,m \cdot s^{-1}$. Although all applied levels of u_0 were in the range $\langle u_{mf-90} - u_t \rangle$ for both PSDs, the oxy-fuel combustion process with LWA 'P3' used as fluidized bed material was not stable for $u_0 \leq 1.5\,m \cdot s^{-1}$ and was accompanied by loss of fluidization. However, at $u_0 \approx 2\,m \cdot s^{-1}$, this coarser material performed very well. External fluidized bed materials were selected according to our study [170], which was published in a peer-reviewed journal.

5.2.3 Experimental tests

Experimental tests performed using the 30 kW_{th} BFB facility

The main experimental part of this thesis was carried out using the $30\,kW_{th}$ BFB facility to investigate the influence of

- global oxygen stoichiometry (expressed as the volumetric fraction of O_2 in the dry flue gas),
- fluidized bed temperature, and
- staged supply of oxygen

on nitrogen oxides formation in oxy-fuel combustion in a BFB.

In the cases of tests with a variable O_2 concentration in the flue gas and a variable fluidized bed temperature, only primary oxygen was introduced into the BFB. In the case of

staged oxygen supply, the ratio of secondary to primary oxygen ψ was variable. This ratio is defined by Equation 5.3.

$$\psi = \frac{\dot{V}_{O_2,sec}}{\dot{V}_{O_2,prim}}, \tag{5.3}$$

where $\dot{V}_{O_2,prim}$ and $\dot{V}_{O_2,sec}$ are the volumetric flows of primary and secondary oxygen. Other than the variable parameters were always kept constant.

Two different approaches to the combustor settings were chosen for a staged supply of oxygen. When changing the secondary to primary oxygen volumetric flow ratio ψ from 0 to approximately 1.25,

- the fluidized bed temperature or
- the O_2 to CO_2 concentration in the primary gas ratio

was kept constant. Although it is very common to study the impact of the oxy-fuel primary gas composition on the formation of gaseous pollutants in facilities with a primary gas made of an artificial mixture of pure gases, the approach of keeping constant O_2/CO_2 volumetric ratio in the primary gas is inconvenient if it should be applied in full-scale facilities. In this case, the primary gas consists of streams of FGR and pure oxygen and has three critical functions, as described in Section 2.1.1 - to fluidize the bed, to oxidize the fuel in the primary zone of combustion, and to moderate the fluidized bed temperature. When it is desired to keep the composition of the primary gas constant while changing a different parameter, control of the combustion process lacks a degree of freedom. In the particular case of staged oxygen supply, it means that it is necessary to decrease the volumetric flow of the FGR to compensate for the decrease in the primary oxygen flow when increasing the ratio ψ at a constant fuel load. This change affects the heat balance of the fluidized bed, then. This results in a lack of possibilities on how to control the fluidized bed temperature. However, this approach was included in this thesis, as it is used in a number of studies carried out on a laboratory-scale using an atmosphere mixed from synthetic gases [50, 56, 117, 156].

Moreover, similar series of experiments were performed in the air-combustion regime to compare the differences between air- and oxy-combustion. In this case, only the impacts of

Table 5.10: Matrix of parameters of the combustion process applied in the experimental tests.

Oxy-fuel combustion					
Parameter	Unit	Impact of:			
		Oxygen stoichiometry	BFB temperature	Oxygen staging at const.	
				t_{BFB}	$(O_2/CO_2)_{prim}$
$\phi_{O_2}^{DFG}$	[% vol.]	3–9	6	6, 9	6
t_{BFB}	[°C]	880	840–960	880	variable
$(O_2/CO_2)_{prim}$	[–]	variable	variable	variable	0.4
ψ	[–]	0	0	0–1.25	

Air-combustion			
Parameter	Unit	Impact of:	
		Oxygen stoichiometry	BFB temperature
$\phi_{O_2}^{DFG}$	[% vol.]	3–9	6
t_{BFB}	[°C]	880	840–960

air stoichiometry (expressed as the volumetric fraction of O_2 in dry flue gas) and fludized bed temperature were studied. The formation of nitrogen oxides in air-combustion in a BFB is well known. Therefore, the air-combustion experiments were performed only using the 30 kW_{th} BFB facility to show the effect of different combustion atmospheres. The numerical part of this thesis is focused only on oxy-fuel combustion.

The matrix of variable parameters of the experimental tests is given in Table 5.10. Except for these main parameters, the impact of the superficial gas velocity (and so of the gas residence time) was studied. Most of the experimental series described in Table 5.10 were repeated at different superficial velocity. However, its change is not quite straightforward. The superficial gas velocity depends on the volumetric flow of the fludization gas and its temperature. Since the flow of oxygen is determined by the stoichiometric ratio to the fuel load and contributes usually to a lesser content of the primary gas, the parameter that is used to control the superficial velocity is the flow rate of the FGR. However, the FGR is also the only available measure to control the temperature of the fluidized bed, except for the

power load [171]. Therefore, the change in the flow rate of the FGR had to be accompanied by a suitable change in power load together with a change in the flow rate of oxygen, as the fluidized bed temperature and the volumetric fraction of O_2 in the dry flue gas were meant to be constant. The experiments of the oxy-fuel combustion of wooden pellets at high superficial velocities were carried out with coarser LWA P3 to prevent pneumatic transport of fluidized bed material.

The experimental results that study the impact of oxygen stoichiometry and fluidized bed temperature on NO_X formation in the oxy-fuel combustion of lignite were partially published in a peer-reviewed journal [158]. The results concerning the impact of staged supply of oxygen were published in another peer-reviewed article [172].

The experimental results of oxy-fuel and air-combustion were compared based on emission factors with a unit $[mg \cdot MJ^{-1}]$, since volumetric fractions or concentrations are misleading in the case of oxy-fuel combustion, where the total volume of formed flue gas is much smaller than in the case of air-combustion. Emission factors, calculated according to Hrdlička et al. [39], represent the amount of formed gaseous pollutant per a unit of released energy. The emssion factors are particularly useful for comparison of emissions from combustion of different fuels under various conditions. The approach of calculation of the flue gas volume and composition in oxy-fuel combustion was published in a book chapter [171]. The results of air combustion were recalculated for a reference volumetric of O_2 in dry flue gas (6 % vol. in the case of lignite, and 10 % vol. in the case of wood combustion).

Experimental tests performed using the 500 kW_{th} pilot-scale BFB facility

To verify the shares of NO, NO_2, and N_2O in the nitrogen oxides formed in the oxy-fuel combustion in a BFB, supplementary experiments were performed using the pilot-scale 500 kW_{th} BFB combustor equipped with analyzers, which can measure the concentrations of these oxides separately. The operation of the pilot-scale combustor requires at least four experienced researchers and is accompanied by significantly higher costs than the operation of the laboratory-scale combustor used for this study. Therefore, only one fuel was used to verify

Table 5.11: Matrix of parameters of the combustion process applied in the pilot-scale experimental tests.

Oxy-fuel combustion				
Parameter	Unit	Impact of:		
		Oxygen stoichiometry	BFB temperature	Oxygen staging at const. t_{BFB}
$\phi_{O_2}^{DFG}$	[% vol.]	6–12	9	8
t_{BFB}	[°C]	880	840–960	880
$(O_2/CO_2)_{prim}$	[−]	variable	variable	variable
ψ	[−]	0	0	0–1.3

the speciation of nitrogen oxides, pellets from spruce wood. These pellets were the same as those used in the experiments carried out using the 30 kW_{th} BFB facility and within the numerical model. Similarly as within the laboratory-scale experiments, the impacts of oxygen excess, fluidized bed temperature, and staged supply of oxygen on the formation of nitrogen oxides in the oxy-fuel combustion were examined. The matrix of variable parameters of the experimental tests on a pilot-scale is given in Table 5.11.

Chapter 6

Analysis of the numerical model

The results of the numerical model of the nitrogen oxides formation in oxy-fuel combustion in a BFB are presented and analyzed in this chapter. Four different kinetic mechanisms applied within the model are compared in Section 6.1. The results obtained with the mechanism selected based on the comparison are presented and discussed in Section 6.2.

6.1 Comparison of different mechanisms of reaction kinetics

The performance of the kinetic mechanisms published by Glarborg et al. [139], Hashemi et al.[127], Miller and Bowman [106], and of GRI-Mech 3.0 [137] mechanism within the proposed model was analyzed. To describe the numerically modeled formation of nitrogen oxides, their concentration profiles along the reactor height were plotted. In these plots, the vertical dashed line indicates the boundary of the dense bed and the freeboard section. The fuel compounds were introduced to the gas mixture only in the dense bed. Finite concentrations at the end of the reactor were also plotted to show effects of the studied parameters in a wider range. In these figures, the volumetric fraction of NO_X refers to the sum of the volumetric fractions of NO and NO_2 in dry flue gas.

6.1.1 Effect of oxygen stoichiometry

The results describing the impact of oxygen stoichiometry expressed using a volumetric fraction of O_2 in dry flue gas on the formation of nitrogen oxides at constant BFB temperature (880 °C) are given in Figures 6.1 and 6.2 for the oxy-fuel combustion of lignite and in Figures 6.3 and 6.4 for the oxy-fuel combustion of spruce wood. No staged supply of oxygen was considered in this case, all the supplied oxygen was introduced in the primary gas stream.

Formation of NO in lignite combustion (Figures 6.1a and 6.1b)

The relative difference in the final concentration of NO (at the outlet of the reactor, that is, at the height of 2 m) calculated using the four mechanisms is more than 200 % compared at $\phi_{O_2} = 6\,\%$ vol. The lowest volumetric fractions of NO in dry flue gas was calculated using the Miller and Bowman [106] mechanism (in the range from 150 to 200 ppmv for ϕ_{O_2} in the range from 3 to 9 % vol.) and the highest by the Hashemi et al. [127] mechanism (in the range from 450 to 550 ppmv for the same range of ϕ_{O_2}). The formation of NO calculated using the Glarborg et al. [139], the Hashemi et al. [127], and the Miller and Bowman [106] mechanisms show a significant sensitivity to oxygen stoichiometry, where the increase in the volumetric fraction of O_2 led to a higher concentration of NO in the flue gas. The formation of NO calculated using the GRI-Mech 3.0 [137] mechanism shows the opposite sensitivity to oxygen stoichiometry, which is more apparent in Figure 6.2b.

Formation of NO_2 in lignite combustion (Figures 6.1c and 6.1d)

In the case of NO_2 final concentration, the maximum relative difference in the results modeled using the four mechanisms was about 210 % compared at $\phi_{O_2} = 6\,\%$ vol. The lowest volumetric fractions of NO_2 in the dry flue gas were calculated using the Hashemi et al. [127] mechanism (in the range from 25 to 50 ppmv for ϕ_{O_2} in the range from 3 to 9 % vol.) and the highest by the GRI-Mech 3.0 [137] mechanism (in the range from 75 to 175 ppmv for ϕ_{O_2} in the range from 3 to 9 % vol.). The formation of NO_2 calculated using all the studied mechanisms showed a sensitivity to oxygen stoichiometry, where the increase in the volumetric

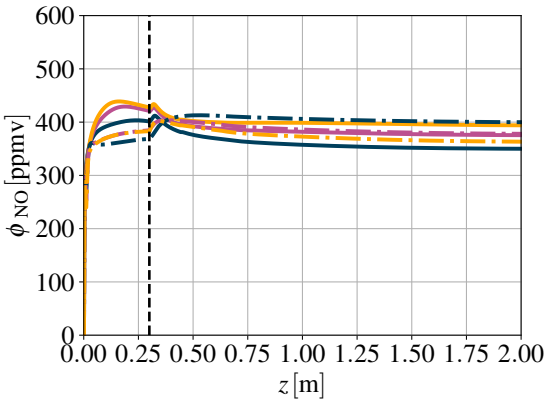

(a) NO formation: Glarborg et al. [139] and GRI-Mech 3.0 [137] mechanisms.

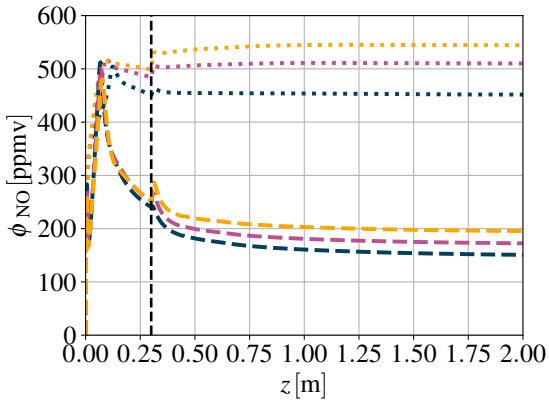

(b) NO formation: Hashemi et al. [127] and Miller and Bowman [106] mechanisms.

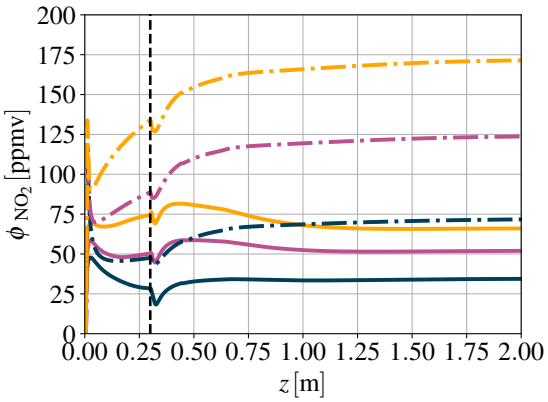

(c) NO_2 formation: Glarborg et al. [139] and GRI-Mech 3.0 [137] mechanisms.

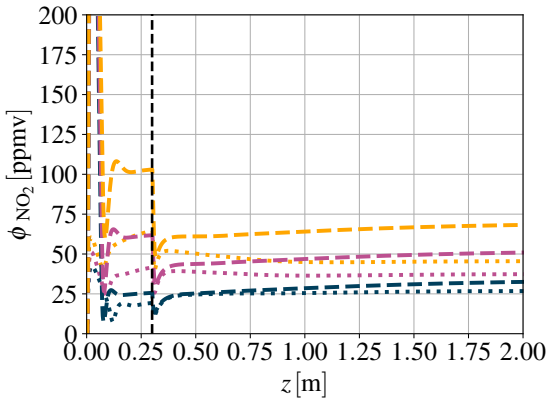

(d) NO_2 formation: Hashemi et al. [127] and Miller and Bowman [106] mechanisms.

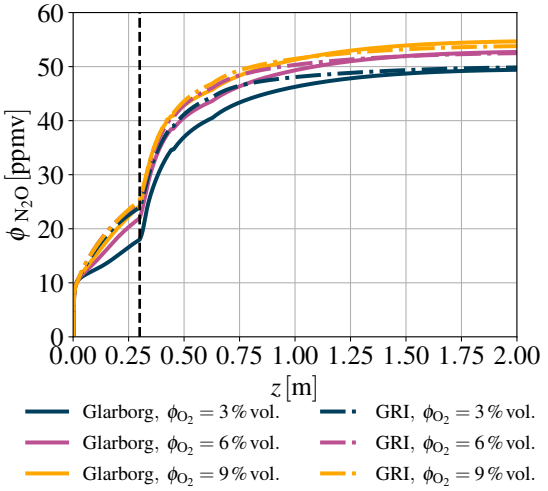

(e) N_2O formation: Glarborg et al. [139] and GRI-Mech 3.0 [137] mechanisms.

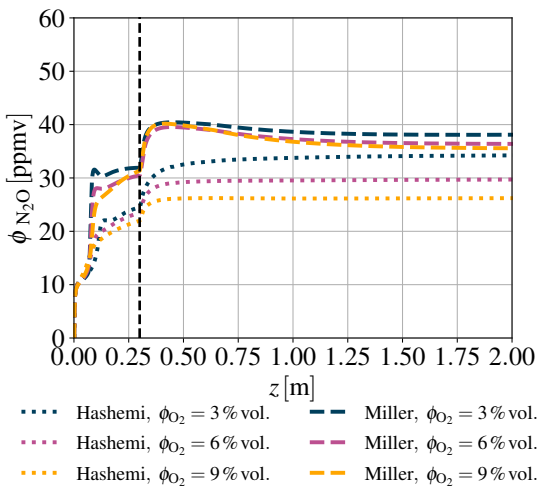

(f) N_2O formation: Hashemi et al. [127] and Miller and Bowman [106] mechanisms.

Figure 6.1: Numerical results, concentration profiles: The dependence of NO, NO_2 and N_2O formation on the oxygen stoichiometry in the oxy-fuel combustion of lignite.

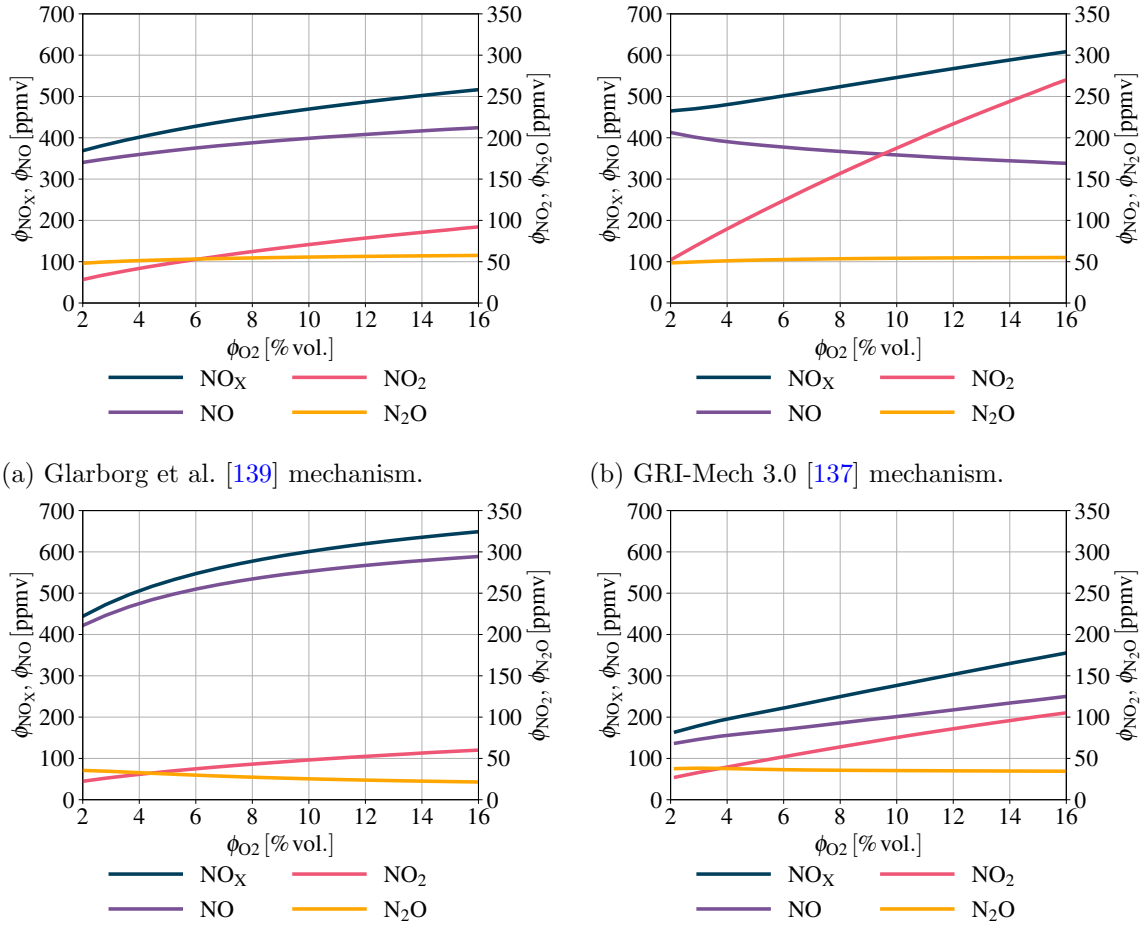

(a) Glarborg et al. [139] mechanism.

(b) GRI-Mech 3.0 [137] mechanism.

(c) Hashemi et al. [127] mechanism.

(d) Miller and Bowman [106] mechanism.

Figure 6.2: Numerical results, final concentrations in dry flue gas: The dependence of NO, NO_2 and N_2O formation on the oxygen stoichiometry in the oxy-fuel combustion of lignite.

fraction of O_2 in dry flue gas led to a promoted formation of NO_2. The sensitivity was the strongest in the case of GRI-Mech 3.0 [137] mechanism, where the increase in the volumetric fraction of O_2 from 3 to 9 % vol. led to a relative increase in the volumetric fraction of NO_2 in dry flue gas of more than 130 %.

Formation of N_2O in lignite combustion (Figures 6.1e and 6.1f)

The maximum relative difference in the final volumetric fractions of N_2O in dry flue gas calculated using the studied mechanisms was up to 35 % compared at $\phi_{O_2} = 6$ % vol. It can be seen that the concentration profiles of the results calculated using the Glarborg et al. [139]

and the GRI-Mech 3.0 [137] mechanisms are similar and that there is also a similarity in the results calculated using the Hashemi et al. [127] and the Miller and Bowman [106] mechanisms. A weak sensitivity of the formation of N_2O to the stoichiometry of oxygen can be observed in the results calculated using all the studied mechanisms, however the effect of the stoichiometry of oxygen predicted by these mechanisms is different. While the volumetric fraction of N_2O increases with the increase in the volumetric fraction of O_2 in dry flue gas using the Glarborg et al. [139] and the GRI-Mech 3.0 [137] mechanisms, a decrease in the volumetric fraction of N_2O is apparent in the results calculated using the Hashemi et al. [127] and the Miller and Bowman [106] mechanisms.

Formation of NO in the combustion of spruce wood (Figures 6.3a and 6.3b)

The concentration profiles of NO in dry flue gas from the oxy-fuel combustion of spruce wood calculated using the Glarborg et al. [139], the GRI-Mech 3.0 [137], and the Miller and Bowman [106] mechanisms are very similar in contrast to the profiles reached using the Hashemi et al. [127] mechanism, which predicted significantly higher final volumetric fractions of NO (at the level of 450 ppmv for $\phi_{O_2} = 6\,\%$ vol., i.e., relative difference in comparison to other mechanisms of more than 2 100 %). The Glarborg et al. [139], the GRI-Mech 3.0 [137], and the Miller and Bowman [106] mechanisms show similar sensitivity to oxygen stoichiometry. According to these mechanisms, the increase in the volumetric fraction of O_2 in dry flue gas leads to a reduced formation of NO, which is caused mainly by the promoted conversion of NO to NO_2. On the contrary, the results calculated with the Hashemi et al. [127] mechanism show opposite sensitivity to oxygen stoichiometry, where the increase in the volumetric fraction of O_2 in dry flue gas leads to a promoted formation of NO. According to the mechanism of Glarborg et al. and GRI-Mech 3.0, NO was converted mainly to NO_2 in the freeboard section, while according to the mechanism of Miller and Bowman, a significant part of NO formed in the dense bed section was also converted to N_2O. In the case of this mechanism, the share of NO in the sum of volumetric fractions of nitrogen oxides was extremely low.

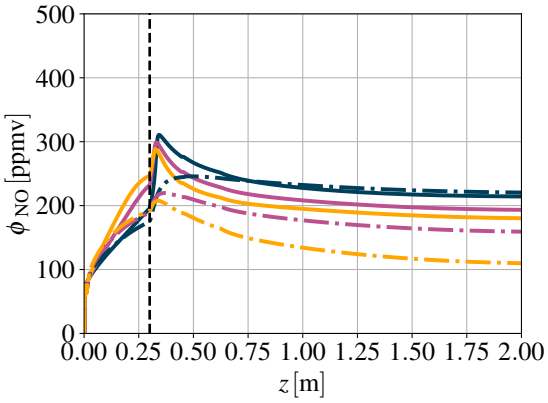

(a) NO formation: Glarborg et al. [139] and GRI-Mech 3.0 [137] mechanisms.

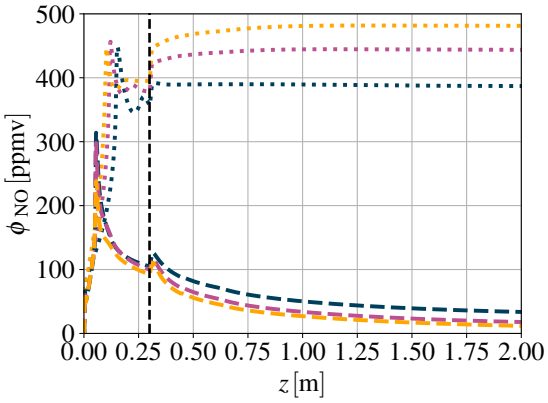

(b) NO formation: Hashemi et al. [127] and Miller and Bowman [106] mechanisms.

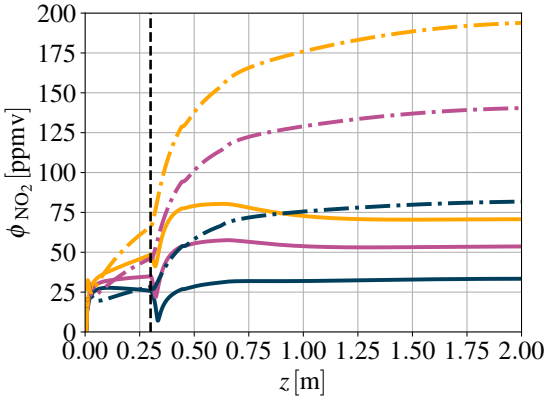

(c) NO_2 formation: Glarborg et al. [139] and GRI-Mech 3.0 [137] mechanisms.

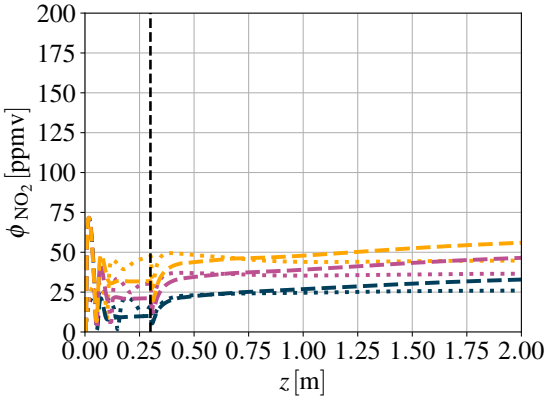

(d) NO_2 formation: Hashemi et al. [127] and Miller and Bowman [106] mechanisms.

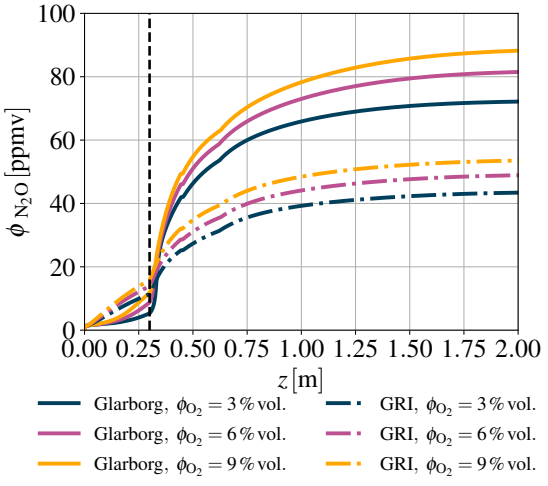

(e) N_2O formation: Glarborg et al. [139] and GRI-Mech 3.0 [137] mechanisms.

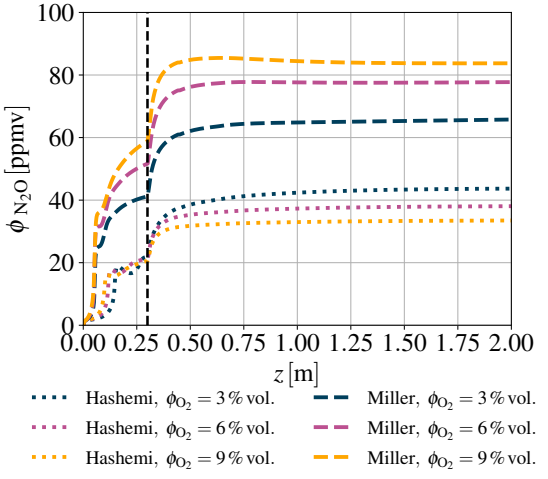

(f) N_2O formation: Hashemi et al. [127] and Miller and Bowman [106] mechanisms.

Figure 6.3: Numerical results, concentration profiles: The dependence of NO, NO_2 and N_2O formation on the oxygen stoichiometry in the oxy-fuel combustion of wooden pellets.

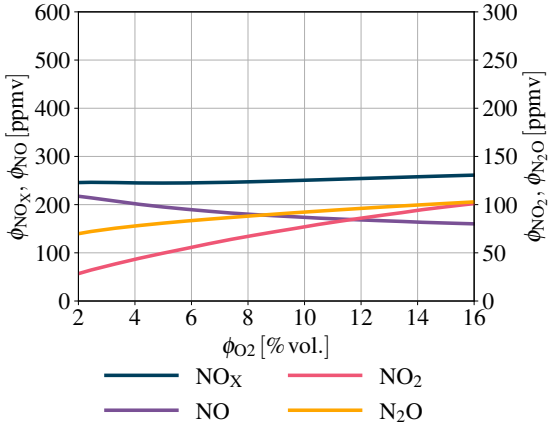

(a) Glarborg et al. [139] mechanism.

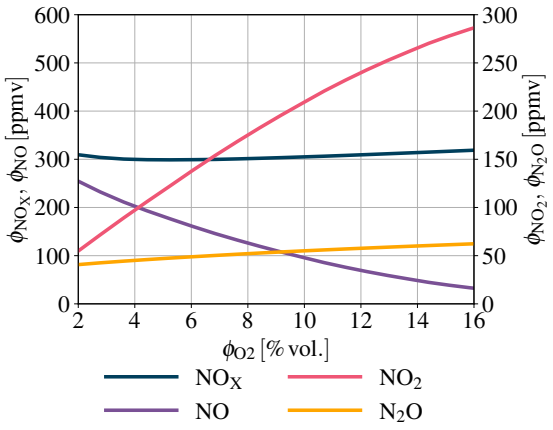

(b) GRI-Mech 3.0 [137] mechanism.

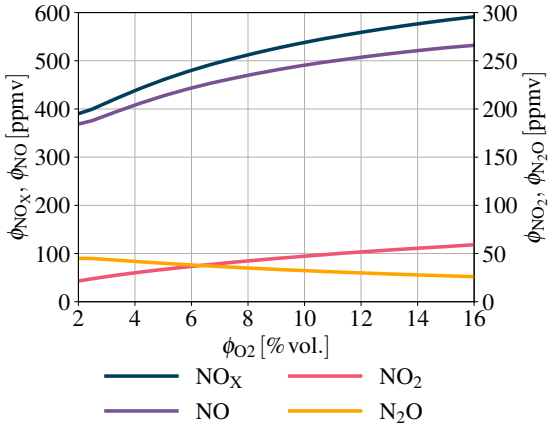

(c) Hashemi et al. [127] mechanism.

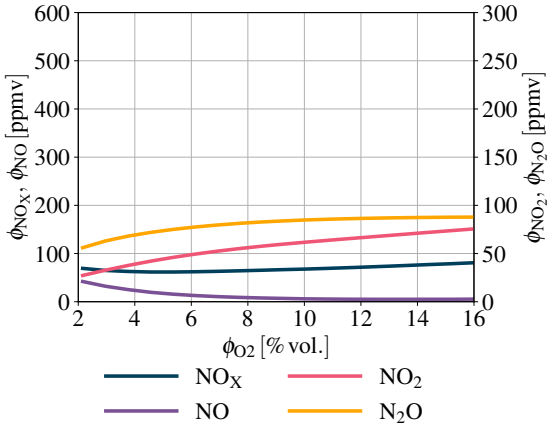

(d) Miller and Bowman [106] mechanism.

Figure 6.4: Numerical results, final concentrations in dry flue gas: The dependence of NO, NO_2 and N_2O formation on the oxygen stoichiometry in the oxy-fuel combustion of wooden pellets.

Formation of NO_2 in the combustion of spruce wood (Figures 6.3c and 6.3d)

Results of the formation of NO_2 reached using the Glarborg et al. [139], the Hashemi et al. [127], and the Miller and Bowman [106] mechanisms were similar (the final NO_2 volumetric fractions were in the range from 40 to 60 ppmv for $\phi_{O_2} = 6\,\%$ vol.) in contrary to the GRI-Mech 3.0 [137] mechanism, which predicted the volumetric fraction of NO_2 of 140 ppmv for the same oxygen stoichiometry. Using all mechanisms, NO_2 formation showed a similar sensitivity to oxygen stoichiometry, where the increase in the volumetric fraction of O_2 in dry flue gas led to an increase in the volumetric fraction of NO_2. This sensitivity

was weakest in the case of the Hashemi et al. [127] mechanism (increase in ϕ_{O_2} from 3 to 9 % vol. led to the increase of ϕ_{NO_2} from 25 to 45 ppmv) and strongest in the case of the GRI-Mech 3.0 [137] mechanism (increase in ϕ_{O_2} from 3 to 9 % vol. led to the increase of ϕ_{NO_2} from 80 to 190 ppmv) and further increase in ϕ_{O_2} led to even higher ϕ_{NO_2} (up to 280 ppmv for $\phi_{O_2} = 16$ %) (Figure 6.4b).

Formation of N_2O in the combustion of spruce wood (Figures 6.3e and 6.3f)

There are significant differences in the results of the formation of N_2O calculated using the studied mechanisms. The Glarborg et al. [139] and the Miller and Bowman [106] mechanisms predicted higher final volumetric fractions of N_2O in dry flue gas (about 80 ppmv for $\phi_{O_2} =$ 6 % vol.). On the contrary, the GRI-Mech 3.0 [137] and the Hashemi et al. [127] mechanisms predicted N_2O volumetric fractions significantly lower (about 40 and 45 ppmv, respectively, for $\phi_{O_2} = 6$ % vol.). Furthermore, there were differences in the sensitivity of N_2O formation to oxygen stoichiometry. Using the Glarborg et al. [139], the GRI-Mech 3.0 [137], and the Miller and Bowman [106] mechanisms, N_2O formation was promoted by increase in oxygen stoichiometry. The results reached using the Hashemi et al. [127] mechanism showed a slight, but opposite, sensitivity.

6.1.2 Effect of fluidized bed temperature

The results describing the impact of the fluidized bed temperature on the formation of nitrogen oxides at a constant volumetric fraction of O_2 in dry flue gas (6 % vol.) are given in Figures A.1 and A.2 for the oxy-fuel combustion of lignite and in Figures A.3 and A.4 for the oxy-fuel combustion of wooden pellets. These figures are given in Appendix A and here are only briefly described. No staged supply of oxygen was considered in this case, all the supplied oxygen was introduced in the primary gas stream.

A very similar effect of fluidized bed temperature on the fate of nitrogen oxides in the modeling of the oxy-fuel combustion of lignite can be observed in the results reached using the Glarborg et al. [139], the GRI-Mech 3.0 [137], and the Hashemi et al. [127] mechanisms,

which all showed an increase in the formation of NO and a decrease in the formation of NO_2 with increasing temperature. The Miller and Bowman [106] mechanism also predicted a decrease in NO_2 formation, but the formation of NO reached using this mechanism differed significantly from the others. The final concentration of NO was significantly higher for lower temperatures, then decreased dramatically with increasing temperatures (in the range from 800 to 875 °C) and for temperatures higher than 875 °C it increased slightly. The formation of N_2O was depressed with increasing fluidized bed temperature for all mechanisms except for the Glarborg et al. [139] mechanism.

The mechanisms of Glarborg et al. [139] and Hashemi et al. [127] led to similar results in the case of modeling of oxy-fuel combustion of wooden pellets as in the case of combustion of lignite, only the concentration of NO was significantly lower in the case of combustion of wooden pellets modeled using Glarborg et al. [139] mechanism. The GRI-Mech 3.0 [137] and the Miller and Bowman [106] mechanisms predicted unrealistically depressed formation of NO for temperatures lower than 850 °C in the case of oxy-fuel combustion of wooden pellets. In the case of the GRI-Mech 3.0 [137] mechanism, NO was oxidized particularly to NO_2. In the case of the Miller and Bowman [106] mechanism, it was also significantly converted to N_2O.

6.1.3 Effect of staged supply of oxygen

Figures describing the impact of the staged supply of oxygen on the formation of nitrogen oxides at a constant volumetric fraction of O_2 in dry flue gas (6 % vol.) and constant fluidized bed temperature (880 °C) are given in Appendix A and here, they are described only briefly. Figures A.5 and A.6 show the results of the oxy-fuel combustion of lignite and the results of the oxy-fuel combustion of spruce wood are given in Figures A.7 and A.8. The vertical dotted lines plotted in Figures A.5 and A.7 indicate the level of the secondary oxygen supply. Generally, the formation of nitrogen oxides was affected by the changing oxygen stoichiometry in the dense bed. No significant changes in the concentration of nitrogen oxides invoked by the supply of secondary oxygen appeared in the freeboard section. Therefore, the impact

of the staged supply of oxygen expressed with an increasing ratio ψ (ratio of secondary to primary oxygen volumetric flows) is similar to the impact of oxygen stoichiometry expressed with decreasing ϕ_{O_2}.

In the case of lignite combustion, the staged supply of oxygen led to a reduced formation of NO for all studied kinetic mechanisms except for the GRI-Mech 3.0, to a reduced formation of NO_2 for all studied mechanisms, to a slightly reduced formation of N_2O in the case of the Glarborg et al. [139] and the GRI-Mech 3.0 [137] mechanisms, and to slightly promoted formation of N_2O in the case of the Hashemi et al. [127] and the Miller and Bowman [106] mechanisms. Changes in the final concentrations of nitrogen oxides were nearly linear in the studied range of the ratio ψ (from 0 to 2).

In the case of oxy-fuel combustion of wooden pellets, the staged supply of oxygen led to a reduced formation of NO_2 for all studied kinetic mechanisms, to a reduced formation of N_2O in the case of the Miller and Bowman [106] mechanism, and to a reduced formation of NO in the case of the Hashemi et al. [127] mechanism. The changes in the final concentrations of nitrogen oxides were also nearly linear in the studied range of the ratio ψ.

6.1.4 Evaluation of the analysis of the kinetic mechanisms

It can be seen that the application of different mechanisms of chemical kinetics led to significant difference in the results calculated at otherwise identical conditions. In the case of lignite combustion, the dominant nitrogen oxide was NO for all four mechanisms. The shares of NO_2 and N_2O were lower and reached from 0 to 75 % of the concentration of NO depending on the parameters of the combustion process. In the case of the combustion of spruce wood, the only mechanism that predicted the dominant formation of NO was that of Hashemi et al. [127]. According to the other mechanism, the final concentrations of NO at the end of the reactor were the same (or even lower) as those of NO_2 and N_2O. The GRI-Mech 3.0 [137] and the Miller and Bowman [106] mechanisms also unrealistically predicted concentrations of NO near zero for low fluidized bed temperatures. It is known that N_2O can be formed in conventional combustion in fluidized beds at a considerable amount [110, 157].

Therefore, its formation predicted by the compared mechanisms does not seem overrated. However, the presence of NO_2 in the flue gas from fluidized bed combustors should be limited by low equilibrium concentrations of NO oxidation to NO_2 [13]. Within the laboratory-scale oxy-fuel experiments, NO_2 was detected only in a very low volumetric fractions (in units of ppmv) [42, 43, 45], or was not detected at all [56]. Therefore, the mechanism of Hashemi et al. [127], which was originally assembled for the study of oxy-fuel combustion of pulverized coal and predicted the lowest shares of NO_2 in the total amount of formed nitrogen oxides, was selected for a more detailed study.

6.2 Analysis of the numerical model with the selected kinetic mechanism

To describe the numerically modeled formation of nitrogen oxides, their concentration profiles along the height of the reactor were plotted. The plots expressing the impacts of oxygen stoichiometry, temperature of the bubbling fluidized bed, and staged supply of oxygen are given in Figures 6.5, 6.7, and 6.9, respectively. In these figures, the solid lines represent the oxy-combustion of lignite, while the dotted lines represent the oxy-combustion of spruce wood. The vertical dashed line indicates the boundary of the dense bed and the freeboard section. The fuel compounds were introduced to the gas mixture only in the dense bed. The black vertical dotted lines in Figure 6.9 indicate the level of secondary oxygen supply. The volumetric fractions ϕ_i are related to the dry flue gas. The NO_X fraction ϕ_{NO_X} was calculated as the sum of ϕ_{NO} and ϕ_{NO_2}.

The applied kinetic mechanism assembled by Hashemi et al. [127] contains 108 reactions, where NO figures as either a reactant or as a product, 78 reactions in which NO_2 figures, and 22 reactions in which N_2O figures. In these reactions, free radicals play a key role in the formation or either in the destruction of nitrogen oxides. Therefore, the concentration profiles of the most important radicals (O, OH, H, and HO_2) along the reactor height were

plotted in Figures 6.6, 6.8, and 6.10 to help understand the impacts of oxygen stoichiometry, bubbling fluidized bed temperature, and staged supply of O_2, respectively.

Generally, there is a significant difference between the modeling of lignite combustion and spruce wood combustion in the distribution of nitrogen compounds in the chars and volatiles that are added in the dense bed zone. As it was indicated in Tables 5.3 and 5.4, the molar nitrogen distribution in the devolatilization phase is following:

- 14 % in NH_3, 6 % in HCN, 27 % in NO, 2 % in NO_2, and 51 % in N_2 for lignite,
- 30 % in NH_3, 50 % in HCN, 15 % in NO, 0.5 % in NO_2, and 2.5 % in N_2 for spruce wood.

While the NO defined directly as the source term contributes mostly to the final NO share in the case of lignite combustion, the HCN and NH_3 oxidation mechanisms contribute the most to the final NO share in the case of spruce wood combustion. This fact causes a significant difference in the modeled nitrogen oxides formation, particularly in the formation of NO_2, which is formed mainly by reaction with HO_2 described in Equation (3.2). The high concentration of NO in the early stage of combustion where HO_2 is present dominantly is a key factor in the promotion of NO_2 formation in the case of lignite combustion.

6.2.1 Effect of oxygen stoichiometry

The effect of the oxygen stoichiometry expressed by the volumetric fraction of oxygen in the dry flue gas appears to be quite clear. The increase of the oxygen excess and thus of the concentration of O_2 available for the oxidation reactions promotes both the formation of NO (Figure 6.5a) and NO_2 (Figure 6.5b). In the case of lignite combustion, the volumetric fractions of NO in flue gas are slightly higher than in the case of spruce wood combustion. The levels of volumetric fractions of NO_2 were nearly the same for both fuels. It can be seen in Figure 6.5c that the effect of oxygen stoichiometry on N_2O formation was opposite to that in NO and NO_2, since N_2O was formed mainly through the reactions of NO with NH

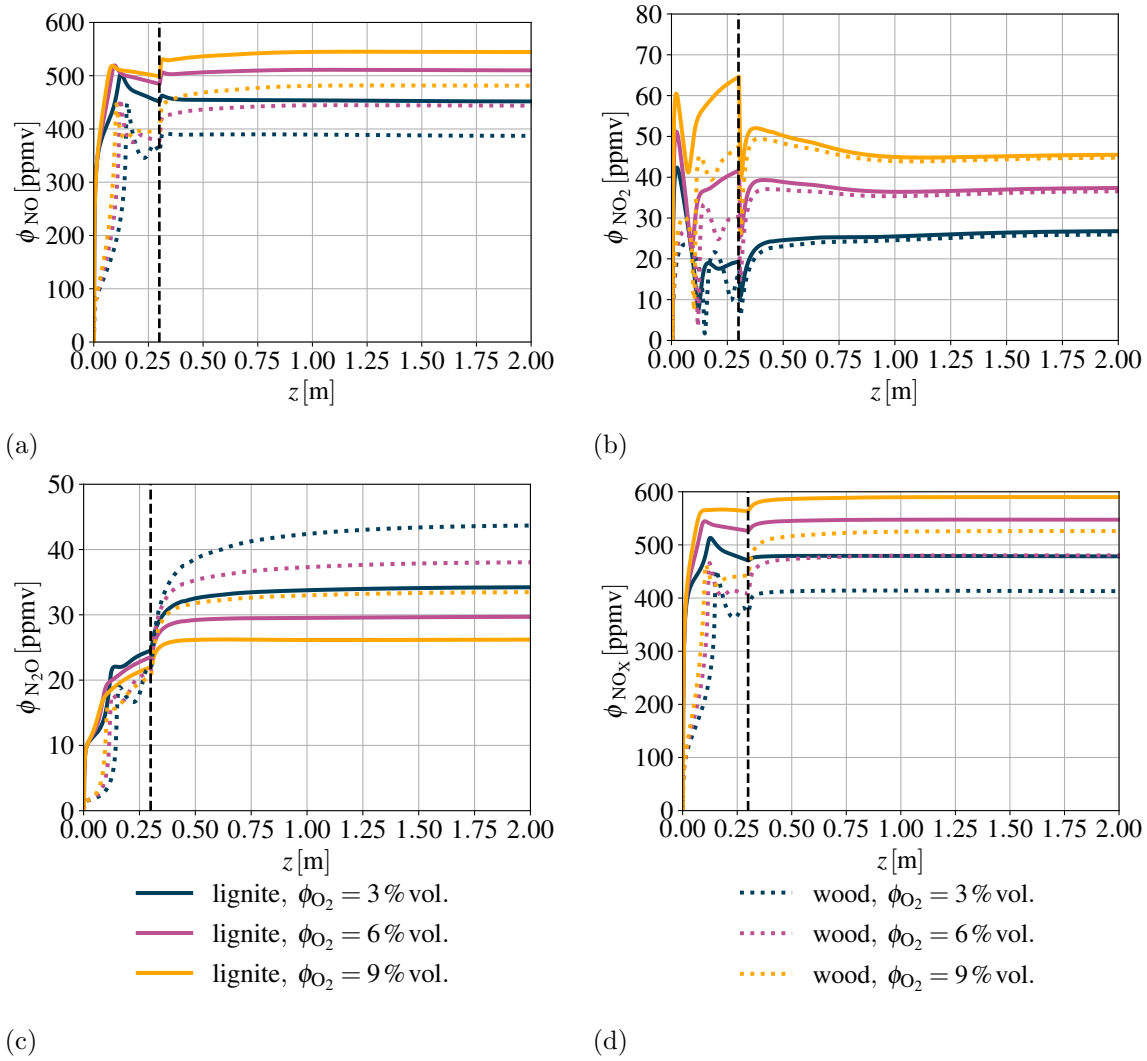

Figure 6.5: Numerical results: The dependence of a) NO, b) NO_2, c) N_2O, and d) NO_X formation on the oxygen stoichiometry.

and NCO described by Equations (3.30) and (3.29), which were negatively affected by the increase in O_2 concentration.

The resulting profiles of NO_X volumetric fraction (Figure 6.5d) show that the increase of ϕ_{O_2} generally promoted the formation of NO_X.

The concentration profiles of radicals (described in Figure 6.6) with an essential impact on the fate of nitrogen oxides show similarity for both studied fuels, which is in agreement with the similarity observed in the concentration profiles of nitrogen oxides. It is appar-

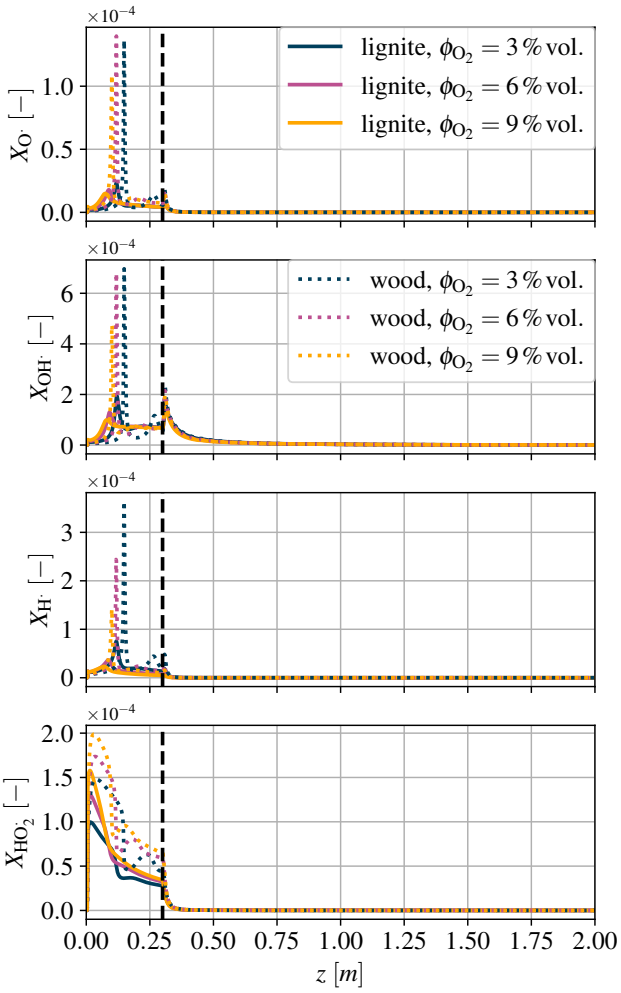

Figure 6.6: Mole fraction of O, OH, H, and HO_2 radicals in dependence on the oxygen stoichiometry.

ent that all reactions significantly affecting nitrogen chemistry take place in the dense bed section, where the fuel is introduced, or slightly above it. In the freeboard section, the concentrations of radicals are reaching zero observed for both fuels. The reactions with the highest net production rates, through which NO_2 was formed or reduced, were described by Equations (3.2) and (3.27). For both fuels, high concentrations of NO and HO_2 were responsible for the higher formation of NO_2 in the early combustion stage in the dense bed section through reaction (3.2). This reaction can also be responsible for increased concentrations of OH radical in the early combustion stage in the dense bed section. The second peak in the concentration profiles of OH radical on the boundary of the dense bed and the freeboard

section can be a consequence of a rapid NO_2 consumption through the reaction (3.27). The concentration profiles of radicals were not affected by the oxygen stoichiometry significantly.

6.2.2 Effect of fluidized bed temperature

Figure 6.7a shows that the NO concentration profiles were not significantly affected by the change in the fluidized bed temperature in the studied temperature range in the case of lignite combustion modeling, since the NO originated from a major part directly in the volatiles and char combustion products added in the dense bed section as part of the fuel. In contrast, the NO profiles showed a slight temperature sensitivity in the case of the modeling of spruce wood combustion, where NO was mainly derived from the oxidation mechanisms of HCN and NH_3. In this case, the formation of NO was slower at the lowest studied temperature (840 °C) which can be seen in the leftmost part of Figure 6.7a indicating the dense bed section. In the freeboard section of the PFR model, no significant changes in the concentrations of NO are apparent.

The increase in the temperature of the fluidized bed significantly decreased the formation of NO_2 for both fuels, as can be seen in Figure 6.7b. For both fuels, NO_2 was formed mainly in the dense bed section through reaction (3.2). The net production rates of both reactions, which are mainly responsible for the fate of NO_2 (3.2) and (3.27) decreased significantly with increasing temperature and were about 1 000 times lower at $t_{BFB} = 960\,°C$ compared to 840 °C. In the case of reaction (3.2), the net production rate is even negative in the freeboard section at 960 °C resulting in NO_2 depletion. The reactions that contribute the most to the NO_2 formation at $t_{BFB} = 960\,°C$ are described by Equations (6.1) and (6.2).

$$NO + O + M \rightleftharpoons NO_2 + M \tag{6.1}$$

$$HONO + OH \rightleftharpoons H_2O + NO_2 \tag{6.2}$$

The main part of N_2O (similarly as of NO) originated directly in the volatiles and char combustion products in the case of lignite combustion modeling. The dependence of the

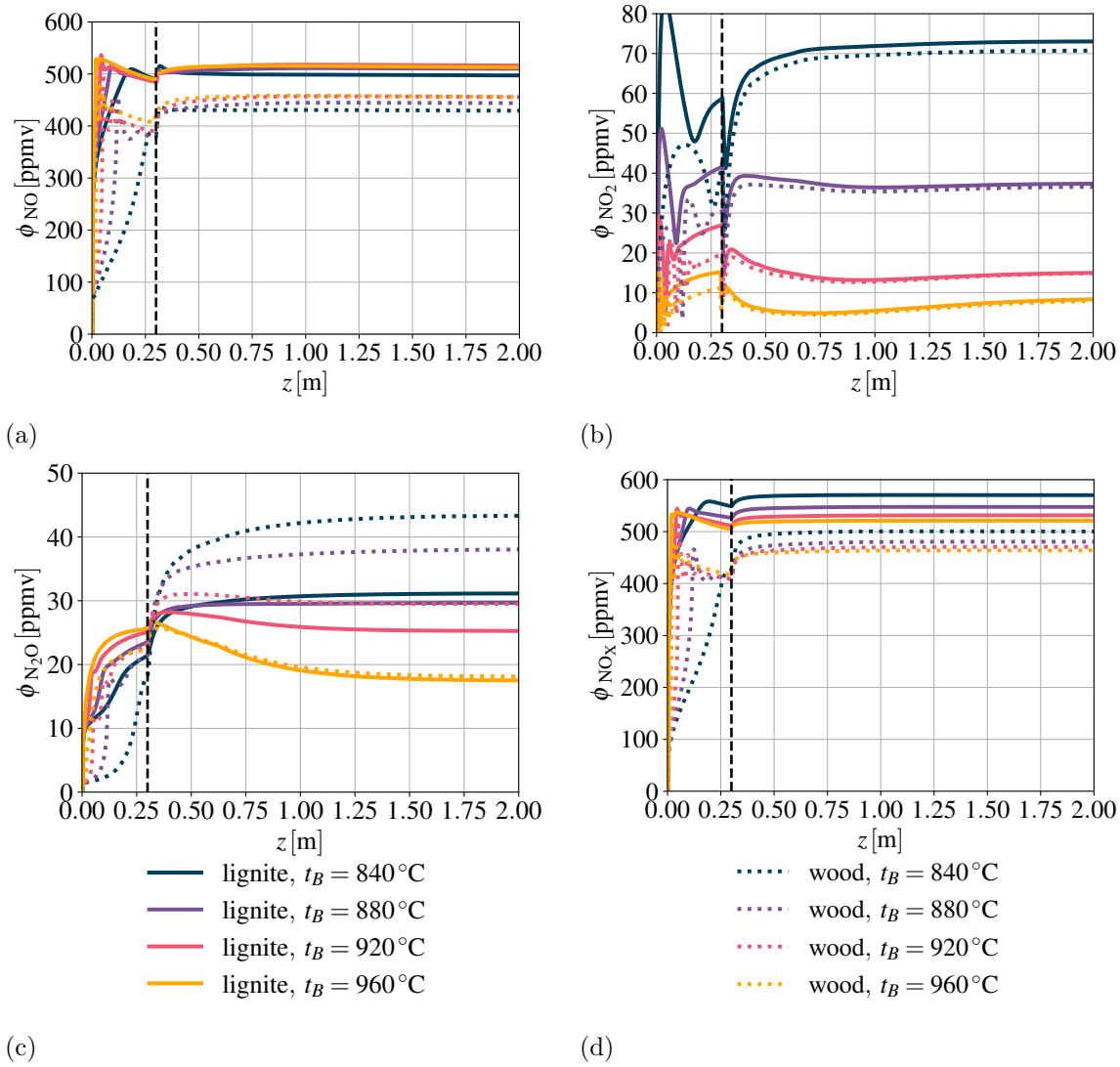

Figure 6.7: Numerical results: The dependence of a) NO, b) NO_2, c) N_2O, and d) NO_X formation on the fluidized bed temperature.

concentration of N_2O on the fluidized bed temperature indicated in Figure 6.7c inheres mainly in the temperature sensitivity of the reaction (3.31), which was the major contributor to the N_2O reduction in the freeboard section at elevated temperatures. In the case of wood combustion modeling, the reaction that contributed mostly to the N_2O formation can be described by Equation (6.3). The net rate of this reaction was highest in the dense bed

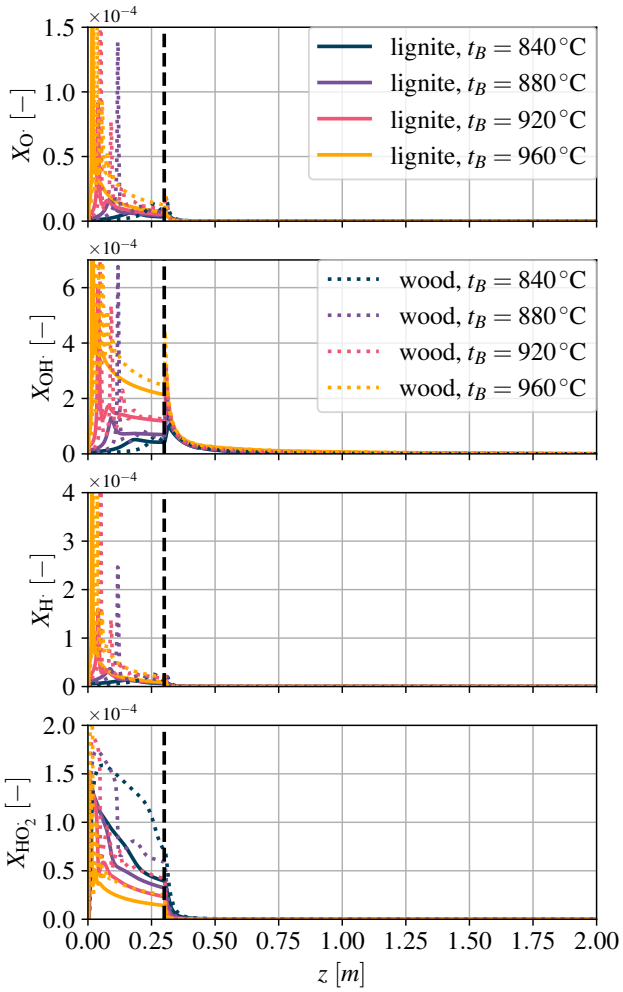

Figure 6.8: Mole fraction of O, OH, H, and HO_2 radicals in dependence on the fluidized bed temperature.

section at lower temperatures, and in the freeboard section at $t_{BFB} = 960\,°C$.

$$NH + NO \rightleftharpoons H + N_2O \tag{6.3}$$

The resulting NO_X fromation was slightly depressed by an increase in the fludized bed temperature for both fuels (Figure 6.7d), which was particularly invoked by the temperature sensitivity of the formation of NO_2 and N_2O.

It can be observed in Figure 6.8, where the impact of the fluidized bed temperature on the concentration profiles of key radicals for the formation and reduction of nitrogen oxides is

given, that the formation of OH radical was significantly promoted in the dense bed section at elevated fluidized bed temperatures. The main reason for that is found in the impact of temperature on reactions (3.2) and (3.27). At higher temperatures, the net production rates of these reactions are very similar. They are competitive in terms of the formation of NO and NO_2, but both produce OH radicals. The decrease in the net production rate of reaction (3.2) with increase in t_{BFB} is also apparent in the decrease in the concentration of HO_2 radical in the dense bed section.

6.2.3 Effect of staged supply of oxygen

The results of the staged supply of oxygen partly extended the effect of oxygen stoichiometry, since sub-stoichiometric conditions were reached in the dense bed section for all ratios $\psi > 0.5$. The changes apparent in Figure 6.9 at heights lower than the height of the secondary O_2 supply were caused due to the same principles, which were described in Section 6.2.1. This is also confirmed by the concentration profiles of key radicals (given in Figure 6.10), which are very similar to those that were reported for the effect of global oxygen stoichiometry in Figure 6.6. It can be seen in Figures 6.9a and 6.9b that each increase in the ratio of secondary to primary oxygen ψ promoted the reduction of NO and NO_2 for both fuels. Similarly as in Section 6.2.1, the results showed that the formation of N_2O was promoted when the oxygen stoichiometry was reduced due to the reduction in the amount of primary oxygen introduced into the dense bed.

The supply of the stream of secondary oxygen did not significantly affect the formation of nitrogen oxides. The concentrations of radicals in the freeboard section were also not affected and remained at zero.

The final total NO_X concentration decreased with each increase in the ratio ψ for both fuels (Figure 6.9d). The maximum NO_X reduction efficiency was 12.7 % in the case of lignite and 17 % in the case of wood combustion modeling.

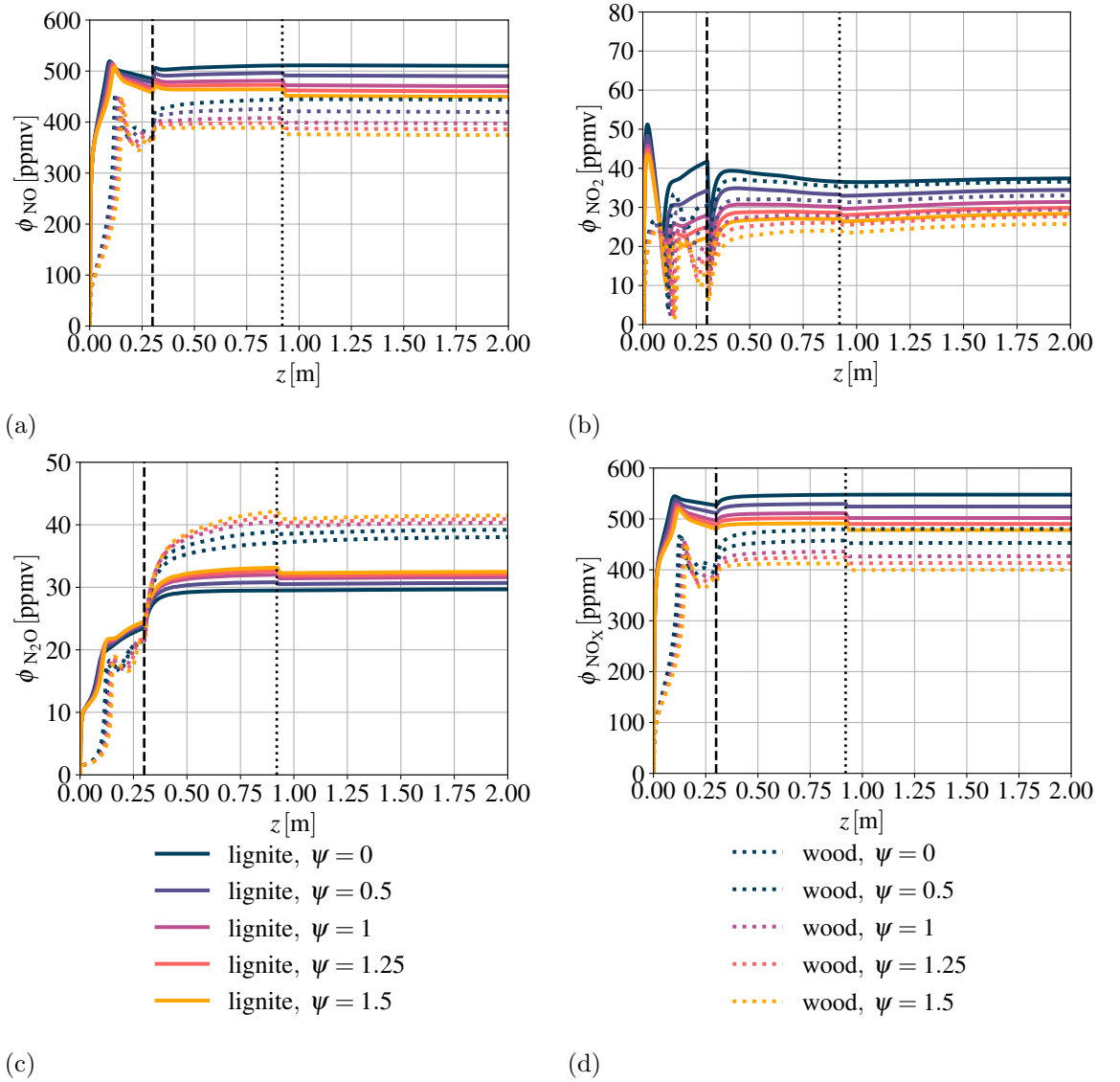

Figure 6.9: Numerical results: The dependence of a) NO, b) NO_2, c) N_2O, and d) NO_X formation on the oxygen staging.

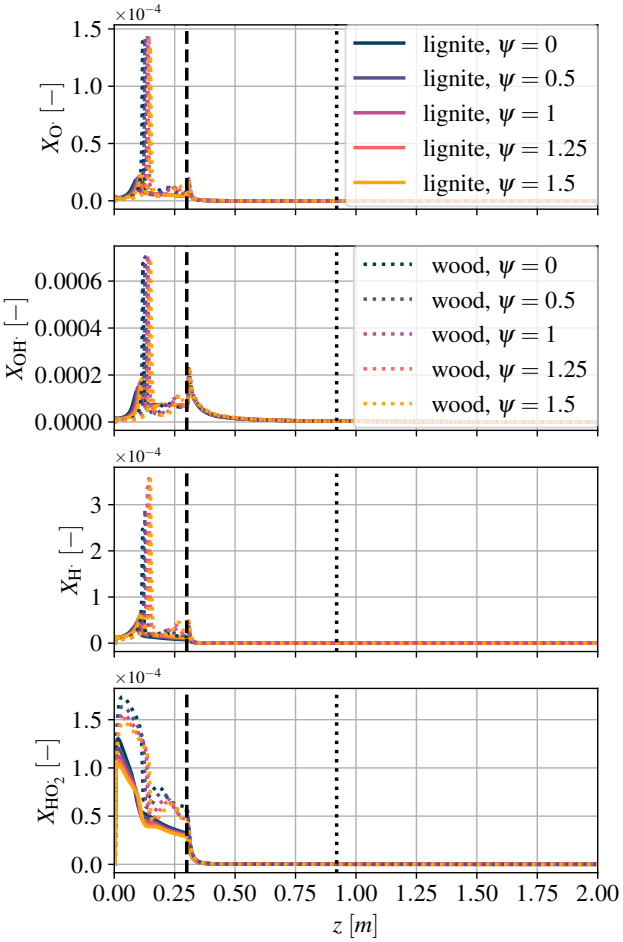

Figure 6.10: Mole fraction of O, OH, H, and HO_2 radicals in dependence on the staged supply of oxygen.

Chapter 7

Experimental results and validation of the numerical model

Experimental results of the formation of nitrogen oxides in oxy-fuel combustion in a BFB are presented and discussed in this chapter. The results showing the original experimental work performed using the 30 kW_{th} laboratory-scale BFB combustor are given in Section 7.1. In relevant scenarios (effect of global stoichiometry and of fluidized bed temperature), the results of experiments conducted in the air-combustion regime are added for comparison of the oxy-fuel and air-combustion. Supplementary experimental results reached using a 500 kW_{th} pilot-scale BFB combustor are presented in Section 7.2 to show the typical formation NO, NO_2 and N_2O in the oxy-fuel combustion in a BFB. Comparison of the experimental and numerical results of oxy-fuel combustion is given in Section 7.3 together with a discussion of the results of already published studies.

7.1 Experimental results of the NO_X formation

In this Section mainly, graphical plots of the dependencies of the concentration of NO_X on key variables are presented. Supplemental tables with complete data are given in Appendix B. The volumetric fraction of CO_2 in dry flue gas varied in the range from 70 to 95 % within the

experimental tests of the oxy-fuel combustion, but its average value was 85.4%. The sum of volumetric fractions of CO_2 and O_2 in dry flue gas was 92.1 % on average, indicating a very low degree of false air ingress.

7.1.1 Effect of oxygen stoichiometry

Combustion of lignite

To describe the effect of oxygen stoichiometry on the formation of NO_X in the case of lignite combustion, two series of experiments in the oxy-fuel and one series in the air-combustion regime were realized (Figure 7.1). The oxy-fuel experimental series differed in the superficial fluidizing gas velocity and so in the fuel load. The averages of these parameters were as follows:

oxy-combustion No 1	$u_0 \approx 1.1\,\mathrm{m \cdot s^{-1}}$	$m_{fuel} = 3\,\mathrm{kg \cdot h^{-1}}$,
oxy-combustion No 2	$u_0 \approx 2.4\,\mathrm{m \cdot s^{-1}}$	$m_{fuel} = 7.1\,\mathrm{kg \cdot h^{-1}}$, and
air-combustion	$u_0 \approx 2.8\,\mathrm{m \cdot s^{-1}}$	$m_{fuel} = 8\,\mathrm{kg \cdot h^{-1}}$.

It can be seen that the parameters of the air-combustion series were closer to those of the oxy-fuel series No 2. In the three experimental series, a clear effect of oxygen stoichiometry on NO_X formation can be seen. With the increase in the volumetric fraction of O_2 in dry flue gas from 3 to 9 %, the NO_X emission factor increased from 32.5 to 68.1 $\mathrm{mg \cdot MJ^{-1}}$ (gain of 110 %) in case of oxy-fuel No 1, from 30 to 58.8 $\mathrm{mg \cdot MJ^{-1}}$ (gain of 96 %) in case of oxy-fuel No 2, and from 119 to 330 $\mathrm{mg \cdot MJ^{-1}}$ (gain of 177 %) in case of air-combustion. Higher oxygen stoichiometry (corresponding to the O_2 volumetric fraction of 12 % in dry flue gas) was used in case of oxy-fuel No 1 - in this case, the NO_X emission factor of 82.2 $\mathrm{mg \cdot MJ^{-1}}$ and gain of 153 % compared to $\phi_{O_2} = 3\,\%$ vol. were reached. All cases with $\phi_{O_2} = 3\,\%$ vol. were accompanied with increased formation of CO (in all experimental series), which could contribute to the reduction of NO through the reaction described by Equation (3.34). Only negligible concentrations of CO were measured for higher levels of O_2 in the dry flue gas. No clear effect of the power load and fluidization gas velocity on NO_X formation can be seen from the comparison of the results of oxy-fuel series No 1 and 2.

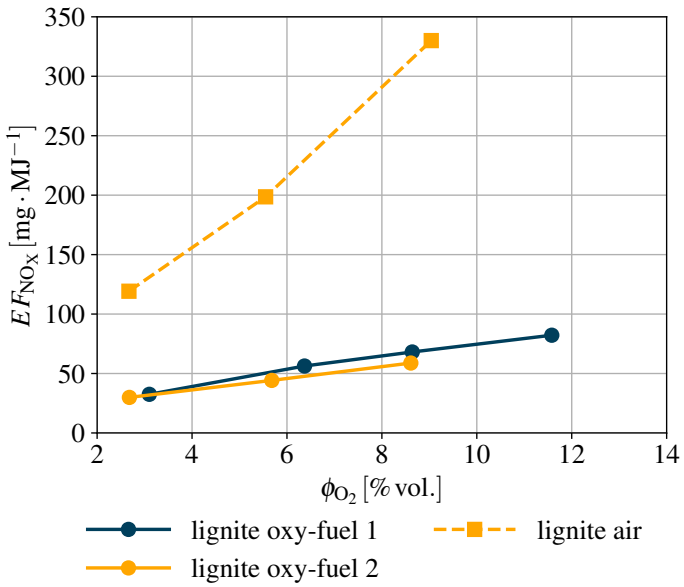

Figure 7.1: Experimental results, combustion of lignite: Emission factors of NO_X in dependence on the oxygen stoichiometry.

Combustion of wooden pellets

In the case of the combustion of spruce wood, three series were performed in oxy-fuel and three series in air-combustion regime (Figure 7.2). The series differed in the superficial gas velocity, the fuel load, and the type of LWA used as the fluidized bed material. The averages of the used superficial fluidizing gas velocities and fuel loads were as follows:

oxy-combustion No 1	$u_0 \approx 1.0\,\mathrm{m \cdot s^{-1}}$	$m_{fuel} \approx 5.2\,\mathrm{kg \cdot h^{-1}}$	LWA 0–2,
oxy-combustion No 2	$u_0 \approx 1.0\,\mathrm{m \cdot s^{-1}}$	$m_{fuel} = 5.6\,\mathrm{kg \cdot h^{-1}}$	LWA 0–2,
oxy-combustion No 3	$u_0 \approx 1.9\,\mathrm{m \cdot s^{-1}}$	$m_{fuel} = 9\,\mathrm{kg \cdot h^{-1}}$	LWA P3,
air-combustion No 1	$u_0 \approx 1.2\,\mathrm{m \cdot s^{-1}}$	$m_{fuel} \approx 4.9\,\mathrm{kg \cdot h^{-1}}$	LWA 0–2,
air-combustion No 2	$u_0 \approx 1.5\,\mathrm{m \cdot s^{-1}}$	$m_{fuel} = 5\,\mathrm{kg \cdot h^{-1}}$	LWA 0–2, and
air-combustion No 3	$u_0 \approx 3.5\,\mathrm{m \cdot s^{-1}}$	$m_{fuel} = 10.8\,\mathrm{kg \cdot h^{-1}}$	LWA P3.

A clear effect of oxygen stoichiometry on NO_X formation can also be seen in the case of spruce wood combustion similar to lignite combustion. The increase in the volumetric fraction of O_2 in dry flue gas from approx. 3 to 9 % brought increases in emission factors

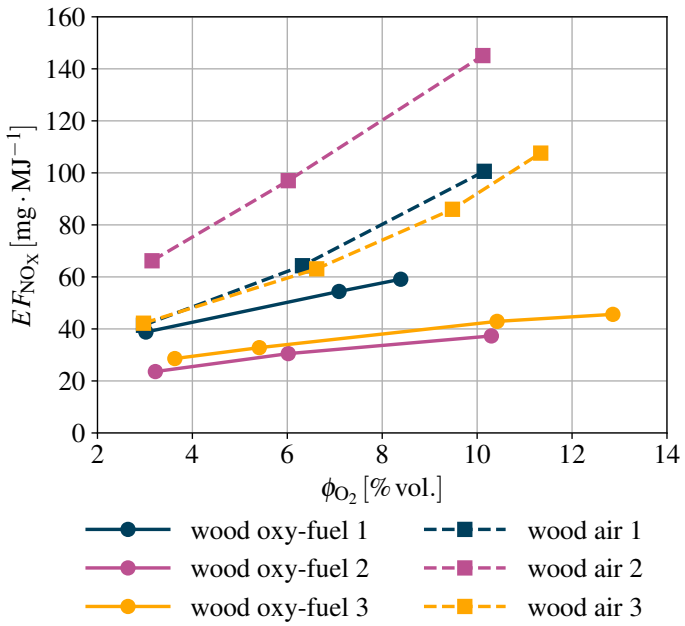

Figure 7.2: Experimental results, combustion of wooden pellets: Emission factors of NO_X in dependence on the oxygen stoichiometry.

of NO_X from 38.8 to 59.1 mg · MJ^{-1} (gain of 52 %) in case of oxy-fuel No 1, from 23.6 to 37.3 mg · MJ^{-1} (gain of 58 %) in case of oxy-fuel No 2, from 28.6 to 42.9 mg · MJ^{-1} (gain of 50 %) in case of oxy-fuel No 3, from 41.4 to 100.6 mg · MJ^{-1} (gain of 143 %) in case of air-combustion No 1, from 66.2 to 145.1 mg · MJ^{-1} (gain of 119 %) in case of air-combustion No 2, and from 42.2 to 86 mg · MJ^{-1} (gain of 104 %) in case of air-combustion No 3. Furthermore, a higher oxygen stoichiometry (corresponding to the O_2 volumetric fraction of 12 % in dry flue gas) was used in cases of oxy-combustion series No 3 and air-combustion series No 3. In these cases, the NO_X emission factors of 45.6 and 107.6 mg · MJ^{-1} (gains of 59 and 155 %) were reached respectively compared to the cases with $\phi_{O_2} = 3$ % vol.. The oxy-combustion cases with $\phi_{O_2} = 3$ % vol. were accompanied with slightly increased formation of CO. In other experiments, the concentrations of CO were negligible. Within the tests of air-combustion No 2, significantly higher level of NO_X emission factors was reached compared to the other air-combustion series and the corresponding ϕ_{O_2} (about $40 \div 50$ %). It is difficult to determine the cause of this difference, as the parameters of air-combustion series No 2 were almost identical to the parameters of series No 1. The series No 1 could be possibly accompanied

with an air ingress into the analyzer, since the sums of the measured volumetric fractions of O_2 and CO_2 are about 1 % lower compared to the series No 2, but this ingress could hardly cause such a significant difference in the NO_X fraction. Other possible explanations can be found in the different compositions of the fuel used in these experiments. However, the spruce wood pellets used in these two experimental series came from the same batch, and unfortunately only one sample from this batch was analyzed. The results do not show a clear effect of the power load, the superficial velocity of the fluidization gas, or the PSD of the fluidized bed material on the formation of NO_X.

Evaluation of the effect of oxygen stoichiometry

The NO_X emission factors were always higher in the case of air-combustion than in oxy-fuel combustion for both fuels, and so were the conversion ratios of fuel-N to NO_X. The difference was greater for higher volumetric fractions of O_2 in the flue gas. In case of lignite combustion, the NO_X emission factors were about $90\,mg \cdot MJ^{-1}$ (300 %) higher for $\phi_{O_2} = 3\,\%\,vol.$ and about $260\,mg \cdot MJ^{-1}$ (370 %) higher for $\phi_{O_2} = 9\,\%\,vol.$ The corresponding N−NO ratios were higher about 11 % mole absolutely (370 % relatively) for $\phi_{O_2} = 3\,\%\,vol.$ and 19 % mole absolutely (270 % relatively) for $\phi_{O_2} = 9\,\%\,vol.$ In the case of spruce wood combustion, the NO_X emission factors reached in air-combustion were in comparison to those reached in oxy-fuel combustion about $20\,mg \cdot MJ^{-1}$ (65 %) higher for $\phi_{O_2} = 3\,\%\,vol.$ and about $70\,mg \cdot MJ^{-1}$ (149 %) higher for $\phi_{O_2} = 9\,\%\,vol.$ The corresponding N−NO ratios were higher about 9 % mole absolutely (169 % relatively) for $\phi_{O_2} = 3\,\%\,vol.$ and 12 % mole absolutely (138 % relatively) for $\phi_{O_2} = 9\,\%\,vol.$ The major difference between air- and oxy-combustion in formation of NO_X inhere in the oxygen availability and in significantly different concentrations of combustion products. The compared experimental series were performed for the same concentrations of O_2 in dry flue gas, which, however, did not bring the same conditions for the reaction of fuel-N. On the one hand, air- and oxy-combustion flue gases contain significantly different water content (higher in oxy-fuel combustion). On the other hand, the volume of flue gas (both wet and dry) is marginally higher in air-combustion.

These facts have opposite effect, but the ratio of O_2 and fuel is higher in air- than in oxy-combustion at the same O_2 volumetric fraction in dry flue gas, as a consequence. A lower O_2 stoichiometry, combined with a higher concentration of products, results in a decrease in the fuel-N conversion to NO_X. Although it appears that the comparison at the same ϕ_{O_2} in dry flue gas is not ideal for the comparison of air- and oxy-combustion, using an approach of the same oxygen excess ratio would lead to an extensive content of O_2 in flue gas from oxy-fuel combustion (e.g., $\phi_{O_2} = 10.45\,\%$ vol. in dry flue gas for the oxygen excess of 20 % in case of lignite combustion, which corresponds to $\phi_{O_2} = 3.07\,\%$ vol. in dry flue gas in the air-combustion regime), as was published in [171]. The higher concentration of oxygen in the flue gas increases the demands on the CO_2 purification process and, therefore, is not desirable. As can be seen in Tables B.1, B.6, B.11, and B.13, the formation of CO and so the completeness of combustion is similar in air- and oxy-combustion at the same ϕ_{O_2} in dry flue gas, so the chosen experimental approach can provide valuable information on the impact of oxygen stoichiometry on the formation of NO_X in the possible operating range of the BFB combustor.

7.1.2 Effect of fluidized bed temperature

Combustion of lignite

Three series of experimental tests were performed in the oxy-fuel combustion and one in the air-combustion of lignite to study the impact of the fluidized bed temperature on the formation of NO_X (Figure 7.3). The averages of the superficial velocities of the fluidizing gas and of the fuel loads within these tests were the following:

oxy-combustion No 1	$u_0 \approx 1.1\,\mathrm{m \cdot s^{-1}}$	$m_{fuel} \approx 4.2\,\mathrm{kg \cdot h^{-1}}$,
oxy-combustion No 2	$u_0 \approx 1.4\,\mathrm{m \cdot s^{-1}}$	$m_{fuel} \approx 4.2\,\mathrm{kg \cdot h^{-1}}$,
oxy-combustion No 3	$u_0 \approx 2.2\,\mathrm{m \cdot s^{-1}}$	$m_{fuel} \approx 7.3\,\mathrm{kg \cdot h^{-1}}$, and
air-combustion	$u_0 \approx 2.7\,\mathrm{m \cdot s^{-1}}$	$m_{fuel} = 8.0\,\mathrm{kg \cdot h^{-1}}$.

A clear dependence of the NO_X emission factors on the fluidized bed temperature can be seen in Figure 7.3 within the studied temperature range. The formation of NO_X was

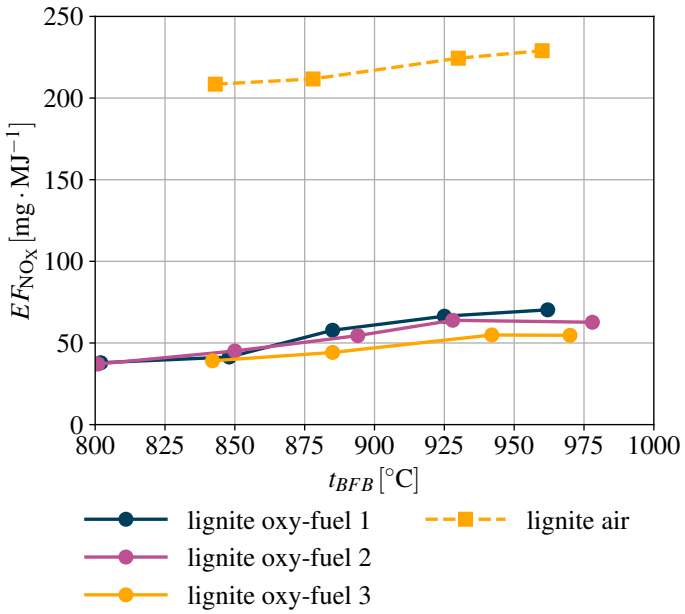

Figure 7.3: Experimental results, combustion of lignite: Emission factors of NO_X in dependence on the fluidized bed temperature.

slightly promoted by the increase in the temperature in all experimental series of lignite combustion. The increase in t_{BFB} from 800 to 960 °C brought an increase in the emission factors of NO_X from 37.9 to 70.3 mg · MJ^{-1} (gain of 85 %) in case of oxy-fuel No 1 and from 37.1 to 62.7 mg · MJ^{-1} (gain of 69 %) in case of oxy-fuel No 2. In the case of the series of oxy-combustion No 3 and air-combustion, the lowest temperature of the studied range was 840 °C. The increase of t_{BFB} from 840 to 960 °C brought an increase of NO_X emission factors from 39.1 to 54.7 mg · MJ^{-1} (gain of 40 %) in case of oxy-fuel No 3 and from 208.5 to 229 mg · MJ^{-1} (gain of 10 %) in case of air-combustion. It can be seen that the gain of EF_{NO_X} is significantly lower in air- than in oxy-combustion despite a similar trend gradient. A small offset can be seen between the lines describing the three series of oxy-fuel combustion. This offset could be possibly caused by differences in the superficial velocities of the fluidization gas and so in the residence time of the flue gas in the combustion chamber. The shorter residence time in the combustion zone in oxy-fuel series No 3 could lead to lower NO_X formation.

Combustion of wooden pellets

In the case of spruce wood combustion, two experimental series were measured in the oxy-fuel and two series in the air-combustion regime to study the dependence of NO_X formation on the temperature of the fluidized bed (Figure 7.4). The averages of the superficial velocities of the fluidizing gas and of the fuel loads within these tests were the following:

oxy-combustion No 1	$u_0 \approx 1.0\,\mathrm{m \cdot s^{-1}}$	$m_{fuel} \approx 6.0\,\mathrm{kg \cdot h^{-1}}$	LWA 0–2,
oxy-combustion No 2	$u_0 \approx 1.7\,\mathrm{m \cdot s^{-1}}$	$m_{fuel} = 9.0\,\mathrm{kg \cdot h^{-1}}$	LWA P3,
air-combustion No 1	$u_0 \approx 1.4\,\mathrm{m \cdot s^{-1}}$	$m_{fuel} = 5\,\mathrm{kg \cdot h^{-1}}$	LWA 0–2, and
air-combustion No 2	$u_0 \approx 2.7\,\mathrm{m \cdot s^{-1}}$	$m_{fuel} \approx 8.6\,\mathrm{kg \cdot h^{-1}}$	LWA P3.

It cannot be clearly concluded how the fluidized bed temperature affects NO_X formation in the case of spruce wood combustion. For both oxy-fuel combustion series, the NO_X emission factors were almost constant in the studied range of t_{BFB}. Their value was in the range from 30.5 to 31.3 $\mathrm{mg \cdot MJ^{-1}}$ with average interval of 95 % confidence $\pm 0.3\,\mathrm{mg \cdot MJ^{-1}}$ in series No 1 and from 33.1 to 34.3 $\mathrm{mg \cdot MJ^{-1}}$ with average interval of 95 % confidence $\pm 0.2\,\mathrm{mg \cdot MJ^{-1}}$ in series No 2. In the case of air-combustion regime, a significant difference is apparent between the two series. The NO_X emission factors decreased from 104.9 to 88.4 $\mathrm{mg \cdot MJ^{-1}}$ (drop of 16 %) when the fluidized bed temperature increased from 840 to 920 °C in the series No 1. In the series No 2, the fludized bed temperature had no effect on EF_{NO_X}, which was in the range from 59.3 to 62.1 $\mathrm{mg \cdot MJ^{-1}}$ for the temperature range from 820 to 950 °C. The detected decrease in air-combustion series No 1 could be caused by a slightly decreasing volumetric fraction of O_2 in the dry flue gas, although we tried to keep it constant. ϕ_{O_2} strongly affects NO_X formation, as was noted in Section 7.1.1. For $t_{BFB} = 840$ °C, the average ϕ_{O_2} was 6.44 %, while for $t_{BFB} = 920$ °C it was only 5.54 %.

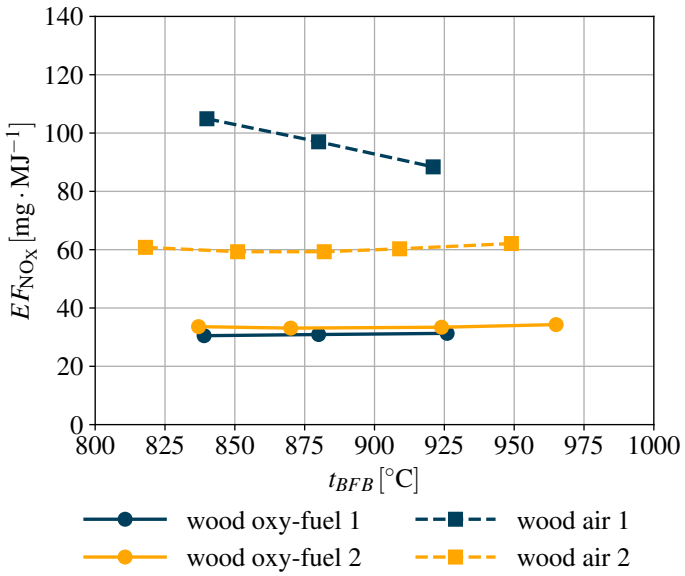

Figure 7.4: Experimental results, combustion of wooden pellets: Emission factors of NO_X in dependence on the fluidized bed temperature.

7.1.3 Effect of staged supply of oxygen

7.1.3.1 NO_X formation

To study the effect of staged oxygen supply on NO_X formation, three different approaches were chosen, as indicated in Section 5.2.3. When changing the variable parameter ψ (ratio of secondary to primary O_2 volumetric flows), the parameters that were kept constant were:

a) $t_{BFB} = 880\,°C$ and $\phi_{O_2} = 6\,\%$ vol.,

b) $t_{BFB} = 880\,°C$ and $\phi_{O_2} = 9\,\%$ vol., and

c) $(\phi_{O_2}/\phi_{CO_2})_{prim} = 40\,\%$ and $\phi_{O_2} = 6\,\%$ vol.

Combustion of lignite

In case of lignite combustion (Figure 7.5), the experimental series '$t_{BFB} = 880\,°C$, $\phi_{O_2} = 6\,\%$ vol.' was measured twice. The series No 1 and 2 differ slightly in fuel load, but other parameters were very similar. While the fuel load was $3.6\,kg \cdot h^{-1}$ in series No 1, in series No 2 it was $3.9\,kg \cdot h^{-1}$.

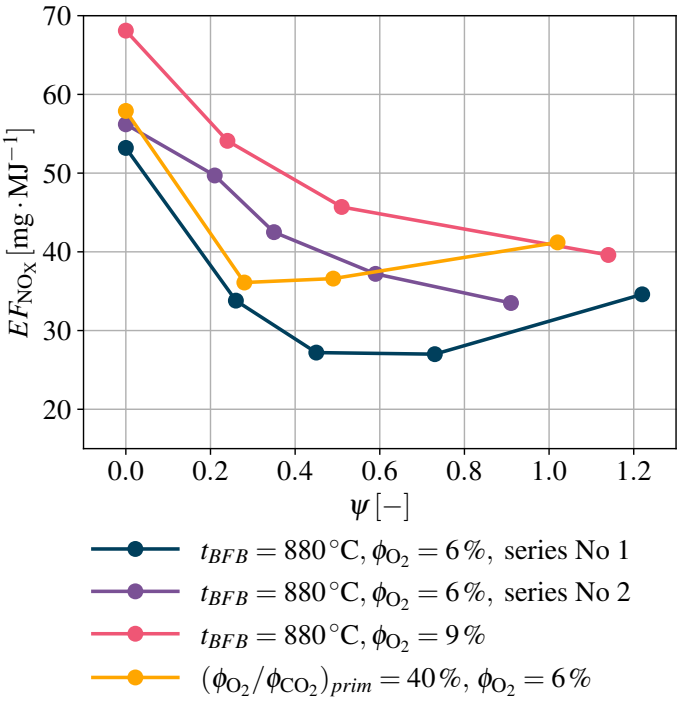

Figure 7.5: Experimental results, combustion of lignite: Emission factors of NO_X in dependence on the staged supply of oxygen expressed using the ratio of the volumetric flows of secondary and primary O_2 ψ.

It can be seen in Figure 7.5 that oxygen staging generally led to a reduced formation of NO_X for all experimental approaches, however, it is not valid that every increase in the ψ ratio always led to a more intensive NO_X reduction. In Tables B.3, B.4, and B.5 it can be seen that each experimental series ended with a strong lack of oxygen in the primary gas ($\lambda_{prim} \in \langle 0.53 - 0.78 \rangle$) for the highest ratio ψ and had to cause a rather gasification environment in the dense bed. Sub-stoichiometric conditions were reached in the primary combustion zone at $\psi = 0.26$ for the series '$t_{BFB} = 880\,°C$, $\phi_{O_2} = 6\,\%$ vol.' No 1, at $\psi = 0.59$ for the series No 2, at $\psi = 0.24$ for the series '$t_{BFB} = 880\,°C$, $\phi_{O_2} = 9\,\%$ vol.', and at $\psi = 0.49$ for the series '$(\phi_{O_2}/\phi_{CO_2})_{prim} = 40\,\%$, $\phi_{O_2} = 6\,\%$ vol'. The most significant reduction of NO_X was detected for the value of ratio ψ of 0.5 (49 %) in the series '$t_{BFB} = 880\,°C$, $\phi_{O_2} = 6\,\%$' No 1, for $\psi = 0.91$ (40 %) in the series No 2, for $\psi = 1.14$ (42 %) in the series '$t_{BFB} = 880\,°C$, $\phi_{O_2} = 9\,\%$', and for $\psi = 0.28$ (38 %) in the series '$(\phi_{O_2}/\phi_{CO_2})_{prim} = 40\,\%$, $\phi_{O_2} = 6\,\%$. Further raising of the ψ ratio led to an increase of the NO_X concentration in the

flue gas in case of the series '$t_{BFB} = 880\,°C$, $\phi_{O_2} = 6\,\%$ No 1' and '$(\phi_{O_2}/\phi_{CO_2})_{prim} = 40\,\%$, $\phi_{O_2} = 6\,\%$'. A higher concentration of CO in the flue gas (about 1 400 - 2 200 ppmv) was measured indicating an incomplete combustion within the oxygen staging experiments for the '$(\phi_{O_2}/\phi_{CO_2})_{prim} = 40\,\%$, $\phi_{O_2} = 6\,\%$' approach, which could possibly affect the formation of NO_X. However, it is known that CO participates in the NO_X reduction, so the increased CO formation is in disagreement with the observed NO_X increased values.

It can be observed that the increase in oxygen stoichiometry (characterized by the increase in the final oxygen concentration from 6 to 9 %) generally promoted the formation of NO_X. The NO_X emission factor was about 21 % ($15.8\,mg \cdot MJ^{-1}$) higher in the reference case without oxygen staging ($\psi = 0$) at the fluidized bed temperature of 880 °C. The partial pressure of oxygen in the combustor is obviously important for the oxidation of N-containing compounds originating in fuel-bound nitrogen, as confirmed in Section 7.1.1.

Combustion of wooden pellets

In the case of the combustion of spruce wood, only three series of experiments were carried out corresponding to the proposed experimental approaches (Figure 7.6). The fuel load was kept at a value of $9\,kg \cdot h^{-1}$ and the LWA P3 was used as the fluidized bed material in all experimental series. It can be seen that this time, each increase in the ψ ratio led to a more intensive NO_X reduction. The emission factors of NO_X decreased almost proportionally with the increasing ratio ψ.

In Tables B.8, B.9, and B.10 it can be observed that each experimental series ended with a strong lack of oxygen in the primary gas ($\lambda_{prim} \in \langle 0.49 - 0.6 \rangle$) for the highest ratio ψ. In all series, sub-stoichiometric conditions were reached in the primary combustion zone already in the first cases of staged O_2 supply at $\psi \approx 0.25$. The maximum NO_X reduction efficiency achieved in the studied range of parameters was about 36 % for $\psi = 0.7$ in the case of '$t_{BFB} = 880\,°C$, $\phi_{O_2} = 6\,\%$ vol.', 48 % for $\psi = 1.16$ in the case of '$t_{BFB} = 880\,°C$, $\phi_{O_2} = 9\,\%$ vol.', and 54 % for $\psi = 0.91$ in the case of '$(\phi_{O_2}/\phi_{CO_2})_{prim} = 40\,\%$, $\phi_{O_2} = 6\,\%$ vol.'.

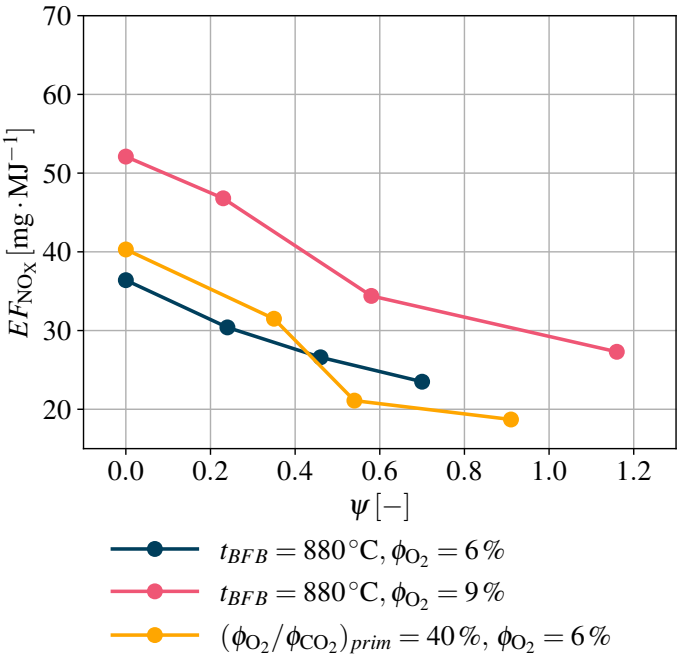

Figure 7.6: Experimental results, combustion of wooden pellets: Emission factors of NO_X in dependence on the staged supply of oxygen expressed using the ratio of the volumetric flows of secondary and primary O_2 ψ.

In all the experiments with spruce wood combustion, the CO concentration in the flue gas was almost negligible (less than 60 ppmv).

The conversion of fuel-bound nitrogen to NO_X was slightly higher for the wooden biomass combustion (N–NO $\in \langle 3.44 - 9.55 \rangle$) compared to lignite combustion in general (N–NO $\in \langle 1.91 - 4.8 \rangle$), as can be seen in appended tables, although the NO_X emission factors measured for biomass combustion were lower. This is due to the significantly different nitrogen content in the fuel. This difference is affected by the nitrogen distribution in the fuels. In lignite, most of the nitrogen is bounded to char, while in wood, nitrogen is particularly found in volatiles [145, 146]. The reaction pathways of both char-N and volatile-N can lead to form NO but as well to form unreactiveN_2 in dependence on the reaction conditions. However, the NO forming routes are favored in the reaction mechanism of volatile nitrogen compounds, while in the case of char-N it is likely the opposite [146]. The definition of $N - NO$ conversion assumes that all nitrogen oxides are formed from the fuel-bound N, as stated in Section 3.5.

7.1.3.2 Temperature profile

Staged injection of the oxidizer can move the dominant combustion zone in the BFB from the dense bed to the freeboard. As a consequence, the temperature profile in the combustor is affected and the freeboard temperature can be raised significantly. This effect is stronger in the oxy-fuel combustion, when pure oxygen is supplied without any additional heat carrier (like nitrogen in air-combustion) to the freeboard. The elevated freeboard temperature creates an opportunity for the effective application of the selective non-catalytic reduction (SNCR).

The need to implement secondary measures for further NO_X reduction is given by the fact that the requirement for CO_2 purity for the transportation and storage systems mentioned in Section 1.2 concerning NO_X up to 100 ppmv is claimed. The disadvantage of the oxy-fuel combustion inhere in a lower specific volume of the off-gas compared to air mode, which results in relatively higher real NO_X concentrations. Even for the best NO_X reduction efficiencies reached within the presented experiments, the NO_X volumetric fractions in the dry flue gas were about 200 ppmv, which is not sufficiently low to meet the requirements.

For lignite combustion, the temperature height profiles in the experimental facility are shown in Figure 7.7. The corresponding results measured for the wooden pellets are given in Figure 7.8. In all charts, the horizontal dash-dot line represents the height at which secondary oxygen is injected. The position of the last thermocouple in the freeboard is 1.64 m above the distributor of the primary gas and is referred to as the height h_{max}. The y axis of the charts represents the ratio of given height to h_{max}.

Combustion of lignite

Because the lignite contains mainly fixed carbon, the highest temperatures were achieved in the bed zone, where heterogeneous combustion occurs. Then, the temperature of the flue gas decreased as the flue gas raised in the facility in the case of non-staged lignite combustion. When the volumetric flow of primary oxygen was reduced with increasing ψ, the

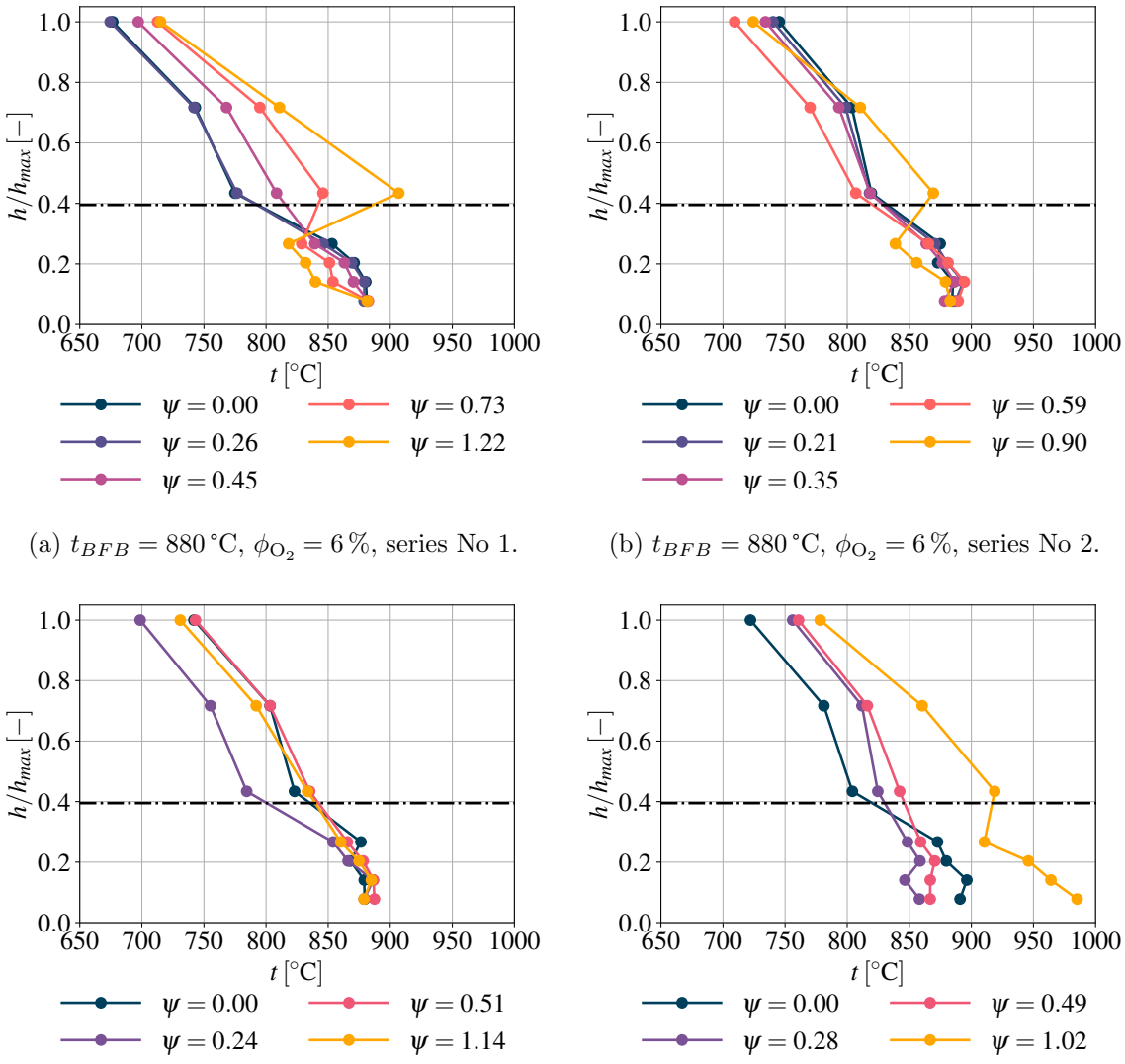

(a) $t_{BFB} = 880\,°C$, $\phi_{O_2} = 6\,\%$, series No 1.

(b) $t_{BFB} = 880\,°C$, $\phi_{O_2} = 6\,\%$, series No 2.

(c) $t_{BFB} = 880\,°C$, $\phi_{O_2} = 9\,\%$.

(d) $(\phi_{O_2}/\phi_{CO_2})_{prim} = 40\,\%$, $\phi_{O_2} = 6\,\%$.

Figure 7.7: Temperature heights profiles in the experimental facility in dependence on the secondary to primary oxygen ratio ψ for lignite combustion.

sub-stoichiometric conditions caused a partial gasification of the lignite in the fluidized bed and the released volatiles oxidized in the freeboard section. The most obvious dependence of the temperature profile on the stoichiometric conditions in the fluidized bed (as a consequence of increasing ψ) can be seen in Figure 7.7a. With increasing ratio ψ, the temperature of the flue gas decreases directly above the bed, but increases when secondary oxygen is injected, although the freeboard temperature did not reach the optimal temperature range

for the SNCR (950 – 1050 °C) in this case. In Figure 7.7b representing the '$t_{BFB} = 880\,°C$, $\phi_{O_2} = 6\,\%$' series No 2, this trend is not so clear, but it can be observed that the temperature profile was changed and the freeboard temperature increased for the highest ratio $\psi = 0.9$. In the case of the '$t_{BFB} = 880\,°C$, $\phi_{O_2} = 9\,\%$' approach (Figure 7.7c), the temperature height profile did not show the same dependence as described above, however, a slight increase in the freeboard temperature can be observed with an increasing ratio ψ. It can be caused by a higher overall oxygen stoichiometry, which could promote oxidation in the dense bed. In case of the '$(\phi_{O_2}/\phi_{CO_2})_{prim} = 40\,\%$, $\phi_{O_2} = 6\,\%$' approach (Figure 7.7d), the increase in the freeboard temperature with the increasing ratio ψ is visible, but the fluidized bed temperatures are different and so the height profile curves are shifted. The higher temperature of the fluidized bed measured for $\psi = 1.02$ might have possibly enhanced the oxidation of char, so there were not enough volatiles to increase the freeboard temperature above the temperature of the fluidized bed.

Combustion of wooden pellets

The different distributions of the combustibles to the char and volatiles among the fuels can be seen in the presented figures very clearly. The high content of volatiles in spruce wood causes a higher freeboard temperature even in non-staged combustion. Only part of the primary oxygen is consumed for char oxidation and the rest is available for combustion of released volatiles. It can be seen that all the temperature height profiles in Figure 7.8 are more straight compared to those obtained for the combustion of lignite. Within all the experiments, the freeboard temperature increased with each increase in the ratio ψ. For the highest measured ψ, the freeboard temperature of about 950 °C was achieved, which is in the optimal temperature range for the SNCR in the oxy-fuel mode.

The flue gas temperature directly above the fluidized bed was not affected by staged injection of oxygen in the cases of approaches '$t_{BFB} = 880\,°C$, $\phi_{O_2} = 6\,\%$' and '$t_{BFB} = 880\,°C$, $\phi_{O_2} = 9\,\%$', as can be observed in Figures 7.8a and 7.8b. Only the temperatures above the secondary oxygen nozzles were affected. The same situation can be observed

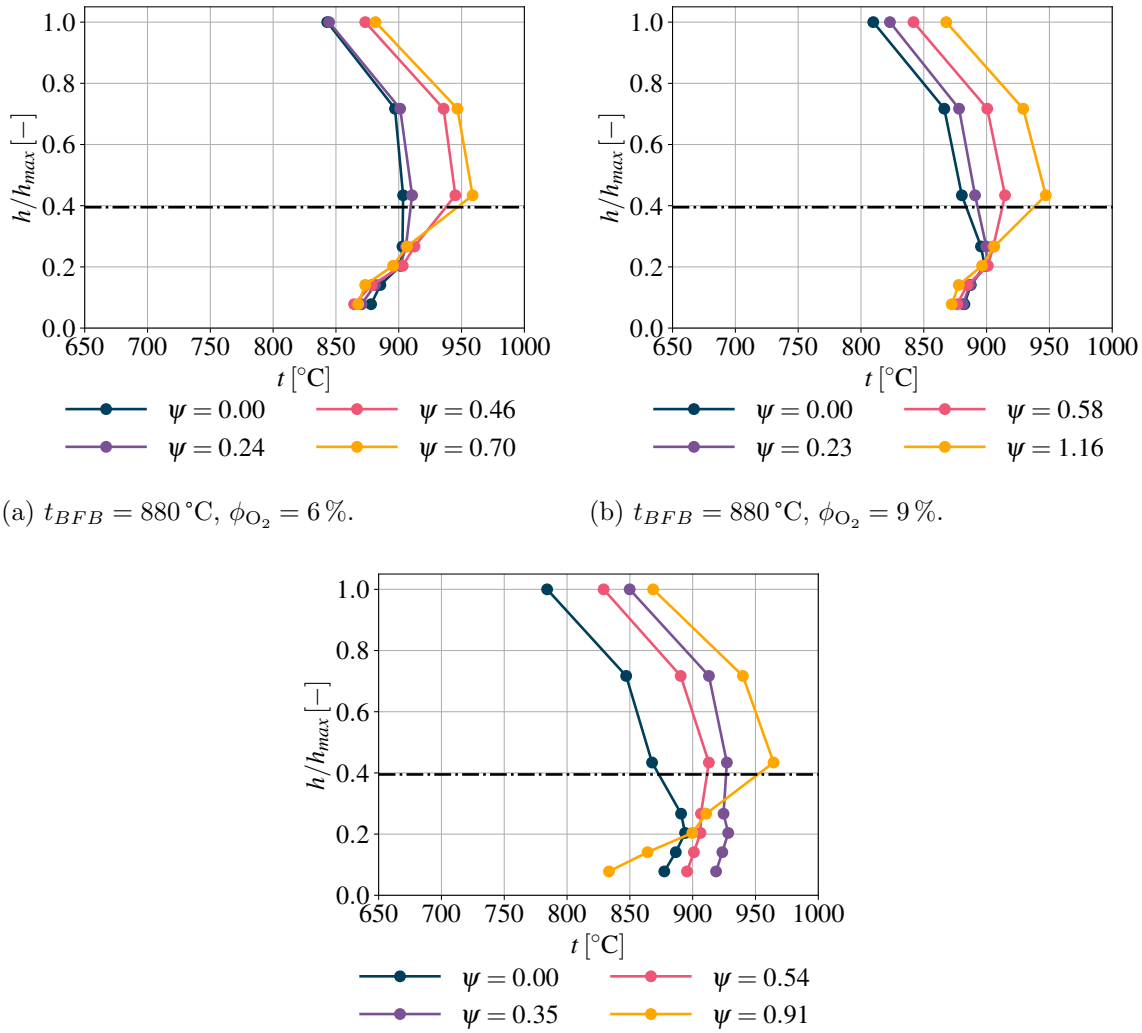

(a) $t_{BFB} = 880\,°\text{C}$, $\phi_{O_2} = 6\,\%$.

(b) $t_{BFB} = 880\,°\text{C}$, $\phi_{O_2} = 9\,\%$.

(c) $(\phi_{O_2}/\phi_{CO_2})_{prim} = 40\,\%$, $\phi_{O_2} = 6\,\%$.

Figure 7.8: Temperature height profiles in the experimental facility in dependence on the secondary to primary oxygen ratio ψ for combustion of wooden pellets.

in the case for constant ϕ_{O_2}/ϕ_{CO_2} ratio in the primary gas where different fluidized bed temperatures were measured. For the highest oxygen staging at $\psi = 0.91$, the temperature gradient was significantly higher between the bed and the freeboard probably due to the combination of low superficial velocity and sub-stoichiometric conditions in the primary zone.

7.2 Pilot-scale experimental results of the NO_X formation and speciation

These supplementary experiments were conducted to study the shares of NO, NO_2, and N_2O in the nitrogen oxides formed in the oxy-fuel combustion in a BFB using the pilot-scale 500 kW_{th} BFB combustor equipped with analyzers, which are able to measure concentrations of these oxides separately.

The operation of the pilot-scale combustor was accompanied by significant air ingress, which caused that the volumetric fraction of CO_2 in the dry flue gas was reached in the range from only 60 to 70 % vol. This ingress was caused by a still unaddressed leakage in the flue gas duct or in the sealing of the shaft of the primary or flue gas fan.

The graphic results of the pilot-scale experiments are given in Figures 7.9, 7.10, and 7.11. The detailed results in tables are given in Appendix C at the end of this thesis. The volumetric fraction of NO_X was measured independently of the volumetric fractions of NO and NO_2. Therefore, the sum of the volumetric fractions of NO and NO_2 is not always equal to the value reported for NO_X. Nevertheless, the agreement of these results is very good.

7.2.1 Effect of oxygen stoichiometry

The dependence of the volumetric fractions of NO, NO_2, N_2O, and NO_X in the dry flue gas on the oxygen stoichiometry expressed using the volumetric fraction of O_2 in the dry flue gas is given in Figure 7.9 and Table C.1. It can be observed that the increase in the volumetric fraction of O_2 in dry flue gas significantly promoted the formation of NO and NO_2. The volumetric fractions of these oxides in dry flue gas rose from 165 ppmv to 200 ppmv (increase of 17.5 %) in the case of NO and from 4 ppmv to 10 ppmv (increase of 150 %) in the case of NO_2 when ϕ_{O_2} was increased from 6.4 to 12.2 % vol. No clear impact of the oxygen stoichiometry on the formation of N_2O was observed within these experiments.

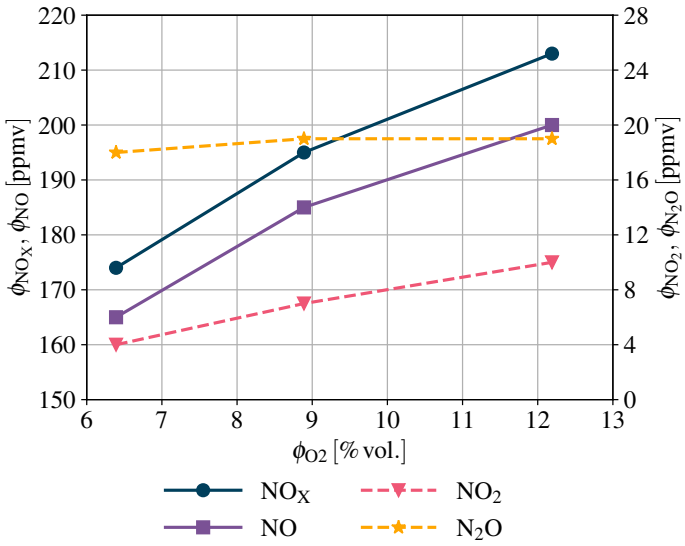

Figure 7.9: Pilot-scale experimental results: Volumetric fractions of NO, NO_2, N_2O, and NO_X in dry flue gas in dependence on the oxygen stoichiometry.

7.2.2 Effect of fluidized bed temperature

The effect of fluidized bed temperature on the formation of NO, NO_2, and N_2O is described in Figure 7.10 and Table C.2. The fluidized bed temperature varied in the range from 840 to 960 °C within these experiments. A slight temperature sensitivity can be observed in the formation of NO and N_2O at temperatures in the range from 880 to 960 °C. With the increase in fluidized bed temperature, the volumetric fraction of NO increased from 160 to 179 ppmv (increase of 11.9 %) and the volumetric fraction of N_2O increased from 13 to 15 ppmv (increase of 15.3 %). The formation of NO_2 did not show any dependence on temperature of the fluidized bed.

7.2.3 Effect of staged supply of oxygen

The results showing the impact of the staged supply of oxygen on the formation of NO, NO_2, and N_2O are given in Figure 7.11 and Table C.3. Six steady-state cases were measured in which the ratio of volumetric flows of secondary and primary oxigen ψ was changed from 0 (non-staged combustion) to 1.31. Similarly as within laboratory-scale experiments,

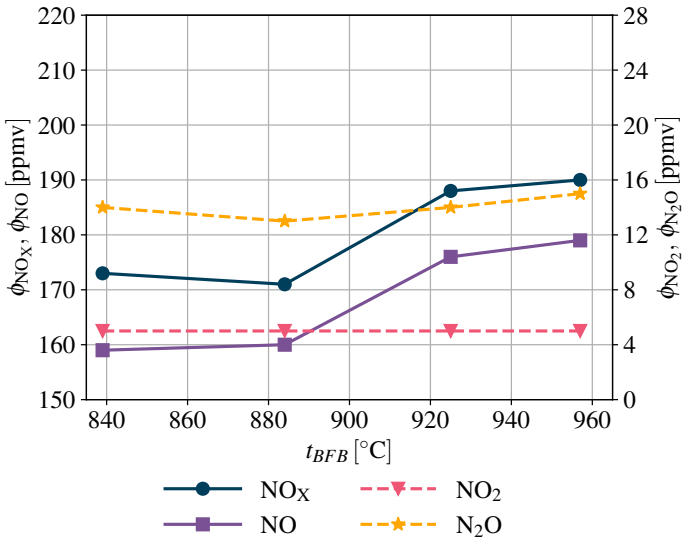

Figure 7.10: Pilot-scale experimental results: Volumetric fractions of NO, NO_2, N_2O, and NO_X in dry flue gas in dependence on the fluidized bed temperature.

the volumetric fraction of oxygen in the dry flue gas ($\phi_{O_2} = 8\,\%$ vol.) and the fluidized bed temperature ($t_{BFB} = 880\,°C$) were kept constant. Sub-stoichiometric conditions in the dense bed were reached even for the first staged case ($\lambda_{prim} = 0.82$) with the ratio $\psi = 0.3$. The staged supply of oxygen slightly promoted the formation of NO in these pilot-scale experiments. The volumetric fraction of NO increased from 160 to 179 ppmv when comparing the cases with the ratio $\psi = 0$ and 1.31. A decrease in the volumetric fraction of NO is apparent for the ratio $\psi = 0.3$, but it was caused by a slightly lower total stoichiometry of oxygen corresponding to $\phi_{O_2} = 6.7\,\%$ vol. No significant impact of the staged supply of oxygen on the formation of NO_2 was observed. The staged supply of oxygen led to an increase in ϕ_{N_2O} from 13 to 20 ppmmv, when the ratio ψ increased from 0 to 0.3. The continued increase in the ratio ψ did not cause significant changes in the concentration of N_2O.

7.2.4 Evaluation of results of the pilot-scale experiments

Despite the low concentration of CO_2 in the flue gas from the pilot-scale combustor within the experiments, the results give valuable insight into the speciation of nitrogen oxides in the

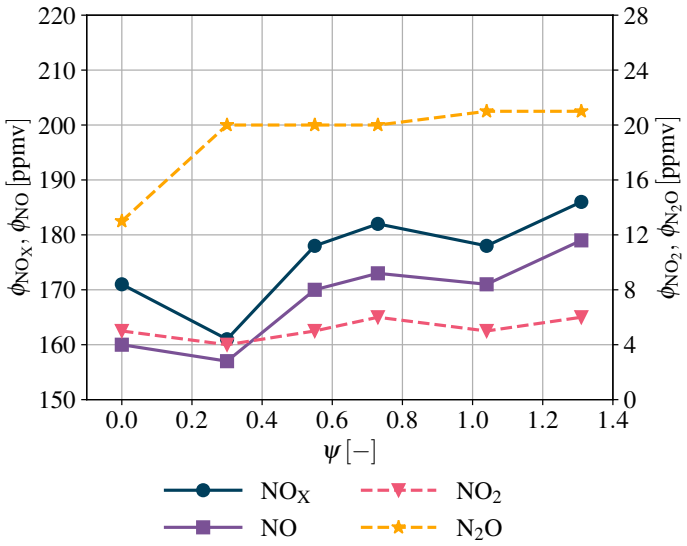

Figure 7.11: Pilot-scale experimental results: Volumetric fractions of NO, NO_2, N_2O, and NO_X in dry flue gas in dependence on the staged supply of oxygen expressed using the ratio of the volumetric flows of secondary and primary oxygen ψ.

oxy-fuel combustion in a BFB. The volumetric fraction of NO in dry flue gas varied in the range from 160 to 200 ppmv in all experimental cases, while the volumetric fraction of NO_2 was in the range from 4 to 10 ppmv, and the volumetric fraction of N_2O was in the range from 13 to 21 ppmv. On average, the shares of the volumetric fractions of NO, NO_2, and N_2O in the total sum of nitrogen oxides were about 88.4 %, 2.8 %, and 8.8 %, respectively.

The pilot-scale experimental results of NO_X (sum of NO and NO_2) agree well with the laboratory-scale experimental results of oxy-fuel combustion of spruce wood, which reported similar trends in the cases of dependence on oxygen stoichiometry and fluidized bed temperature. Only the staged supply of oxygen did not lead to a reduction of NO_X in the case of pilot-scale experiments. This could probably be due to the short residence time in the reduction zone, since the secondary oxygen inlets are placed very near above the dense bed section (only 550 mm above the distributor of fluidizing gas).

7.3 Comparison of numerical and experimental results of NO_X formation and discussion

7.3.1 Effect of oxygen stoichiometry

NO_X is formed mainly by the oxidation of fuel-bound nitrogen in oxy-fuel combustion in a BFB, hence the oxygen stoichiometry is clearly of importance when examining the key parameters affecting NO_X formation. In addition to the fact that the concentration of O_2 affects the kinetics of the oxidation reactions of the precursors of NO_X, it also affects the peak temperature of the char particles and the concentration of CO in the flue gas. While the peak temperature of char raises with increasing O_2 concentration, which promotes the conversion of char-N to NO_X, the concentration CO in the flue gas decreases, which inhibits the reduction of already formed NO_X. The comparison of experimental and numerical results of the overall volumetric fraction of NO_X is given in Figure 7.12. Here, the numbering of the experimental series corresponds to the denomination used in Section 7.1.1 based on different superficial velocities and power loads for the results of oxy-fuel combustion. In particular, the averages of superficial fluidizing gas velocities and fuel loads were as follows:

lignite, experiment 1	$u_0 \approx 1.1\,\mathrm{m \cdot s^{-1}}$	$m_{fuel} = 3\,\mathrm{kg \cdot h^{-1}}$,
lignite, experiment 2	$u_0 \approx 2.4\,\mathrm{m \cdot s^{-1}}$	$m_{fuel} = 7.1\,\mathrm{kg \cdot h^{-1}}$,
wooden pellets, experiment 1	$u_0 \approx 1.0\,\mathrm{m \cdot s^{-1}}$	$m_{fuel} \approx 5.2\,\mathrm{kg \cdot h^{-1}}$,
wooden pellets, experiment 2	$u_0 \approx 1.0\,\mathrm{m \cdot s^{-1}}$	$m_{fuel} = 5.6\,\mathrm{kg \cdot h^{-1}}$, and
wooden pellets, experiment 3	$u_0 \approx 1.9\,\mathrm{m \cdot s^{-1}}$	$m_{fuel} = 9\,\mathrm{kg \cdot h^{-1}}$.

The obvious impact of the stoichiometry of oxygen can be seen for both fuels. The numerical model with kinetic mechanism assembled by Hashemi et al. predicts a positive dependence of the NO_X formation on the oxygen stoichiometry, which is strongest at the lowest volumetric fraction of O_2 in dry flue gas and weakens with increasing ϕ_{O_2}. The experimental results showed the same trends in the studied range of $\phi_{O_2} \in \langle 3-9\,(12)\rangle\,\%$, although only a weak decrease in the gradient was observed for higher ϕ_{O_2} in the case of experimental

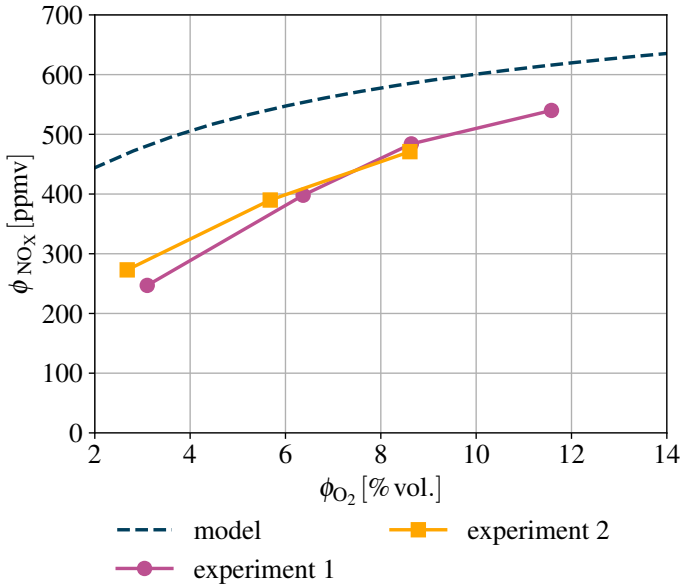

(a) Combustion of lignite.

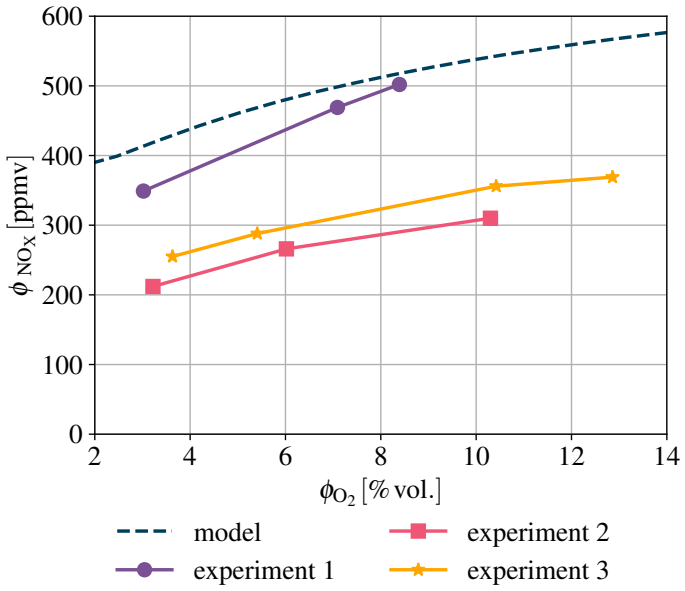

(b) Combustion of wood.

Figure 7.12: Comparison of numerical and experimental results: Volumetric fraction of NO_X in dry flue gas in dependence on the oxygen stoichiometry.

series No 1 of spruce wood oxy-fuel combustion (Figure 7.12b). The gradients of the studied dependence were always slightly higher in the case of experimental results compared to numerical results. An offset of about 100–200 ppmv can be observed in the comparison of

the numerical and experimental results of lignite oxy-fuel combustion (Figure 7.12a). The observed differences can be explained by the low dimensionality of the numerical approach and by the possibly inaccurate composition of volatiles, which was determined using data published for a different type of lignite. Therefore, the model should be used rather to compare trends than the absolute values. Although the numerical results do not match the experimental results exactly, they are still in very good agreement.

A positive effect of oxygen stoichiometry on NO_X formation was observed also by Lupiáñez et al. [49], who studied the oxy-fuel combustion of different types of coal in a laboratory-scale $90\,kW_{th}$ BFB with simulated FGR. They reached values of NO_X emission factors from 60 to $110\,mg \cdot MJ^{-1}$ for ϕ_{O_2} from 13 to 19 % in the case of lignite combustion. The values of emission factors presented within this thesis are similar, however, the range of ϕ_{O_2} measured by Lupiáñez et al. is significantly higher.

7.3.2 Effect of fluidized bed temperature

The comparison of numerical and experimental results of the effect of fluidized bed temperature on NO_X formation is given in Figure 7.13. Here, the numbering of the experimental series corresponds to the denomination used in Section 7.1.2 based on different superficial velocities and power loads for the results of oxy-fuel combustion. In particular, the averages of superficial fluidizing gas velocities and fuel loads were as follows:

lignite, experiment 1	$u_0 \approx 1.1\,m \cdot s^{-1}$	$m_{fuel} \approx 4.2\,kg \cdot h^{-1}$,
lignite, experiment 2	$u_0 \approx 1.4\,m \cdot s^{-1}$	$m_{fuel} \approx 4.2\,kg \cdot h^{-1}$,
lignite, experiment 3	$u_0 \approx 2.2\,m \cdot s^{-1}$	$m_{fuel} \approx 7.3\,kg \cdot h^{-1}$,
wooden pellets, experiment 1	$u_0 \approx 1.0\,m \cdot s^{-1}$	$m_{fuel} \approx 6.0\,kg \cdot h^{-1}$, and
wooden pellets, experiment 2	$u_0 \approx 1.7\,m \cdot s^{-1}$	$m_{fuel} = 9.0\,kg \cdot h^{-1}$.

The results did not show as clear agreement as in the case of the effect of O_2 stoichiometry. In the case of lignite combustion (Figure 7.13a), all experimental series showed a positive dependence of the NO_X concentration on the fluidized bed temperature in the

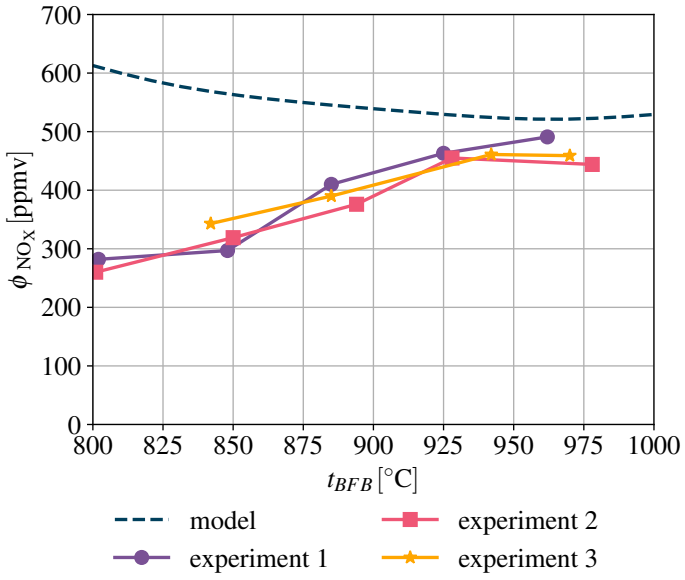

(a) Combustion of lignite.

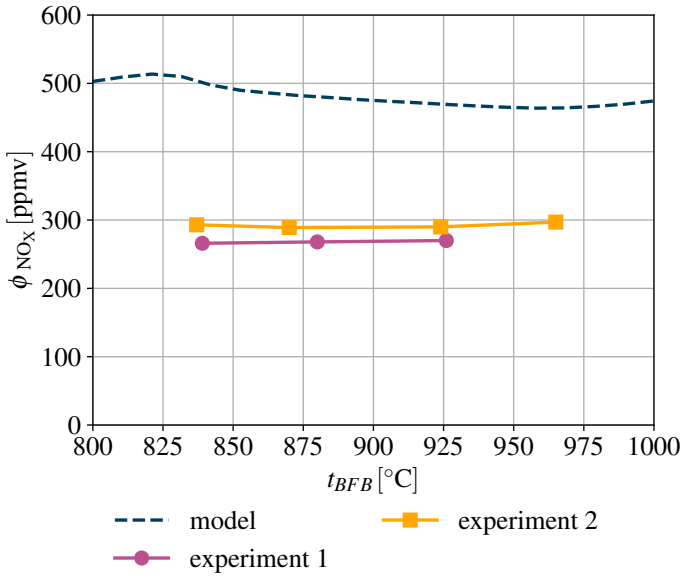

(b) Combustion of wood.

Figure 7.13: Comparison of numerical and experimental results: Volumetric fraction of NO_X in dry flue gas in dependence on the fluidized bed temperature.

studied temperature range at least for temperatures up to 920 °C. Similar effect was observed also by de las Obras-Loscertales et al. [42] and de Diego et al. [43] who studied the oxy-fuel combustion of anthracite in a 3 kW_{th} BFB with simulated FGR, by de las Obras-

Loscertales et al. [45] who studied oxy-fuel combsution of anthracite, lignite, and bituminous coal in the same device, or by Lupiáñez et al. [49].

The negative effect of the fluidized bed temperature apparent in the numerical results is caused particularly by the temperature sensitivity of the modeled NO_2 formation. The model did not predict any strong temperature sensitivity of NO formation in the case of lignite. Unfortunately, NO_2 concentration could not be measured separately within the experiments. De las Obras-Loscertales et al. [42, 45] and de Diego et al. [43] did not detect any NO_2 fractions higher than 10 ppmv. Therefore, the NO_2 formation predicted by the numerical model seems slightly over-rated. However, any of the other examined kinetic mechanisms did not provide lower NO_2 concentrations, as can be seen in Section 6.1. Therefore, the reason for the high formation of NO_2 could be the possibly inaccurate composition of volatiles and chars used within the numerical model.

In the case of spruce wood combustion, no effect of the fluidized bed temperature on the formation of NO_X was observed within the studied range (Figure 7.13b). The NO_X volumetric fraction provided by the numerical model also does not show any strong temperature sensitivity. The impacts of the fluidized bed temperature on the formation of NO and NO_2 were opposite and equalized in the overall volumetric fraction of NO_X. There is no reference in the published literature on oxy-fuel combustion of biomass in a BFB with which the results could be compared.

7.3.3 Effect of staged supply of oxygen

Staged oxygen supply theoretically leads to reduced fuel-N conversion to NO_X and increased conversion to N_2 in the sub-stoichiometric primary combustion zone. Subsequently, the unburned carbon components are oxidized in the secondary combustion zone in the freeboard section, where the secondary oxidizer is introduced. The conditions in this section should not allow any significant oxidation of N_2 and therefore the method of the staged oxygen supply should lead to significantly reduced NO_X formation. The comparison of numerical and experimental results on the impact of the staged supply of O_2 on the formation of NO_X

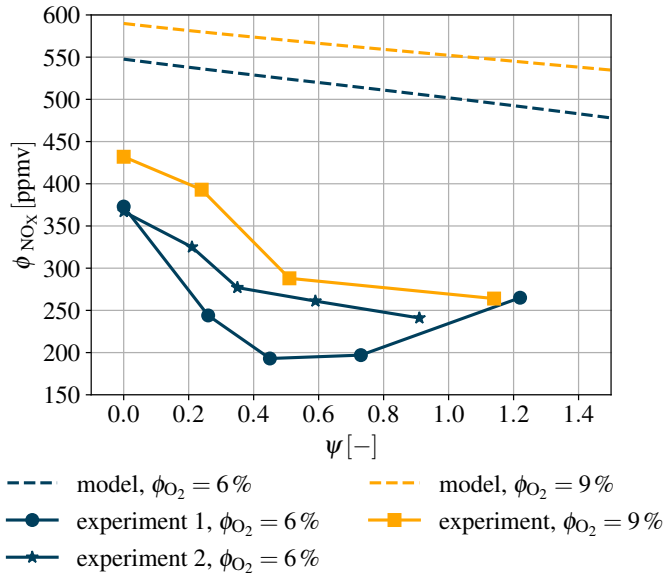

(a) Combustion of lignite.

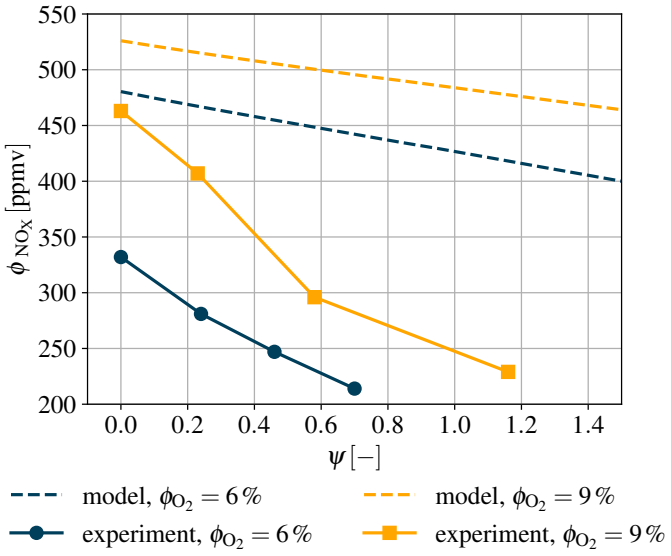

(b) Combustion of wood.

Figure 7.14: Comparison of numerical and experimental results: Volumetric fraction of NO_X in dry flue gas in dependence on the staged supply of oxygen expressed using the ratio of the volumetric flows of secondary and primary O_2 ψ.

is shown in Figure 7.14. The experimental series with constant fluidized bed temperature were selected for comparison with the numerical results. The composition of the primary gas changes within the numerical model with the change in the distribution of the supplied

oxygen, therefore the experimental results with the approach of constant composition of the primary gas are not suitable for comparison. The experimental series given in Figure 7.14 are referred to in a similar way to those in Section 7.1.3. In the case of lignite combustion (Figure 7.14a), the experimental series with constant fluidized bed temperature and $\phi_{O_2} = 6\,\%$ vol. was measured twice. The series No 1 and 2 differ slightly in fuel load, but other parameters were very similar. While the fuel load was $3.6\,\mathrm{kg \cdot h^{-1}}$ in series No 1, in series No 2 it was $3.9\,\mathrm{kg \cdot h^{-1}}$.

The comparison of numerical and experimental results shows good agreement in terms of trends. For both fuels, two experimental and numerical series are presented, differing in the final ϕ_{O_2} in the dry flue gas. The ϕ_{O_2} of $9\,\%$ vol. led to higher NO_X concentrations compared to $\phi_{O_2} = 6\,\%$ vol. in each case. In all series except for lignite combustion at $\phi_{O_2} = 6\,\%$ vol., every increase of the secondary to primary oxygen ratio ψ led to a decrease in the NO_X volumetric fraction. In the case of lignite combustion at $\phi_{O_2} = 6\,\%$ vol., the NO_X reduction had an optimum at $\psi = 0.5$ for the experimental results. For higher ratios ψ, the NO_X volumetric fraction was raised again. The numerical model predicted a still decreasing concentration of NO in the flue gas at an increasing ratio ψ for both fuels, both oxygen stoichiometries, and for the ratio ψ in the studied range ($\psi \leq 2$).

It can be seen in Figure 7.14 that the effect of the staged supply of oxygen on the reduction of NO_X was more intensive throughout all experimental series for both fuels than it was predicted by the numerical model. Gradients of the curves that describe the experimental and corresponding numerical results are steeper in the case of experimental results. In addition, offsets of approximately 300 ppmv between the experimental and corresponding numerical results can be seen, the numerical model predicted higher volumetric fractions of NO_X in flue gas than were measured within the experiments. The reasons explaining the source of this discrepancy were discussed in previous sections.

The effect of staged supply of oxidizer on the formation of NO_X in oxy-fuel combustion in a BFB was studied by Lupiáñez et al. [50], Díez et al. [51], or Jankowska et al. [56]. Lupiáñez et al. observed a strong positive effect on the reduction of NO in the case of lignite

combustion, but a small to no effect in the case of anthracite combustion. They used two artificial mixtures of O_2 and CO_2 (27/78 and 45/55 %, respectively) for both the primary and secondary oxidizer. Using the mixture of 28/72 % O_2/CO_2 they achieved a reduction of about 25 % in the case of anthracite and about 38 % in the case of lignite for the ratio of secondary to primary oxidizer 0.2. With the mixture of 45/55 % O_2/CO_2 they achieved almost no reduction in the case of anthracite and about 45 % in the case of lignite. The maximum ratio of secondary to primary oxidizer was also 0.2. Almost identical results for anthracite combustion were reached by Díez et al. [51] using the same experimental facility. Jankowska et al. [56] studied the impact of the staged supply of oxidizer on nitrogen chemistry in oxy-fuel combustion of bituminous coal in a 0.1 MW_{th} CFB. They used a constant ratio of volumetric flows of the secondary and primary oxidizer of 0.43 and changed the volumetric fraction of O_2 in the artificial mixtures of the secondary oxidizer from 21 to 35 % vol. The primary gas was a mixture of 21/79 % O_2/CO_2. They observed that an increase in the concentration of O_2 in secondary gas results in a significant decrease in N_2O concentrations and an increased conversion of fuel-N to NO. They did not detect any NO_2 in the flue gas downstream the combustor. Their conclusions are opposite to the numerical results, but they are similar to the pilot-scale experimental results presented in this thesis. The discrepancy in the results can be caused by the to short residence time of the gas in the reduction zone or by different fuel and experimental approach used by Jankowska et al.

Chapter 8

Conclusions

In this thesis, the characterization of NO_X formation in oxy-fuel combustion of two fuels (a Czech lignite and spruce wood pellets) in a BFB combustor was presented. The main goals of this study were: creation of a numerical model describing the formation of nitrogen oxides in oxy-fuel combustion in a BFB using chemical kinetics; design and preparation of a lab-scale BFB combustor operating under oxy-fuel conditions with real flue gas recirculation; an experimental evaluation of the nitrogen oxides formation in the laboratory-scale BFB facility; and validation of the numerical model. These goals were fully achieved.

8.1 Evaluation of the presented results

A 1-D plug flow reactor was used to model the oxy-fuel combustion in a BFB within the numerical part of this thesis. Four different kinetic mechanisms were used to calculate the progress of homogeneous gaseous reactions and the results were compared. There were significant differences in the formation of nitrogen oxides predicted by these mechanisms, particularly in the shares of NO, NO_2, and N_2O. Using all mechanisms except one, the model calculated unrealistically high final concentrations of NO_2. Nitrogen dioxide should not be formed in significant amounts at temperatures typical for BFBs, therefore, the mechanism that led to the lowest formation of NO_2 was selected for further analysis. This mechanism

was proposed by Hashemi et al. [127] for modeling of nitrogen chemistry in the oxy-fuel combustion of pulverized coal. The results obtained using this mechanism were analyzed in detail and compared with the experimental results.

The experimental part was carried out using a 30 kW_{th} BFB combustor with real flue gas recirculation. The effects of key operating parameters, oxygen stoichiometry and fluidized bed temperature, on NO_X (sum of NO and NO_2) formation were studied, as well as the efficiency of the only primary measure applicable in oxy-fuel combustion in a BFB, the staged supply of oxygen. The results showed that the formation of NO_X is highly sensitive to oxygen stoichiometry for both fuels, since oxygen availability is essential for the oxidation of fuel-N. The sensitivity of NO_X formation to fluidized bed temperature was observed only in the case of lignite combustion, where increasing temperature promoted NO_X formation. In the case of wood combustion, no clear impact of the fluidized bed temperature on the concentration of NO_X in the flue gas was observed in the studied temperature range from 820 to 960 °C. Repeating these experimental series at different power loads of the combustor and so at different fluidization velocities did not reveal any significant effect of these parameters on the formation of NO_X. The comparison of results achieved in the oxy-fuel combustion and in the air-combustion regime showed that the sensitivity of the NO_X formation to the studied parameters is comparable, but the conversion rate of fuel-N to NO_X is significantly lower in the case of oxy-fuel combustion for both fuels. The results of the staged supply of oxygen showed that a significant NO_X reduction can be achieved (about $40 - 50\,\%$) deploying the sub-stoichiometric conditions of oxygen in the dense bed and subsequent oxidation conditions in the freeboard section. However, it was possible to reach the volumetric fraction of NO_X in the dry flue gas of only about 200 ppmv at minimum within the experiments, which is still about 100 ppmv higher than is required in CO_2 processing and transport processes. This shows the limits of NO_X reduction achievable by adjusting the parameters of the combustion process and applying primary measures.

It can be concluded that the numerical and experimental results show quite good agreement in the overall production of NO_X. The sensitivity of the formation of NO_X to the

oxygen stoichiometry observed within the experimental part was confirmed by the numerical model, as was the extension of this sensitivity within the reduction of NO_X by the staged supply of oxygen. The effect of the fluidized bed temperature observed in the case of lignite combustion was not confirmed within the studied temperature range, where the numerical model predicted the negative effect of the fluidized bed temperature on the formation of NO_X. On the contrary, there was an agreement of the numerical and experimental results in the case of the oxy-fuel combustion of wood, where no effect of the fludized bed temperature on the formation of NO_X was observed. It appeared that the numerical model predicted slightly higher NO_2 formation than was expected and was also observed within competitive studies. The concentration of NO_2 could not be measured separately within the experimental part of this thesis performed using the laboratory-scale combustor. Therefore, additional pilot-scale experimental tests were performed using a 500 kW_{th} BFB combustor equipped with analyzers to measure the concentrations of NO, NO_2, and N_2O separately to verify the accuracy of the model. These experimental tests were carried out with only one fuel, spruce wood pellets. The results were in good agreement with the laboratory-scale experimental test (in terms of concentrations of NO_X) except for the effect of the staged supply of oxygen, which did not lead to a reduction of NO_X in the case of pilot-scale experiments, probably due to the very short residence time of the flue gas in the primary reduction zone. Within pilot-scale experiments, the average volumetric shares of NO, NO_2, and N_2O in the flue gas were 88.4 %, 2.8 %, and 8.8 %, respectively. These results confirmed that, in particular, the formation of NO_2 calculated by the numerical model with all studied kinetic mechanisms except for the Hashemi et al. [127] mechanism is unrealistically high. In the case of the Hashemi et al. [127] mechanism, the shares of the volumetric fractions of NO, NO_2, and N_2O in the total sum of nitrogen oxides were in the ranges 79.1–94.1 %, 1.7–13.5 %, and 3.1–8.5 %, respectively, in dependence on the parameters of the combustion process. In this case, the numerical results correspond well to the pilot-scale experiments.

The numerical model is based on a very significant simplification, which allows the application of kinetic mechanisms of gaseous reactions on heterogeneous combustion in a BFB,

where the solid fuel is replaced with a mixture of gaseous products of the fuel devolatilization. The composition of volatiles was calculated on the basis of conversion ratios found in the published literature because it was not possible to measure it experimentally directly at the stage of fuel decomposition. Although the calculation was adjusted to the fuels used within the experiments, the resulting composition of volatiles can be questioned. The composition of the devolatilized fuel is considered constant in all sets of boundary conditions applied within the model to simulate the effects of the operating parameters studied in the experimental part. This is also inaccurate because the operating parameters of the combustion process also affect the heterogeneous reactions. Despite these facts, the presented simplified model provided valuable information and was in reasonable agreement with the experimental results. Creating an accurate model that would include heterogeneous reactions with all interconnected issues like heat and mass transfers, catalytic effects, and fluidized bed hydrodynamics would require enormous amounts of numerical work, which is out of the scope of this thesis.

8.2 Future prospects of the study

The study presented in this thesis brought important results on NO_X formation in the oxy-fuel combustion in a BFB and characterization of the impacts of key operating parameters of the combustion process on nitrogen chemistry. It was not possible to reach the limiting volumetric fraction of NO_X in dry flue gas (100 ppmv) either by adjusting operating parameters or by a primary measure of NO_X reduction (staged supply of oxygen). It indicates that the application of secondary measures of NO_X reduction in the post-combustion process is inevitable. These measures can be the selective non-catalytic reduction (SNCR) and the selective catalytic reduction (SCR). These methods have been well known and applied in industry for years, however, only in conventional air-combustion conditions. The completely changed composition of the reaction atmosphere in the oxy-fuel combustion can significantly affect the performance of both reduction methods. Therefore, it is necessary to experimentally characterize their efficiencies in oxy-fuel conditions in dependence on the

most important parameters, which are the process temperature and the stoichiometry of the reducing agent. The results presented within this thesis suggested that the cost-effective SNCR method may be sufficient to meet the required NO_X concentration in the flue gas. At the time of writing of this thesis, a project "Research centre for low-carbon energy technologies" focused on oxy-fuel combustion of biomass in fluidized beds is being solved at the Czech Technical University in Prague (CTU). This project is in part focused on SNCR and SCR. These topics are currently investigated and are in the scope of two Ph.D. studies at CTU.

Another prospect for further study is the accurate numerical model of the nitrogen chemistry including heterogeneous reactions in the oxy-fuel combustion in a BFB, which was mentioned in the previous Section. However, the combustion of solid fuels in a fluidized bed is a very complex and difficult to describe process. Additionally, gathering the boundary conditions for the model can be very difficult and will require a detailed study of the fuel, particularly of the nitrogen-containing compounds. Such a study can explain the effect of fluidized bet temperature on the formation of nitrogen oxides, which was not clearly managed within this thesis, however, the benefit for real practice of such a challenging study can be questioned.

8.3 Practical experience with oxy-fuel combustion

The experimental tests carried out within this study revealed that oxy-fuel combustion brings two very challenging problems that must be managed to achieve stable, safe and continuous operation and required CO_2 purity simultaneously. The first is condensation of water vapor in the FGR stream, and the second is ingress of air into all gas streams and throughout the combustion process.

It was mentioned that the flue gas from oxy-fuel combustion contains a significant fraction of water vapor that originates in the H and H_2O content in the fuel. For the overall CO_2 purity, the water vapor is not a considerable problem, since it can be separated easier than O_2

or non-condensable gases. However, it can cause significant problems in the treatment of the flue gas immediately downstream the combustion process. The oxy-fuel technology requires a large volume of FGR. To prevent extensive abrasion in the FGR duct and fan, the FGR inlet should be downstream of the solid particle separation unit. If the water vapor condenses anywhere in the FGR duct or in the solid particle separation unit, it negatively affects the lifetime of the equipment and usually leads to shutdown of the facility. Water and condensed acid gases can be very dangerous to the fan since they can pass through the shaft seal to the electric motor where they can cause a short circuit. In the solid particle separation unit, the water in contact with the ash can make a mud, reducing the particle separation effect or blocking the fly ash dump. Experiments have shown that keeping the temperature of FGR at a value of 150 °C is not always sufficient to prevent condensation of water vapor, since in some places with a longer gas residence time (particularly in the solid particle separation unit) the temperature can locally decrease below the dew point and condensation can appear. On the contrary, higher temperatures than 150 °C can be hazardous to the bearings of the FGR fan and are not desired for stable and continuous operation. A possible way to resolve this issue appears in cooling the FGR in a heat exchanger prior to the particle separation unit and the FGR fan, where a considerable part of H_2O would condense and then heating the FGR above the dew point temperature. This condenser would have to be robust and resistant to corrosion, abrasion, and blocking by the mixture of fly ash and water.

The conventional combustors of solid fuels operating slightly below atmospheric pressure are characterized by a certain level of air ingress. This ingress does not pose a bigger problem in air-combustion, furthermore, it prevents the leakage of the flue gas to the boiler room. However, the situation is quite different in the case of oxy-fuel combustion. Experiments have shown that to achieve low air ingress and high concentrations of CO_2, the combustor had to be operated over the atmospheric pressure. Although the experimental facility allows for very good sealing (which would not be possible on a larger scale, as was confirmed within the pilot-scale experiments), significant air ingress was achieved for pressures lower than atmospheric. The air was probably sucked in mainly by leaks in the fan shafts. The

over-pressure conditions in the combustor have consequences that have to be dealt with to ensure a safe environment and stable operation conditions. Since the flue gas leaks from the combustor, the boiler room must be equipped with very good air conditioning or ventilation. Particularly at non-standard conditions of the combustor operation (e.g., start-up or change of the combustion regime), the risk of health effects can be serious. Additionally, the atmosphere of the fuel feeding system must be separated from the atmosphere in the combustion chamber (e.g., by a set of turnstile fuel feeders) to prevent premature ignition of the fuel and fire in the hopper.

As a consequence, oxy-fuel combustion seems to be a promising technology for CO_2 capture from a flue gas, but requires a number of modifications of the combustor and its equipment, so retrofitting the technology to conventional air-combustion systems can be very difficult.

Bibliography

1. YORO, Kelvin O.; DARAMOLA, Michael O. Advances in Carbon Capture. In: Elsevier Inc., 2020, chap. CO_2 emission sources, greenhouse gases, and the global warming effect, pp. 3–28. ISBN 9780128196571. Available from DOI: 10.1016/b978-0-12-819657-1.00001-3.
2. UNITED NATIONS AND CANADA. *United Nations Framework Convention on Climate Change*. New York, 1992. Tech. rep. United Nations, General Assembly.
3. BUDINIS, Sara; KREVOR, Samuel; DOWELL, Niall Mac; BRANDON, Nigel; HAWKES, Adam. An assessment of CCS costs, barriers and potential. *Energy Strategy Reviews*. 2018, vol. 22, pp. 61–81. Available from DOI: 10.1016/j.esr.2018.08.003.
4. EUROPEAN COMMISSION. *EU Emissions Trading System (EU ETS)* [https://ec.europa.eu/clima/eu-action/eu-emissions-trading-system-eu-ets_en]. 2005. accessed: 3 June 2022.
5. TOFTEGAARD, Maja B.; BRIX, Jacob; JENSEN, Peter A.; GLARBORG, Peter; JENSEN, Anker D. Oxy-fuel combustion of solid fuels. *Progress in Energy and Combustion Science*. 2010, vol. 36, no. 5, pp. 581–625. Available from DOI: 10.1016/j.pecs.2010.02.001.
6. PEHNT, Martin; HENKEL, Johannes. Life cycle assessment of carbon dioxide capture and storage from lignite power plants. *International Journal of Greenhouse Gas Control*. 2009, vol. 3, no. 1, pp. 49–66. Available from DOI: 10.1016/j.ijggc.2008.07.001.
7. BEÉR, János M. High efficiency electric power generation: The environmental role. *Progress in Energy and Combustion Science*. 2007, vol. 33, no. 2, pp. 107–134. Available from DOI: 10.1016/j.pecs.2006.08.002.
8. YADAV, Sujeet; MONDAL, S.S. A review on the progress and prospects of oxy-fuel carbon capture and sequestration (CCS) technology. *Fuel*. 2022, vol. 308, p. 122057. Available from DOI: 10.1016/j.fuel.2021.122057.
9. SIMMONDS, Mark; MIRACCA, Ivano; GERDES, Karl. Oxyfuel technologies for CO2 capture: A techno-economic overview. In: RUBIN, E.S.; KEITH, D.W.; GILBOY, C.F.; WILSON, M.; MORRIS, T.; GALE, J.; THAMBIMUTHU, K. (eds.). *Greenhouse Gas Control Technologies 7*. Oxford: Elsevier Science Ltd, 2005, pp. 1125–1130. Available from DOI: 10.1016/B978-008044704-9/50117-8.

10. VARAGANI, Rajani K; CHÂTEL-PÉLAGE, Fabienne; PRANDA, Pavol; ROSTAM-ABADI, Massoud; LU, Yongqi; BOSE, Arun C. Performance simulation and cost assessment of oxy-combustion process for CO2 capture from coal-fired power plants. In: *The Fourth Annual Conference on Carbon Sequestration, May*. 2005, pp. 2–5.

11. OKAWA, M; KIMURA, N; KIGA, T; TAKANO, S; ARAI, K; KATO, M. Trial design for a CO2 recovery power plant by burning pulverized coal in O2/CO2. *Energy Conversion and Management*. 1997, vol. 38, S123–S127. Available from DOI: 10.1016/S0196-8904(96)00257-9.

12. KOORNNEEF, Joris; JUNGINGER, Martin; FAAIJ, André. Development of fluidized bed combustion - An overview of trends, performance and cost. *Progress in Energy and Combustion Science*. 2007, vol. 33, no. 1, pp. 19–55. Available from DOI: 10.1016/j.pecs.2006.07.001.

13. JOHNSSON, Jan E. Formation and reduction of nitrogen oxides in fluidized-bed combustion. *Fuel*. 1994, vol. 73, no. 9, pp. 1398–1415. Available from DOI: 10.1016/0016-2361(94)90055-8.

14. HARTMAN, M.; SVOBODA, K.; POHOŘELÝ, M.; TRNKA, O. Combustion of dried sewage sludge in a fluidized-bed reactor. *Industrial and Engineering Chemistry Research*. 2005, vol. 44, no. 10, pp. 3432–3441. Available from DOI: 10.1021/ie040248n.

15. ABBAS, Zeina; MEZHER, Toufic; ABU-ZAHR, Mohammad R.M. Evaluation of CO_2 purification requirements and the selection of processes for impurities deep removal from the CO_2 product stream. *Energy Procedia*. 2013, vol. 37, pp. 2389–2396. Available from DOI: 10.1016/j.egypro.2013.06.120.

16. LARIBI, Sinda; DUBOIS, Lionel; DE WEIRELD, Guy; THOMAS, Diane. Optimization of the Sour Compression Unit (SCU) process for CO_2 Purification Applied to Flue Gases Coming from Oxy-combustion Cement Industries. *Energy Procedia*. 2017, vol. 114, pp. 458–470. Available from DOI: 10.1016/j.egypro.2017.03.1188.

17. LAKO, P.; VAN DER WELLE, A. J.; HARMELINK, M.; VAN DER KUIP, M. D.C.; HAAN-KAMMINGA, A.; BLANKE, F.; DE WOLFFE, J.; NEPVEUC, M. Issues concerning the implementation of the CCS Directive in the Netherlands. *Energy Procedia*. 2011, vol. 4, no. 2010, pp. 5479–5486. Available from DOI: 10.1016/j.egypro.2011.02.533.

18. WANG, Jinsheng; RYAN, David; ANTHONY, Edward J.; WILDGUST, Neil; AIKEN, Toby. Effects of impurities on CO2 transport, injection and storage. *Energy Procedia*. 2011, vol. 4, pp. 3071–3078. Available from DOI: 10.1016/j.egypro.2011.02.219.

19. NORMANN, Fredrik; JANSSON, Erik; PETERSSON, Tobias; ANDERSSON, Klas. Nitrogen and sulphur chemistry in pressurised flue gas systems: A comparison of modelling and experiments. *International Journal of Greenhouse Gas Control*. 2013, vol. 12, pp. 26–34. Available from DOI: 10.1016/j.ijggc.2012.11.012.

20. HORN, Frederick L.; STEINBERG, Meyer. Control of carbon dioxide emissions from a power plant (and use in enhanced oil recovery). *Fuel*. 1982, vol. 61, no. 5, pp. 415–422. Available from DOI: 10.1016/0016-2361(82)90064-3.

21. ABRAHAM, B. M.; ASBURY, J. G.; LYNCH, E. P.; TEOTIA, A. P. S. Coal-oxygen process provides CO_2 for enhanced recovery. *Oil & Gas Journal*. 1982, vol. 80, no. 11, pp. 68–70.

22. STRÖMBERG, Lars; LINDGREN, Göran; JACOBY, Jürgen; GIERING, Rainer; ANHEDEN, Marie; BURCHHARDT, Uwe; ALTMANN, Hubertus; KLUGER, Frank; STAMATELOPOULOS, Georg-Nikolaus. Update on Vattenfall's 30 MWth oxyfuel pilot plant in Schwarze Pumpe. *Energy Procedia*. 2009, vol. 1, no. 1, pp. 581–589. Available from DOI: 10.1016/j.egypro.2009.01.077.

23. CIEUTAT, Denis; SANCHEZ-MOLINERO, Ivan; TSIAVA, Rémi; RECOURT, Patrick; AIMARD, Nicolas; PRÉBENDÉ, Claude. The oxy-combustion burner development for the CO_2 pilot at Lacq. *Energy Procedia*. 2009, vol. 1, no. 1, pp. 519–526. Available from DOI: 10.1016/j.egypro.2009.01.069.

24. LUPION, Monica; ALVAREZ, Iñaki; OTERO, Pedro; KUIVALAINEN, Reijo; LANTTO, Jouni; HOTTA, Arto; HACK, Horst. 30 MWth CIUDEN oxy-CFB boiler - first experiences. *Energy Procedia*. 2013, vol. 37, pp. 6179–6188. Available from DOI: 10.1016/j.egypro.2013.06.547.

25. KOMAKI, Akihiro; GOTOU, Takahiro; UCHIDA, Terutoshi; YAMADA, Toshihiko; KIGA, Takashi; SPERO, Chris. Operation experiences of oxyfuel power plant in Callide oxyfuel project. *Energy Procedia*. 2014, vol. 63, pp. 490–496. Available from DOI: 10.1016/j.egypro.2014.11.053.

26. AGENCE FRANCE PRESSE (AFP). *Vattenfall abandons research on CO2 storage*. 2014-05. Available also from: https://www.thelocal.se/20140507/vattenfall-abandons-research-on-co2-storage/. Accessed: 10 March 2021.

27. VATTENFALL. *Vattenfall and Aker Carbon Capture to achieve negative emissions in bio CCS-projects*. 2020-10. Available also from: https://group.vattenfall.com/press-and-media/pressreleases/2020/vattenfall-and-aker-carbon-capture-to-achieve-negative-emissions-in-bio-ccs-projects. Accessed: 10 March 2021.

28. WALL, Terry; LIU, Yinghui; SPERO, Chris; ELLIOTT, Liza; KHARE, Sameer; RATHNAM, Renu; ZEENATHAL, Farida; MOGHTADERI, Behdad; BUHRE, Bart; SHENG, Changdong; GUPTA, Raj; YAMADA, Toshihiko; MAKINO, Keiji; YU, Jianglong. An overview on oxyfuel coal combustion – State of the art research and technology development. *Chemical Engineering Research and Design*. 2009, vol. 87, no. 8, pp. 1003–1016. Available from DOI: 10.1016/j.cherd.2009.02.005.

29. SCHEFFKNECHT, Günter; AL-MAKHADMEH, Leema; SCHNELL, Uwe; MAIER, Jörg. Oxy-fuel coal combustion – A review of the current state-of-the-art. *International Journal of Greenhouse Gas Control*. 2011, vol. 5, S16–S35. Available from DOI: 10.1016/j.ijggc.2011.05.020.

30. OBERNBERGER, Ingwald. Decentralized biomass combustion: state of the art and future development. *Biomass and Bioenergy*. 1998, vol. 14, no. 1, pp. 33–56. Available from DOI: 10.1016/S0961-9534(97)00034-2.

31. ERGUDENLER, A.; GHALY, A. E. Agglomeration of alumina sand in a fluidized bed straw gasifier at elevated temperatures. *Bioresource Technology*. 1993, vol. 43, no. 3, pp. 259–268. Available from DOI: 10.1016/0960-8524(93)90039-E.

32. GHALY, A. E.; ERGÜDENLER, A.; LAUFER, E. Agglomeration characteristics of alumina sand-straw ash mixtures at elevated temperatures. *Biomass and Bioenergy*. 1993, vol. 5, no. 6, pp. 467–480. Available from DOI: 10.1016/0961-9534(93)90042-3.

33. SHIMIZU, Tadaaki; HAN, Jun; CHOI, Sunyong; KIM, Laehyun; KIM, Heejoon. Fluidized-bed combustion characteristics of cedar pellets by using an alternative bed material. *Energy and Fuels*. 2006, vol. 20, no. 6, pp. 2737–2742. Available from DOI: 10.1021/ef0601723.

34. HAN, Jun; KIM, Heejoon; MINAMI, Wataru; SHIMIZU, Tadaaki; WANG, Guanghui. The effect of the particle size of alumina sand on the combustion and emission behavior of cedar pellets in a fluidized bed combustor. *Bioresource Technology*. 2008, vol. 99, no. 9, pp. 3782–3786. Available from DOI: 10.1016/j.biortech.2007.07.010.

35. VUTHALURU, Hari B.; ZHANG, Dong Ke. Effect of Ca- and Mg-bearing minerals on particle agglomeration defluidization during fluidized-bed combustion of a South Australian lignite. *Fuel processing technology*. 2001, vol. 69, no. 1, pp. 13–27. Available from DOI: 10.1016/S0378-3820(00)00129-6.

36. DE GEYTER, Sigrid; ÖHMAN, Marcus; BOSTRÖM, Dan; ERIKSSON, Morhan; NORDIN, Anders. Effects of non-quartz minerals in natural bed sand on agglomeration characteristics during fluidized bed combustion of biomass fuels. *Energy and Fuels*. 2007, vol. 21, no. 5, pp. 2663–2668. Available from DOI: 10.1021/ef070162h.

37. KUBA, Matthias; HE, Hanbing; KIRNBAUER, Friedrich; SKOGLUND, Nils; BOSTRÖM, Dan; ÖHMAN, Marcus; HOFBAUER, Hermann. Mechanism of layer formation on olivine bed particles in industrial-scale dual fluid bed gasification of wood. *Energy and Fuels*. 2016, vol. 30, no. 9, pp. 7410–7418. Available from DOI: 10.1021/acs.energyfuels.6b01522.

38. BOZAGHIAN, Marjan; REBBLING, Anders; LARSSON, Sylvia H.; THYREL, Mikael; XIONG, Shaojun; SKOGLUND, Nils. Combustion characteristics of straw stored with CaCO3 in bubbling fluidized bed using quartz and olivine as bed materials. *Applied Energy*. 2018, vol. 212, pp. 1400–1408. Available from DOI: 10.1016/j.apenergy.2017.12.112.

39. HRDLIČKA, Jan; SKOPEC, Pavel; OPATŘIL, Jan; DLOUHÝ, Tomáš. Oxyfuel combustion in a bubbling fluidized bed combustor. *Energy Procedia*. 2016, vol. 86, pp. 116–123. Available from DOI: 10.1016/j.egypro.2016.01.012.

40. CHYANG, Chien-Song; DUAN, Feng; LIN, Shih-Min; TSO, Jim. A study on fluidized bed combustion characteristics of corncob in three different combustion modes. *Bioresource Technology*. 2012, vol. 116, pp. 184–189. Available from DOI: 10.1016/j.biortech.2012.04.041.

41. ARROMDEE, Porametr; SIRISOMBOON, Kasama. Effects of In-bed Stoichiometric and Flue Gas Recirculation on Combustion and Environmental Performances of a Swirling Fluidized-bed Combustor. *Engineering Journal*. 2021, vol. 25, pp. 207–214. Available from DOI: 10.4186/ej.2021.25.2.207.

42. DE LAS OBRAS-LOSCERTALES, M.; RUFAS, A.; DE DIEGO, L.F.; GARCÍA-LABIANO, F.; GAYÁN, P.; ABAD, A.; ADÁNEZ, J. Effects of temperature and flue gas recycle on the SO_2 and NO_X emissions in an oxy-fuel fluidized bed combustor. *Energy Procedia*. 2013, vol. 37, pp. 1275–1282. Available from DOI: 10.1016/j.egypro.2013.06.002.

43. DE DIEGO, L.F.; DE LAS OBRAS-LOSCERTALES, M.; RUFAS, A.; GARCÍA-LABIANO, F.; GAYÁN, P.; ABAD, A.; ADÁNEZ, J. Pollutant emissions in a bubbling fluidized bed combustor working in oxy-fuel operating conditions: Effect of flue gas recirculation. *Applied Energy*. 2013, vol. 102, pp. 860–867. Available from DOI: 10.1016/j.apenergy.2012.08.053.

44. DE DIEGO, L.F.; RUFAS, A.; GARCÍA-LABIANO, F.; DE LAS OBRAS-LOSCERTALES, M.; ABAD, A.; GAYÁN, P.; ADÁNEZ, J. Optimum temperature for sulphur retention in fluidised beds working under oxy-fuel combustion conditions. *Fuel*. 2013, vol. 114, pp. 106–113. Available from DOI: 10.1016/j.fuel.2012.02.064.

45. DE LAS OBRAS-LOSCERTALES, M.; MENDIARA, T.; RUFAS, A.; DE DIEGO, L.F.; GARCÍA-LABIANO, F.; GAYÁN, P.; ABAD, A.; ADÁNEZ, J. NO and N_2O emissions in oxy-fuel combustion of coal in a bubbling fluidized bed combustor. *Fuel*. 2015, vol. 150, pp. 146–153. Available from DOI: 10.1016/j.fuel.2015.02.023.

46. DE LAS OBRAS-LOSCERTALES, M.; IZQUIERDO, M.T.; RUFAS, A.; DE DIEGO, L.F.; GARCÍA-LABIANO, F.; ABAD, A.; GAYÁN, P.; ADÁNEZ, J. The fate of mercury in fluidized beds under oxy-fuel combustion conditions. *Fuel*. 2016, vol. 167, pp. 75–81. Available from DOI: 10.1016/j.fuel.2015.11.045.

47. DUAN, Lunbo; ZHAO, Changsui; REN, Qiangqiang; WU, Zhou; CHEN, Xiaoping. NO_X precursors evolution during coal heating process in CO_2 atmosphere. *Fuel*. 2011, vol. 90, no. 4, pp. 1668–1673. Available from DOI: 10.1016/j.fuel.2010.12.014.

48. DUAN, Lunbo; DUAN, Yuanqiang; ZHAO, Changsui; ANTHONY, Edward J. NO emission during co-firing coal and biomass in an oxy-fuel circulating fluidized bed combustor. *Fuel*. 2015, vol. 150, pp. 8–13. Available from DOI: 10.1016/j.fuel.2015.01.110.

49. LUPIÁÑEZ, Carlos; GUEDEA, Isabel; BOLEA, Irene; DÍEZ, Luis I.; ROMEO, Luis M. Experimental study of SO_2 and NO_X emissions in fluidized bed oxy-fuel combustion. *Fuel Processing Technology*. 2013, vol. 106, pp. 587–594. Available from DOI: 10.1016/j.fuproc.2012.09.030.

50. LUPIÁÑEZ, Carlos; DÍEZ, Luis I.; ROMEO, Luis M. Influence of gas-staging on pollutant emissions from fluidized bed oxy-firing. *Chemical Engineering Journal*. 2014, vol. 256, pp. 380–389. Available from DOI: 10.1016/j.cej.2014.07.011.

51. DÍEZ, Luis I.; LUPIÁÑEZ, Carlos; GUEDEA, Isabel; BOLEA, Irene; ROMEO, Luis M. Anthracite oxy-combustion characteristics in a 90 kWth fluidized bed reactor. *Fuel Processing Technology*. 2015, vol. 139, pp. 196–203. Available from DOI: 10.1016/j.fuproc.2015.07.021.

52. LUPIÁÑEZ, Carlos; CARMEN MAYORAL, M.; DÍEZ, Luis I.; PUEYO, Eloy; ESPATOLERO, Sergio; MANUEL ANDRÉS, J. The role of limestone during fluidized bed oxy-combustion of coal and biomass. *Applied Energy*. 2016, vol. 184, pp. 670–680. Available from DOI: 10.1016/j.apenergy.2016.11.018.

53. LUPIÁÑEZ, Carlos; MAYORAL, M. Carmen; GUEDEA, Isabel; ESPATOLERO, Sergio; DÍEZ, Luis I.; LAGUARTA, Sergio; ANDRÉS, J. Manuel. Effect of co-firing on emissions and deposition during fluidized bed oxy-combustion. *Fuel*. 2016, vol. 184, pp. 261–268. Available from DOI: 10.1016/j.fuel.2016.07.027.

54. LUPIÁÑEZ, Carlos; MAYORAL, M. Carmen; DÍEZ, Luis I.; PUEYO, Eloy; ESPATOLERO, Sergio; ANDRÉS, J. Manuel. On the oxy-combustion of lignite and corn stover in a lab-scale fluidized bed reactor. *Biomass and Bioenergy*. 2017, vol. 96, pp. 152–161. Available from DOI: 10.1016/j.biombioe.2016.11.013.

55. MAYORAL, M. Carmen; DÍEZ, Luis I.; LUPIÁÑEZ, Carlos; ESPATOLERO, Sergio; ANDRÉS, J. Manuel. Oxy-co-firing in fluidized beds: Control of sulfur emissions and assessment of corrosion issues. *Energy Procedia*. 2017, vol. 114, pp. 6003–6009. Available from DOI: 10.1016/j.egypro.2017.03.1735.

56. JANKOWSKA, Sylwia; CZAKIERT, Tomasz; KRAWCZYK, Grzegorz; BORECKI, Paweł; JESIONOWSKI, Łukasz; NOWAK, Wojciech. The effect of oxygen staging on nitrogen conversion in oxy-fuel CFB environment. *Chemical and Process Engineering - Inzynieria Chemiczna i Procesowa*. 2014, vol. 35, no. 4, pp. 489–496. Available from DOI: 10.2478/cpe-2014-0036.

57. PIKKARAINEN, Toni; SAASTAMOINEN, Jaakko; SAASTAMOINEN, Heidi; LEINO, Timo; TOURUNEN, Antti. Development of 2nd generation oxyfuel CFB technology - small scale combustion experiments and model development under high oxygen concentrations. *Energy Procedia*. 2014, vol. 63, pp. 372–385. Available from DOI: 10.1016/j.egypro.2014.11.040.

58. SHER, Farooq; PANS, Miguel A.; SUN, Chenggong; SNAPE, Colin; LIU, Hao. Oxy-fuel combustion study of biomass fuels in a 20 kWth fluidized bed combustor. *Fuel*. 2018, vol. 215, pp. 778–786. Available from DOI: 10.1016/j.fuel.2017.11.039.

59. SINGH, Ravi Inder; KUMAR, Rajesh. Current status and experimental investigation of oxy-fired fluidized bed. *Renewable and Sustainable Energy Reviews*. 2016, vol. 61, pp. 398–420. Available from DOI: 10.1016/j.rser.2016.04.021.

60. KUMAR, Rajesh; SINGH, Ravi Inder. An investigation of co-combustion municipal sewage sludge with biomass in a 20 kW BFB combustor under air-fired and oxygen-enriched condition. *Waste Management*. 2017, vol. 70, pp. 114–126. Available from DOI: 10.1016/j.wasman.2017.09.005.

61. MOON, Ji-Hong; JO, Sung-Ho; PARK, Sung Jin; KHOI, Nguyen Hoang; SEO, Myung Won; RA, Ho Won; YOON, Sang-Jun; YOON, Sung-Min; LEE, Jae-Goo; MUN, Tae-Young. Carbon dioxide purity and combustion characteristics of oxy firing compared to air firing in a pilot-scale circulating fluidized bed. *Energy*. 2019, vol. 166, pp. 183–192. Available from DOI: 10.1016/j.energy.2018.10.045.

62. NGUYEN, Hoang Khoi; MOON, Ji-Hong; JO, Sung-Ho; PARK, Sung Jin; SEO, Myung Won; RA, Ho Won; YOON, Sang-Jun; YOON, Sung-Min; SONG, Byungho; LEE, Uendo; YANG, Chang Won; MUN, Tae-Young; LEE, Jae-Goo. Oxy-combustion characteristics as a function of oxygen concentration and biomass co-firing ratio in a 0.1 MWth circulating fluidized bed combustion test-rig. *Energy*. 2020, vol. 196, p. 117020. Available from DOI: 10.1016/j.energy.2020.117020.

63. YANG, Changwon; KIM, Youngdoo; BANG, Byeongryeol; JEONG, Soohwa; MOON, Jihong; MUN, Tae-Young; JO, Sungho; LEE, Jaegoo; LEE, Uendo. Oxy-CFB combustion technology for use in power-generation applications. *Fuel*. 2020, vol. 267, p. 117206. Available from DOI: 10.1016/j.fuel.2020.117206.

64. WU, Yinghai; WANG, Chunbo; TAN, Yewen; JIA, Lufei; ANTHONY, Edward J. Characterization of ashes from a 100 kWth pilot-scale circulating fluidized bed with oxy-fuel combustion. *Applied Energy*. 2011, vol. 88, no. 9, pp. 2940–2948. Available from DOI: 10.1016/j.apenergy.2011.03.007.

65. STEWART, Michael C.; SYMONDS, Robert T.; MANOVIC, Vasilije; MACCHI, Arturo; ANTHONY, Edward J. Effects of steam on the sulfation of limestone and NO_X formation in an air- and oxy-fired pilot-scale circulating fluidized bed combustor. *Fuel*. 2012, vol. 92, no. 1, pp. 107–115. Available from DOI: 10.1016/j.fuel.2011.06.054.

66. VAROL, Murat; SYMONDS, Robert; ANTHONY, E.J.; LU, Dennis; JIA, Lufei; TAN, Yewen. Emissions from co-firing lignite and biomass in an oxy-fired CFBC. *Fuel Processing Technology*. 2018, vol. 173, pp. 126–133. Available from DOI: 10.1016/j.fuproc.2018.01.002.

67. TAN, Y.; JIA, L.; WU, Y.; ANTHONY, E.J. Experiences and results on a 0.8 MWth oxy-fuel operation pilot-scale circulating fluidized bed. *Applied Energy*. 2012, vol. 92, pp. 343–347. Available from DOI: 10.1016/j.apenergy.2011.11.037.

68. JIA, L.; TAN, Y.; MCCALDEN, D.; WU, Y.; HE, I.; SYMONDS, R.; ANTHONY, E.J. Commissioning of a 0.8 MWth CFBC for oxy-fuel combustion. *International Journal of Greenhouse Gas Control*. 2012, vol. 7, pp. 240–243. Available from DOI: 10.1016/j.ijggc.2011.10.009.

69. XU, Mingxin; LI, Shiyuan; WU, Yinghai; JIA, Lufei; LU, Qinggang. The characteristics of recycled NO reduction over char during oxy-fuel fluidized bed combustion. *Applied Energy*. 2017, vol. 190, pp. 553–562. Available from DOI: 10.1016/j.apenergy.2016.12.073.

70. XU, Mingxin; LI, Shiyuan; WU, Yinghai; JIA, Lufei. Reduction of recycled NO over char during oxy-fuel fluidized bed combustion: Effects of operating parameters. *Applied Energy*. 2017, vol. 199, pp. 310–322. Available from DOI: 10.1016/j.apenergy.2017.05.028.

71. NDIBE, Collins; SPÖRL, Reinhold; MAIER, Jörg; SCHEFFKNECHT, Günter. Experimental study of NO and NO_2 formation in a PF oxy-fuel firing system. *Fuel*. 2013, vol. 107, pp. 749–756. Available from DOI: 10.1016/j.fuel.2013.01.055.

72. AL-MAKHADMEH, L.; MAIER, J.; AL-HARAHSHEH, M.; SCHEFFKNECHT, G. Oxy-fuel technology: An experimental investigations into oil shale combustion under oxy-fuel conditions. *Fuel*. 2013, vol. 103, pp. 421–429. Available from DOI: 10.1016/j.fuel.2012.05.054.

73. SPÖRL, Reinhold; MAIER, Jörg; BELO, Lawrence; SHAH, Kalpit; STANGER, Rohan; WALL, Terry; SCHEFFKNECHT, Günter. Mercury and SO_3 Emissions in Oxy-fuel Combustion. *Energy Procedia*. 2014, vol. 63, pp. 386–402. Available from DOI: 10.1016/j.egypro.2014.11.041.

74. AL-MAKHADMEH, L.; MAIER, J.; SCHEFFKNECHT, G. Oxyfuel technology: NO reduction during oxy-oil shale combustion. *Fuel*. 2014, vol. 128, pp. 155–161. Available from DOI: 10.1016/j.fuel.2014.03.003.

75. HOFBAUER, G.; BEISHEIM, T.; DIETER, H.; SCHEFFKNECHT, G. Experiences from Oxy-fuel Combustion of Bituminous Coal in a 150 kWth Circulating Fluidized Bed Pilot Facility. *Energy Procedia*. 2014, vol. 51, pp. 24–30. Available from DOI: 10.1016/j.egypro.2014.07.003.

76. CARRASCO-MALDONADO, Francisco; BAKKEN, Jørn; DITARANTO, Mario; HAUGEN, Nils E.L.; LANGØRGEN, Øyvind; GRATHWOHL, Simon; MAIER, Jörg. Oxy-fuel burner investigations for CO_2 capture in cement plants. *Energy Procedia*. 2017, vol. 120, pp. 120–125. Available from DOI: 10.1016/j.egypro.2017.07.160.

77. ROY, Bithi; BHATTACHARYA, Sankar. Oxy-fuel fluidized bed combustion using Victorian brown coal: An experimental investigation. *Fuel Processing Technology*. 2014, vol. 117, pp. 23–29. Available from DOI: 10.1016/j.fuproc.2013.02.019.

78. ROY, Bithi; BHATTACHARYA, Sankar. Combustion of single char particles from Victorian brown coal under oxy-fuel fluidized bed conditions. *Fuel*. 2016, vol. 165, pp. 477–483. Available from DOI: 10.1016/j.fuel.2015.10.099.

79. ROY, Bithi; BHATTACHARYA, Sankar. Ash characteristics during oxy-fuel fluidized bed combustion of a Victorian brown coal. *Powder Technology*. 2016, vol. 288, pp. 1–5. Available from DOI: 10.1016/j.powtec.2015.10.036.

80. ROY, Bithi; BHATTACHARYA, Sankar. Release behavior of Hg, Se, Cr and As during oxy-fuel combustion using Loy Yang brown coal in a bench-scale fluidized bed unit. *Powder Technology*. 2016, vol. 302, pp. 328–332. Available from DOI: 10.1016/j.powtec.2016.08.073.

81. MYÖHÄNEN, Kari; DIEGO, Ruth; KUIVALAINEN, Reijo; HYPPÄNEN, Timo. Modelling supported development of oxy-CFB combustion. *Energy Procedia*. 2017, vol. 114, pp. 589–599. Available from DOI: 10.1016/j.egypro.2017.03.1201.

82. STANGER, Rohan; TING, Timothy; BELO, Lawrence; SPERO, Chris; WALL, Terry. Field measurements of NO_X and mercury from oxy-fuel compression condensates at the Callide Oxyfuel Project. *International Journal of Greenhouse Gas Control*. 2015, vol. 42, pp. 485–493. Available from DOI: 10.1016/j.ijggc.2015.08.021.

83. STANGER, Rohan; TING, Tim; SPERO, Chris; WALL, Terry. Oxyfuel derived CO_2 compression experiments with NO_X, SO_X and mercury removal—Experiments involving compression of slip-streams from the Callide Oxyfuel Project (COP). *International Journal of Greenhouse Gas Control*. 2015, vol. 41, pp. 50–59. Available from DOI: 10.1016/j.ijggc.2015.06.022.

84. LIU, Dunyu; WALL, Terry; STANGER, Rohan. CO2 quality control in Oxy-fuel technology for CCS: SO_2 removal by the caustic scrubber in Callide Oxy-fuel Project. *International Journal of Greenhouse Gas Control*. 2016, vol. 51, pp. 207–217. Available from DOI: 10.1016/j.ijggc.2016.05.026.

85. STANGER, Rohan; BELO, Lawrence; TING, Timothy; SPERO, Chris; WALL, Terry. Mercury and SO_3 measurements on the fabric filter at the Callide Oxy-fuel Project during air and oxy-fuel firing transitions. *International Journal of Greenhouse Gas Control*. 2016, vol. 47, pp. 221–232. Available from DOI: 10.1016/j.ijggc.2016.01.049.

86. KUNII, Daizo; LEVENSPIEL, Octave. *Fluidization Engineering*. 2nd. Elsevier, 1991. Available from DOI: 10.1016/C2009-0-24190-0.

87. WERTHER, J.; SAENGER, M.; HARTGE, E.-U.; OGADA, T.; SIAGI, Z. Combustion of agricultural residues. *Progress in Energy and Combustion Science*. 2000, vol. 26, no. 1, pp. 1–27. Available from DOI: 10.1016/S0360-1285(99)00005-2.

88. OLOFSSON, Göran; YE, Zhicheng; BJERLE, Ingemar; ANDERSSON, Arne. Bed agglomeration problems in fluidized-bed biomass combustion. *Industrial and Engineering Chemistry Research*. 2002, vol. 41, no. 12, pp. 2888–2894. Available from DOI: 10.1021/ie010274a.

89. BARTELS, Malte; LIN, Weigang; NIJENHUIS, John; KAPTEIJN, Freek; OMMEN, J. Ruud van. Agglomeration in fluidized beds at high temperatures: Mechanisms, detection and prevention. *Progress in Energy and Combustion Science*. 2008, vol. 34, no. 5, pp. 633–666. Available from DOI: 10.1016/j.pecs.2008.04.002.

90. MORRIS, Jonathan D.; DAOOD, Syed Sheraz; CHILTON, Stephen; NIMMO, William. Mechanisms and mitigation of agglomeration during fluidized bed combustion of biomass: A review. *Fuel*. 2018, vol. 230, pp. 452–473. Available from DOI: 10.1016/j.fuel.2018.04.098.

91. SCALA, Fabrizio. Particle agglomeration during fluidized bed combustion: Mechanisms, early detection and possible countermeasures. *Fuel Processing Technology*. 2018, vol. 171, pp. 31–38. Available from DOI: 10.1016/j.fuproc.2017.11.001.

92. KUBA, Matthias; SKOGLUND, Nils; ÖHMAN, Marcus; HOFBAUER, Hermann. A review on bed material particle layer formation and its positive influence on the performance of thermo-chemical biomass conversion in fluidized beds. *Fuel*. 2021, vol. 291. Available from DOI: 10.1016/j.fuel.2021.120214.

93. SERRANO, D.; SÁNCHEZ-DELGADO, S.; SOBRINO, C.; MARUGÁN-CRUZ, C. Defluidization and agglomeration of a fluidized bed reactor during Cynara cardunculus L. gasification using sepiolite as a bed material. *Fuel Processing Technology*. 2015, vol. 131, pp. 338–347. Available from DOI: 10.1016/j.fuproc.2014.11.036.

94. MORRIS, Jonathan D.; DAOOD, Syed Sheraz; NIMMO, William. Agglomeration and the effect of process conditions on fluidized bed combustion of biomasses with olivine and silica sand as bed materials: Pilot-scale investigation. *Biomass and Bioenergy*. 2020, vol. 142, p. 105806. Available from DOI: 10.1016/j.biombioe.2020.105806.

95. CRAMER, E. S.; BRIGGS, M. S.; LIU, N.; MAILYAN, B.; DWYER, J. R.; RASSOUL, H. K. The impact on the ozone layer from NO_X produced by terrestrial gamma ray flashes. *Geophysical Research Letters*. 2017, vol. 44, no. 10, pp. 5240–5245. Available from DOI: 10.1002/2017GL073215.

96. LAW, C.S. Air–Sea Transfer: N_2O, NO, CH_4, CO. In: STEELE, John H. (ed.). *Encyclopedia of Ocean Sciences*. Second edition. Oxford: Academic Press, 2001, pp. 163–170. ISBN 978-0-12-374473-9. Available from DOI: 10.1016/B978-012374473-9.00064-3.

97. VEJVODA, Josef; MACHAČ, Pavel; BURYAN, Petr. *Technologie ochrany ovzduší a čištění odpadních plynů*. Vysoká škola chemicko-technologická v Praze, 2003. ISBN 80-7080-517-X.

98. GREENWOOD, N. N.; EARNSHAW, Alan. *Chemie prvků*. 1st ed. Praha: Informatorium, 1993. ISBN 80-85427-38-9.

99. GLASSMAN, Irvin; YETTER, Richard A.; GLUMAC, Nick G. *Combustion*. Elsevier, 2015. ISBN 9780124079137. Available from DOI: 10.1016/C2011-0-05402-9.

100. VÍDEN, Ivan. *Chemie ovzduší*. Vysoká škola chemicko-technologická v Praze, 2005. ISBN 80-7080-571-4.

101. CRUTZEN, Paul J. The role of NO and NO_2 in the chemistry of the troposphere and stratosphere. *Annual Review of Earth and Planetary Sciences*. 1979, vol. 7, pp. 443–472.

102. LIN, C. L.; LEU, M. T. Temperature and third-body dependence of the rate constant for the reaction O + O2 + M → O3 + M. *International Journal of Chemical Kinetics*. 1982, vol. 14, no. 4, pp. 417–434. Available from DOI: 10.1002/kin.550140408.

103. IPCC, 2013. *Climate Change 2013: The Physical Science Basis. Contribution of Working Group I to the Fifth Assessment Report of the Intergovernmental Panel on Climate Change*. Ed. by STOCKER, T.F.; QIN, D.; PLATTNER, G.-K.; TIGNOR, M.; ALLEN, S.K.; BOSCHUNG, J.; NAUELS, A.; XIA, Y.; BEX, V.; MIDGLEY, P.M. Cambridge, United Kingdom: Cambridge University Press, 2013.

104. ZELDOVICH, Ya. B.; SADOVNIKOV, P. Ya.; FRANK-KAMENETSKII, D. A. *Oxidation of Nitrogen in Combustion*. Moscow-Leningrad, 1947. Tech. rep. Academy of Sciences of USSR, Institute of Chemical Physics. transl. by M. Shelef.

105. FENIMORE, C.P. Formation of nitric oxide in premixed hydrocarbon flames. *Symposium (International) on Combustion*. 1971, vol. 13, no. 1, pp. 373–380. Available from DOI: 10.1016/S0082-0784(71)80040-1.

106. MILLER, James A.; BOWMAN, Craig T. Mechanism and modeling of nitrogen chemistry in combustion. *Progress in Energy and Combustion Science*. 1989, vol. 15, no. 4, pp. 287–338. Available from DOI: 10.1016/0360-1285(89)90017-8.

107. BOWMAN, Craig T. Control of combustion-generated nitrogen oxide emissions: Technology driven by regulation. *Symposium (International) on Combustion*. 1992, vol. 24, no. 1, pp. 859–878. Available from DOI: 10.1016/S0082-0784(06)80104-9.

108. BOWMAN, Craig T. Gas-Phase Reaction Mechanisms for Nitrogen Oxide Formation and Removal in Combustion. In: *Pollutants from Combustion: Formation and Impact on Atmospheric Chemistry*. Ed. by VOVELLE, C. Springer, Dordrecht, 2000, pp. 123–144. Available from DOI: 10.1007/978-94-011-4249-6_7.

109. HAYHURST, A.N.; VINCE, I.M. The origin and nature of "prompt" nitric oxide in flames. *Combustion and Flame*. 1983, pp. 41–57. Available from DOI: 10.1016/0010-2180(83)90047-0.

110. GLARBORG, P.; JENSEN, A. D.; JOHNSSON, J. E. Fuel nitrogen conversion in solid fuel fired systems. *Progress in Energy and Combustion Science*. 2003, vol. 29, no. 2, pp. 89–113. Available from DOI: 10.1016/S0360-1285(02)00031-X.

111. NINOMIYA, Y.; YOKOI, K.; ARAI, Norio; HASATANI, M. Characteristics of emission of char NO during the combustion of a single particle of coal char. *International Chemical Engineering*. 1989, vol. 29, pp. 512–516.

112. AIHARA, Toshiaki; MATSUOKA, Koichi; KYOTANI, Takashi; TOMITA, Akira. Mechanism of N_2 formation during coal char oxidation. *Proceedings of the Combustion Institute*. 2000, vol. 28, no. 2, pp. 2189–2195. Available from DOI: 10.1016/S0082-0784(00)80628-1.

113. ASHMAN, Peter J.; HAYNES, Brian S.; NICHOLLS, Patricia M.; NELSON, Peter F. Interactions of gaseous NO with char during the low-temperature oxidation of coal chars. *Proceedings of the Combustion Institute*. 2000, vol. 28, no. 2, pp. 2171–2179. Available from DOI: 10.1016/S0082-0784(00)80626-8.

114. ZHU, Chuanqiang; LIU, Shuyuan; LIU, Huan; YANG, Juan; LIU, Xiaoxing; XU, Guangwen. NO_X emission characteristics of fluidized bed combustion in atmospheres rich in oxygen and water vapor for high-nitrogen fuel. *Fuel*. 2015, vol. 139, pp. 346–355. Available from DOI: 10.1016/j.fuel.2014.08.058.

115. GIMÉNEZ-LÓPEZ, J.; MILLERA, A.; BILBAO, R.; ALZUETA, M. U. HCN oxidation in an O2/CO2 atmosphere: An experimental and kinetic modeling study. *Combustion and Flame*. 2010, vol. 157, no. 2, pp. 267–276. Available from DOI: 10.1016/j.combustflame.2009.07.016.

116. NORMANN, Fredrik; ANDERSSON, Klas; LECKNER, Bo; JOHNSSON, Filip. Emission control of nitrogen oxides in the oxy-fuel process. *Progress in Energy and Combustion Science*. 2009, vol. 35, no. 5, pp. 385–397. Available from DOI: 10.1016/j.pecs.2009.04.002.

117. ZHOU, Hao; LI, Yuan; LI, Ning; QIU, Runchao; CEN, Kefa. Conversions of fuel-N to NO and N_2O during devolatilization and char combustion stages of a single coal particle under oxy-fuel fluidized bed conditions. *Journal of the Energy Institute*. 2019, vol. 92, no. 2, pp. 351–363. Available from DOI: 10.1016/j.joei.2018.01.001.

118. SVOBODA, Karel; HARTMAN, Miloslav; POHOŘELÝ, Michael; TRNKA, Otakar. Modelling of effects of operating conditions and coal reactivity on temperature of burning particles in fluidized bed combustion. *Acta Geodynamica et Geomaterialia*. 2004, vol. 1, no. 2, pp. 261–274.

119. BHUNIA, Shyamal; SADHUKHAN, Anup Kumar; GUPTA, Parthapratim. Modelling and experimental studies on oxy-fuel combustion of coarse size coal char. *Fuel Processing Technology*. 2017, vol. 158, pp. 73–84. Available from DOI: 10.1016/j.fuproc.2016.11.015.

120. SALINERO, J.; GÓMEZ-BAREA, A.; FUENTES-CANO, D.; LECKNER, B. The influence of CO_2 gas concentration on the char temperature and conversion during oxy-fuel combustion in a fluidized bed. *Applied Energy*. 2018, vol. 215, pp. 116–130. Available from DOI: 10.1016/J.APENERGY.2018.01.038.

121. KOSOWSKA-GOLACHOWSKA, Monika; LUCKOS, Adam; KIJO-KLECZKOWSKA, Agnieszka. Pollutant Emissions during Oxy-Fuel Combustion of Biomass in a Bench Scale CFB Combustor. *Energies*. 2022, vol. 15, no. 3, pp. 1–23. Available from DOI: 10.3390/en15030706.

122. SKOPEC, Pavel. *Desulphurization during oxyfuel combustion in a fluidized bed*. Prague, 2019. Available also from: https://dspace.cvut.cz/bitstream/handle/10467/85546/F2-D-2019-Skopec-Pavel-DP_Skopec_final.pdf?sequence=-1&isAllowed=y. PhD thesis. Czech Technical University in Prague, Faculty of Mechanical Engineering, Department of Energy Engineering. Accessed: 31 January, 2023.

123. STADLER, Hannes; CHRIST, Dominik; HABERMEHL, Martin; HEIL, Peter; KELLERMANN, Arno; OHLIGER, Andreas; TOPOROV, Dobrin; KNEER, Reinhold. Experimental investigation of NO_X emissions in oxycoal combustion. *Fuel*. 2011, vol. 90, no. 4, pp. 1604–1611. Available from DOI: 10.1016/j.fuel.2010.11.026.

124. FAN, Weidong; LI, Yu; GUO, Qinghong; CHEN, Can; WANG, Yong. Coal-nitrogen release and NO_X evolution in the oxidant-staged combustion of coal. *Energy*. 2017, vol. 125, pp. 417–426. Available from DOI: 10.1016/j.energy.2017.02.130.

125. SPLIETHOFF, Hartmut; GREUL, Ulrich; RÜDIGER, Helmut; HEIN, Klaus R.G. Basic effects on NO_X emissions in air staging and reburning at a bench-scale test facility. *Fuel*. 1996, vol. 75, no. 5, pp. 560–564. Available from DOI: 10.1016/0016-2361(95)00281-2.

126. OKAZAKI, K.; ANDO, T. NO_X reduction mechanism in coal combustion with recycled CO_2. *Energy*. 1997, vol. 22, no. 2, pp. 207–215. Available from DOI: 10.1016/S0360-5442(96)00133-8. International Symposium on CO_2 Fixation and Efficient Utilization of Energy.

127. HASHEMI, Hamid; HANSEN, Stine; TOFTEGAARD, Maja B.; PEDERSEN, Kim H.; JENSEN, Anker D.; DAM-JOHANSEN, Kim; GLARBORG, Peter. A model for nitrogen chemistry in oxy-fuel combustion of pulverized coal. *Energy and Fuels*. 2011, vol. 25, no. 10, pp. 4280–4289. Available from DOI: 10.1021/ef200853t.

128. KRZYWAŃSKI, J.; CZAKIERT, T.; MUSKAŁA, W.; NOWAK, W. Modelling of CO_2, CO, SO_2, O_2 and NO_x emissions from the oxy-fuel combustion in a circulating fluidized bed. *Fuel Processing Technology*. 2011, vol. 92, no. 3, pp. 590–596. Available from DOI: 10.1016/j.fuproc.2010.11.015.

129. KRZYWAŃSKI, Jaroslaw; CZAKIERT, Tomasz; MUSKALA, Waldemar; SEKRET, Robert; NOWAK, Wojciech. Modeling of solid fuels combustion in oxygen-enriched atmosphere in circulating fluidized bed boiler. Part 1. The mathematical model of fuel combustion in oxygen-enriched CFB environment. *Fuel Processing Technology*. 2010, vol. 91, no. 3, pp. 290–295. Available from DOI: 10.1016/j.fuproc.2009.10.011.

130. SCHLUCKNER, C.; GABER, C.; LANDFAHRER, M.; DEMUTH, M.; HOCHENAUER, C. Fast and accurate CFD-model for NO_X emission prediction during oxy-fuel combustion of natural gas using detailed chemical kinetics. *Fuel*. 2020, vol. 264, p. 116841. Available from DOI: 10.1016/j.fuel.2019.116841.

131. PEETERS, Timotheus Willem Joannes. *Numerical modeling of turbulent natural-gas diffusion flames*. 1995. PhD thesis. TU Delft.

132. SCHLUCKNER, C.; GABER, C.; DEMUTH, M.; HOCHENAUER, C. Scrutiny of residual nitrogen content and different nozzle designs on NO_X formation during oxy-fuel combustion of natural gas. *Fuel*. 2020, vol. 277, p. 118065. Available from DOI: 10.1016/j.fuel.2020.118065.

133. YADAV, Sujeet; MONDAL, S. S. Numerical investigation of the influence of operating parameters on NO_X emission characteristics under oxy-coal combustion atmosphere in a tubular combustor. *International Communications in Heat and Mass Transfer*. 2020, vol. 119, p. 104915. Available from DOI: 10.1016/j.icheatmasstransfer.2020.104915.

134. LIANG, Xiaorui; WANG, Qinhui; LUO, Zhongyang; EDDINGS, Eric; RING, Terry; LI, Simin; YU, Peng; YAN, Jiqing; YANG, Xudong; JIA, Xin. Experimental and numerical investigation on nitrogen transformation in pressurized oxy-fuel combustion of pulverized coal. *Journal of Cleaner Production*. 2021, vol. 278, p. 123240. Available from DOI: 10.1016/j.jclepro.2020.123240.

135. AHO, M. J.; PAAKKINEN, K. M.; PIRKONEN, P. M.; KILPINEN, P.; HUPA, M. The effects of pressure, oxygen partial pressure, and temperature on the formation of N_2O, NO, and NO_2 from pulverized coal. *Combustion and Flame*. 1995, vol. 102, no. 3, pp. 387–400. Available from DOI: 10.1016/0010-2180(95)00019-3.

136. MENDIARA, Teresa; GLARBORG, Peter. Ammonia chemistry in oxy-fuel combustion of methane. *Combustion and Flame*. 2009, vol. 156, no. 10, pp. 1937–1949. Available from DOI: 10.1016/j.combustflame.2009.07.006.

137. SMITH, Gregory P.; GOLDEN, David M.; FRENKLACH, Michael; MORIARTY, Nigel W.; EITENEER, Boris; GOLDENBERG, Mikhail; BOWMAN, C. Thomas; HANSON, Ronald K.; SONG, Soonho; GARDINER JR., William C.; LISSIANSKI, Vitali V.; QIN, Zhiwei. *GRI-MECH 3.0*. Gas Research Institute, 1999. Available also from: http://combustion.berkeley.edu/gri-mech/version30/text30.html. Accessed: 3 January 2022.

138. RAHMAN, Zia ur; ZHANG, Jiaye; ZHANG, Lan; WANG, Xuebin; YANG, Zhiwei; TAN, Houzhang; AXELBAUM, Richard L. A kinetic evaluation and optimization study on NO_X reduction by reburning under pressurized oxy-combustion. *Journal of Environmental Management*. 2021, vol. 290, p. 112690. Available from DOI: 10.1016/j.jenvman.2021.112690.

139. GLARBORG, P.; MILLER, J. A.; RUSCIC, B.; KLIPPENSTEIN, S. Modeling nitrogen chemistry in combustion. *Progress in Energy and Combustion Science*. 2018, vol. 67, pp. 31–68. Available from DOI: 10.1016/j.pecs.2018.01.002.

140. RAHMAN, Zia ur; WANG, Xuebin; MIKULCIC, Hrvoje; ZHOU, Shangkun; ZHANG, Jiaye; VUJANOVIC, Milan; TAN, Houzhang. Numerical assessment of NO_X evolution in ammonia oxidation and its control by reburning in pressurized oxy-combustion. *Journal of the Energy Institute*. 2022, vol. 100, pp. 89–98. Available from DOI: 10.1016/j.joei.2021.11.002.

141. BOWMAN, C.T.; HANSON, R.K.; DAVIDSON, D.F.; GARDINER JR., W.C.; LISSIANSKI, V.; SMITH, G.P.; GOLDEN, D.M.; FRENKLACH, M.; GOLDENBERG, M. *GRI-MECH 2.11*. Gas Research Institute, 1997. Available also from: http://combustion.berkeley.edu/gri-mech/new21/version21/text21.html. Accessed: 3 January 2022.

142. GOODWIN, David G.; MOFFAT, Harry K.; SCHOEGL, Ingmar; SPETH, Raymond L.; WEBER, Bryan W. *Cantera: An Object-oriented Software Toolkit for Chemical Kinetics, Thermodynamics, and Transport Processes* [https://www.cantera.org]. 2021. Available from DOI: 10.5281/zenodo.4527812. Version 2.5.1.

143. MULVIHILL, Clayton R.; MATHIEU, Olivier; PETERSEN, Eric L. H_2O time histories in the H_2-NO_2 system for validation of NO_X hydrocarbon kinetics mechanisms. *International Journal of Chemical Kinetics*. 2019, vol. 51, no. 9, pp. 669–678. Available from DOI: 10.1002/kin.21286.

144. GOODWIN, David G.; MOFFAT, Harry K.; SCHOEGL, Ingmar; SPETH, Raymond L.; WEBER, Bryan W. *Modeling Chemical Reactions in Cantera* [https://cantera.org/science/kinetics.html]. 2022. accessed: 28 June 2022.

145. WINTER, Franz; WARTHA, Christian; LÖFFLER, Gerhard; HOFBAUER, Hermann. The NO and N_2O formation mechanism during devolatilization and char combustion under fluidized-bed conditions. *Symposium (International) on Combustion*. 1996, vol. 26, no. 2, pp. 3325–3334. Available from DOI: 10.1016/S0082-0784(96)80180-9.

146. KONTTINEN, Jukka; KALLIO, Sirpa; HUPA, Mikko; WINTER, Franz. NO formation tendency characterization for solid fuels in fluidized beds. *Fuel*. 2013, vol. 108, pp. 238–246. Available from DOI: 10.1016/j.fuel.2013.02.011.

147. ANCA-COUCE, Andrés; SOMMERSACHER, Peter; EVIC, Nikola; MEHRABIAN, Ramin; SCHARLER, Robert. Experiments and modelling of NO_X precursors release (NH_3 and HCN) in fixed-bed biomass combustion conditions. *Fuel*. 2018, vol. 222, pp. 529–537. Available from DOI: 10.1016/j.fuel.2018.03.003.

148. BRUNNER, Thomas; BIEDERMANN, Friedrich; KANZIAN, Werner; EVIC, Nikola; OBERNBERGER, Ingwald. Advanced biomass fuel characterization based on tests with a specially designed lab-scale reactor. *Energy and Fuels*. 2013, vol. 27, no. 10, pp. 5691–5698. Available from DOI: 10.1021/ef400559j.

149. SKOPEC, Pavel; HRDLIČKA, Jan; OPATŘIL, Jan; ŠTEFANICA, Jiří. NO_X emissions from bubbling fluidized bed combustion of lignite coal. *Acta Polytechnica*. 2015, vol. 55, no. 4, pp. 275–281. Available from DOI: 10.14311/AP.2015.55.0275.

150. *ISO 1928 - Solid mineral fuels - Determination of gross calorific value by the bomb calorimetric method, and calculation of net calorific value*. Geneva, 1995. Standard. International Organization for Standardization.

151. *ČSN 44 1377 - Solid mineral fuels - Determination of moisture*. Prague, 2004. Standard. Czech Standardization Agency.

152. *ISO 1171 - Solid mineral fuels - Determination of ash*. Geneva, 2010. Standard. International Organization for Standardization.

153. ALLEN, Terence. *Particle Size Measurement*. 3rd. Boston: Springer, 1981. Available from DOI: 10.1007/978-1-4899-3063-7.

154. GELDART, D. Types of gas fluidization. *Powder Technology*. 1973, vol. 7, no. 5, pp. 285–292. Available from DOI: 10.1016/0032-5910(73)80037-3.

155. DRYDEN, I. G. C. (ed.). Fluidized-bed combustion. In: *The Efficient Use of Energy*. 2nd. Butterworth-Heinemann, 1982, pp. 58–63. Available from DOI: 10.1016/B978-0-408-01250-8.50014-3.

156. HU, Y; NAITO, S; KOBAYASHI, N; HASATANI, M. CO2, NOx and SO2 emissions from the combustion of coal with high oxygen concentration gases. *Fuel*. 2000, vol. 79, no. 15, pp. 1925–1932. Available from DOI: 10.1016/S0016-2361(00)00047-8.

157. SHEN, B. X.; MI, T.; LIU, D. C.; FENG, B.; YAO, Q.; WINTER, Franz. N_2O emission under fluidized bed combustion condition. *Fuel Processing Technology*. 2003, vol. 84, no. 1–3, pp. 13–21. Available from DOI: 10.1016/S0378-3820(02)00104-2.

Author's own publications

158. VODIČKA, Matěj; HAUGEN, Nils Erland; GRUBER, Andrea; HRDLIČKA, Jan. NO_X formation in oxy-fuel combustion of lignite in a bubbling fluidized bed - Modelling and experimental verification. *International Journal of Greenhouse Gas Control*. 2018, vol. 76, pp. 208–214. Available from DOI: 10.1016/j.ijggc.2018.07.007.

159. VODIČKA, Matěj; HAUGEN, Nils Erland; GRUBER, Andrea; HRDLIČKA, Jan. Vznik NO_X při oxy-fuel spalování v bublinkující fluidní vrstvě - modelování a experimentální ověření. In: *Energie z biomasy XVIII*. Lednice: Brno University of Technology, Faculty of Mechanical Engineering, 2017, pp. 124–133. ISBN 978-80-214-5584-9.

160. SKOPEC, Pavel; HRDLIČKA, Jan; VODIČKA, Matěj. Desulfurization in co-firing of sewage sludge and wooden biomass in a bubbling fluidized bed combustor under air and oxy-fuel conditions. *Fuel*. 2023, vol. 342, p. 127709. Available from DOI: 10.1016/j.fuel.2023.127709.

161. SKOPEC, Pavel; HRDLIČKA, Jan; VODIČKA, Matěj. Dry additive desulfurization in oxyfuel bubbling fluidized bed combustor. *Fuel*. 2021, vol. 283, p. 118945. Available from DOI: 10.1016/j.fuel.2020.118945.

162. SKOPEC, Pavel; HRDLIČKA, Jan; VODIČKA, Matěj; PILAŘ, Lukáš; OPATŘIL, Jan. Combustion of Lignite Coal in a Bubbling Fluidized Bed Combustor under Oxy-fuel Conditions. In: *Energy Procedia - 13th International Conference on Greenhouse Gas Control Technologies*. Lausanne: Elsevier, 2017, pp. 600–607. Available from DOI: 10.1016/j.egypro.2017.03.1202.

163. VODIČKA, Matěj; HRDLIČKA, Jan; SKOPEC, Pavel. Emise oxidů dusíku při oxyfuel spalování dřevních pelet v ohništi se stacionární fluidní vrstvou. In: *Energie z biomasy XVII*. Lednice: Brno University of Technology, Faculty of Mechanical Engineering, 2016, pp. 111–117. ISBN 978-80-214-5441-5.

164. SKOPEC, Pavel; HRDLIČKA, Jan; VODIČKA, Matěj. Porovnání experimentálních výsledků oxyfuel spalování ve fluidní vrstvě s numerickým modelem. In: *Energie z biomasy XVII*. Lednice: Brno University of Technology, Faculty of Mechanical Engineering, 2016, pp. 105–110. ISBN 978-80-214-5441-5.

165. SKOPEC, Pavel; HRDLIČKA, Jan; VODIČKA, Matěj. Zkušenosti s oxy-fuel spalováním ve stacionární fluidní vrstvě. In: *Energie z biomasy XVI*. Lednice: Brno University of Technology, Faculty of Mechanical Engineering, 2015, pp. 100–105. ISBN 978-80-214-5286-2.

166. VODIČKA, Matěj; MICHALIKOVÁ, Kristýna; HRDLIČKA, Jan; SKOPEC, Pavel; JENÍKOVÁ, Jitka. Experimental verification of the impact of the air staging on the NO_X production and on the temperature profile in a BFB. *Acta Polytechnica*. 2022, vol. 62, no. 3, pp. 400–408. Available from DOI: 10.14311/AP.2022.62.0400.

167. JENÍKOVÁ, Jitka; MICHALIKOVÁ, Kristýna; HRDLIČKA, František; HRDLIČKA, Jan; PILAŘ, Lukáš; VODIČKA, Matěj; SKOPEC, Pavel. Applicability of secondary denitrification measures on a fluidized bed boiler. *Acta Polytechnica*. 2022, vol. 62, no. 3, pp. 341–351. Available from DOI: 10.14311/AP.2022.62.0341.

168. MICHALIKOVÁ, Kristýna; HRDLIČKA, Jan; VODIČKA, Matěj; SKOPEC, Pavel; JENÍKOVÁ, Jitka; PILAŘ, Lukáš. Experimental verification of the efficiency of selective non-catalytic reduction in a bubbling fluidized bed combustor. *Acta Polytechnica*. 2022, vol. 62, no. 3, pp. 361–369. Available from DOI: 10.14311/AP.2022.62.0361.

169. MICHALIKOVÁ, Kristýna; HRDLIČKA, Jan; VODIČKA, Matěj; SKOPEC, Pavel; JENÍKOVÁ, Jitka. Účinnost selektivní nekatalytické redukce oxidů dusíku při spalování v BFB. In: *Energie z biomasy XX*. Lednice: Brno University of Technology, Faculty of Mechanical Engineering, 2019, pp. 72–77. ISBN 978-80-214-5825-3.

170. VODIČKA, Matěj; MICHALIKOVÁ, Kristýna; HRDLIČKA, Jan; HOFBAUER, Cornelia; WINTER, Franz; SKOPEC, Pavel; JENÍKOVÁ, Jitka. External bed materials for the oxy-fuel combustion of biomass in a bubbling fluidized bed. *Journal of Cleaner Production*. 2021, vol. 321, p. 128882. Available from DOI: 10.1016/j.jclepro.2021.128882.

171. HRDLIČKA, Jan; VODIČKA, Matěj; SKOPEC, Pavel; HRDLIČKA, František; DLOUHÝ, Tomáš. CO_2 Capture by Oxyfuel Combustion. In: WINTER, Franz; AGARWAL, Rashmi Avinash; HRDLICKA, Jan; VARJANI, Sunita (eds.). *CO_2 Separation, Purification and Conversion to Chemicals and Fuels*. Singapore: Springer, 2019, pp. 55–78. Available from DOI: 10.1007/978-981-13-3296-8_5.

172. VODIČKA, Matěj; HRDLIČKA, Jan; SKOPEC, Pavel. Experimental study of the NO_X reduction through the staged oxygen supply in the oxy-fuel combustion in a 30 kW_{th} bubbling fluidized bed. *Fuel*. 2021, vol. 286, p. 119343. Available from DOI: 10.1016/j.fuel.2020.119343.

Appendix A

Supplementary numerical results achieved using different chemical kinetic mechanisms

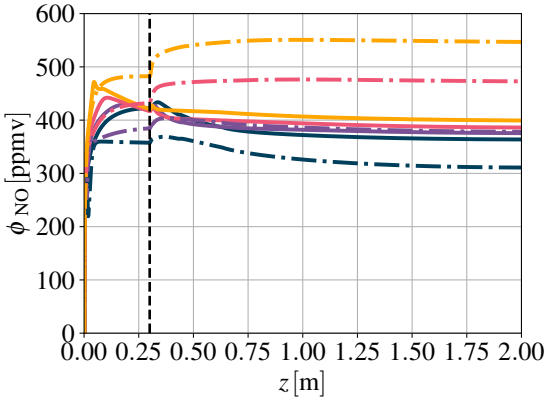

(a) NO formation: Glarborg et al. [139] and GRI-Mech 3.0 [137] mechanisms.

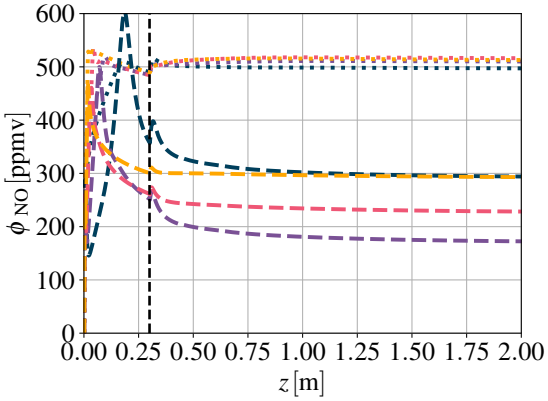

(b) NO formation: Hashemi et al. [127] and Miller and Bowman [106] mechanisms.

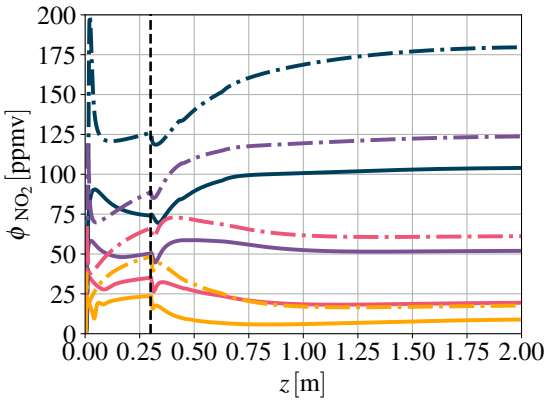

(c) NO_2 formation: Glarborg et al. [139] and GRI-Mech 3.0 [137] mechanisms.

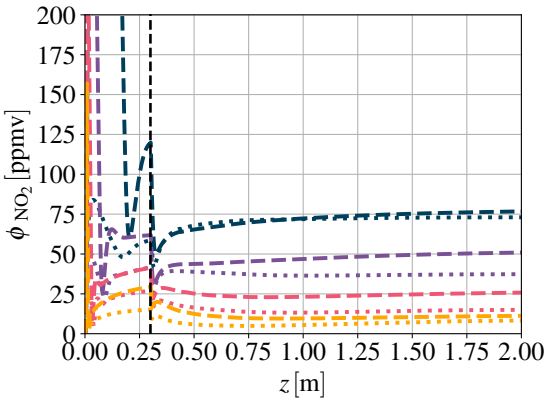

(d) NO_2 formation: Hashemi et al. [127] and Miller and Bowman [106] mechanisms.

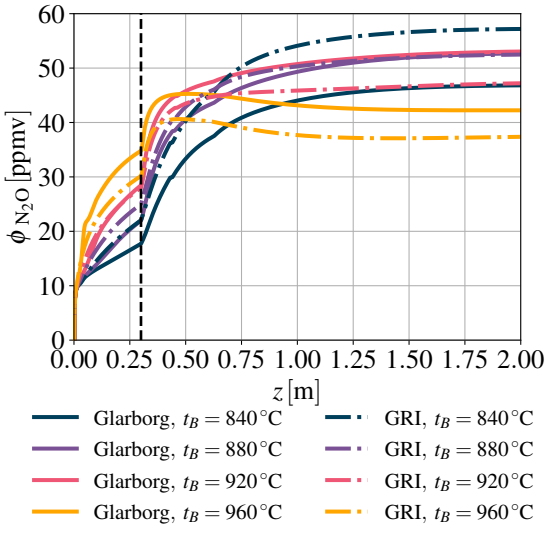

(e) N_2O formation: Glarborg et al. [139] and GRI-Mech 3.0 [137] mechanisms.

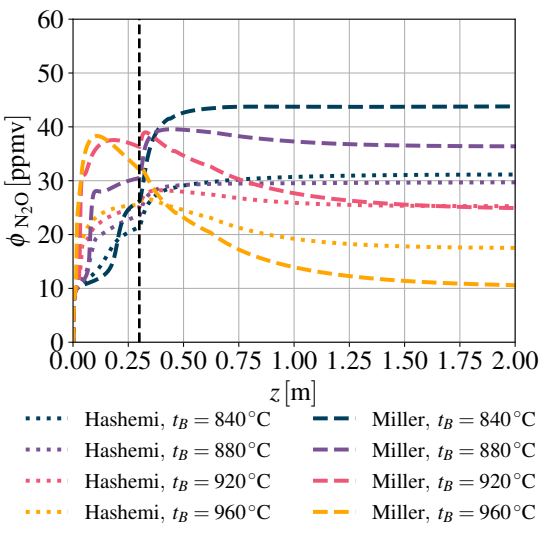

(f) N_2O formation: Hashemi et al. [127] and Miller and Bowman [106] mechanisms.

Figure A.1: Numerical results, concentration profiles: The dependence of NO, NO_2 and N_2O formation on the fluidized bed temperature in the oxy-fuel combustion of lignite.

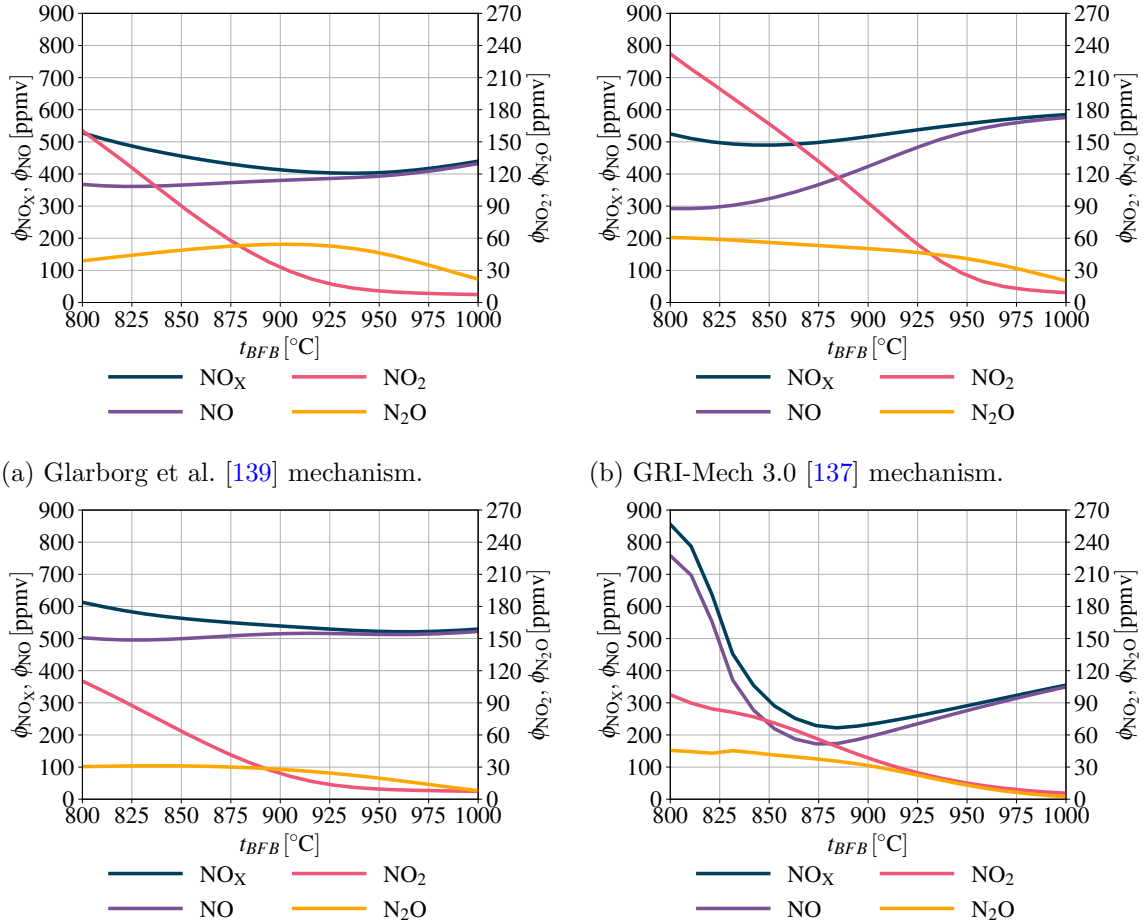

(a) Glarborg et al. [139] mechanism.

(b) GRI-Mech 3.0 [137] mechanism.

(c) Hashemi et al. [127] mechanism.

(d) Miller and Bowman [106] mechanism.

Figure A.2: Numerical results, final concentrations in dry flue gas: The dependence of NO, NO_2 and N_2O formation on the fluidized bed temperature in the oxy-fuel combustion of lignite.

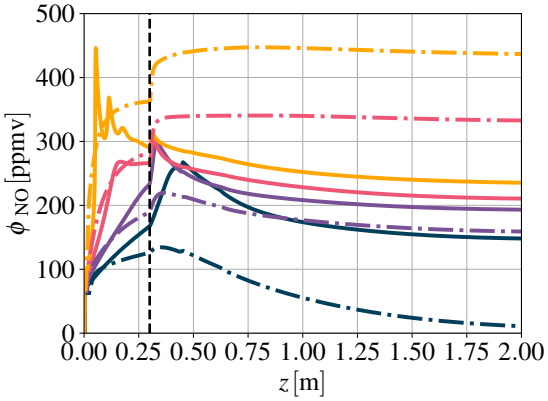

(a) NO formation: Glarborg et al. [139] and GRI-Mech 3.0 [137] mechanisms.

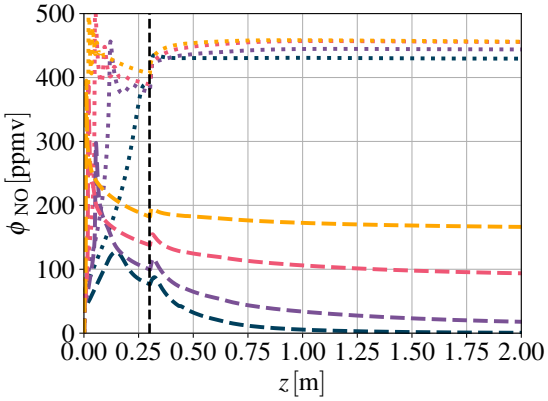

(b) NO formation: Hashemi et al. [127] and Miller and Bowman [106] mechanisms.

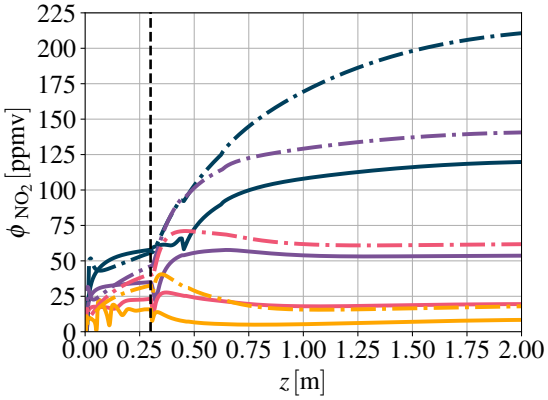

(c) NO_2 formation: Glarborg et al. [139] and GRI-Mech 3.0 [137] mechanisms.

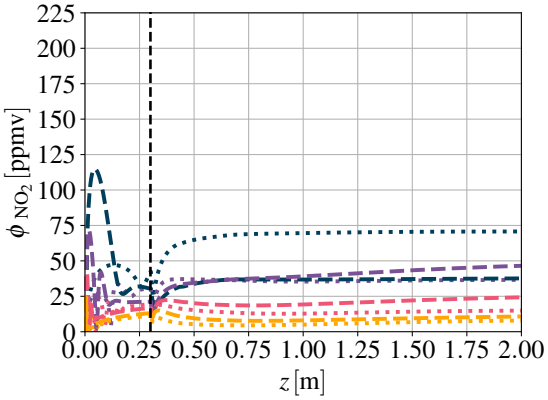

(d) NO_2 formation: Hashemi et al. [127] and Miller and Bowman [106] mechanisms.

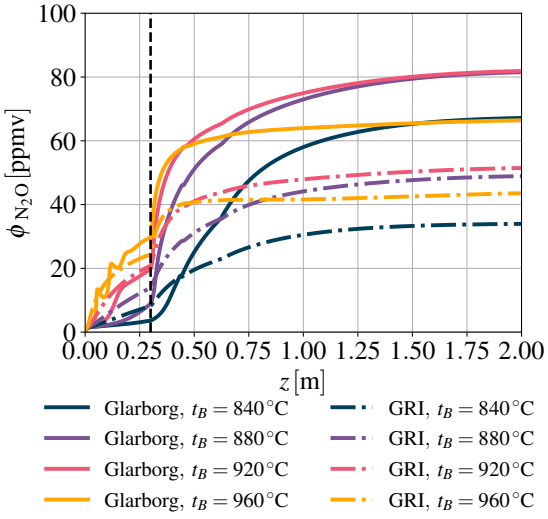

(e) N_2O formation: Glarborg et al. [139] and GRI-Mech 3.0 [137] mechanisms.

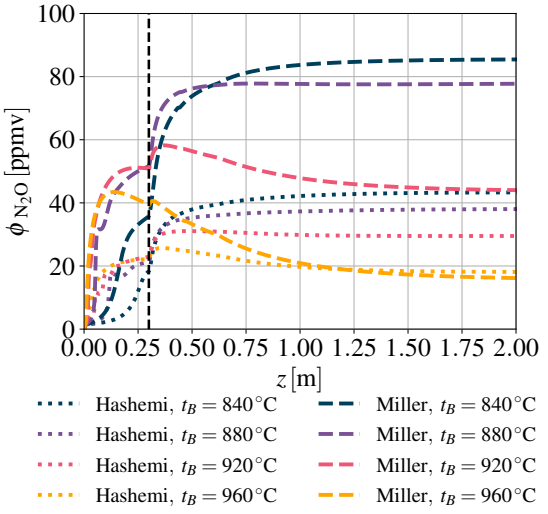

(f) N_2O formation: Hashemi et al. [127] and Miller and Bowman [106] mechanisms.

Figure A.3: Numerical results: The dependence of NO, NO_2 and N_2O formation on the fluidized bed temperature in the oxy-fuel combustion of wooden pellets.

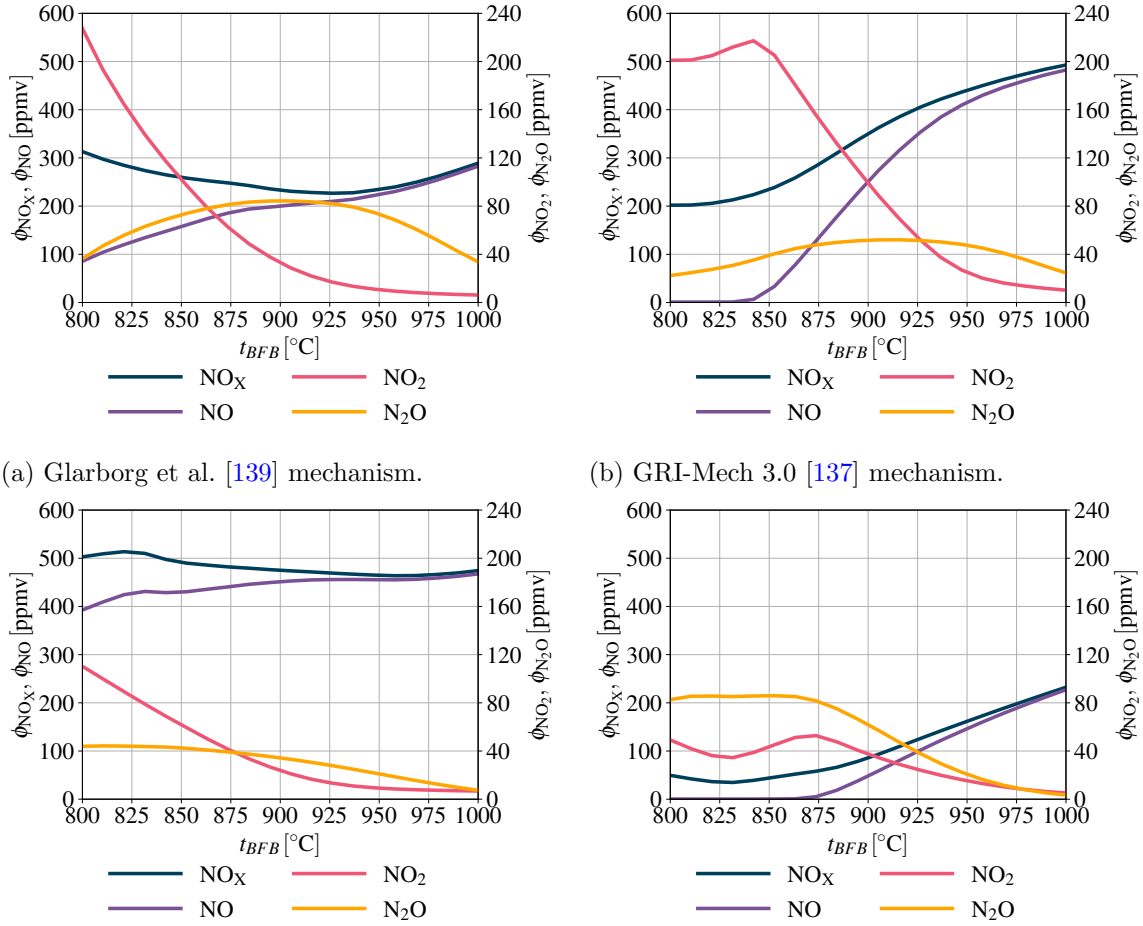

(a) Glarborg et al. [139] mechanism.

(b) GRI-Mech 3.0 [137] mechanism.

(c) Hashemi et al. [127] mechanism.

(d) Miller and Bowman [106] mechanism.

Figure A.4: Numerical results, final concentrations in dry flue gas: The dependence of NO, NO_2 and N_2O formation on the fluidized bed temperature in the oxy-fuel combustion of wooden pellets.

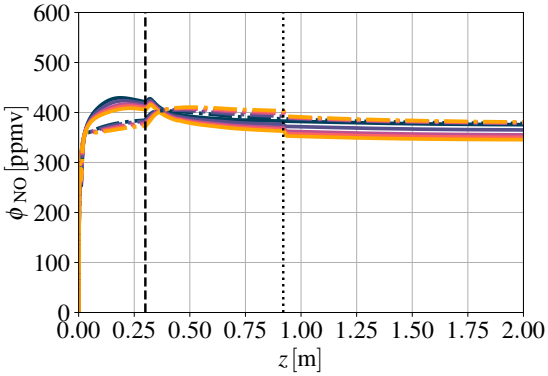

(a) NO formation: Glarborg et al. [139] and GRI-Mech 3.0 [137] mechanisms.

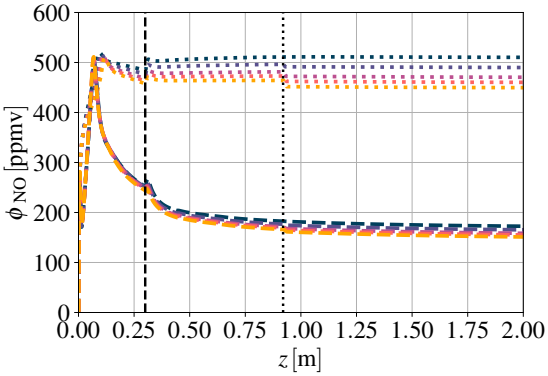

(b) NO formation: Hashemi et al. [127] and Miller and Bowman [106] mechanisms.

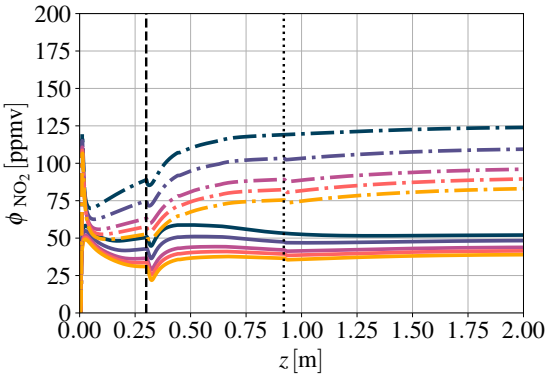

(c) NO_2 formation: Glarborg et al. [139] and GRI-Mech 3.0 [137] mechanisms.

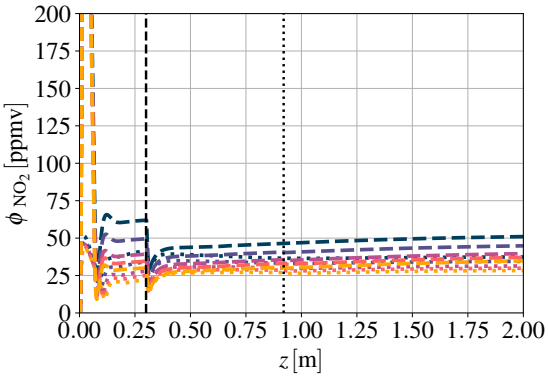

(d) NO_2 formation: Hashemi et al. [127] and Miller and Bowman [106] mechanisms.

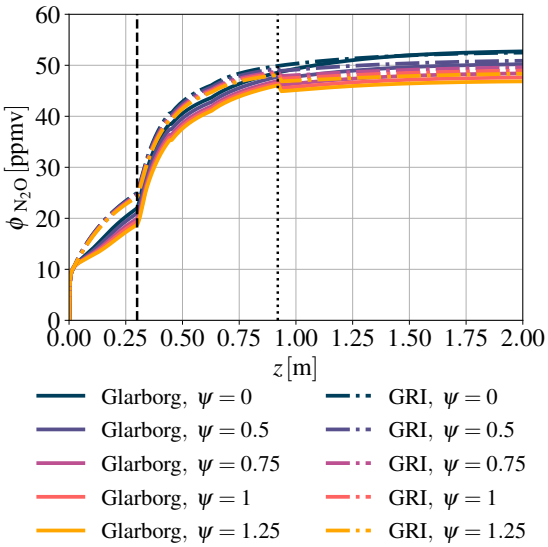

(e) N_2O formation: Glarborg et al. [139] and GRI-Mech 3.0 [137] mechanisms.

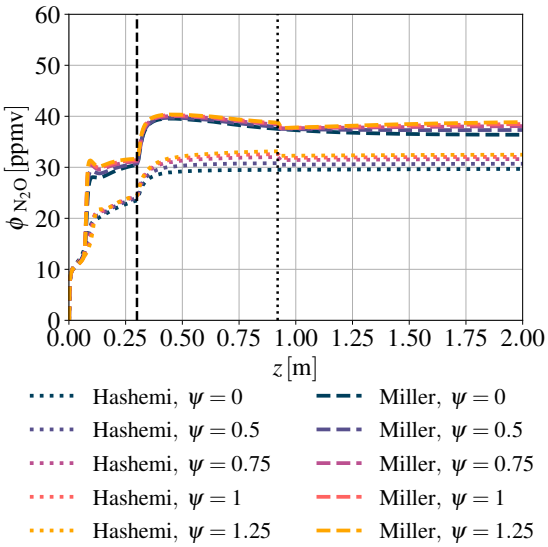

(f) N_2O formation: Hashemi et al. [127] and Miller and Bowman [106] mechanisms.

Figure A.5: Numerical results: The dependence of NO, NO_2 and N_2O formation on the staged supply of oxygen in the oxy-fuel combustion of lignite.

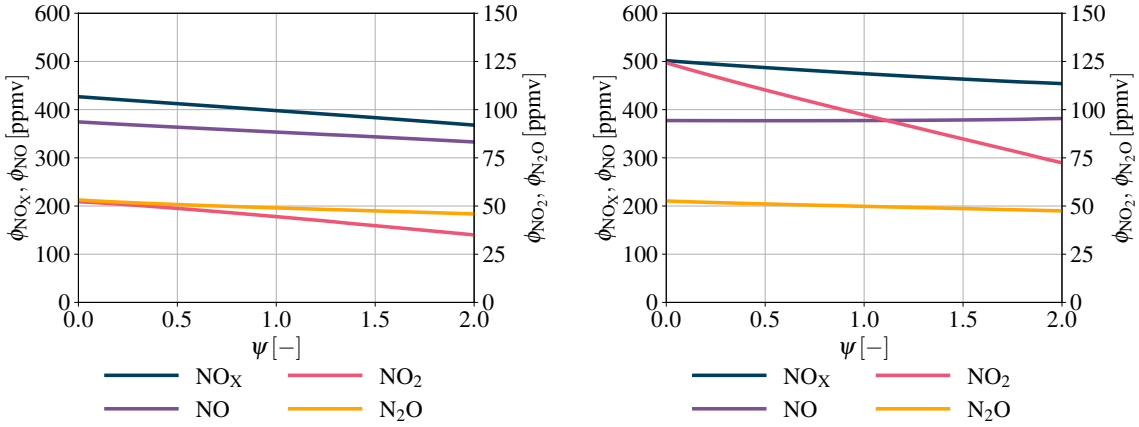

(a) Glarborg et al. [139] mechanism.

(b) GRI-Mech 3.0 [137] mechanism.

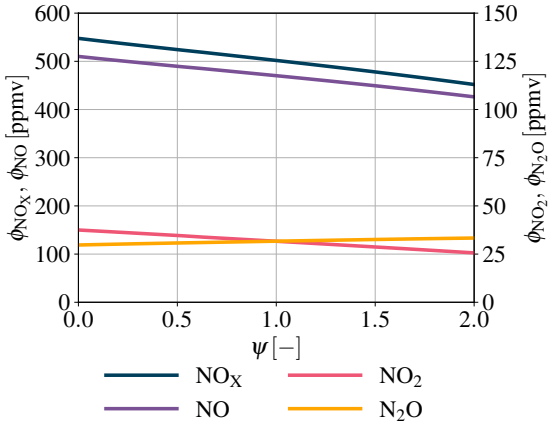

(c) Hashemi et al. [127] mechanism.

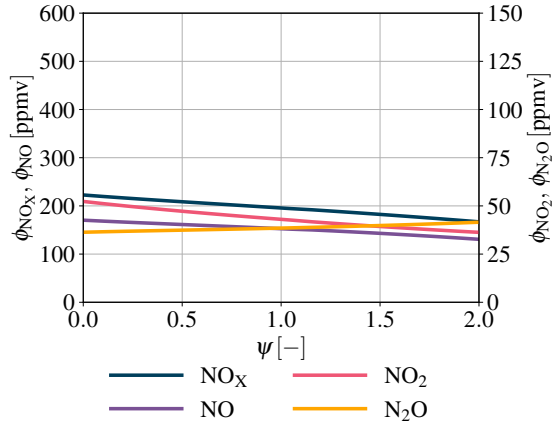

(d) Miller and Bowman [106] mechanism.

Figure A.6: Numerical results, final concentrations in dry flue gas: The dependence of NO, NO_2 and N_2O formation on the staged supply of oxygen in the oxy-fuel combustion of lignite.

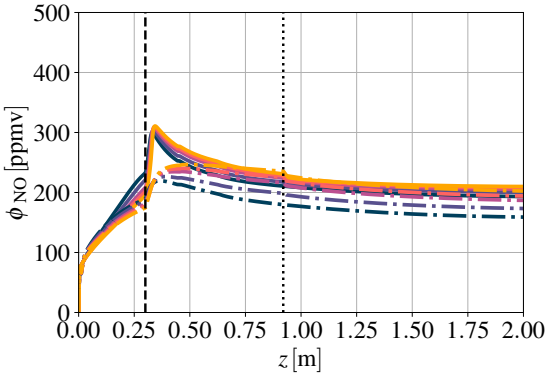

(a) NO formation: Glarborg et al. [139] and GRI-Mech 3.0 [137] mechanisms.

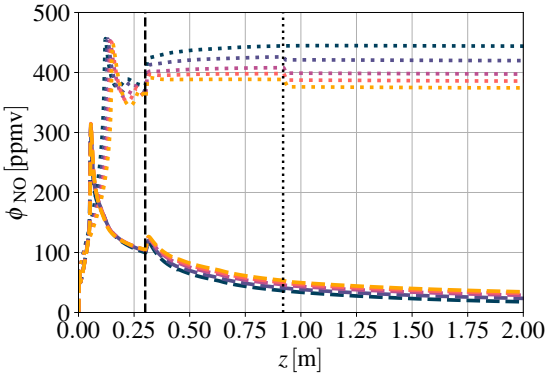

(b) NO formation: Hashemi et al. [127] and Miller and Bowman [106] mechanisms.

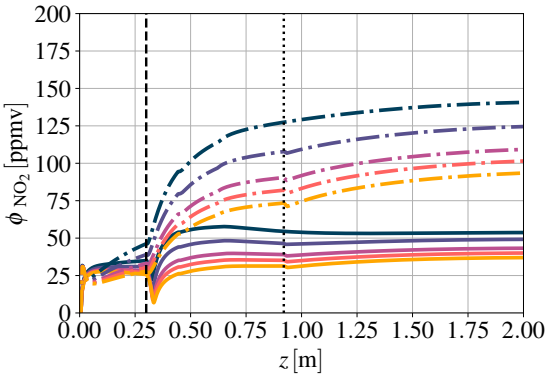

(c) NO_2 formation: Glarborg et al. [139] and GRI-Mech 3.0 [137] mechanisms.

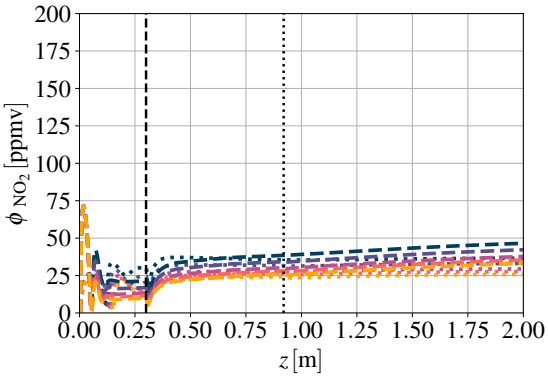

(d) NO_2 formation: Hashemi et al. [127] and Miller and Bowman [106] mechanisms.

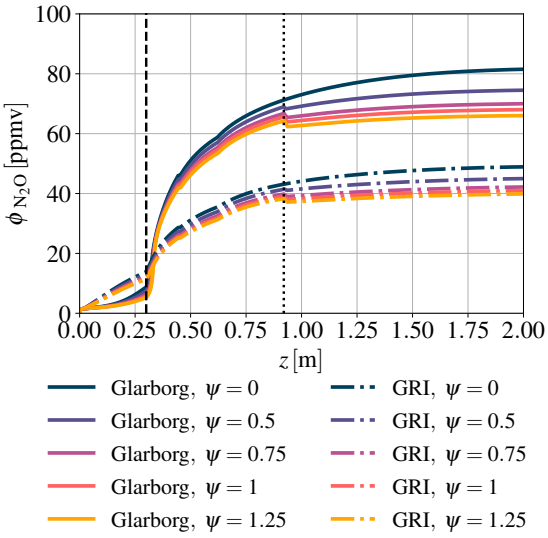

(e) N_2O formation: Glarborg et al. [139] and GRI-Mech 3.0 [137] mechanisms..

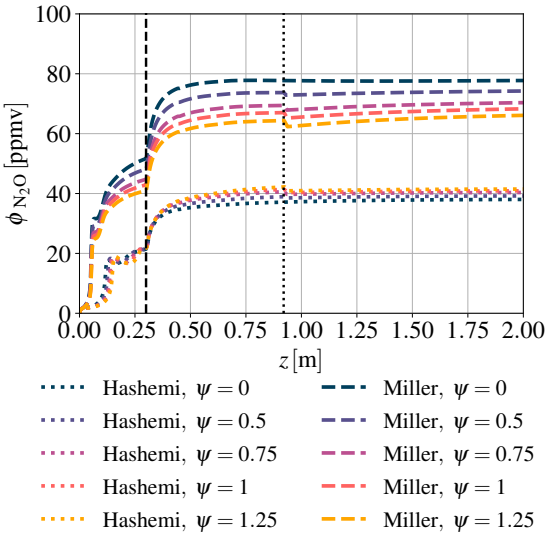

(f) NO_2 formation: Hashemi et al. [127] and Miller and Bowman [106] mechanisms.

Figure A.7: Numerical results: The dependence of NO, NO_2 and N_2O formation on the oxygen staging in the oxy-fuel combustion of wooden pellets.

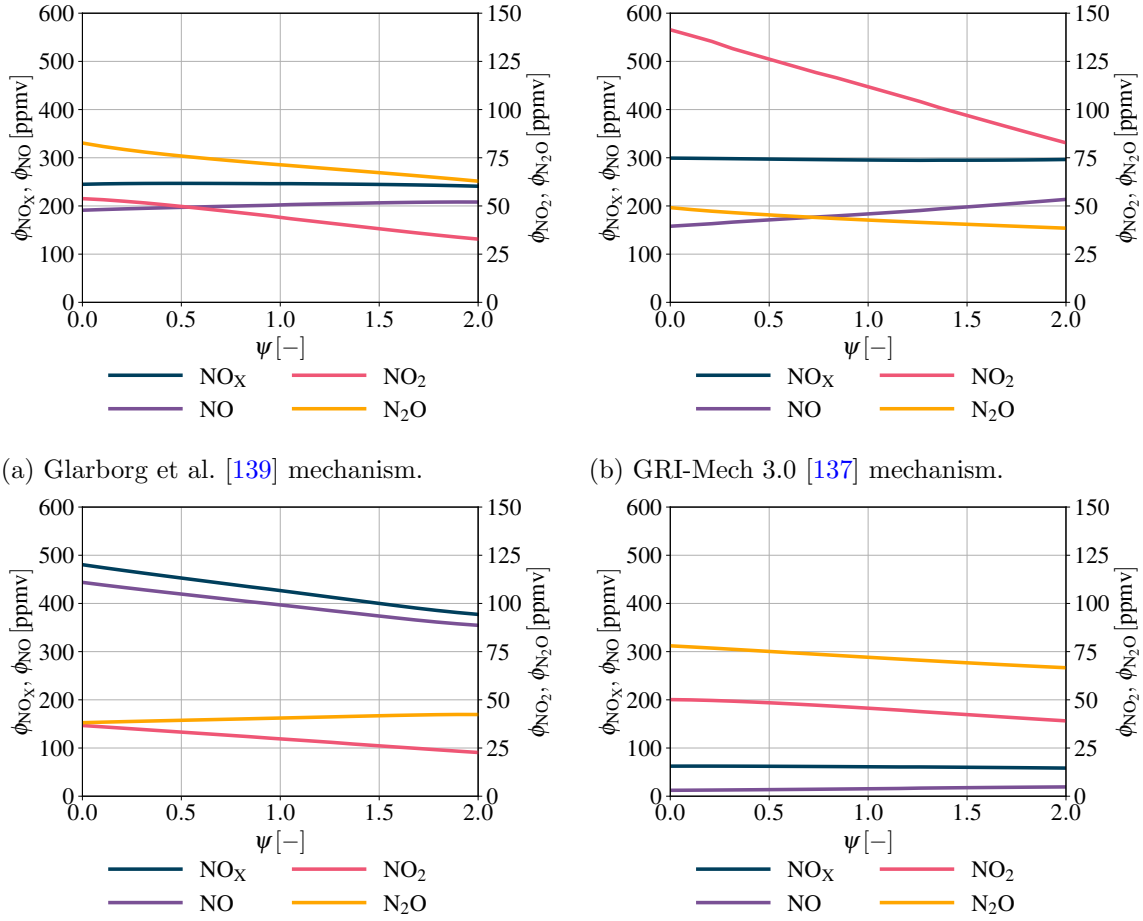

(a) Glarborg et al. [139] mechanism.

(b) GRI-Mech 3.0 [137] mechanism.

(c) Hashemi et al. [127] mechanism.

(d) Miller and Bowman [106] mechanism.

Figure A.8: Numerical results, final concentrations in dry flue gas: The dependence of NO, NO_2 and N_2O formation on the staged supply of oxygen in the oxy-fuel combustion of wooden pellets.

Appendix B

Supplementary experimental results of the NO_X formation

B.1 Oxy-fuel combustion of lignite

B.1.1 Effect of oxygen stoichiometry

Parameter	Unit	'Case 1'	'Case 2'	'Case 3'	'Case 4'
ϕ_{O_2}	[% vol.]	3.1 ± 0.07	6.37 ± 0.09	8.64 ± 0.08	11.58 ± 0.12
t_{BFB}	[°C]	881 ± 0.5	882 ± 0.3	881 ± 0.5	882 ± 0.4
ϕ_{NO_X}	[ppmv]	247 ± 2	398 ± 3	484 ± 2	540 ± 2
EF_{NO_X}	$[mg \cdot MJ^{-1}]$	32.5 ± 0.3	56.3 ± 0.4	68.1 ± 0.3	82.2 ± 0.4
ϕ_{CO}	[ppmv]	2249 ± 68	219 ± 13	152 ± 2	152 ± 4
EF_{CO}	$[mg \cdot MJ^{-1}]$	296.4 ± 8.9	31.0 ± 1.8	21.4 ± 0.3	23.1 ± 0.6
ϕ_{CO_2}	[% vol.]	89.5 ± 0.14	87.3 ± 0.08	84.7 ± 0.1	81.7 ± 0.17
u_0	$[m \cdot s^{-1}]$	0.86	0.98	1.24	1.26
$(\phi_{O_2}/\phi_{CO_2})_{prim}$	[−]	0.44	0.42	0.32	0.36
N − NO	[% mole]	3.15	5.45	6.59	7.96
m_{fuel}	$[kg \cdot h^{-1}]$	3.9	3.9	3.9	3.9

(a) Experimental series No. 1.

Parameter	Unit	'Case 1'	'Case 2'	'Case 3'
ϕ_{O_2}	[% vol.]	2.68 ± 0.11	5.68 ± 0.16	8.61 ± 0.2
t_{BFB}	[°C]	881 ± 0.5	885 ± 0.8	901 ± 0.4
ϕ_{NO_X}	[ppmv]	273 ± 2	390 ± 4	471 ± 3
EF_{NO_X}	$[mg \cdot MJ^{-1}]$	29.9 ± 0.3	44.2 ± 0.5	58.8 ± 0.5
ϕ_{CO}	[ppmv]	2038 ± 70	679 ± 32	889 ± 34
EF_{CO}	$[mg \cdot MJ^{-1}]$	222.9 ± 7.7	77.0 ± 3.6	110.8 ± 4.2
ϕ_{CO_2}	[% vol.]	91.5 ± 0.08	90.6 ± 0.13	87.3 ± 0.18
u_0	$[m \cdot s^{-1}]$	2.39	2.4	2.48
$(\phi_{O_2}/\phi_{CO_2})_{prim}$	[−]	0.22	0.23	0.25
N − NO	[% mole]	2.89	4.28	5.69
m_{fuel}	$[kg \cdot h^{-1}]$	7.1	7.1	7.1

(b) Experimental series No. 2.

Table B.1: Experimental results of the impact of oxygen stoichimetry on the NO_X formation in the oxy-fuel combustion of lignite.

B.1.2 Effect of fluidized bed temperature

Parameter	Unit	'Case 1'	'Case 2'	'Case 3'	'Case 4'	'Case 5'
ϕ_{O_2}	[% vol.]	6.03 ± 0.09	4.97 ± 0.07	6.49 ± 0.12	6.55 ± 0.1	6.39 ± 0.08
t_{BFB}	[°C]	802 ± 1.0	848 ± 0.3	885 ± 0.6	925 ± 0.4	962 ± 0.2
ϕ_{NO_X}	[ppmv]	282 ± 3	297 ± 2	410 ± 5	463 ± 4	491 ± 4
EF_{NO_X}	$[mg \cdot MJ^{-1}]$	37.9 ± 0.4	41.4 ± 0.3	57.8 ± 0.7	66.4 ± 0.6	70.3 ± 0.5
ϕ_{CO}	[ppmv]	289 ± 8	242 ± 30	84 ± 7	168 ± 16	165 ± 9
EF_{CO}	$[mg \cdot MJ^{-1}]$	38.7 ± 1.0	33.7 ± 4.2	11.9 ± 1.0	24.1 ± 2.3	23.6 ± 1.2
ϕ_{CO_2}	[% vol.]	87.4 ± 0.1	89.0 ± 0.08	87.4 ± 0.11	87.7 ± 0.1	87.8 ± 0.16
u_0	$[m \cdot s^{-1}]$	0.87	0.94	1.33	1.36	1.1
$(\phi_{O_2}/\phi_{CO_2})_{prim}$	[−]	0.44	0.43	0.31	0.34	0.46
$N - NO$	[% mole]	3.67	4.0	5.6	6.42	6.81
m_{fuel}	$[kg \cdot h^{-1}]$	4.1	4.1	4.1	4.4	4.4

(a) Experimental series No. 1.

Parameter	Unit	'Case 1'	'Case 2'	'Case 3'	'Case 4'	'Case 5'
ϕ_{O_2}	[% vol.]	6.05 ± 0.12	6.26 ± 0.08	6.34 ± 0.07	7.04 ± 0.11	6.55 ± 0.07
t_{BFB}	[°C]	801 ± 0.7	850 ± 0.3	894 ± 0.2	928 ± 0.5	978 ± 0.3
ϕ_{NO_X}	[ppmv]	260 ± 4	319 ± 2	376 ± 2	455 ± 4	444 ± 2
EF_{NO_X}	$[mg \cdot MJ^{-1}]$	37.1 ± 0.5	45.1 ± 0.3	54.5 ± 0.4	63.9 ± 0.6	62.7 ± 0.3
ϕ_{CO}	[ppmv]	186 ± 12	98 ± 2	146 ± 7	61 ± 3	158 ± 9
EF_{CO}	$[mg \cdot MJ^{-1}]$	26.5 ± 1.6	13.8 ± 0.2	21.2 ± 1.0	8.5 ± 0.4	22.3 ± 1.2
ϕ_{CO_2}	[% vol.]	86.7 ± 0.17	86.2 ± 0.13	87.2 ± 0.07	86.6 ± 0.1	87.3 ± 0.06
u_0	$[m \cdot s^{-1}]$	1.34	1.41	1.54	1.64	1.15
$(\phi_{O_2}/\phi_{CO_2})_{prim}$	[−]	0.27	0.27	0.29	0.27	0.43
$N - NO$	[% mole]	3.59	4.37	5.27	6.18	6.07
m_{fuel}	$[kg \cdot h^{-1}]$	3.9	3.9	4.4	4.4	4.4

(b) Experimental series No. 2.

Parameter	Unit	'Case 1'	'Case 2'	'Case 3'	'Case 4'
ϕ_{O_2}	[% vol.]	5.93 ± 0.19	5.68 ± 0.16	6.48 ± 0.28	5.33 ± 0.19
t_{BFB}	[°C]	842 ± 0.7	885 ± 0.8	942 ± 0.7	970 ± 0.3
ϕ_{NO_X}	[ppmv]	343 ± 3	390 ± 4	461 ± 7	459 ± 3
EF_{NO_X}	$[mg \cdot MJ^{-1}]$	39.1 ± 0.4	44.2 ± 0.5	54.9 ± 0.9	54.7 ± 0.5
ϕ_{CO}	[ppmv]	1119 ± 45	679 ± 32	1614 ± 60	2088 ± 57
EF_{CO}	$[mg \cdot MJ^{-1}]$	127.8 ± 5.1	77.0 ± 3.6	192.3 ± 7.2	248.6 ± 6.8
ϕ_{CO_2}	[% vol.]	90.7 ± 0.16	90.6 ± 0.13	90.2 ± 0.24	91.2 ± 0.15
u_0	$[m \cdot s^{-1}]$	2.02	2.4	2.26	2.21
$(\phi_{O_2}/\phi_{CO_2})_{prim}$	[−]	0.26	0.23	0.28	0.29
$N - NO$	[% mole]	3.79	4.28	5.32	5.29
m_{fuel}	$[kg \cdot h^{-1}]$	7.1	7.1	7.4	7.4

(c) Experimental series No. 3.

Table B.2: Experimental results of the impact of fluidized bed temperature on the NO_X formation in the oxy-fuel combustion of lignite.

B.1.3 Effect of staged supply of oxygen

Parameter	Unit	'Case 1'	'Case 2'	'Case 3'	'Case 4'	'Case 5'
ψ	[−]	0.0	0.26	0.45	0.73	1.22
$V_{O_2,sec}$	$[m^3_N \cdot h^{-1}]$	0.0	1.0	1.5	2.0	2.5
$V_{O_2,prim}$	$[m^3_N \cdot h^{-1}]$	4.92	3.78	3.36	2.74	2.05
λ_{prim}	[−]	1.26	0.97	0.86	0.7	0.53
ϕ_{O_2}	[% vol.]	6.2 ± 0.07	5.64 ± 0.11	5.98 ± 0.05	5.45 ± 0.06	5.56 ± 0.1
t_{BFB}	[°C]	881 ± 0.5	879 ± 0.8	882 ± 0.9	882 ± 0.5	881 ± 1.2
ϕ_{NO_X}	[ppmv]	373 ± 3	244 ± 4	193 ± 1	197 ± 1	265 ± 2
EF_{NO_X}	$[mg \cdot MJ^{-1}]$	53.2 ± 0.4	33.8 ± 0.6	27.2 ± 0.1	27.0 ± 0.1	34.6 ± 0.3
ϕ_{CO}	[ppmv]	401 ± 26	128 ± 4	168 ± 7	268 ± 10	60 ± 26
EF_{CO}	$[mg \cdot MJ^{-1}]$	34.8 ± 2.3	10.8 ± 0.3	14.4 ± 0.6	22.4 ± 0.9	4.8 ± 2.1
ϕ_{CO_2}	[% vol.]	86.5 ± 0.11	84.9 ± 0.12	84.6 ± 0.08	85.9 ± 0.07	86.7 ± 0.12
u_0	$[m \cdot s^{-1}]$	1.15	1.14	1.34	1.21	0.86
$(\phi_{O_2}/\phi_{CO_2})_{prim}$	[−]	0.44	0.35	0.28	0.24	0.25
$N - NO$	[% mole]	3.76	2.38	1.92	1.91	2.44
m_{fuel}	$[kg \cdot h^{-1}]$	3.6	3.6	3.6	3.6	3.6

(a) Experimental series No. 1.

Parameter	Unit	'Case 1'	'Case 2'	'Case 3'	'Case 4'	'Case 5'
ψ	[−]	0.0	0.21	0.35	0.59	0.91
$V_{O_2,sec}$	$[m^3_N \cdot h^{-1}]$	0.0	1.0	1.5	2.0	2.5
$V_{O_2,prim}$	$[m^3_N \cdot h^{-1}]$	5.74	4.73	4.25	3.37	2.76
λ_{prim}	[−]	1.35	1.11	1.0	0.79	0.65
ϕ_{O_2}	[% vol.]	6.33 ± 0.06	6.56 ± 0.05	6.55 ± 0.05	7.5 ± 0.06	5.36 ± 0.05
t_{BFB}	[°C]	885 ± 0.2	887 ± 0.3	878 ± 0.4	889 ± 0.5	883 ± 0.7
ϕ_{NO_X}	[ppmv]	367 ± 2	325 ± 2	277 ± 2	261 ± 2	241 ± 1
EF_{NO_X}	$[mg \cdot MJ^{-1}]$	56.2 ± 0.3	49.7 ± 0.2	42.5 ± 0.3	37.2 ± 0.2	33.5 ± 0.2
ϕ_{CO}	[ppmv]	827 ± 24	332 ± 19	198 ± 14	71 ± 3	54 ± 6
EF_{CO}	$[mg \cdot MJ^{-1}]$	77.1 ± 2.3	30.9 ± 1.8	18.5 ± 1.3	6.2 ± 0.3	4.6 ± 0.5
ϕ_{CO_2}	[% vol.]	89.1 ± 0.05	88.7 ± 0.05	88.0 ± 0.05	86.4 ± 0.05	83.0 ± 0.03
u_0	$[m \cdot s^{-1}]$	1.18	1.18	1.11	1.12	0.75
O_2/CO_2	[−]	0.49	0.41	0.39	0.34	0.39
$N - NO$	[% mole]	3.96	3.51	3.0	2.63	2.37
m_{fuel}	$[kg \cdot h^{-1}]$	3.9	3.9	3.9	3.9	3.9

(b) Experimental series No. 2.

Table B.3: Experimental results of the impact of staged supply of oxygen on the NO_X formation in the oxy-fuel combustion of lignite. Constant fluidized bed temperature at 880 °C, constant O_2 volumetric fraction in dry flue gas $\phi_{O_2} = 6$ % vol.

Parameter	Unit	'Case 1'	'Case 2'	'Case 3'	'Case 4'
ψ	[−]	0.0	0.24	0.51	1.14
$V_{O_2,sec}$	$[m^3_N \cdot h^{-1}]$	0.0	1.0	2.0	3.0
$V_{O_2,prim}$	$[m^3_N \cdot h^{-1}]$	5.88	4.21	3.91	2.64
λ_{prim}	[−]	1.38	0.99	0.92	0.62
ϕ_{O_2}	[% vol.]	8.03 ± 0.09	9.24 ± 0.07	8.12 ± 0.08	9.97 ± 0.07
t_{BFB}	[°C]	879 ± 0.5	879 ± 0.4	887 ± 0.6	879 ± 0.5
ϕ_{NO_X}	[ppmv]	432 ± 3	393 ± 2	288 ± 2	264 ± 2
EF_{NO_X}	$[mg \cdot MJ^{-1}]$	68.1 ± 0.4	54.1 ± 0.3	45.7 ± 0.2	39.6 ± 0.2
ϕ_{CO}	[ppmv]	463 ± 19	87 ± 2	353 ± 29	73 ± 3
EF_{CO}	$[mg \cdot MJ^{-1}]$	44.4 ± 1.8	7.3 ± 0.2	34.0 ± 2.8	6.6 ± 0.2
ϕ_{CO_2}	[% vol.]	85.6 ± 0.08	83.3 ± 0.07	84.3 ± 0.08	82.4 ± 0.08
u_0	$[m \cdot s^{-1}]$	1.42	1.37	1.31	1.29
$(\phi_{O_2}/\phi_{CO_2})_{prim}$	[−]	0.45	0.37	0.35	0.29
N − NO	[% mole]	4.8	3.82	3.22	2.8
m_{fuel}	$[kg \cdot h^{-1}]$	3.9	3.9	3.9	3.9

Table B.4: Experimental results of the impact of staged supply of oxygen on the NO_X formation in the oxy-fuel combustion of lignite. Constant fluidized bed temperature at 880 °C, constant O_2 volumetric fraction in dry flue gas $\phi_{O_2} = 9$ % vol.

Parameter	Unit	'Case 1'	'Case 2'	'Case 3'	'Case 4'
ψ	[−]	0.0	0.28	0.49	1.02
$V_{O_2,sec}$	$[m^3_N \cdot h^{-1}]$	0.0	1.3	2.0	3.0
$V_{O_2,prim}$	$[m^3_N \cdot h^{-1}]$	5.51	4.69	4.07	2.95
λ_{prim}	[−]	1.24	1.06	0.92	0.67
ϕ_{O_2}	[% vol.]	6.62 ± 0.05	6.02 ± 0.06	6.24 ± 0.04	5.91 ± 0.06
t_{BFB}	[°C]	891 ± 0.2	858 ± 2.3	867 ± 1.0	985 ± 2.6
ϕ_{NO_X}	[ppmv]	413 ± 2	234 ± 2	234 ± 2	270 ± 2
EF_{NO_X}	$[mg \cdot MJ^{-1}]$	57.9 ± 0.3	36.1 ± 0.3	36.6 ± 0.3	41.2 ± 0.3
ϕ_{CO}	[ppmv]	144 ± 4	1489 ± 38	1355 ± 35	2213 ± 79
EF_{CO}	$[mg \cdot MJ^{-1}]$	12.3 ± 0.3	139.4 ± 3.5	128.8 ± 3.3	205.6 ± 7.4
ϕ_{CO_2}	[% vol.]	87.1 ± 0.05	88.5 ± 0.07	88.0 ± 0.04	86.6 ± 0.09
u_0	$[m \cdot s^{-1}]$	1.3	1.07	0.96	0.88
$(\phi_{O_2}/\phi_{CO_2})_{prim}$	[−]	0.44	0.43	0.42	0.37
N − NO	[% mole]	4.08	2.55	2.58	2.91
m_{fuel}	$[kg \cdot h^{-1}]$	4.1	4.1	4.1	4.1

Table B.5: Experimental results of the impact of staged supply of oxygen on the NO_X formation in the oxy-fuel combustion of lignite. Constant $(\phi_{O_2}/\phi_{CO_2})_{prim}$ ratio in the primary gas, constant O_2 volumetric fraction in dry flue gas $\phi_{O_2} = 6$ % vol.

B.2 Oxy-fuel combustion of wooden pellets

B.2.1 Effect of oxygen stoichiometry

Parameter	Unit	'Case 1'	'Case 2'	'Case 3'
ϕ_{O_2}	[% vol.]	3.02 ± 0.13	7.09 ± 0.18	8.39 ± 0.22
t_{BFB}	[°C]	881 ± 0.5	883 ± 0.4	879 ± 0.6
ϕ_{NO_X}	[ppmv]	349 ± 6	469 ± 3	502 ± 5
EF_{NO_X}	$[mg \cdot MJ^{-1}]$	38.8 ± 0.6	54.4 ± 0.4	59.1 ± 0.6
ϕ_{CO}	[ppmv]	516 ± 79	10 ± 1	14 ± 1
EF_{CO}	$[mg \cdot MJ^{-1}]$	57.3 ± 8.8	1.2 ± 0.1	1.7 ± 0.1
ϕ_{CO_2}	[% vol.]	92.0 ± 0.11	88.1 ± 0.17	87.4 ± 0.2
u_0	$[m \cdot s^{-1}]$	0.97	0.98	1.02
$(\phi_{O_2}/\phi_{CO_2})_{prim}$	[−]	0.48	0.48	0.48
$N - NO$	[% mole]	7.11	9.97	10.84
m_{fuel}	$[kg \cdot h^{-1}]$	5.4	5.1	5.0

(a) Experimental series No. 1.

Parameter	Unit	'Case 1'	'Case 2'	'Case 3'
ϕ_{O_2}	[% vol.]	3.22 ± 0.07	6.02 ± 0.1	10.3 ± 0.1
t_{BFB}	[°C]	841 ± 0.6	839 ± 0.8	836 ± 0.3
ϕ_{NO_X}	[ppmv]	212 ± 2	266 ± 1	310 ± 1
EF_{NO_X}	$[mg \cdot MJ^{-1}]$	23.6 ± 0.2	30.5 ± 0.2	37.3 ± 0.1
ϕ_{CO}	[ppmv]	457 ± 69	28 ± 2	26 ± 1
EF_{CO}	$[mg \cdot MJ^{-1}]$	50.8 ± 7.6	3.2 ± 0.2	3.1 ± 0.1
ϕ_{CO_2}	[% vol.]	95.0 ± 0.06	92.8 ± 0.09	88.2 ± 0.1
u_0	$[m \cdot s^{-1}]$	0.97	1.02	1.11
$(\phi_{O_2}/\phi_{CO_2})_{prim}$	[−]	0.46	0.45	0.45
$N - NO$	[% mole]	4.33	5.6	6.84
m_{fuel}	$[kg \cdot h^{-1}]$	5.6	5.6	5.6

(b) Experimental series No. 2.

Parameter	Unit	'Case 1'	'Case 2'	'Case 3'	'Case 4'
ϕ_{O_2}	[% vol.]	3.63 ± 0.12	5.41 ± 0.13	10.42 ± 0.12	12.86 ± 0.17
t_{BFB}	[°C]	879 ± 0.7	886 ± 0.5	894 ± 0.6	884 ± 0.4
ϕ_{NO_X}	[ppmv]	255 ± 2	288 ± 2	356 ± 1	369 ± 1
EF_{NO_X}	$[mg \cdot MJ^{-1}]$	28.6 ± 0.3	32.8 ± 0.3	42.9 ± 0.1	45.6 ± 0.1
ϕ_{CO}	[ppmv]	323 ± 66	366 ± 58	45 ± 0	52 ± 0
EF_{CO}	$[mg \cdot MJ^{-1}]$	36.1 ± 7.4	41.6 ± 6.6	5.4 ± 0.0	6.4 ± 0.0
ϕ_{CO_2}	[% vol.]	91.9 ± 0.09	90.2 ± 0.12	85.7 ± 0.11	83.3 ± 0.16
u_0	$[m \cdot s^{-1}]$	1.73	1.82	2.05	2.18
$(\phi_{O_2}/\phi_{CO_2})_{prim}$	[−]	0.35	0.36	0.35	0.34
$N - NO$	[% mole]	5.24	6.01	7.86	8.37
m_{fuel}	$[kg \cdot h^{-1}]$	9.0	9.0	9.0	9.0

(c) Experimental series No. 3.

Table B.6: Experimental results of the impact of oxygen stoichimetry on the NO_X formation in the oxy-fuel combustion of wooden pellets.

B.2.2 Effect of fluidized bed temperature

Parameter	Unit	'Case 1'	'Case 2'	'Case 3'
ϕ_{O_2}	[% vol.]	6.02 ± 0.1	6.48 ± 0.16	7.21 ± 0.23
t_{BFB}	[°C]	839 ± 0.8	880 ± 0.5	926 ± 0.3
ϕ_{NO_X}	[ppmv]	266 ± 1	268 ± 2	270 ± 3
EF_{NO_X}	$[mg \cdot MJ^{-1}]$	30.5 ± 0.2	30.9 ± 0.3	31.3 ± 0.4
ϕ_{CO}	[ppmv]	28 ± 2	76 ± 25	17 ± 2
EF_{CO}	$[mg \cdot MJ^{-1}]$	3.2 ± 0.2	8.7 ± 2.9	2.0 ± 0.2
ϕ_{CO_2}	[% vol.]	92.8 ± 0.09	91.9 ± 0.15	91.3 ± 0.23
u_0	$[m \cdot s^{-1}]$	1.02	0.95	1.1
$(\phi_{O_2}/\phi_{CO_2})_{prim}$	[−]	0.45	0.5	0.55
N − NO	[% mole]	5.6	5.66	5.74
m_{fuel}	$[kg \cdot h^{-1}]$	5.6	5.6	6.7

(a) Experimental series No. 1.

Parameter	Unit	'Case 1'	'Case 2'	'Case 3'	'Case 4'
ϕ_{O_2}	[% vol.]	6.15 ± 0.11	6.02 ± 0.12	6.26 ± 0.12	6.73 ± 0.13
t_{BFB}	[°C]	837 ± 1.3	870 ± 1.0	924 ± 0.5	965 ± 0.4
ϕ_{NO_X}	[ppmv]	293 ± 2	289 ± 2	290 ± 2	297 ± 1
EF_{NO_X}	$[mg \cdot MJ^{-1}]$	33.6 ± 0.2	33.1 ± 0.2	33.4 ± 0.2	34.3 ± 0.2
ϕ_{CO}	[ppmv]	26 ± 2	41 ± 4	43 ± 5	40 ± 6
EF_{CO}	$[mg \cdot MJ^{-1}]$	3.0 ± 0.2	4.7 ± 0.4	4.9 ± 0.6	4.6 ± 0.7
ϕ_{CO_2}	[% vol.]	89.9 ± 0.1	89.9 ± 0.11	89.7 ± 0.11	89.2 ± 0.11
u_0	$[m \cdot s^{-1}]$	1.64	1.74	1.73	1.7
$(\phi_{O_2}/\phi_{CO_2})_{prim}$	[−]	0.34	0.34	0.37	0.4
N − NO	[% mole]	6.16	6.07	6.12	6.29
m_{fuel}	$[kg \cdot h^{-1}]$	9.0	9.0	9.0	9.0

(b) Experimental series No. 2.

Table B.7: Experimental results of the impact of fluidized bed temperature on the NO_X formation in the oxy-fuel combustion of wooden pellets.

B.2.3 Effect of staged supply of oxygen

Parameter	Unit	'Case 1'	'Case 2'	'Case 3'	'Case 4'
ψ	[−]	0.0	0.24	0.46	0.7
$V_{O_2,sec}$	$[m^3_N \cdot h^{-1}]$	0.0	1.5	2.4	3.18
$V_{O_2,prim}$	$[m^3_N \cdot h^{-1}]$	7.75	6.16	5.22	4.56
λ_{prim}	[−]	1.02	0.81	0.69	0.6
ϕ_{O_2}	[% vol.]	6.08 ± 0.13	6.71 ± 0.08	6.1 ± 0.1	5.54 ± 0.08
t_{BFB}	[°C]	878 ± 0.8	870 ± 0.6	864 ± 0.6	868 ± 1.2
ϕ_{NO_X}	[ppmv]	332 ± 4	281 ± 1	247 ± 1	214 ± 1
EF_{NO_X}	$[mg \cdot MJ^{-1}]$	36.4 ± 0.5	30.4 ± 0.1	26.6 ± 0.1	23.5 ± 0.1
ϕ_{CO}	[ppmv]	37 ± 8	39 ± 0	29 ± 0	36 ± 5
EF_{CO}	$[mg \cdot MJ^{-1}]$	2.5 ± 0.6	2.6 ± 0.0	1.9 ± 0.0	2.4 ± 0.3
ϕ_{CO_2}	[% vol.]	69.5 ± 0.13	71.4 ± 0.08	73.5 ± 0.09	75.0 ± 0.35
u_0	$[m \cdot s^{-1}]$	2.05	1.84	1.67	1.58
$(\phi_{O_2}/\phi_{CO_2})_{prim}$	[−]	0.48	0.43	0.38	0.34
$N - NO$	[% mole]	6.68	5.58	4.88	4.3
m_{fuel}	$[kg \cdot h^{-1}]$	9.0	9.0	9.0	9.0

Table B.8: Experimental results of the impact of staged supply of oxygen on the NO_X formation in the oxy-fuel combustion of wooden pellets. Constant fluidized bed temperature at 880 °C, constant O_2 volumetric fraction in dry flue gas $\phi_{O_2} = 6$ % vol.

Parameter	Unit	'Case 1'	'Case 2'	'Case 3'	'Case 4'
ψ	[−]	0.0	0.23	0.58	1.16
$V_{O_2,sec}$	$[m^3_N \cdot h^{-1}]$	0.0	1.5	3.0	4.5
$V_{O_2,prim}$	$[m^3_N \cdot h^{-1}]$	7.92	6.57	5.17	3.87
λ_{prim}	[−]	1.04	0.86	0.68	0.51
ϕ_{O_2}	[% vol.]	9.32 ± 0.09	9.43 ± 0.08	8.79 ± 0.1	8.86 ± 0.13
t_{BFB}	[°C]	882 ± 0.3	881 ± 0.3	877 ± 0.8	872 ± 0.7
ϕ_{NO_X}	[ppmv]	463 ± 3	407 ± 2	296 ± 1	229 ± 1
EF_{NO_X}	$[mg \cdot MJ^{-1}]$	52.1 ± 0.4	46.8 ± 0.2	34.4 ± 0.1	27.3 ± 0.1
ϕ_{CO}	[ppmv]	46 ± 0	56 ± 0	51 ± 0	45 ± 4
EF_{CO}	$[mg \cdot MJ^{-1}]$	3.1 ± 0.0	3.9 ± 0.0	3.6 ± 0.0	3.3 ± 0.3
ϕ_{CO_2}	[% vol.]	69.7 ± 0.13	69.6 ± 0.08	70.9 ± 0.1	71.8 ± 0.37
u_0	$[m \cdot s^{-1}]$	2.2	2.2	1.98	1.77
$(\phi_{O_2}/\phi_{CO_2})_{prim}$	[−]	0.51	0.44	0.38	0.33
$N - NO$	[% mole]	9.55	8.58	6.32	5.02
m_{fuel}	$[kg \cdot h^{-1}]$	9.0	9.0	9.0	9.0

Table B.9: Experimental results of the impact of staged supply of oxygen on the NO_X formation in the oxy-fuel combustion of wooden pellets. Constant fluidized bed temperature at 880 °C, constant O_2 volumetric fraction in dry flue gas $\phi_{O_2} = 9$ % vol.

Parameter	Unit	'Case 1'	'Case 2'	'Case 3'	'Case 4'
ψ	[−]	0.0	0.35	0.54	0.91
$V_{O_2,sec}$	$[m^3_N \cdot h^{-1}]$	0.0	2.1	2.58	3.42
$V_{O_2,prim}$	$[m^3_N \cdot h^{-1}]$	8.01	6.09	4.74	3.76
λ_{prim}	[−]	1.05	0.8	0.62	0.49
ϕ_{O_2}	[% vol.]	6.41 ± 0.12	6.25 ± 0.12	7.04 ± 0.12	6.03 ± 0.09
t_{BFB}	[°C]	877 ± 0.5	919 ± 1.0	895 ± 1.0	833 ± 2.2
ϕ_{NO_X}	[ppmv]	354 ± 2	271 ± 2	205 ± 1	186 ± 1
EF_{NO_X}	$[mg \cdot MJ^{-1}]$	40.3 ± 0.3	31.5 ± 0.3	21.1 ± 0.1	18.7 ± 0.1
ϕ_{CO}	[ppmv]	42 ± 1	44 ± 1	33 ± 0	38 ± 3
EF_{CO}	$[mg \cdot MJ^{-1}]$	2.9 ± 0.1	3.1 ± 0.0	2.1 ± 0.0	2.3 ± 0.2
ϕ_{CO_2}	[% vol.]	74.5 ± 0.11	76.4 ± 0.12	76.8 ± 0.08	79.4 ± 0.07
u_0	$[m \cdot s^{-1}]$	2.24	2.05	1.71	1.4
$(\phi_{O_2}/\phi_{CO_2})_{prim}$	[−]	0.43	0.37	0.35	0.3
$N - NO$	[% mole]	7.39	5.79	3.88	3.44
m_{fuel}	$[kg \cdot h^{-1}]$	9.0	9.0	9.0	9.0

Table B.10: Experimental results of the impact of staged supply of oxygen on the NO_X formation in the oxy-fuel combustion of wooden pellets. Constant $(\phi_{O_2}/\phi_{CO_2})_{prim}$ ratio in the primary gas, constant O_2 volumetric fraction in dry flue gas $\phi_{O_2} = 6\,\%\,vol.$

B.3 Air-combustion of lignite

B.3.1 Effect of air stoichiometry

Parameter	Unit	'Case 1'	'Case 2'	'Case 3'
ϕ_{O_2}	[% vol.]	2.67 ± 0.06	5.55 ± 0.06	9.04 ± 0.09
t_{BFB}	[°C]	885 ± 0.5	891 ± 0.5	874 ± 0.7
ϕ_{NO_X}	[ppmv]	247 ± 0	292 ± 0	290 ± 0
EF_{NO_X}	$[mg \cdot MJ^{-1}]$	119.2 ± 0.4	198.6 ± 0.2	330.0 ± 0.7
ϕ_{CO}	[ppmv]	1132 ± 19	328 ± 4	322 ± 10
EF_{CO}	$[mg \cdot MJ^{-1}]$	546.1 ± 9.4	222.9 ± 2.7	366.9 ± 11.1
ϕ_{CO_2}	[% vol.]	15.7 ± 0.05	13.2 ± 0.05	9.8 ± 0.08
u_0	$[m \cdot s^{-1}]$	2.78	2.7	3.08
$N - NO$	[% mole]	14.09	19.8	25.47
m_{fuel}	$[kg \cdot h^{-1}]$	8.0	8.0	8.0

Table B.11: Experimental results of the impact of air stoichimetry on the NO_X formation in the air-combustion of lignite.

B.3.2 Effect of fluidized bed temperature

Parameter	Unit	'Case 1'	'Case 2'	'Case 3'	'Case 4'
ϕ_{O_2}	[% vol.]	6.19 ± 0.08	6.07 ± 0.11	6.07 ± 0.09	6.15 ± 0.09
t_{BFB}	[°C]	843 ± 0.6	878 ± 1.4	930 ± 0.3	960 ± 0.3
ϕ_{NO_X}	[ppmv]	281 ± 0	290 ± 1	308 ± 0	310 ± 0
EF_{NO_X}	$[mg \cdot MJ^{-1}]$	208.5 ± 0.4	211.7 ± 0.8	224.4 ± 0.3	229.0 ± 0.3
ϕ_{CO}	[ppmv]	370 ± 6	414 ± 17	291 ± 5	211 ± 3
EF_{CO}	$[mg \cdot MJ^{-1}]$	274.2 ± 4.5	302.0 ± 12.6	212.5 ± 3.9	155.8 ± 2.6
ϕ_{CO_2}	[% vol.]	12.4 ± 0.07	12.5 ± 0.09	12.6 ± 0.08	12.5 ± 0.07
u_0	$[m \cdot s^{-1}]$	2.72	2.67	2.63	2.63
$N - NO$	[% mole]	19.91	20.4	21.62	21.93
m_{fuel}	$[kg \cdot h^{-1}]$	8.0	8.0	8.0	8.0

Table B.12: Experimental results of the impact of fluidized bed temperature on the NO_X formation in the air-combustion of lignite.

B.4 Air-combustion of wooden pellets

B.4.1 Effect of air stoichiometry

Parameter	Unit	'Case 1'	'Case 2'	'Case 3'
ϕ_{O_2}	[% vol.]	2.97 ± 0.05	6.32 ± 0.04	10.15 ± 0.38
t_{BFB}	[°C]	876 ± 0.2	881 ± 0.5	888 ± 0.4
ϕ_{NO_X}	[ppmv]	105 ± 0	108 ± 0	92 ± 1
EF_{NO_X}	$[mg \cdot MJ^{-1}]$	41.4 ± 0.2	64.3 ± 0.1	100.6 ± 1.1
ϕ_{CO}	[ppmv]	71 ± 15	45 ± 1	53 ± 7
EF_{CO}	$[mg \cdot MJ^{-1}]$	27.8 ± 5.9	26.7 ± 0.8	58.0 ± 7.3
ϕ_{CO_2}	[% vol.]	15.7 ± 0.05	12.5 ± 0.05	8.9 ± 0.1
u_0	$[m \cdot s^{-1}]$	0.98	0.96	1.54
$N - NO$	[% mole]	12.45	15.74	18.2
m_{fuel}	$[kg \cdot h^{-1}]$	5.4	4.3	5.0

(a) Experimental series No. 1.

Parameter	Unit	'Case 1'	'Case 2'	'Case 3'
ϕ_{O_2}	[% vol.]	3.15 ± 0.05	6.02 ± 0.04	10.12 ± 0.05
t_{BFB}	[°C]	887 ± 0.5	880 ± 0.5	883 ± 0.8
ϕ_{NO_X}	[ppmv]	165 ± 0	170 ± 0	133 ± 0
EF_{NO_X}	$[mg \cdot MJ^{-1}]$	66.2 ± 0.3	97.0 ± 0.2	145.1 ± 0.8
ϕ_{CO}	[ppmv]	20 ± 1	44 ± 1	43 ± 1
EF_{CO}	$[mg \cdot MJ^{-1}]$	7.9 ± 0.4	25.3 ± 0.4	47.1 ± 1.2
ϕ_{CO_2}	[% vol.]	16.8 ± 0.05	14.1 ± 0.04	9.9 ± 0.05
u_0	$[m \cdot s^{-1}]$	1.41	1.48	1.53
$N - NO$	[% mole]	19.7	24.24	26.32
m_{fuel}	$[kg \cdot h^{-1}]$	5.0	5.0	5.0

(b) Experimental series No. 2.

Parameter	Unit	'Case 1'	'Case 2'	'Case 3'	'Case 4'
ϕ_{O_2}	[% vol.]	2.97 ± 0.04	6.62 ± 0.05	9.48 ± 0.05	11.34 ± 0.04
t_{BFB}	[°C]	885 ± 0.8	883 ± 0.8	864 ± 0.9	873 ± 1.1
ϕ_{NO_X}	[ppmv]	107 ± 0	102 ± 0	89 ± 0	78 ± 0
EF_{NO_X}	$[mg \cdot MJ^{-1}]$	42.2 ± 0.1	63.1 ± 0.1	86.0 ± 0.2	107.6 ± 0.3
ϕ_{CO}	[ppmv]	55 ± 3	110 ± 2	176 ± 1	207 ± 2
EF_{CO}	$[mg \cdot MJ^{-1}]$	21.8 ± 1.3	68.1 ± 1.1	170.4 ± 1.0	286.2 ± 2.1
ϕ_{CO_2}	[% vol.]	16.9 ± 0.04	13.2 ± 0.05	10.4 ± 0.05	8.4 ± 0.05
u_0	$[m \cdot s^{-1}]$	3.1	3.4	3.7	3.87
$N - NO$	[% mole]	12.68	15.14	16.52	17.35
m_{fuel}	$[kg \cdot h^{-1}]$	10.8	10.8	10.8	10.8

(c) Experimental series No. 3.

Table B.13: Experimental results of the impact of air stoichimetry on the NO_X formation in the air-combustion of wooden pellets.

B.4.2 Effect of fluidized bed temperature

Parameter	Unit	'Case 1'	'Case 2'	'Case 3'
ϕ_{O_2}	[% vol.]	6.44 ± 0.04	6.02 ± 0.04	5.54 ± 0.05
t_{BFB}	[°C]	840 ± 0.5	880 ± 0.5	921 ± 0.6
ϕ_{NO_X}	[ppmv]	173 ± 0	170 ± 0	165 ± 0
EF_{NO_X}	$[mg \cdot MJ^{-1}]$	104.9 ± 0.2	97.0 ± 0.2	88.4 ± 0.1
ϕ_{CO}	[ppmv]	103 ± 2	44 ± 1	30 ± 1
EF_{CO}	$[mg \cdot MJ^{-1}]$	62.3 ± 1.4	25.3 ± 0.4	15.8 ± 0.6
ϕ_{CO_2}	[% vol.]	13.8 ± 0.04	14.1 ± 0.04	14.4 ± 0.05
u_0	$[m \cdot s^{-1}]$	1.46	1.48	1.14
$N - NO$	[% mole]	25.47	24.24	22.79
m_{fuel}	$[kg \cdot h^{-1}]$	5.0	5.0	5.0

(a) Experimental series No. 1.

Parameter	Unit	'Case 1'	'Case 2'	'Case 3'	'Case 4'	'Case 5'
ϕ_{O_2}	[% vol.]	6.53 ± 0.04	6.25 ± 0.03	6.29 ± 0.05	6.41 ± 0.04	6.6 ± 0.05
t_{BFB}	[°C]	818 ± 0.5	851 ± 0.4	882 ± 0.8	909 ± 0.4	949 ± 0.4
ϕ_{NO_X}	[ppmv]	99 ± 0	101 ± 0	100 ± 0	100 ± 0	100 ± 0
EF_{NO_X}	$[mg \cdot MJ^{-1}]$	60.8 ± 0.1	59.3 ± 0.0	59.3 ± 0.1	60.3 ± 0.1	62.1 ± 0.1
ϕ_{CO}	[ppmv]	62 ± 1	77 ± 1	82 ± 1	75 ± 1	66 ± 1
EF_{CO}	$[mg \cdot MJ^{-1}]$	37.7 ± 0.3	45.5 ± 0.3	48.3 ± 0.5	45.5 ± 0.3	40.8 ± 0.4
ϕ_{CO_2}	[% vol.]	13.4 ± 0.04	13.6 ± 0.03	13.5 ± 0.05	13.3 ± 0.04	13.1 ± 0.05
u_0	$[m \cdot s^{-1}]$	2.28	2.83	2.81	2.75	2.72
$N - NO$	[% mole]	14.68	14.6	14.56	14.67	14.91
m_{fuel}	$[kg \cdot h^{-1}]$	7.2	9.0	9.0	9.0	9.0

(b) Experimental series No. 2.

Table B.14: Experimental results of the impact of fluidized bed temperature on the NO_X formation in the air-combustion of wooden pellets.

Appendix C

Pilot-scale experimental results of the NO, NO_2, and N_2O formation

C.1 Oxy-fuel combustion of wooden pellets

C.1.1 Effect of oxygen stoichiometry

Parameter	Unit	'Case 1'	'Case 2'	'Case 3'
ϕ_{O_2}	[% vol.]	6.4 ± 0.4	8.9 ± 0.2	12.2 ± 0.2
t_{BFB}	[°C]	877 ± 3	892 ± 2	887 ± 3
ϕ_{NO_X}	[ppmv]	174 ± 3.5	195 ± 0.6	213 ± 0.6
ϕ_{NO}	[ppmv]	165 ± 3.3	185 ± 0.6	200 ± 0.5
ϕ_{NO_2}	[ppmv]	4 ± 0.3	7 ± 0.2	10 ± 0.2
ϕ_{N_2O}	[ppmv]	18 ± 0.1	19 ± 0.1	19 ± 0.1
ϕ_{CO}	[ppmv]	72 ± 2.6	70 ± 1.7	67 ± 0.9
ϕ_{CO_2}	[% vol.]	69.8 ± 0.5	72.2 ± 0.3	69.6 ± 0.3
u_0	$[m \cdot s^{-1}]$	3.12	3.4	3.52
$(\phi_{O_2}/\phi_{CO_2})_{prim}$	[−]	0.19	0.25	0.36
$N - NO$	[% mole]	3.7	4.2	4.8
m_{fuel}	$[kg \cdot h^{-1}]$	69.0	70.2	64.2

Table C.1: Pilot-scale experimental results: Experimental characterization of the effect of the oxygen stoichiometry on the formation of NO, NO_2, N_2O, and NO_X in the oxy-fuel combustion process of wooden pellets.

C.1.2 Effect of fluidized bed temperature

Parameter	Unit	'Case 1'	'Case 2'	'Case 3'	'Case 4'
t_{BFB}	[°C]	839 ± 2	884 ± 2	925 ± 1	957 ± 2
ϕ_{O_2}	[% vol.]	9.5 ± 0.3	8.8 ± 0.2	9.1 ± 0.2	8.9 ± 0.3
ϕ_{NO_X}	[ppmv]	173 ± 2.2	171 ± 1.4	188 ± 1.1	190 ± 1.2
ϕ_{NO}	[ppmv]	159 ± 1.7	160 ± 1.1	176 ± 1.0	179 ± 1.1
ϕ_{NO_2}	[ppmv]	5 ± 0.3	5 ± 0.2	5 ± 0.2	5 ± 0.2
ϕ_{N_2O}	[ppmv]	14 ± 0.1	13 ± 0.2	14 ± 0.1	15 ± 0.1
ϕ_{CO}	[ppmv]	76 ± 2.9	92 ± 2.7	66 ± 0.9	53 ± 1.2
ϕ_{CO_2}	[% vol.]	57.2 ± 0.3	59.1 ± 0.5	63.8 ± 0.3	63.8 ± 0.3
u_0	$[m \cdot s^{-1}]$	2.78	3.12	3.0	2.86
$(\phi_{O_2}/\phi_{CO_2})_{prim}$	[−]	0.19	0.24	0.24	0.21
$N - NO$	[% mole]	3.8	3.7	4.1	4.1
m_{fuel}	$[kg \cdot h^{-1}]$	65.0	67.0	65.0	65.0

Table C.2: Pilot-scale experimental results: Experimental characterization of the effect of the fluidized bed temperature on the formation of NO, NO_2, N_2O, and NO_X in the oxy-fuel combustion process of wooden pellets.

C.1.3 Effect of staged supply of oxygen

Parameter	Unit	'Case 1'	'Case 2'	'Case 3'	'Case 4'	'Case 5'	'Case 6'
ψ	[−]	0.0	0.3	0.55	0.73	1.04	1.31
λ_{prim}	[−]	1.04	0.82	0.67	0.56	0.49	0.43
t_{BFB}	[°C]	884 ± 2	898 ± 1	902 ± 1	899 ± 1	876 ± 2	889 ± 1
ϕ_{O_2}	[% vol.]	8.8 ± 0.2	6.7 ± 0.1	7.8 ± 0.1	8.4 ± 0.1	7.8 ± 0.1	8.5 ± 0.1
ϕ_{NO_X}	[ppmv]	171 ± 1.4	161 ± 0.5	178 ± 0.3	182 ± 0.1	178 ± 0.3	186 ± 0.2
ϕ_{NO}	[ppmv]	160 ± 1.1	157 ± 0.4	170 ± 0.2	173 ± 0.1	171 ± 0.3	179 ± 0.2
ϕ_{NO_2}	[ppmv]	5 ± 0.2	4 ± 0.03	5 ± 0.04	6 ± 0.02	5 ± 0.02	6 ± 0.03
ϕ_{N_2O}	[ppmv]	13 ± 0.2	20 ± 0.02	20 ± 0.03	20 ± 0.02	21 ± 0.03	21 ± 0.02
ϕ_{CO}	[ppmv]	92 ± 2.7	52 ± 0.2	53 ± 0.3	62 ± 0.2	59 ± 0.3	59 ± 0.2
ϕ_{CO_2}	[% vol.]	59.1 ± 0.5	66.9 ± 0.1	67.3 ± 0.1	68.0 ± 0.1	68.4 ± 0.1	68.7 ± 0.1
u_0	$[m \cdot s^{-1}]$	3.12	2.87	2.82	2.89	2.53	2.52
$(\phi_{O_2}/\phi_{CO_2})_{prim}$	[−]	0.24	0.18	0.15	0.09	0.08	0.07
$N - NO$	[% mole]	3.7	3.4	3.8	3.9	3.8	4.0
m_{fuel}	$[kg \cdot h^{-1}]$	67.0	69.0	69.0	69.0	69.0	69.0

Table C.3: Pilot-scale experimental results: Experimental characterization of the effect of the staged supply of oxygen on the formation of NO, NO_2, N_2O, and NO_X in the oxy-fuel combustion process of wooden pellets.